



UNIVERSITY OF  
BIRMINGHAM

**Development of force and electron microscopy for the  
quantification of nanoparticle number concentration  
measurements**

by

**ASHWINI PRASAD**

A thesis submitted to  
The University of Birmingham  
For the degree of

**DOCTOR OF PHILOSOPHY**

**The University of Birmingham**  
April 2015

UNIVERSITY OF  
BIRMINGHAM

**University of Birmingham Research Archive**

**e-theses repository**

This unpublished thesis/dissertation is copyright of the author and/or third parties. The intellectual property rights of the author or third parties in respect of this work are as defined by The Copyright Designs and Patents Act 1988 or as modified by any successor legislation.

Any use made of information contained in this thesis/dissertation must be in accordance with that legislation and must be properly acknowledged. Further distribution or reproduction in any format is prohibited without the permission of the copyright holder.

## **ABSTRACT**

The development of metrological and analytical methods for the detection and quantification of nanomaterials (NMs) has been identified as one of the most urgent and important research priorities to advance eco-responsible nanotechnology (Alvarez et al., 2009). Several nanometrics such as mass, number and surface area are currently under scrutiny by nano(eco)toxicologists in order to identify the most appropriate metrics to express the hazard of NMs and therefore to perform risk assessments. Currently, NM mass concentration is almost universally used as a metric because of challenges with analytical measurements, while the mass concentration is measured by a analytical technique called inductive coupled plasma mass spectroscopy. For example, the mass concentration doesn't facilitate to quantify the NM aggregation in an exposure media but can be quantified by particle number measurement. The particle number concentration is an important metric in nano-ecotoxicology and environmental systems to better understand biological uptake and toxicity, aggregation, dissolution and other fate processes. However tools/methods capable of providing fully quantitative assessment of the number size distribution and number particle concentration are lacking and are urgently needed. Microscopy techniques are the only suitable techniques available that can provide accurate information on nanoparticle (NM) number size distribution and number concentration at low concentrations, although others such as single particle- inductive coupled plasma mass spectroscopy (SP-ICPMS) are being developed. However, sample handling issues such as quantitative recovery of NMs from suspension are key challenges hampering their routine application for this purpose. This project has successfully fulfilled the key challenges and developed a novel sampling technique for force and electron microscopy to detect and to quantify the particle number concentration both in realistic environmental relevant conditions and exposure media.

## **ACKNOWLEDGEMENTS**

My first and foremost gratitude goes to my supervisor, Professor Jamie Lead for his honest and friendly guidance, his extremely useful ideas and endless professional support throughout the project. Thank you very much for your valuable time and immeasurable patience. I am extremely thankful to Dr Mohammed Baalousha for his continuous and endless support and guidance throughout my PhD studies.

I am thankful to all of my colleagues in the Environmental Health Research group in the School of Geography, Earth and Environmental Science at the University of Birmingham, support needed for the continuation of the PhD project, Dr Ruth Merrifield for provision of training on various analytical equipment. I owe special thanks to the group of Microscopic Centre at the University of Birmingham for both the training and technical support of the imaging of my samples. The data of this project will be incomplete without the support of Dr Stephen Baker for the ICPM-MS measurements, thank you infinitely for your help.

I am also very grateful to my friend and colleagues for continuous encouragement and support with the structure of the dissertation. I would particularly like to thank the Natural Environmental Research Council (NERC) for the funding of my project.

Finally, I am extremely grateful to my family for their patience, compromise, continuous moral support and understanding during the last three and a half years in which most of my time and energy was devoted to the completion of this project

## CONTENTS

<b>ABSTRACT</b> .....	<b>III</b>
<b>ACKNOWLEDGEMENTS</b> .....	<b>IV</b>
<b>CONTENTS</b> .....	<b>V</b>
<b>LIST OF ABBREVIATIONS</b> .....	<b>IX</b>
<b>LIST OF FIGURES</b> .....	<b>XI</b>
<b>LIST OF TABLES</b> .....	<b>XVII</b>
<b>CHAPTER 1 INTRODUCTION</b> .....	<b>1</b>
<b>1.1 Nanoscience and Nanotechnology</b> .....	<b>1</b>
<b>1.2 Thesis outline</b> .....	<b>3</b>
<b>CHAPTER 2 RESEARCH BACKGROUND</b> .....	<b>5</b>
<b>2.1 Introduction</b> .....	<b>5</b>
2.1.1 Evolve of nanotechnology .....	6
2.1.2 Natural and manufactured NMs .....	8
2.1.3 Classification of nanomaterials (NMs) .....	11
2.1.4 Sources and production of engineered NMs .....	14
2.1.5 Release of NMs to the environment .....	16
2.1.6 Nanoparticle aggregation and DVLO theory .....	20
2.1.7 Limitation for the measurement of NM metrics .....	22
2.1.8 Review on techniques related to particle number concentration .....	26
2.1.9 Analytical Instrumentation .....	29
<b>2.2 Research aims and objectives</b> .....	<b>31</b>
<b>CHAPTER 3 THEORY OF SYNTHESIS AND CHARACTERISATION OF NMS</b> .....	<b>32</b>
<b>3.1 Theory for the synthesis of nanoparticles</b> .....	<b>32</b>
3.1.1 Chemical Synthesis Methods .....	33
3.1.1.1 Hydrochemical Method .....	33
3.1.1.2 Ultrasonification method .....	33
3.1.1.3 Non-hydrochemical Method .....	34
3.1.2 Physical Synthesis Methods .....	34
3.1.2.1 Arc Discharge Method .....	35
3.1.2.2 Spark discharge method .....	35

<b>3.2</b>	<b>Conclusion for Synthesis Procedure .....</b>	<b>37</b>
<b>3.3</b>	<b>Theory of characterisation Techniques .....</b>	<b>38</b>
<b>3.4</b>	<b>Dynamic Light scattering (DLS) .....</b>	<b>38</b>
3.4.1	Electrophoretic Mobility (EPM) and Zeta Potential .....	40
3.4.2	Ultra violet – visible spectroscopy .....	42
3.4.3	Flow field-flow fractionation (F/FFF).....	43
3.4.4	Atomic force microscopy (AFM) .....	46
3.4.5	Transmission electron microscopy (TEM) .....	48
3.4.6	Nanoparticle tracking analysis (NTA) .....	50
3.4.7	Inductively coupled plasma mass spectrometry (ICP-MS).....	50
<b>CHAPTER 4</b>	<b>MATERIALS AND METHODOLOGY .....</b>	<b>53</b>
<b>4.1</b>	<b>Chapter summary .....</b>	<b>53</b>
<b>4.2</b>	<b>Synthesis of gold nanoparticles.....</b>	<b>54</b>
4.2.1	Materials .....	54
4.2.2	Synthesis of Au NMs capped with citrate .....	55
4.2.3	Synthesis of Au NMs capped with polymer (PVP <sub>10</sub> ) .....	55
4.2.3.1	Hot process .....	55
4.2.3.2	Cold process.....	56
<b>4.3</b>	<b>Multi-method approach used to characterise the synthesised gold nanoparticles ..</b>	<b>57</b>
4.3.1	Hydrodynamic and zeta potential measurement with dynamic light scattering (DLS) .....	58
4.3.2	Nanoparticle Tracking Analysis (NTA).....	58
4.3.3	Ultraviolet -Visible spectroscopy .....	59
<b>4.4</b>	<b>Mass concentration of gold with Inductively Coupled Plasma Mass spectrometry (ICP-MS) .....</b>	<b>59</b>
<b>4.5</b>	<b>Sample preparation .....</b>	<b>60</b>
4.5.1	Drop Deposition Method .....	62
4.5.1.1	TEM sample preparation with drop deposition method.....	62
4.5.1.2	AFM sample preparation with drop deposition method.....	63
4.5.2	Ultracentrifugation Method for both TEM and AFM substrates .....	64
4.5.3	Ultracentrifugation with surface functionalisation of the substrate .....	65
<b>4.6</b>	<b>Simple and complex media.....</b>	<b>66</b>
4.6.1	EPA synthetic soft water .....	67
4.6.2	Suwannee river fulvic acid (SRFA).....	68
4.6.3	Natural Surface Water/Lake Water .....	69
<b>4.7</b>	<b>Imaging NMs for size and number concentration measurements from both TEM and AFM analysis .....</b>	<b>69</b>
4.7.1	Imaging for number measurements by TEM .....	69

4.7.2	Imaging for size Measurements by TEM and AFM.....	70
4.7.3	Height Measurements by AFM.....	72
4.7.4	Validation of the AFM and TEM sample preparation for number concentration measurements .....	72
4.7.5	Number of images required for representative measurement of number concentration. ....	75

**CHAPTER 5 NANOPARTICLE CHARACTERISATION USING MULTI-METHOD APPROACH ..... 76**

<b>5.1</b>	<b>Introduction .....</b>	<b>76</b>
<b>5.2</b>	<b>Results and discussion .....</b>	<b>77</b>
<b>5.3</b>	<b>Synthesis and growth of gold NMs .....</b>	<b>78</b>
<b>5.4</b>	<b>Characterisation of Au NMs capped with citrate and PVP .....</b>	<b>82</b>
5.4.1	In-house synthesised NMs used for characterisation .....	82
5.4.2	Wavelength measurement by Ultraviolet-visible Spectroscopy (Uv-vis) .....	83
5.4.3	Z-average Hydrodynamic Diameter (Z-dh) and zeta potential .....	86
5.4.4	Particle spherical diameter measurement by TEM .....	89
5.4.5	Hydrodynamic diameter measurement by NTA.....	91
5.4.6	Particle height measurement by (AFM) .....	94
5.4.7	Particle shape factor .....	96
5.4.8	Mass concentration measurement by ICP-MS .....	98
5.4.9	Comparison of the sizes of NMs measured using different techniques.....	98
<b>5.5</b>	<b>Characterisation of PVP Ag NMs.....</b>	<b>100</b>
<b>5.6</b>	<b>Conclusion.....</b>	<b>105</b>

**CHAPTER 6 NUMBER CONCENTRATION MEASUREMENT OF CITRATE AND PVP AUNMS BY SIMPLE MEDIA USING AFM TECHNIQUE..... 107**

<b>6.1</b>	<b>Chapter Summary .....</b>	<b>107</b>
<b>6.2</b>	<b>Distribution of NMs on the AFM substrate .....</b>	<b>108</b>
<b>6.3</b>	<b>NM suspension on non-functionalised substrate .....</b>	<b>109</b>
6.3.1	PVP capped Au NMs on non-functionalised substrate .....	109
6.3.2	Citrate capped Au NMs on non-functionalised substrate.....	112
6.3.3	Adding CaCl <sub>2</sub> to the NM suspension before ultracentrifugation .....	113
6.3.4	PLL functionalised Au NMs suspended in UHPW .....	118
<b>6.4</b>	<b>Recovery of NMs .....</b>	<b>121</b>
<b>6.5</b>	<b>Particle number measurement of NMs.....</b>	<b>125</b>
<b>6.6</b>	<b>Correlation between the mass and number concentration .....</b>	<b>131</b>

<b>6.7</b>	<b>Number of images required for representative measurement of particle number.....</b>	<b>133</b>
<b>6.8</b>	<b>Conclusion.....</b>	<b>138</b>
<b>CHAPTER 7</b>	<b>NUMBER CONCENTRATION MEASUREMENT OF CITRATE AND PVP AU NMS BY SIMPLE AND COMPLEX MEDIA AND AG NMS WITH E3 MEDIA USING TEM TECHNIQUE .....</b>	<b>140</b>
<b>7.1</b>	<b>Chapter Summary .....</b>	<b>140</b>
<b>7.2</b>	<b>Measurement of particle number concentration by simple media and complex media.....</b>	<b>143</b>
7.2.1	Measurement of particle number of Au NMs in simple media by TEM technique	145
7.2.1.1	Introduction.....	145
7.2.1.2	Distribution of NMs in simple media on TEM grids .....	146
7.2.1.3	Percentage recovery of NMs by simple media .....	158
7.2.1.4	Number of images required for representative measurement of particle number .....	161
7.2.1.5	Correlation between the mass and number concentration .....	166
7.2.2	Detection and quantification of engineered NMs in environmentally representative complex media .....	169
7.2.2.1	Au NMs added to SRFA media .....	170
7.2.2.2	Au NMs added to the synthetic EPA soft water .....	181
7.2.2.3	Au NMs added to lake water/Natural surface water .....	185
7.2.3	Conclusions .....	196
<b>7.3</b>	<b>Particle number and size measurement analysis of Ag NMs by simple media (pure water) and complex media (E3) .....</b>	<b>197</b>
7.3.1	Quantifying the particle number of Ag NMs in pure water/simple media.....	197
7.3.2	Detection and quantification of engineered Ag NMs in E3 media. ....	203
<b>7.4</b>	<b>Conclusion.....</b>	<b>210</b>
<b>CHAPTER 8</b>	<b>CONCLUSION AND FUTURE WORK .....</b>	<b>211</b>
<b>REFERENCES</b>	<b>.....</b>	<b>214</b>
<b>APPENDIX A</b> .....	<b>.....</b>	<b>225</b>
<b>APPENDIX B</b> .....	<b>.....</b>	<b>232</b>



## LIST OF ABBREVIATIONS

$\beta$	angular aperture
$\delta$	distance between two objects
$\mu$	refractive index
AFM	atomic force microscope
AuNMs	gold nanoparticles
CNT	carbon nanotube
DLS	dynamic light scattering
DVLO	Derjaguin, Verwe, Landau, and Overbeek
E	field strength
EDS	energy dispersive X-ray spectrometer
EDX	energy dispersive x-ray
ESA	electrostatic analyser FC centrifugal acceleration
EPA	environmental protection agency
FFF	Field flow fractionation
ICP-MS	Inductively Coupled Plasma Mass Spectrometry
K	stiffness of the lever.
kDa	kilodalton
KV	kilovolt Kw water constant
LED	light emitting diodes
LSPR	localised surface Plasmon resonance
MDM	Minimal Davis Media MRI magnetic resonance imaging
MWCNTs	multi-walled carbon nanotubes
N	rotational speed

NMs	Nanomaterials
NOM	natural organic matter
NTA	nanoparticle tracking analysis
ENMs	engineered nanoparticles
OD	optical density
OECD	Organization for Economic Cooperation and Development
PEG	polyethylene glycol
PPb	part per billion
PPM	part per million
PVP	polyvinylpyrrolidone
PVPNMs	polyvinylpyrrolidone nanoparticles
r	radius
RF	radio frequency
SRFA	Suwannee River Fulvic acid
STM	scanning tunneling microscopy
SWCNTs	single-walled carbon nanotubes
TEM	transmission electron microscope
TOC	total organic carbon
UV_VIS	ultraviolet-visible spectroscopy
Z	deflection distance
$\zeta$	zeta potential
$\lambda$	wavelength
$\omega$	angular speed

## LIST OF FIGURES

FIGURE 1-1 NANOSCOPIC PARTICLES LIE BETWEEN MESOSCOPIC AND MICROSCOPIC PARTICLE (KLABUNDE AND RICHARDS, 2001).....	1
FIGURE 1-2 SIZE OF THE NANOMATERIALS COMPARED TO 'MICRO' AND 'NANO' SIZES.(BUZEA ET AL., 2007).....	2
FIGURE 2-1. ILLUSTRATION OF HOW SURFACE AREA-TO-VOLUME RATIO OF NANOMATERIALS IS INCREASED COMPARED WITH NON-NANOSCALE-SIZED MATERIALS. (TAKEN FROM NATIONAL NANOTECHNOLOGY INITIATIVE ).....	6
FIGURE 2-2. MARKET TIMELINE PROJECTION OF THE WORLDWIDE PRODUCTS THAT INCORPORATE NANOTECHNOLOGY (ROCO 2011).....	7
FIGURE 2-3. PRODUCTION OF NMS (MADHUMITHA AND ROOPAN, 2013A).....	15
<b>FIGURE 2-4:</b> RELEASE OF NP FROM PRODUCTS AND (INTENDED OR UNINTENDED) APPLICATIONS: (A) RELEASE OF FREE NP, (B) RELEASE OF AGGREGATES OF NM, (C) RELEASE OF NM EMBEDDED IN A MATRIX AND (D) RELEASE OF FUNCTIONALIZED NM. ENVIRONMENTAL FACTORS (E.G. LIGHT, MICROORGANISMS) RESULT IN FORMATION OF FREE NM THAT CAN UNDERGO AGGREGATION REACTIONS. MOREOVER, SURFACE MODIFICATIONS (E.G. COATING WITH NATURAL COMPOUNDS) CAN AFFECT THE AGGREGATION BEHAVIOUR OF THE NM (NOWACK AND BUCHELI, 2007).....	16
FIGURE 2-5: PLAUSIBLE ENVIRONMENTAL TRANSPORT OF NANOSCALE MATERIALS BASED ON CURRENT AND POTENTIAL FUTURE APPLICATIONS (STONE ET AL., 2010).....	18
FIGURE 2-7 COMPARISON OF THE MEASURED PARTICLE NUMBER CONCENTRATION WITH MATHEMATICAL CALCULATION AND THE EXPERIMENTAL CONCENTRATION OF THE NIST PRECISION NANOBEADS (DU ET AL., 2010).....	27
FIGURE 2-8 BASED ON THE ABOVE SIGNAL, PARTICLE NUMBER CONCENTRATION CAN BE OBTAINED (DEGUELDRE AND FAVARGER, 2003B).....	28
FIGURE 3-1. TYPES OF NM SYNTHESIS .....	32
FIGURE 3-2. SCHEMATIC ILLUSTRATION OF AN ULTRASONICALLY IRRADIATED PROCESS (AMENDOLA ET AL.).....	34
FIGURE 3-3. DC ARC DISCHARGE SYSTEM (LEE AND PARK, 2007, LUNG ET AL., 2007, ASHKARRAN ET AL., 2009, TIEN ET AL., 2010).....	35
FIGURE 3-4. SCHEMATIC OF ARC DISCHARGE METHOD (TSENG ET AL., 2009).....	36
FIGURE 3-5. SCHEMATIC ILLUSTRATION OF SPARK DISCHARGE METHOD (TABRIZI ET AL., 2008, TABRIZI ET AL., 2009).....	36
FIGURE 3-6. PRINCIPLE OF OPERATION OF DYNAMIC LIGHT SCATTERING INSTRUMENT .....	38
FIGURE 3-7. HYDRODYNAMIC RADIUS OF A PARTICLE COATED WITH IONIC POLYMER (PECORA, 2000, SARTOR). .....	40
FIGURE 3-8 SCHEMATIC REPRESENTATION OF ZETA POTENTIAL (JÉRÔME F. L. DUVAL, 2007). .....	41
FIGURE 3-9. EFFECT OF PH ON ZETA POTENTIAL (KIRBY AND HASSELBRINK, 2004).....	42
FIGURE 3-10 SCHEMATIC DIAGRAM OF F/FFF CHANNEL (ASSEMI ET AL., 2004). .....	44
FIGURE 3-11 SCHEMATIC ILLUSTRATION F/ FFF SEPARATION MECHANISM.(GIDDINGS, 1993, ASSEMI ET AL., 2004, FRAUNHOFER AND WINTER, 2004). .....	45
FIGURE 3-12 (A) SCHEMATIC DIAGRAM SHOWING THE OPERATING PRINCIPLES OF THE AFM IN THE CONTACT MODE (PICTURE FROM DIGITAL INSTRUMENTS, CA) (B) SCHEMATIC ILLUSTRATION OF THE CANTILEVER AND THE DISTANCE BETWEEN THE PROBE AND THE SAMPLE SURFACE, (C) SEM IMAGE OF THE SPM CANTILEVER WITH THE PROBE. (PICTURE TAKEN FROM MIKROMASCH).(MEYER, 1992).....	47
FIGURE 3-13. FEI PHILIPS TECNAI F204 (OXFORD INSTRUMENTATION).....	48

FIGURE 3-14. SCHEMATIC ILLUSTRATION OF THE INTERNAL FUNCTION OF TEM (TAKEN FROM THE OXFORD INSTRUMENTS).....	49
FIGURE 3-15. SCHEMATIC ILLUSTRATION F THE ICP-MS INSTRUMENT WHICH WAS FIRST INTRODUCED IN THE YEAR 1983 (JARVIS AND JARVIS, 1992) .....	51
FIGURE 3-16. A DIAGRAM SHOWING THE CROSS SECTION OF THE DIFFERENT COMPONENTS OF MODERN ICPMS (DE WIT ET AL., 1993) .....	52
FIGURE 4-6 AREAS AND IMAGES SCANNED BY AFM FOR EACH SAMPLE. THREE AREAS AT DIFFERENT LOCATIONS ON THE AFM SUBSTRATE AND (A) 5 AND (B) 9 IMAGES WERE COLLECTED BY AREA, RESULTING IN COLLECTING 15-29 IMAGES FOR EACH SAMPLE. ....	71
FIGURE 5-1 A TYPICAL TEM IMAGES OF PVP CAPPED AU NMS SYNTHESISED BY TWO DIFFERENT SYNTHESIS PROCESSES SUCH AS: (A) HOT PROCESS AND (B) COLD PROCESS. ....	79
FIGURE 5-2 TEM IMAGES OF CITRATE CAPPED AU NMS SYNTHESISED BY TRIAL AND ERROR METHOD USING CHEMICAL SYNTHESIS PROCESSES, IMAGES (A, B AND C) ARE AGGREGATED AND (D) NON-AGGREGATED. ....	81
FIGURE 5-10. PARTICLE SIZE DISTRIBUTION AS MEASURED BY ATOMIC FORCE MICROSCOPY (A) CIT-AU NMS (13.3±2.1) AND (B) PVP-AU NMS (12.2±2.2) NM. ....	95
<b>FIGURE 5-11.</b> TEM IMAGE OF THE SYNTHESISED AU NMS SHOWING HIGHLY SPHERICAL AND MONODISPERSED .....	97
FIGURE 5-12 SHAPE FACTOR OF (A) CIT-AU NMS AND (B) PVP-AU NMS CALCULATED FROM THE MICROGRAPH OF TEM IMAGE OF APPROXIMATELY 1500 NMS FROM 30 IMAGES. ....	97
FIGURE 6-1 AFM MICROGRAPHS OF PVP CAPPED AU NMS SUSPENDED IN UHPW AND ULTRACENTRIFUGED ON FRESHLY CLEAVED NON-FUNCTIONALISED MICA SUBSTRATE AT DIFFERENT CONCENTRATIONS OF AU NMS (33.5-670.5 PPB). ....	110
FIGURE 6-2 AFM MICROGRAPHS (5 MM X 5 MM) OF PVP CAPPED AU NMS SUSPENDED IN UHPW AND ULTRACENTRIFUGED ON FRESHLY CLEAVED NON-FUNCTIONALISED MICA SUBSTRATE AT DIFFERENT CONCENTRATIONS OF AU NMS (1.7-67.1 PPB). ....	111
FIGURE 6-3 AFM MICROGRAPHS (5 MM X 5 MM) OF CIT-AUNMS IN ULTRAHIGH PURITY WATER (UHPW) PREPARED ON FRESHLY CLEAVED NON-FUNCTIONALISED MICA SUBSTRATE AT DIFFERENT CONCENTRATIONS (A) 101.6 PPB AU AND (B) 40.64 PPB AU. ....	112
FIGURE 6-4 AFM MICROGRAPHS (5 MM X 5 MM) OF CIT-AUNMS SUSPENDED IN 100 MM $CaCl_2$ AND ULTRACENTRIFUGED ON FRESHLY CLEAVED NON-FUNCTIONALISED MICA SUBSTRATE AT DIFFERENT CONCENTRATIONS OF AUNMS (1-203.2 PPB) EXPRESSED AS PPB AU. ....	114
FIGURE 6-5 AFM MICROGRAPHS OF CIT-AUNMS SUSPENDED IN 200 MM $CaCl_2$ AND ULTRACENTRIFUGED ON FRESHLY CLEAVED NON-FUNCTIONALISED MICA SUBSTRATE AT DIFFERENT CONCENTRATIONS OF AUNMS (1-203.2 PPB) EXPRESSED AS PPB AU. ....	115
FIGURE 6-6 AFM MICROGRAPHS OF PVP-AU NMS SUSPENDED IN 10 MM $CaCl_2$ AND ULTRACENTRIFUGED NON-FUNCTIONALISED MICA SUBSTRATE AT DIFFERENT CONCENTRATIONS OF AU NMS (0.34-33.5 PPB) EXPRESSED AS PPB AU. ....	117
FIGURE 6-7 AFM MICROGRAPHS OF CITRATE CAPPED AU NMS IN UHPW AND ULTRACENTRIFUGED ON POLY-L-LYSINE FUNCTIONALIZED MICA SUBSTRATE AT DIFFERENT CONCENTRATIONS OF AU NMS (1.0-101.6 PPB). ....	119
FIGURE 6-8 AFM MICROGRAPHS OF PVP CAPPED AU NMS IN UHPW AND ULTRACENTRIFUGED ON POLY-L-LYSINE FUNCTIONALIZED MICA SUBSTRATE AT CONCENTRATION OF 1 PPB. ....	120

FIGURE 6-9 AFM MICROGRAPHS (5 MM X 5 MM) OF PVP-AU NMS SUSPENDED IN UHPW AND ULTRACENTRIFUGED ON POLY-L-LYSINE FUNCTIONALIZED MICA SUBSTRATE NOT WASHED. .... 124

FIGURE 6-10 REPRESENTATIVE ATOMIC FORCE MICROSCOPY IMAGES OF PVP-AUNMS SUSPENDED IN 10 MM  $\text{CaCl}_2$  SHOWING A UNIFORM DISTRIBUTION OF PVP-AUNMS ON NON-FUNCTIONALISED AFM SUBSTRATE AND THE DECREASE OF THE NUMBER OF NMS RECOVERED WITH THE DECREASE IN NM MASS CONCENTRATION IN PPB (A) 67.1, (B) 33.5, (C)16.8, (D)3.4, (E) 1.7 AND (F) 0.34. ALL IMAGES ARE  $2 \mu\text{M} \times 2 \mu\text{M}$ . 130

FIGURE 6-11 CORRELATION BETWEEN THE MASS AND NUMBER CONCENTRATION OF NMS (A) NM/L IN DILUTED SUSPENSION AND (B)  $\text{NM}/\text{MM}^2$  ON THE MICA SUBSTRATE. CIT-AUNMS WAS PREPARED BY ULTRACENTRIFUGATION ON A POLY-L-LYSINE FUNCTIONALIZED MICA SUBSTRATE AND PVP-AU NMS IN 10 MM  $\text{CaCl}_2$  WAS PREPARED BY ULTRACENTRIFUGATION ON A NON-FUNCTIONALISED MICA SUBSTRATE. ALL NUMBER CONCENTRATIONS REPRESENT AVERAGE AND STANDARD DEVIATION OF TWO INDEPENDENT REPLICATES. .... 132

FIGURE 6-12 DEPENDENCE OF THE CALCULATED MEAN NUMBER CONCENTRATION AND STANDARD DEVIATION OF THE MEAN ON THE NUMBER OF IMAGES SCANNED BY ATOMIC FORCE MICROSCOPY OF THE CIT-AUNMS PREPARED BY ULTRACENTRIFUGATION AT 150 000 G ON POLY-L-LYSINE FUNCTIONALIZED AFM SUBSTRATES AT DIFFERENT CONCENTRATIONS (PPB): (A) 101.6, (B) 20.3, (C) 10.2, (D) 2.0 AND (E) 1.0. .... 134

FIGURE 6-13 DEPENDENCE OF THE CALCULATED MEAN NUMBER CONCENTRATION AND STANDARD DEVIATION OF THE MEAN ON THE NUMBER OF IMAGES SCANNED BY ATOMIC FORCE MICROSCOPY OF THE PVP-COATED AUNMS PREPARED BY ADDING 10 MM  $\text{CaCl}_2$  ON A NON-FUNCTIONALISED SUBSTRATE AT DIFFERENT CONCENTRATIONS EXPRESSED AS PPB AU: (A) 67.1, (B) 33.5, (C) 16.8, (D) 3.4, (E) 1.7 AND (F) 0.34. .... 136

FIGURE 6-14 DEPENDENCE OF THE CALCULATED MEAN NUMBER CONCENTRATION AND STANDARD DEVIATION OF THE MEAN ON THE NUMBER OF IMAGES SCANNED BY ATOMIC FORCE MICROSCOPY OF THE CIT-COATED AUNMS PREPARED BY ADDING 300 MM  $\text{CaCl}_2$  ON A NON FUNCTIONALISED MICA SUBSTRATE AT DIFFERENT CONCENTRATIONS EXPRESSED AS PPB AU: (A) 101.6, (B) 20.3, (C) 10.2 (D) 2.0 AND (E) 1.0. .... 137

FIGURE 7-1: TRANSMISSION ELECTRON MICROSCOPY IMAGES OF (A) CITRATE-AUNMS (20.3 PPB) AND (B) PVP-AUNMS (15.79 PPB) ON BARE-TEM GRID. SAMPLES WERE PREPARED BY DROP DEPOSITION METHOD. .... 148

FIGURE 7-2: TRANSMISSION ELECTRON MICROSCOPY IMAGES OF CITRATE- AND PVP-CAPPED-AUNMS ON BARED-TEM GRID (A) CIT-AUNMS AT 9.49 PPB AND (B) PVP-AUNMS AT 15.79PPB. NMS WERE SUSPENDED IN UHPW. SAMPLES WERE PREPARED BY ULTRACENTRIFUGATION METHOD ON NON-FUNCTIONALISED TEM GRID. .... 149

FIGURE 7-3: REPRESENTATIVE TRANSMISSION ELECTRON MICROSCOPY IMAGES SHOWING A UNIFORM DISTRIBUTION OF CITRATE CAPPED-AUNMS ON TEM GRID THAT IS TREATED WITH 0.1% W/V POLY-L-LYSINE AND THE DECREASE OF THE NUMBER OF NMS RECOVERED WITH THE DECREASE IN NM MASS CONCENTRATION IN PPB (A) 17.96, (B) 9.49, (C) 1.85, (D) 0.89 AND (E) 0.19. NMS WERE SUSPENDED IN UHPW. .... 151

FIGURE 7-4: REPRESENTATIVE TRANSMISSION ELECTRON MICROSCOPY IMAGES SHOWING A UNIFORM DISTRIBUTION OF PVP-AUNMS ON TEM GRID THAT IS FUNCTIONALIZED WITH 0.1% W/V POLY-L-LYSINE AND THE DECREASE OF THE NUMBER OF NMS RECOVERED WITH THE DECREASE IN NM MASS CONCENTRATION IN PPB (A) 31.38, (B) 15.79, (C) 3.34, (D) 1.55 AND (E) 0.34. NMS WERE SUSPENDED IN UHPW. .... 153

FIGURE 7-5: REPRESENTATIVE TRANSMISSION ELECTRON MICROSCOPY IMAGES SHOWING A UNIFORM DISTRIBUTION OF CITRATE COATED-AUNMS ON TEM GRID THAT IS

TREATED WITH 0.1% W/V POLY-L-LYSINE AND THE DECREASE OF THE NUMBER OF NMS RECOVERED WITH THE DECREASE IN NM MASS CONCENTRATION IN PPB (A) 101.5, (B) 17.96, (C) 9.49, (D) 1.85, (E) 0.89 AND (F) 0.19. SCALE BAR IN ALL IMAGES IS 100 NM. THE CIT-AUNMS WERE SUSPENDED IN UHPW. ....	154
FIGURE 7-6: REPRESENTATIVE TRANSMISSION ELECTRON MICROSCOPY IMAGES SHOWING A UNIFORM DISTRIBUTION OF PVP COATED-AUNMS ON TEM GRID THAT IS TREATED WITH 0.1% W/V POLY-L-LYSINE AND THE DECREASE OF THE NUMBER OF NMS RECOVERED WITH THE DECREASE IN NM MASS CONCENTRATION IN PPB (A) 101.5, (B) 31.38, (C) 15.79, (D) 9.49, (E) 1.55 AND (F) 0.34. SCALE BAR IN ALL IMAGES IS 100 NM. THE CIT-AUNMS WERE SUSPENDED IN UHPW. ....	155
FIGURE 7-7:DEPENDENCE OF THE CALCULATED MEAN NUMBER CONCENTRATION AND STANDARD DEVIATION OF THE MEAN ON THE NUMBER OF IMAGES SCANNED BY TRANSITION ELECTRON MICROSCOPY OF THE CIT-AUNMS PREPARED BY (A) DROP DEPOSITION (17.96 PPB) AND PVP-AUNMS PREPARED BY (B) DROP DEPOSITION (15.79 PPB).THE Y AXES ARE NOT CORRECT HERE. ....	162
FIGURE 7-8: CALCULATED MEAN NUMBER CONCENTRATION AND STANDARD DEVIATION OF THE MEAN ON THE NUMBER OF IMAGES SCANNED BY TRANSITION ELECTRON MICROSCOPY OF THE CIT-AUNMS PREPARED BY (A) ULTRACENTRIFUGATION ON NON FUNCTIONALISED TEM GRID (20.3 PPB) AND (B) ULTRACENTRIFUGATION NON FUNCTIONALISED TEM GRID (10.2 PPB); AND PVP-AUNMS PREPARED BY (C) ULTRACENTRIFUGATION ON NON FUNCTIONALISED TEM GRID (33.5 PPB) AND (D) ULTRACENTRIFUGATION ON NON FUNCTIONALISED TEM GRID (16.8 PPB).....	163
FIGURE 7-9 DEPENDENCE OF THE CALCULATED MEAN NUMBER CONCENTRATION AND STANDARD DEVIATION OF THE MEAN ON THE NUMBER OF IMAGES SCANNED BY TRANSITION ELECTRON MICROSCOPY OF THE PVP-AUNMS PREPARED BY ULTRACENTRIFUGATION AT 150 000 G ON POLY-L-LYSINE FUNCTIONALIZED TEM GRID AT DIFFERENT CONCENTRATIONS (PPB): (A) 31.5, (B) 16.8, (C) 3.4, (D) 1.7 AND (E) 0.34. ....	164
FIGURE 7-10 CALCULATED MEAN NUMBER CONCENTRATION AND STANDARD DEVIATION OF THE MEAN ON THE NUMBER OF IMAGES ANALYZED BY TRANSMISSION ELECTRON MICROSCOPY. TEM SAMPLES WERE PREPARED BY ULTRACENTRIFUGATION OF CIT-AU NMS AT 150 000 G ON POLY-L-LYSINE FUNCTIONALIZED TEM GRID AT DIFFERENT CONCENTRATIONS ( $\mu\text{G L}^{-1}$ ): (A) 20.3, (B) 10.2, (C) 2.0, (D) 1.0 AND (E) 0.20. ....	165
FIGURE 7-11 CORRELATION BETWEEN THE MASS AND NUMBER CONCENTRATION OF AU NMS (A) CITRATE-AU NMS SUSPENDED IN MQ WATER, (B) PVP-AU NMS SUSPENDED IN MQ WATER. SAMPLES PREPARED BY ULTRACENTRIFUGATION ON A POLY-L-LYSINE FUNCTIONALIZED TEM GRID. ....	167
FIGURE 7-12 CONCENTRATION-DEPENDENT AGGREGATION OF NMS REVEALED AT ENVIRONMENTALLY REALISTIC NM CONCENTRATION BY THE NEWLY DEVELOPED FULLY QUANTITATIVE SAMPLE PREPARATION APPROACH FOR TEM ANALYSIS OF NMS (A) $2.0 \mu\text{G L}^{-1}$ AND (B) $20.3 \mu\text{G L}^{-1}$ .....	171
FIGURE 7-13 TRANSMISSION ELECTRON MICROSCOPY IMAGES OF CIT-AU NMS SPIKED IN SYNTHETIC EPA SOFT WATER CONTAINING $5 \text{ MG L}^{-1}$ SUWANNEE RIVER FULVIC ACID. MASS CONCENTRATION OF CIT-AU NMS IN $\mu\text{G L}^{-1}$ WAS (A) 20.3, (B) 2.0, (C) 1.0. (D) A REPRESENTATIVE X-EDS SPECTRUM COLLECTED FROM THE DARK PARTICLES IDENTIFIED AS AU NMS. ALL SAMPLES WERE PREPARED BY ULTRACENTRIFUGATION ON POLY-L-LYSINE FUNCTIONALIZED TEM GRID.....	173
FIGURE 7-14 DEPENDENCE OF THE CALCULATED MEAN NUMBER CONCENTRATION AND STANDARD DEVIATION OF THE MEAN ON THE NUMBER OF IMAGES SCANNED BY TRANSMISSION ELECTRON MICROSCOPY OF THE CIT-AU NMS SPIKED WITH EPA SOFT WATER CONTAINING $5 \text{ MG L}^{-1}$ SUWANNEE RIVER FULVIC ACID PREPARED BY	

ULTRACENTRIFUGATION AT 150 000 G ON POLY-L-LYSINE FUNCTIONALIZED TEM GRID AT DIFFERENT CONCENTRATIONS (PPB) : (A) 20.3, (B) 2.0 AND (C) 1.0 .....	179
FIGURE 7-15 CORRELATION BETWEEN THE MASS AND NUMBER CONCENTRATION OF CITRATE CAPPED AU NMS CIT-AU NMS SPIKED WITH EPA SOFT WATER CONTAINING 5 MG L <sup>-1</sup> SUWANNEE RIVER FULVIC ACID PREPARED BY ULTRACENTRIFUGATION AT 150 000 G ON POLY-L-LYSINE FUNCTIONALIZED TEM GRID AT DIFFERENT CONCENTRATIONS (PPB).....	180
FIGURE 7-16 REPRESENTATIVE TRANSMISSION ELECTRON MICROSCOPY IMAGES SHOWING A UNIFORM DISTRIBUTION OF PVP-AUNMS SPIKED IN EPA SOFT WATER ON TEM GRID THAT IS FUNCTIONALIZED WITH 0.1% W/V POLY-L-LYSINE AND THE DECREASE OF THE NUMBER OF NMS RECOVERED WITH THE DECREASE IN NM MASS CONCENTRATION IN PPB (A) 31.38, (B) 15.79, (C) 3.34 AND (D) 1.55. NMS WERE SUSPENDED IN UHPW.....	182
FIGURE 7-17 DEPENDENCE OF THE CALCULATED MEAN NUMBER CONCENTRATION AND STANDARD DEVIATION OF THE MEAN ON THE NUMBER OF IMAGES SCANNED BY TRANSMISSION ELECTRON MICROSCOPY OF THE PVP-AUNMS PREPARED BY ULTRACENTRIFUGATION AT 150 000 G ON POLY-L-LYSINE FUNCTIONALIZED TEM GRID AT DIFFERENT CONCENTRATIONS (PPB): (A) 31.5, (B) 16.8, (C) 3.4, (D) 1.7 AND (E) 0.34. ....	184
FIGURE 7-18 REPRESENTATIVE TRANSMISSION ELECTRON MICROSCOPY IMAGES SHOWING DISTRIBUTION OF PVP-AUNMS SUSPENDED IN COMPLEX MEDIA (9.1 % OF LAKE WATER) AND UHPW OF 90.9 % PREPARED BY ULTRACENTRIFUGATION ON POLY-L-LYSINE FUNCTIONALIZED TEM GRID AT THE CONCENTRATION OF (A) OVERLOADED WITH 100% OF LAKE WATER WITHOUT NMS, NONE OF NMS VISIBLE (B) 10 FOLDS DILUTED LAKE WATER SPIKED WITH 3.4 µG L <sup>-1</sup> OF NMS AND (C AND D) 10 FOLDS DILUTED LAKE WATER SPIKED WITH 1.7 µG L <sup>-1</sup> OF AU NMS .....	186
FIGURE 7-19 REPRESENTATIVE TEM IMAGES SHOWING DISTRIBUTION OF PVP-AUNMS SUSPENDED IN COMPLEX MEDIA (9.1 % OF LAKE WATER) AND UHPW OF 90.9 % PREPARED BY ULTRACENTRIFUGATION ON POLY-L-LYSINE FUNCTIONALIZED TEM GRID AT THE CONCENTRATION OF 3.4 µG L <sup>-1</sup> AND 1.7 µG L <sup>-1</sup> AND ITS REPRESENTATIVE X-EDS SPECTRUM COLLECTED FROM THE DARK PARTICLES IDENTIFIED AS AU NMS.....	189
FIGURE 7-20 REPRESENTATIVE TRANSMISSION ELECTRON MICROSCOPY IMAGES SHOWING DISTRIBUTION OF CIT-AUNMS SUSPENDED IN COMPLEX MEDIA (LAKE WATER) PREPARED BY ULTRACENTRIFUGATION ON POLY-L-LYSINE FUNCTIONALIZED TEM GRID AT THE CONCENTRATION OF 3.4 PPB (A-C) AND 1.7 NMS (D-F). ....	191
FIGURE 7-21 DEPENDENCE OF THE CALCULATED MEAN NUMBER CONCENTRATION AND STANDARD DEVIATION OF THE MEAN ON THE NUMBER OF IMAGES SCANNED BY TRANSMISSION ELECTRON MICROSCOPY OF THE PVP-AUNMS WITH COMPLEX MEDIA (9.1% LAKE WATER AND 90.9% OF UHPW+NMS) PREPARED BY ULTRACENTRIFUGATION AT 150 000 G ON POLY-L-LYSINE FUNCTIONALIZED TEM GRID AT THE CONCENTRATIONS OF (PPB) : (A) 3.4 AND (B) 1.7. ....	195
FIGURE 7-22 PARTICLE SIZE DISTRIBUTION AS MEASURED BY TRANSMISSION ELECTRON MICROSCOPY OF AGNMS (19.4±6.8) SUSPENDED IN UHPW AND ULTRACENTRIFUGED ON POLY-L-LYSINE FUNCTIONALIZED TEM SUBSTRATE. ....	101
FIGURE 7-23 SHAPE FACTOR OF AG NMS CALCULATED FROM THE MICROGRAPH OF TEM IMAGE OF APPROXIMATELY 2000 NMS.....	103
FIGURE 7-24 EDX SPECTRA OF AG NMS OBTAINED FROM THE TECNAI PHILIPS F20 TEM.	104
FIGURE 7-25 REPRESENTATIVE TRANSMISSION ELECTRON MICROSCOPY IMAGES SHOWING A DISTRIBUTION OF AGNMS ON TEM GRID PREVIOUSLY TREATED WITH 0.1% W/V POLY-L-LYSINE AND THE DECREASE OF THE NUMBER OF NMS	

RECOVERED WITH THE DECREASE IN NM MASS CONCENTRATION IN PPB (A AND B) 55.40, (C AND D) 11.08, (E AND F) 5.54. SCALE BAR IN ALL IMAGES IS 50 NM. THE AGNMS WERE SUSPENDED IN UHPW.....	198
FIGURE 7-26 DEPENDENCE OF THE CALCULATED MEAN NUMBER CONCENTRATION AND STANDARD DEVIATION OF THE MEAN ON THE NUMBER OF IMAGES SCANNED BY TRANSITION ELECTRON MICROSCOPY OF THE PVP-AUNMS PREPARED BY ULTRACENTRIFUGATION AT 150 000 G ON POLY-L-LYSINE FUNCTIONALIZED TEM GRID AT DIFFERENT CONCENTRATIONS IN PPB: (A) 55.40, (B) 11.08 (C) 5.54 AND (D) 1.10.....	201
FIGURE 7-27 CORRELATION BETWEEN THE MASS AND NUMBER CONCENTRATION OF PVP CAPPED AG NMS IN MQ WATER. SAMPLES PREPARED BY ULTRACENTRIFUGATION ON A POLY-L-LYSINE FUNCTIONALIZED TEM GRID. ....	202
FIGURE 7-28 REPRESENTATIVE TRANSMISSION ELECTRON MICROSCOPY IMAGES SHOWING A DISTRIBUTION OF PVP AG NMS ON TEM GRID THAT IS TREATED WITH 0.1% W/V POLY-L-LYSINE , THE DIFFERENT CONCENTRATION IMAGED WERE AS FOLLOWS IN PPB (A) 2770, (B) 1110, (C) 220, (D) 45, (E)8.5 PPB IN 62.5 MM CaCl <sub>2</sub> .....	205
FIGURE 7-29 DEPENDENCE OF THE CALCULATED MEAN NUMBER CONCENTRATION AND STANDARD DEVIATION OF THE MEAN ON THE NUMBER OF IMAGES SCANNED BY TRANSITION ELECTRON MICROSCOPY OF THE PVP-AGNMS IN E3 MEDIA PREPARED BY ULTRACENTRIFUGATION AT 150 000 G ON POLY-L-LYSINE FUNCTIONALIZED TEM GRID AT DIFFERENT CONCENTRATIONS : (A) 220 PPB, (B) 45 PPB AND (E) 8.5 PPB.	208
FIGURE 7-30 X-EDS SPECTRUM OF PVP AG NMS.....	209



## LIST OF TABLES

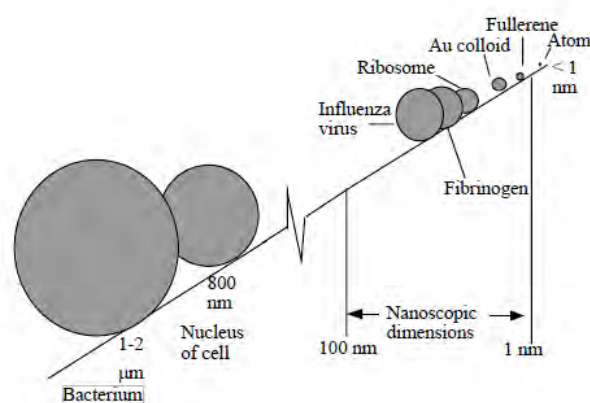
TABLE 2-1: DEFINITIONS OF ENVIRONMENTAL BEHAVIOUR/DISTRIBUTION PROCESS FOR ENMS IN THE CONTEXT OF THIS REPORT BASED ON DEFINITIONS IN (HARTMANN ET AL., 2014, STONE, (2010), NOWACK ET AL., 2012). .....	19
<b>TABLE 4-1</b> CONCENTRATIONS OF THE REACTANT USED FOR THE SYNTHESIS OF AUNMS CAPPED WITH PVP .....	57
TABLE 4-2 PREPARATION OF SYNTHETIC FRESHWATER AFTER USING REAGENT GRADE CHEMICALS <sup>1</sup> .....	67
TABLE 5-1 HYDRODYNAMIC DIAMETER (Z-AVERAGE) AND ZETA POTENTIAL OF PVP AND CITRATE CAPPED AU NMS.....	88
<b>TABLE 5-2: PARTICLE SPHERICAL DIAMETER MEASUREMENT BY TEM</b> .....	91
TABLE 5-3: PARTICLE HEIGHT MEASURE USING AFM TECHNIQUE.....	95
TABLE 5-4 PHYSICO-CHEMICAL PROPERTIES OF CITRATE AND PVP COATED AUNMS MEASURED BY DIFFERENT ANALYTICAL TECHNIQUES .....	99
TABLE 6-1: RECOVERY OF CIT- AND PVP-AUNMS BY IGNORING AND CONSIDERING SIZE POLYDISPERSITY. THE CITRATE AND PVP AUNMS PREPARED BY ULTRACENTRIFUGATION ON A MICA SUBSTRATE FUNCTIONALIZED BY POLY-L-LYSINE. THE PVP-AUNMS WERE PREPARED BY ULTRACENTRIFUGATION ON A NON-FUNCTIONALISED MICA SUBSTRATE FROM 10 MM CaCl <sub>2</sub> SUSPENSION.....	122
TABLE 6-2 RECOVERY OF CITRATE AND PVP COATED AU NMS GIVEN IN BRIEF ON NON FUNCTIONALISED, ON ADDITION OF CaCl <sub>2</sub> AND PLL FUNCTIONALISED SUBSTRATES .....	123
<b>TABLE 6-3</b> NUMBER OF NMS COUNTED PER MM <sup>2</sup> OF AFM SUBSTRATE FOR CIT-AUNMS ....	126
TABLE 6-4: NUMBER OF NMS COUNTED PER MM <sup>2</sup> OF AFM SUBSTRATE FOR PVP-AU NMS .	127
TABLE 6-5 NUMBER CONCENTRATION (PARTICLE.L <sup>-1</sup> ) OF CIT-AU NMS IN DILUTED SAMPLES .....	128
<b>TABLE 6-6</b> NUMBER CONCENTRATION (PARTICLE.L <sup>-1</sup> ) OF PVP-AUNMS IN DILUTED SAMPLES .....	129
TABLE 7-1: NUMBER CONCENTRATION (PARTICLE L <sup>-1</sup> ) OF CIT-AU NMS IN STOCK SOLUTIONS .....	156
<b>TABLE 7-2:</b> NUMBER CONCENTRATION (PARTICLE.L <sup>-1</sup> ) OF PVP-AU NMS IN STOCK SOLUTIONS.....	157
TABLE 7-3: RECOVERY (%) OF CIT-AU NMS .....	159
TABLE 7-4 RECOVERY (%) OF PVP CAPPED AU NMS .....	160
<b>TABLE 7-5 :</b> NUMBER CONCENTRATION (PARTICLE L <sup>-1</sup> ) OF CIT-AU NMS IN STOCK SOLUTIONS.....	174
TABLE 7-6 % NUMBER FRACTION OF AGGREGATES CONTAINING A CERTAIN NUMBER OF PRIMARY NMS IN SOFT EPA WATER CONTAINING 5 MG L <sup>-1</sup> SRFA AT A RANGE OF NM CONCENTRATIONS CA. 1-20 µG L <sup>-1</sup> . ANALYSIS WAS PERFORMED ON 15 IMAGES COLLECTED AT DIFFERENT LOCATIONS ON THE TEM GRID.....	176
TABLE 7-7 RECOVERY (%) OF CIT-AU NMS .....	177
TABLE 7-8 NUMBER CONCENTRATION (PARTICLE.L <sup>-1</sup> ) AND PERCENTAGE RECOVERY OF PVP AU NMS IN EPA SOFT WATER IN STOCK SOLUTIONS	
183	
TABLE 7-9 NUMBER CONCENTRATION (PARTICLE.L <sup>-1</sup> ) OF PVP-AU NMS IN STOCK SOLUTIONS .....	193

TABLE 7-10 RECOVERY (%) OF CIT-AU NMS AND PVP-AU NMS .....	194
TABLE 7-11 PHYSICOCHEMICAL PROPERTIES OF PVP COATED AG NMS MEASURED BY DIFFERENT ANALYTICAL TECHNIQUES .....	100
TABLE 7-12 ELEMENTAL ANALYSIS FOR NMA AS OBTAINED BY EDX.....	104
<b>TABLE 7-13</b> NUMBER CONCENTRATION (PARTICLE.L <sup>-1</sup> ) AND % RECOVERY OF AG NMS IN STOCK SOLUTIONS .....	199
<b>TABLE 7-14:</b> NUMBER CONCENTRATION (PARTICLE.L <sup>-1</sup> ) OF AGNMS IN BOTH UHPW AND E3 MEDIA .....	206
TABLE 8-1: SUMMARY OF THE NMS ADDED TO DIFFERENT MEDIA AND CONCENTRATION RANGE VALIDATED .....	212

## Chapter 1 INTRODUCTION

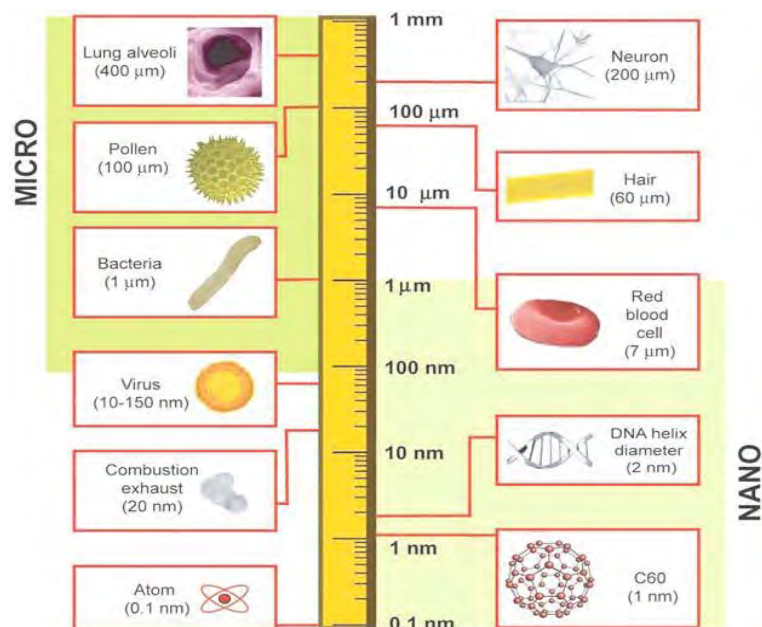
### 1.1 Nanoscience and Nanotechnology

Nano is generally defined as the length of scale between 1-100 nm, matter at the nanoscale often exist in between the mesoscopic and microscopic as shown in the Figure 1-1, called as nanoscopic dimensions and displays novel properties within the nanoscale range (Lead and Valsami-Jones, 2014). Nanoscience involves in understanding of processes and properties at the nanoscale range 1-100 nm (Stone et al., 2010). The current advances in the technology enabled the manipulation, imaging and controlling the matter exist in nanoscale range (Lead and Valsami-Jones, 2014). The products obtained by such manipulations within the nanoscale range are said to be nanomaterials (NMs) (Baalousha Mohammed et al., 2014, Baalousha et al., 2014b, Lead and Valsami-Jones, 2014). The study of these NMs in terms of characterisation, design, production and application of structures, devices and systems by controlling shape and size at nanometre scale is known as nanotechnology (Xu, 2004). Nanotechnology is having huge benefits in many areas such as engineering, medicine, environmental sciences and bioscience and so on.



**Figure 1-1** Nanoscopic particles lie between mesoscopic and microscopic particle (Klabunde and Richards, 2001).

Nanoscience and nanotechnology are concerned with the nanoscale, which is usually defined between 1 to 100 nm (ASTM, 2006) in size. Figure 1-2, below puts the size of the NMs in comparison with the micro sizes (Buzea et al., 2007) which lies between 1-100 nm. At the nanometer scale, materials exhibit new physical properties by manipulating its atoms and molecules (Hasselov et al., 2008, Louie et al., 2014) . Nanomaterial is “a material having one or more external dimensions in the nanoscale or which is nanostructured” and whereas nanoparticle is a “nano-object with all three dimensions in the nanoscale” taken from BSI definition. Nanostructures exhibit their unique properties leading to improved applications (Leppard, 2008). NMs have been used in many scientific disciplines for the manufacture of nano-electronic circuits (Wang and Chou, 1992), cryptology (Benjamin Arazi, 2006), aerospace engineering (Baur and Silverman, 2007), space exploration and automotive, environmental remediation. However, concerns have been raised that the release of NMs into the environment will pose significant risks to human health (Gaiser et al., 2009) and ecosystem functioning (Roco, 2005a, Pedro J. J. Alvarez, 2009).



**Figure 1-2** size of the nanomaterials compared to ‘micro’ and ‘nano’ sizes.(Buzea et al., 2007)

However, the production volume of NMs (Piccino et al, 2012) and the number of nano-enabled consumer products has grown rapidly in the last decade and is expected to increase even faster in the near future. Several concentration measures such as: mass, number, and surface area, which are currently under scrutiny by nano(eco)toxicologists, environmental scientists and metrologists in order to identify the most appropriate dose metrics to express the hazard, fate and behaviour of NMs and therefore to perform risk assessments,(Liang et al., 2011, Donaldson et al., 2013, Donaldson and Poland, 2013, Duffin et al., 2002, Duffin et al., 2007, Sager and Castranova, 2009). However, only mass concentration measurement can be unambiguously performed currently. Similar considerations apply for understanding NM environmental fate and behavior, where number concentration is of particular importance in understanding NM aggregation behavior.

## **1.2 Thesis outline**

This PhD thesis consists of seven chapters whose topics are summarised below:

**Chapter 1** Introduces the concepts of nanomaterials (NMs) and describes both the aims and objectives of the thesis. It also gives outline of the thesis.

**Chapter 2** Introduces nanomaterial (NM) concepts, types and classification, NM source and production, NM transportation and risks in the release of NMs to the environment, analytical techniques limitations to measure the NMs, the review on various analytical techniques based on particle number, aims and objectives of the thesis.

**Chapter 3** Describes the theory of synthesis and characterisation of NMs

**Chapter 4** The first section of this chapter gives a detailed description of the methodology used to synthesise gold NMs and multi method approach to characterise the in-house synthesised NMs for its various physical properties. The second section is based on the detailed explanation of the sample preparation techniques which is vital part of the thesis. Whereas, different types of sample preparation was employed to image the NMs by force

and electron microscopy which eventually lead to the development of the appropriate sample preparation technique that satisfy the critical aim of the research. The third section of this chapter is based on the different media added to the NMs to observe the NMs fate and behaviour. Detailed explanation for the preparation of the different media is given. The last section is paramount importance which is the main objective of the thesis gives the detailed protocol on how to scan the images by microscopies and how to validate the sample preparation technique which is adapted to measure the particle number.

**Chapter 5** is based on the characterisation results, which are divided into two sections. The first section is on in-house synthesis of NMs whereas; the second section is on characterisation results using different analytical techniques.

**Chapter 6** is on results and discussion based on the measurement of particle number using atomic force microscopy. This chapter gives the validation of sample preparation techniques and how the NMs distributed on the AFM substrates and recovery of NMs on its substrates and finally the measurement of particle number.

**Chapter 7** This chapter is based on results and discussion using transmission electron microscopy to validate the sampling technique by adding NMs to both simple and complex media. This chapter is divided three sections. The first section is based on the measurement of particle number concentration by adding simple media to Au NMs. The second section is based on adding synthesised NMs to the three different complex media and measuring the number concentration and later compared for the change in fate and behaviour of NMs. Lastly, the third section uses silver Ag NMs for the measurement of particle number concentration both in pure water and by complex media.

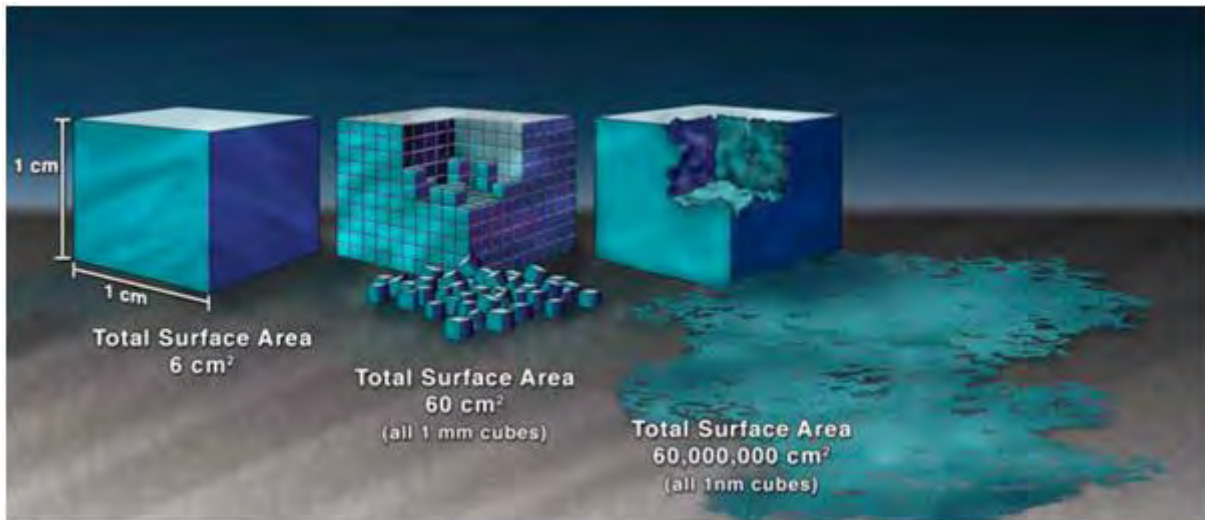
**Chapter 8** is based on the conclusion of the thesis and further work of the technique to control NM arrangement on the substrates.

## Chapter 2 RESEARCH BACKGROUND

### 2.1 Introduction

Nanotechnology is an innovative technology that uses the concepts of nanoscience to develop novel products and applications incorporating nanomaterials (NMs, materials within the size range 1-100 nm, with novel, size dependent properties) (Christian et al., 2008). Nanoscience is the manipulation of NMs at atomic and molecular scales (size range 1-100 nm), that leads to the new NM properties (Lead et al., 1999, Hannah and Thompson, 2008). Nanomaterial properties can differ significantly when compared to those materials having a larger or smaller scale than 1-100 nm (Ju-Nam and Lead, 2008). In nanoscale materials, the percentage of atoms on the surface of a material becomes more significant when compared to bulk materials (Heitbrink et al., 2009), one of the main reasons is spatial confinement of electronic properties. NMs have increased surface-volume ratio compared to bulk material that is, for a given volume of material the external surface is greater that results in domination of the surface properties of the NMs compared to the bulk material properties (Lead and Smith, 2009). An illustration of surface-volume ratio of NMs is shown in the Figure 2-1 in comparison with the non-nanoscale materials. The larger external specific surface area (SSA) of NMs is useful for all those that uses material surface to perform specific applications (Heitbrink et al., 2009), that is chemical reactions takes place at the NM surface, thereby NMs having larger specific surface area is vital when compared to the bulk material(see Figure 2-1). Few examples: (i) at the macroscale gold is not very reactive, while at nanoscale gold NMs are very reactive and (ii)a bulk silver material is inactive compared to Ag NMs; for instance, the silver NMs is toxic, can kill viruses upon contact (Baalousha and Jamie, 2011). Thereby, materials with a size range between 1-100 nm are of particular interest because of their chemical and physical properties. These distinctive physical-chemical properties allow for novel applications within the nanoscale materials,

hence nanotechnology promised to revolutionise the many different fields of science and technology.



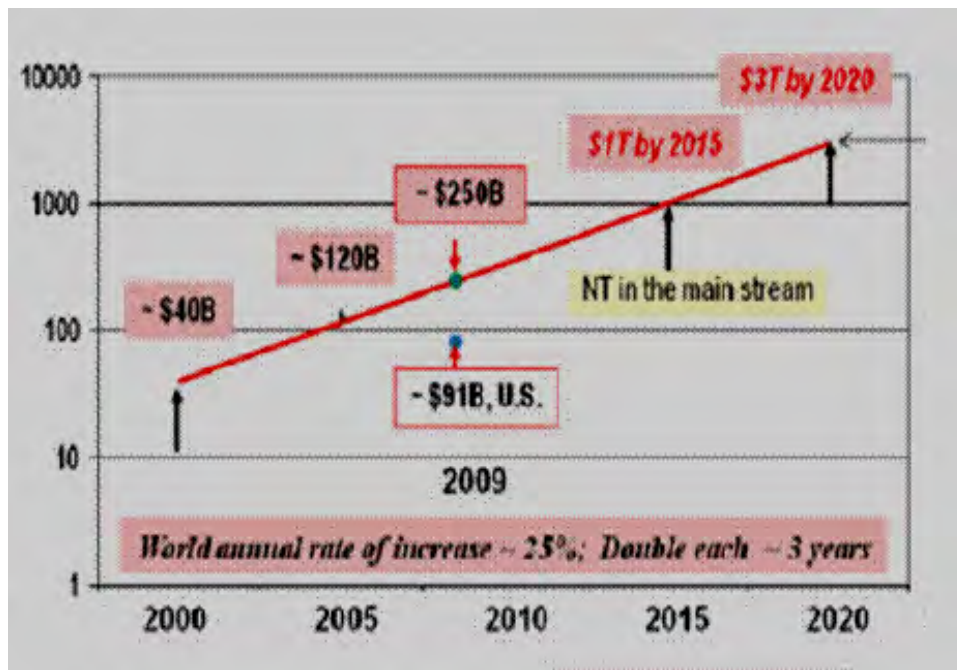
**Figure 2-1.** Illustration of how surface area-to-volume ratio of nanomaterials is increased compared with non-nanoscale-sized materials. (Taken from National Nanotechnology Initiative )

### 2.1.1 Evolve of nanotechnology

The first academic nanotechnology journal was published in the year 1990 (first initiated by Japan's STA funding on nanotechnology projects), which provoked rapid growth in nanotechnology (Roco, 2005b). Later, National Nanotechnology Initiative (NNI) (US government research) and other nanotechnology proponents such as National Initiative on Nanotechnology (NION) in UK, similar nanoscience initiatives in EU and worldwide, initiated to revolutionise the production of nano-enabled tools which are stronger, lighter, low-cost and durable materials and which are used in drug development, water decontamination and communication technologies (Donaldson et al., 2013). Thereafter, the production of nanomaterials (that is the matter in the range of 1-100 nm ) and the number of consumer products has grown rapidly in the last decade and continues to grow.(Piccinno et al., 2012, Wilson, 2012). Figure 2-2 below shows the timeline projection related to the investments and business ongoing in the worldwide market of nanotechnology and its production. USA is the



leading country in terms of its market both investments and technology which is followed by European Union, China, Japan and South Korea. As per the market timeline graph shows the process of production and investment is 25% doubling each three years with respect to the usage increase in nanoscale products (Roco 2011).



**Figure 2-2.** Market timeline projection of the worldwide products that incorporate nanotechnology (Roco 2011).

The following sections were based on the different types of NMs and its classification, sources and production of NMs followed by the release of NMs to the environment and its transportation into the environment. Later section is discussed on the risks involved by the release of NMs and NM exposure level measurement metric which is the highlight of this current project. Thereby, special attention is given to the measurement of nanomaterial number followed by the analytical instruments that can facilitate the accurate characterisation and measurement of the NMs.

## 2.1.2 Natural and manufactured NMs

There are three types of NMs: natural, incidental and manufactured. Natural NMs are distributed everywhere in the oceans, soil systems, atmosphere, air, both underground water and surface water (Nowack and Bucheli, 2007). They are formed mainly because of hydrolysis, erosion, volcanic eruption, minerals, and plant roots on rocks, spray, fine sand, and dust and so on by the results of naturally occurring physical, chemical and biological processes (Wagner et al., 2014, Handy et al., 2008). The other formation of naturally occurring NMs are biogenic NMs formed by microorganisms to fulfil metabolic requirements (Duffin et al., 2007), geogenic and atmospheric such as aerosols (Lead, 2011). Some of the natural NMs include silica, potassium, Mg, Fe which is hydrated aluminosilicates, Iron oxides/hydroxides and aluminium oxides/hydroxides (Gottschalk et al., 2013b). Therefore, the naturally occurring NMs were present in the environment not from recent revolution in nanotechnology, NMs present in the environment the day the earth was born but concern on rapid growth of engineered NMs release into the environment (Nowack and Bucheli, 2007). The different types of NMs and its formation through various roots as explained above such as through biogenic, pyrogenic, geogenic and atmospheric with examples summarised in Table 2-1.

The incidental NMs are man-made NMs that has been emerging rapidly in leading business and industrial research companies which make NM release to environment almost certain. For example through industrial emission which is known to have many health impacts by the release of toxic to environment and while other examples are diesel exhaust, welding fumes, industrial effluents, sandblasting, ambient air, rural areas such as human activities like wood burning; cooking, urban areas and some workplaces such as particles released during manufacture, smaller particles remain airborne for longer period in comparison with the larger particles (Balmes et al., 2015).

The ENMs are manufactured nanoparticles with specific nanoscale dimensions used for specific applications, for example, nano-diamonds which are attached to chemotherapy drugs to treat brain tumors and leukaemia. (Wang et al., 2014), metal oxides NMs such as titanium oxide NMs, zinc oxide NMs and iron oxide NMs are used in skincare products (Gottschalk et al., 2011), zinc oxide NMs are used in photovoltaic cells, as a coating agent to protect wood, plastic and textiles from the exposure to UV rays (Dark, 2006, Meredith et al., 2013), silver NMs are used in fabric to kill bacteria and so on, iron oxide NMs to clean arsenic from water wells and thereby engineered NMs have enormous uses.

In brief, a review of the origin of different types NMs in the environment, they fall into three genera: such as

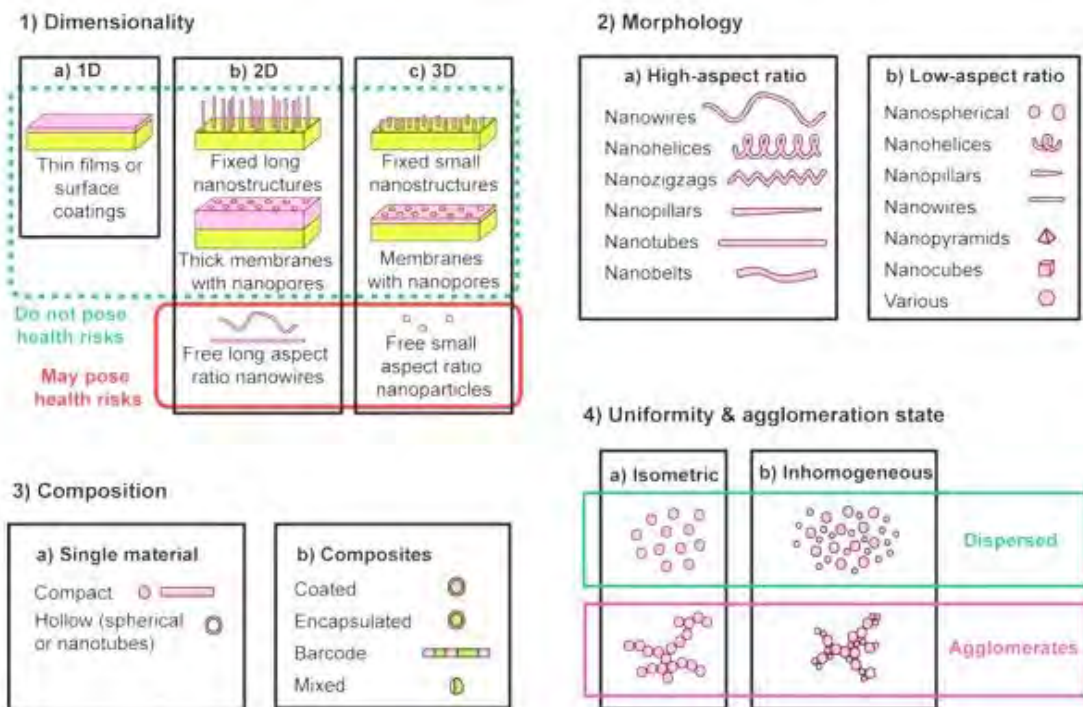
- i. Naturally occurring NMs from plant process, volcanic ash, sea spray, geological constructions, mining and various other human activities,
- ii. Incidental NMs produced by man from cooking, diesel exhaust and
- iii. Engineered NMs are produced synthetically; this is one of the focuses in this research work.

**Table 2-1** Classification of nanomaterials (Nowack and Bucheli, 2007)

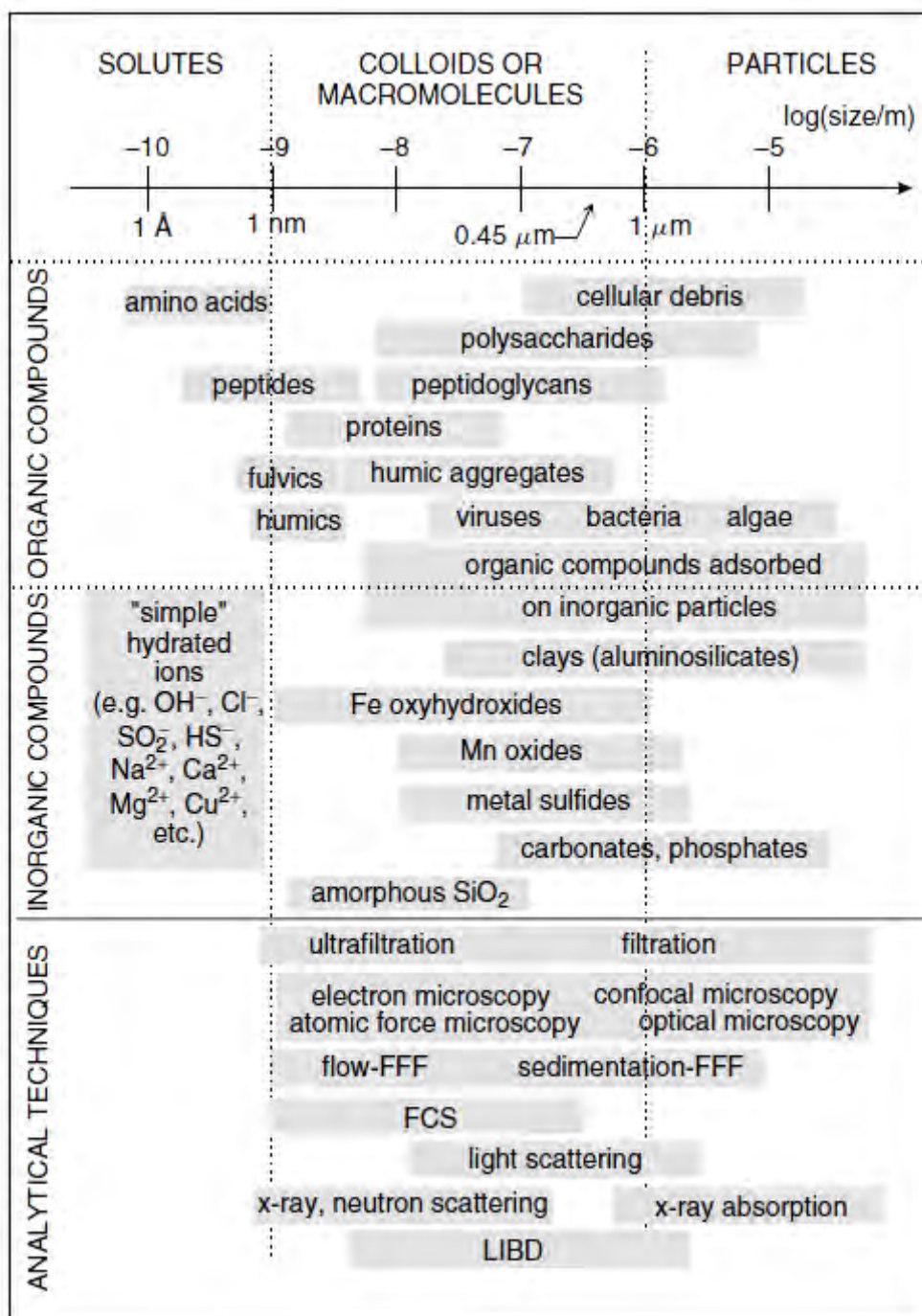
		Formation		Examples
Natural	C-containing	Biogenic	Organic colloids	Humic, fulvic acids
			Organisms	Viruses
		Geogenic	Soot	Fullerenes
		Atmospheric	Aerosols	Organic acids
		Pyrogenic	Soot	CNT
				Fullerenes
	Inorganic	Biogenic	Oxides	Magnetite
			Metals	Ag, Au
		Geogenic	Oxides	Fe-oxides
			Clays	Allophane
Atmospheric	Aerosols	Sea salt		
Anthropogenic (manufactured, engineered)	C-containing	By-product	Combustion by-products	CNT
				Nanoglobules, onion-shaped nanospheres
		Engineered	Soot	Carbon Black
				Fullerenes
	Polymeric NP	Polyethyleneglycol (PEG) NP		
		Functionalized CNT, fullerenes		
	Inorganic	By-product	Combustion by-products	Platinum group metals
				Oxides
		Engineered	Metals	Ag, iron
			Salts	Metal-phosphates
Aluminosilicates	Zeolites, clays,			

### **2.1.3 Classification of nanomaterials (NMs)**

In general NMs are classified based on their composition, dimensionality, morphology, and uniformity (Aitken et al., 2009). Nanoparticle composition consists of composite of several materials or single material composition (See Figure 2-2). Single material composition which can be easily produced/ synthesised, NM synthesis is explained in detail in further Section 2.7. Composition further divided into organic and inorganic (Nowack and Bucheli, 2007) (see Figure 2-3). Based on dimensionality of NMs such as 1D, 2D and 3D, for example in quantum well where electrons are confined in one dimension (1D) at nanoscale but the other two dimensions are not, example., nanocoating, nanofilms etc., and while 2D nanostructures that is quantum wires include nanowires, nanotubes where electrons are confined in two dimensions at nanoscale while the other dimension is not in nanoscale and finally spherical NMs are three dimensional (3D), where electrons are confined in all three dimensions in nanoscale as in quantum dots, clusters, nano-crystallites etc. The third classification is the morphology i.e. based on the shape of NMs for example; flatness, sphericity and aspect ratio. Aspect ratio further classified based on high aspect ratio (examples: nanowires, nanotubes and other various shapes such as zigzag, helices and so on) and low aspect ratio (examples; spherical, oval, prism cube and so on). The fourth classification is NM uniformity and agglomeration, i.e. the dispersion of individual NMs either in aerosols or in suspension without flocculation otherwise presence of NMs in the form of agglomeration that is the formation of flocculation (NMs tends to cluster, explained in detail in further section 2.1.6). The following section is based on the discussion of how these NMs are produced and in this thesis main focus is on the production of engineered NMs.



**Figure 2-2.** Classification of NMs based on nanostructure dimensions, morphology, composition, uniformity and agglomeration state (Duffin et al., 2002).



**Figure 2-3:** Size distribution of various types of environmental colloids and particle and several analytical instruments used to characterise NPs. Techniques abbreviated are: field-flow fractionation (F/FFF). fluorescence correlation spectroscopy (FCS). Laser induced breakdown detections (LIBD). Taken from (Lead and Wilkinson, 2006).

#### 2.1.4 Sources and production of engineered NMs

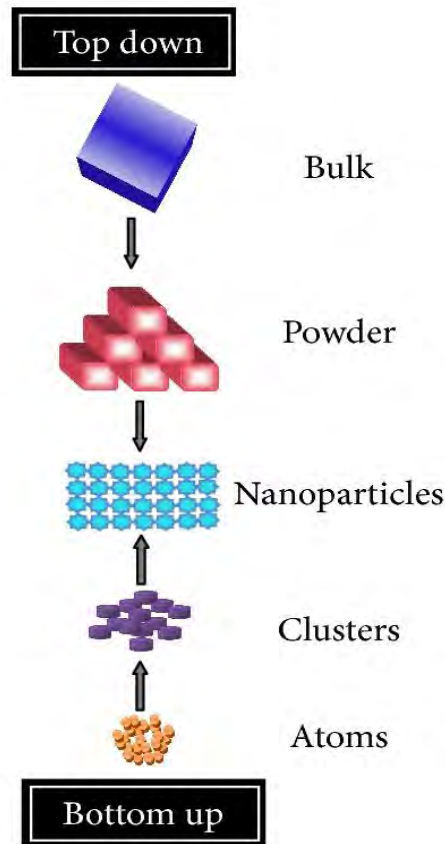
The main focus of this study is production of engineered NMs. There are two approaches to manufacture the engineered NMs, they are top-down and bottom-up (see Figure 2-5). The bottom-up method is a chemical approach refers to the build-up of a material from the bottom: atom by atom, molecule by molecule or cluster by cluster, where the atoms and molecules were assembled or manipulated based on the required applications to generate nanostructure (Madhumitha and Roopan, 2013b). While the top-down is the physical method, breaking down of bulk material into nanoscale materials (Tiruvannamalai-Annamalai et al., 2014), the breaking down is performed by milling, grinding or volatilisation of solid materials which is later followed by condensation and leaving behind the nanostructure (Madhumitha and Roopan, 2013a).

The advantages of the bottom-up approaches are as follows: (i) better chance to obtain nano structures with less defects (ii) homogeneous chemical composition and (iii) better short and long range ordering and few while disadvantages of top-down approaches are: (i) introduces internal stress (ii) surface defects ( i.e. imperfections of the surface structure) and (iii) contaminations. But the top-down approach leads to the bulk production of nano material (Iqbal et al., 2012). Regardless of the defects produced by top down approach, they will continue to play an important role in the synthesis of nano structures. But in turn leads to extra challenges in the device design and fabrication due to its imperfections of the surface structure (Biswas et al., 2012).

The production of NMs in this research is based on the bottom-up approach using chemical synthesis methodology which is given in detail in Section 2.3. The bottom-up approach leads to the creation of the near-identical structures of NMs to obtain the required shape and size by fine tuning/ changing of the reducing agent, temperature, dispersing agent and the reaction time which results in monodispersed NMs. Some of the examples are: semiconductor quantum dots for lasers (Agarwal et al., 2007), hydrothermal synthesis of



metal NMs (Piccinno et al., 2012) and self-organised PVP polymer architectures (Rosa et al., 2010).

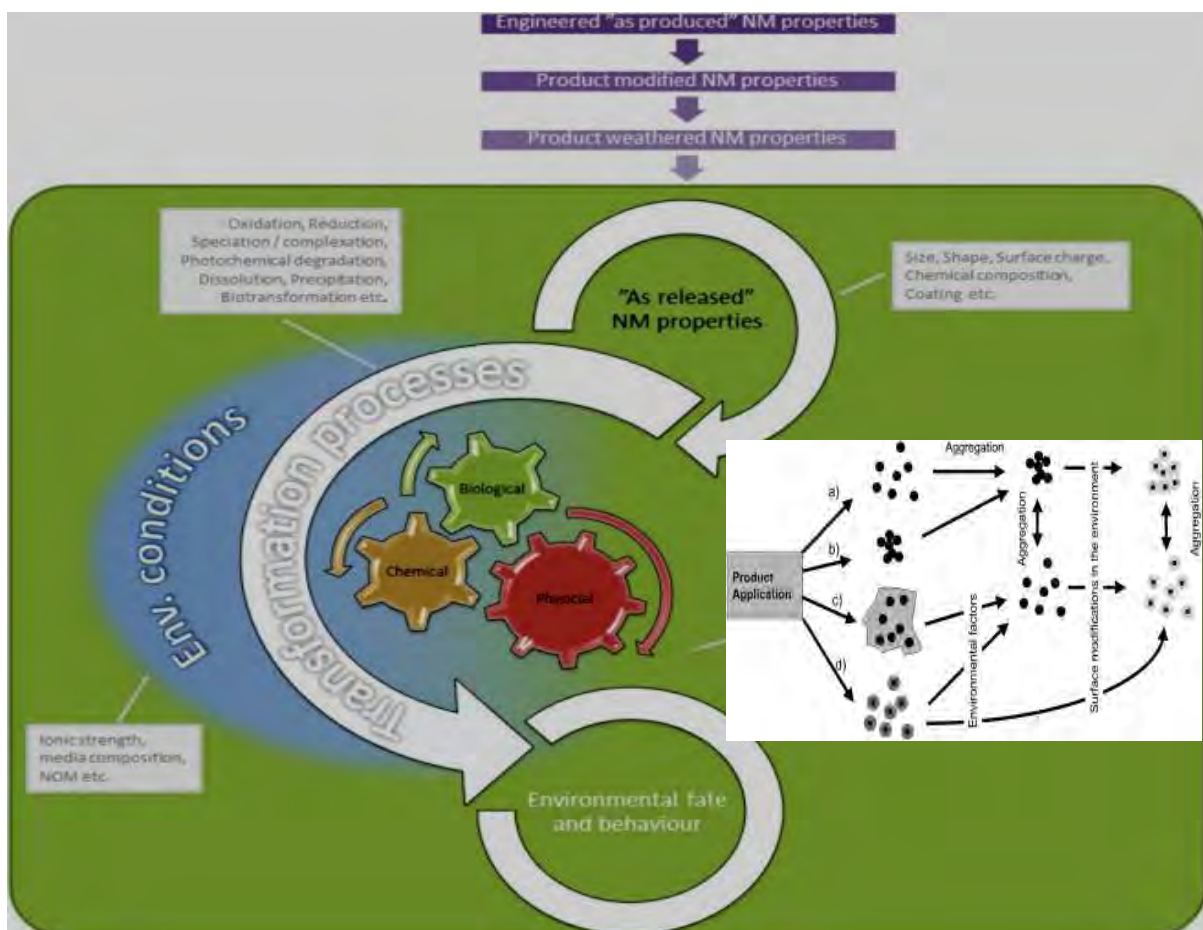


**Figure 2-3.** Production of NMs (Madhumitha and Roopan, 2013b)

At higher end for the more sophisticated applications of nanotechnology such as molecular nanotechnology (Al Globus et al., 2000, Cunha et al., 2015), graphene as a next-generation conducting material to replace traditional electrode materials (Jo et al., 2012), transceiver nanoantennas (Cunha et al., 2015) and made the manufactures more competitiveness to fabricate the nanomaterials having specific physical –chemical properties such as: (i) identical sized particles (all are mono sized and with uniform size distribution (ii) particles having similar shapes (iii) monodispersed that is NMs should be equally spaced by as per the coulombs law and (iv) particle composition (Ju-Nam and Lead 2008). The following section describes the how these engineered NMs released into the environment.

## 2.1.5 Release of NMs to the environment

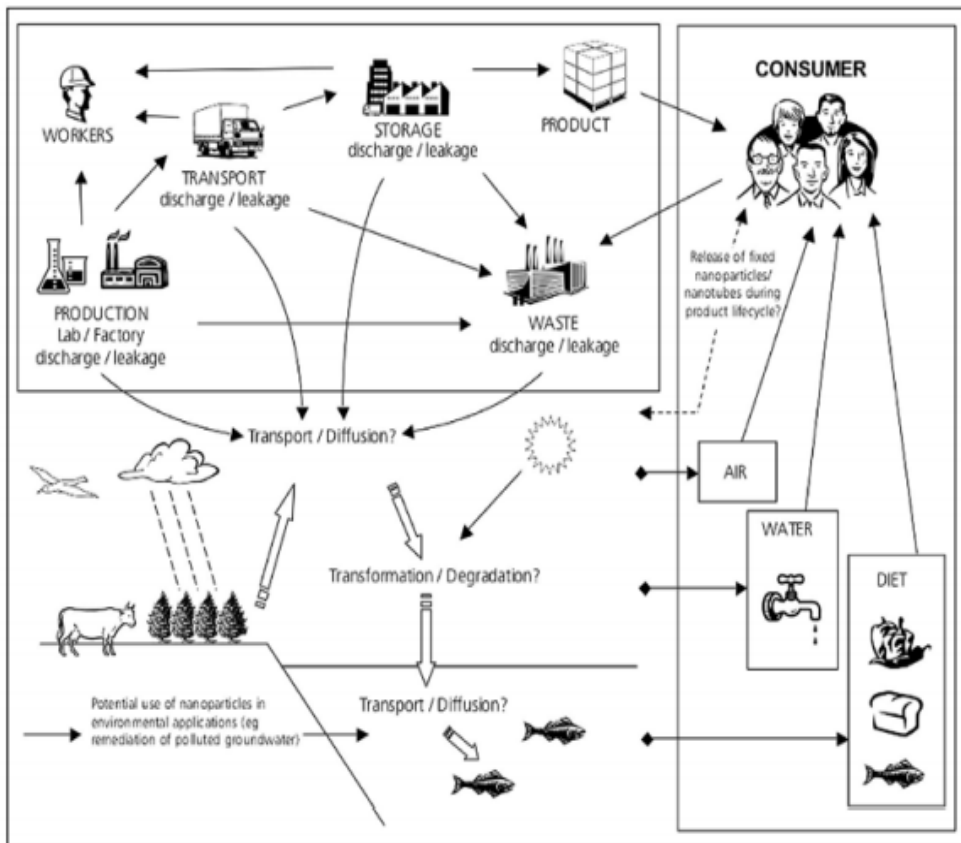
The release of NMs into the environment occurs through the production of NM containing products e.g. release of NMs from commercial textiles during washing and disposal (Hartmann et al., 2014). With the increased presence of NMs in commercial products, it is vital to know what form the NMs were released and the amount of NM released into the environment (Hitchman et al., 2013). The lack of knowledge based on the amount of NMs released into the environment during production is a growing debate due to the unavailability of reliable data (Klaine, 2008, Colvin, 2003). Therefore, it is necessary to have clear guidelines or protocol to quantify these NMs the effects on environmental and human health, which is the main objective of the research.



**Figure 2-4:** Schematic overview of the possible transformation of ENMs in the environment and release of NP from products and (intended or unintended) applications: (a) release of free NP, (b) release of aggregates of NM, (c) release of NM embedded in a matrix and (d)

release of functionalized NM. Environmental factors (e.g. light, microorganisms) result in formation of free NM that can undergo aggregation reactions. Moreover, surface modifications (e.g. coating with natural compounds) can affect the aggregation behaviour of the NM (Nowack and Bucheli, 2007)

Release of NMs to the environment not necessarily as a single NM but also as shown in Figure 2-4 may be release of NMs embedded in a matrix form (Koehler et al 2008), aggregates of NM and release of functionalised NMs, the environmental factors such as light, microorganisms that result in the formation of free NM or that can undergo aggregation reactions (Nowack and Bucheli, 2007). Thereby the released NMs in various forms as well as the nature of the consumer products that contains NMs may have an harmful impact on the environment and humans which is not known (Smita et al., 2012). With the rapid and huge production of the engineered NMs and it's release to the environment concurrently, the released/ exposure NMs having undesirable intrinsic features leads the harmful impacts on the organisms also it is vague about the benefits of NMs that can offset the hazard associated (Colvin, 2003). Thereby it is necessary to have appropriate guidelines to evaluate and quantify these effects and it is crucial to know physical and chemical properties of NMs accurately that confer toxicity. However, after such increased use of NMs and their release into the environment (Health & Safety Laboratory, 2011) giving rise to poorly understood environmental risk. The reason for poor understanding of environmental risk is lack of knowledge regarding amount of NM released into the environment, thereby further research is required to fulfil the gaps (Keune et al., 2012). In order to fulfil the gaps many nanotechnology proponents, commissioned and funded research to review and have a good knowledge on amount of NMs released and identify the gaps in the research to till date with the view to formulate proposals (Report, 2007). Further, discussion is based on the plausible transformation of the released engineered NMs.



**Figure 2-5:** Plausible environmental transport of nanoscale materials based on current and potential future applications (Stone et al., 2010)

The plausible exposures related to engineered NMs transport or diffusion into environment is given in the Figure 2-5 which is taken from royal society and royal academy of engineering (RS/RAEngg 2004) (Stone et al., 2010).

The above Figure 2-5 shows the overview of the possible transformation that occurs after the release of ENMs into the environment. ENM transformations can be classified as physical, chemical and biological in nature. Their definitions of these transformations are summarised in the Table 2-1 (Hartmann et al., 2014).

**Table 2-1:** Definitions of environmental behaviour/distribution process for ENMs in the context of this report based on definitions in (Hartmann et al., 2014, Stone, (2010), Nowack et al., 2012).

<b>Environmental process</b>	<b>Definition</b>
<b>1. Photo/chemical transformation</b>	
1.1.a Photocatalytic degradation	Chemical change induced by light, which includes excitation of photocatalytic ENMs (absorption of a photon causing generation of free radical species) and photolysis of the ENM or components of the ENM (e.g. decomposition of coating material)
1.1.b Oxidation (chemical)	The nanoparticle surface atoms or molecules are oxidized by loss of electrons
1.1.c Reduction (chemical)	The nanoparticle surface atoms or molecules are reduced by uptake of electrons.
1.2.a Speciation/ complexation	ENMs (or released ions / molecules) associating with other molecular or ionic dissolved chemical substances in the environmental matrix. This includes interactions with macromolecules (e.g. chemisorption to the ENM surface, forming a surface coating).
1.2.b Dissolution	Process whereby a solid ENM dissolves (release of individual ions or molecules) in water.
1.2.c Precipitation	The process of dissolved species forming a solid phase (such as metal ions released from an ENM precipitating into a solid material)
<b>2. Physical transformation</b>	
2.1.a Agglomeration	Reversible coagulation of primary particles to form clusters
2.1.b Aggregation (homoaggregation)	Irreversible fusing of primary particles to form larger particles of the same material.
2.2.a Sedimentation	Process whereby ENMs in suspension settle out of the water phase.
<b>3. Interactions with other surfaces and substances</b>	
3.1.a Adsorption/ 'heteroaggregation'	The association of the ENM with other solid surfaces in water. This can be divided into: ENM as sorbent: When other substances adsorb onto the ENM surface. ENMs as sorbate: When ENMs adsorb onto other surfaces.
3.1.b Desorption	Detachment of the ENM from other surfaces into water.
<b>4. Biological transformation</b>	
4.1.a Biologically mediated processes	whereby an ENM undergoes a transformation due to the presence of living organisms. This may include processes such as biological oxidation and degradation, interactions with bio-macromolecules excreted by organisms (e.g. leading to surface coating of the ENM).

Four types of transformations of manufactured nanomaterials which takes place in the environment detailed with subclasses for each transformations and process.

### 2.1.6 Nanoparticle aggregation and DVLO theory

ENMs when released to the environment becomes unmanageable, example when ENMs released into the natural water or humic acid, ENMs might come in contact with organic matter and their size, shape or any other physical properties change. Particle agglomeration, aggregation or sedimentation occurs and individual ENMs exist is unpredictable. Stability is said to be 'resistance to aggregate' of ENMs (Diegoli et al., 2008). The process of aggregation is explained in detail below.

NM aggregation in suspension is mainly due the low energy barrier towards aggregation (Baalousha et al., 2008) which can be explained through DLVO theory quantitatively, which was developed by DeJaguin–Landau–Verwey–Overbeek (DVLO). Theoretically, the process of stability is described by DVLO theory (Merk et al.). The DVLO theory combines van der Waals attraction (Eq. 2.1) and electrostatic repulsion (Eq. 2.2) which results in the total interaction energy ( $V_T = V_A + V_R$ ) (Baalousha et al. 2008);

$$V_A(h) = -\frac{A}{6} \left[ \frac{2R^2}{h^2 + 4Rh} + \frac{2R^2}{(h + 2R)^2} + \ln \left( 1 - \frac{4R^2}{(h + 2R)^2} \right) \right] \quad \text{Eq. 2.1}$$

$$V_R(h) = 32\pi\epsilon R \left( \frac{kT}{ze} \right)^2 \gamma^2 \exp(-kh) \quad \text{Eq. 2.2}$$

Where  $\epsilon$  is the permittivity of the medium; R is the particle radius;  $\psi$  is the surface potential (dimensionless); k is the Boltzmann Constant; T is the absolute temperature; h is the surface separation between particles; e is the electron charge; A is the Hamaker Constant;  $\kappa$  is the inverse-Debye Huckel screening length and can be calculated for electrolyte solutions containing different salts (Baalousha et al. 2008):

$$k = \sqrt{\frac{e^2 \sum n_i z_i^2}{\epsilon k T}} \quad \text{Eq. 2.3}$$

where, n, is the number concentration of ion, i, and z, is the valence of the ions.

Law of physics on electrostatic interactions i.e. the theory of Coulomb's law states by considering two NMs having similar charge and of same type in suspension, the force due to this charge is identical, NMs stay isolated due to the existence of repulsive force between them that leads to a stable suspension. As the distance between the NMs increases the coulombic repulsive force will remain otherwise attractive forces will eventually dominate resulting in the NM aggregation. The surface charge of NM in the suspension is affected either increase or decrease of pH and ionic strength of a suspension, which leads to the process of aggregation, but if the pH is higher aggregation/agglomeration occurs regardless of the salt concentration (Nichols et al., 2002). The process of aggregation and agglomeration of NMs also occurs when exposed to environment has been published in many studies (Baalousha, 2009, Baalousha et al., 2008, Chen et al., 2006). However, highly stabilised NMs can decrease their stability and aggregate/agglomerate when exposed to highly concentrated NOM (Gimbert et al., 2007). Measurement of surface charge of ENMs or zeta potential describes the stability of the colloidal suspension. If NM aggregates are larger particles, these larger NMs settle through gravitational force said to be sedimentation. Gravitational settling of NMs is given by the Stokes' law:

$$F_d = 6\pi\eta r V_d \quad \text{Eq. 2.4}$$

Where,  $F_d$  = is the drag force of the aggregates,  $\eta$  is the fluid viscosity,  $V$  is the velocity of the aggregate relative to the fluid, and  $r$  is the particle radius. Stokes' law states that the larger aggregates settles quicker compared to the dispersed NMs.

The fate and behaviour (example: dissolution, aggregation, disaggregation) of NMs in environmental and toxicology media have been under investigation for many years with misleading assumptions made typically based on NM concentration, for example: NM aggregates in exposure media (behaviour) and their fate is subjected to sedimentation and eventually removal from the water column. Further discussion is based on different metrics used for the quantification of NMs and limitations in analytical tools to quantify the appropriate metrics. Thereby, prior to the assessment of fate and behaviour of NMs there is a need for higher and more consistence standards to characterise NMs and the metrological analysis should be fully reported, without such information our understanding of the human and environmental hazard and risks of nanotechnology is of doubtful and questionable.

### **2.1.7 Limitation for the measurement of NM metrics**

Measurement of NM concentrations are currently under scrutiny by nano(eco)toxicologists related to exposure media and at realistic environmental relevant conditions, in order to identify the most appropriate dose metrics to express the hazard of NMs and therefore to perform risk assessments (Oberdörster et al., 2005; Oberdörster et al., 2007). The first step in implementing such risk assessment is to have the ability to accurately measure NM properties and concentration. Although there is a considerable improvement in the characterisation of NMs when compared to the early efforts uncertainties since knowledge gaps limiting in the measurement of dose metrics which is of concern as the dispersion of tested NMs in exposures will alter both the effective NM dose and the nature of the toxicant (dispersed and aggregated form) (Dale et al., 2015).



There are three main dose metrics utilised in toxicology and environmental studies:

- i. mass concentrations (units  $\text{mg L}^{-1}$ )
- ii. particle number concentrations (particles.  $\text{L}^{-1}$ )
- iii. surface area concentrations ( $\text{m}^2 \text{L}^{-1}$ )

**NM mass concentration measurement** by ICP-MS (or graphite furnace atomic absorption spectroscopy - GF-AAS) is very widely used metric for inorganic NMs because it is relatively accurate and widely available. Some of the advantages and limitations of ICP-MS when compared to other analytical techniques such as atomic absorption spectroscopy (AAS), ICP atomic emission spectroscopy and GFAAS are (i) ICP-MS detection limits is in the range of 1-10 ppt (parts per trillion) for solutions but whereas the limitations, ICP-MS have detection limits to simple solutions having low level of other dissolved materials and degrades because of very poorly dissolved capability i.e. some elements such as S, Ca, Fe, K and Se have serious interferences in ICP-MS (Gschwind et al., 2011). (ii) ICP-MS also gives isotope information (Krystek et al., 2011) (iii) ICP-MS having good sensitivity able to detect at lower concentration as low as below ppb ( $\text{ng/g}$ ) and (iv) ICP-MS have major advantage with high sample throughput i.e. to analyse vast number of samples for trace elements typically less than 5 minutes/sample (Krystek et al., 2011). If six or more elements/sample at sub ppb concentrations ICP-MS is better in comparison with the GFAAS (one to three elements/sample at sub ppb concentration) (Wimuktiwan et al., 2015). Hence the mass concentrations metrics by ICP-MS is widely used to measure accurate NM mass concentration and well established but being questioned as none of the method is as yet fully validated for alternative metrics, especially in complex media. Due its limitation such as incapable to measure the accurate number of NMs irrespective of morphology, density or optical properties, unable to distinguish aggregates/agglomerates from primary nanoparticles

and unable to isolate target NM matrices of naturally occurring NMs, hence particle number and surface area concentrations put forward as an alternative metrics.

**Particle number measurement** is an alternative metrics considered as appropriate (Oberdörster et al., 2007) in nano-ecotoxicology and environmental studies because of the various reasons as stated above i.e. the limitations acknowledged by mass concentration measurement. Currently less attention is paid to the quantification in NM suspensions, which leads to the incompetence and misleading to fully understand the NM behaviour and fate. While there is a requisition to have most relevant and appropriate metric system relating dose measurement to observe environmental and biological fate, behaviour, and health effects. The particle number measurements are widely suggested as an appropriate metric (Seaton et al., 1999, Oberdörster et al., 2007). In atmospheric studies, particle number is easy to measure but in aquatic systems it is not. Hence development of methodology for number concentration is a prerequisite. In aquatic systems, there is a current gap, and whereas in atmospheric numerous papers were published on the measurement of particle number concentration but they were related to the atmospheric nanomaterials (NMs) such as aerosols in road traffic, atmospheric nucleation processes, combustion sources, and sources of semi-volatile materials (Borucu et al., 2010, Gidhagen et al., 2005) by using an instrument called condensation particle counter (CPC) which counts particles one at a time (Aalto et al., 2005) but NONE for aquatic. Scientists have undertaken a significant amount of research into the effects of nanomaterials over the past few years. To date this has often produced conflicting and contradictory results from different studies on the same NM. It is now widely recognized that the major problem with existing studies is the inability to adequately characterize the dose of nanomaterials. More specifically, toxicologically relevant dose metrics to describe nanoparticle dose-response relationships, in particular based on number concentration.

Thereby, there are a number of challenges associated with the measurement the particle number concentration, which will be discussed in detail in further section mainly analytical techniques suffer inherent limitations and also sampling preparation methodology to these analytical techniques is critical to produce accurate results. Hence appropriate sampling techniques must be investigated and validated before carrying on with the analytical techniques to perform particle number measurement. Hence, this project is on to find the methodology/protocol to obtain the appropriate dose metric that can be utilised to both environmental and exposure media characterisation otherwise data obtained is meaningless without suitable, reliable and detailed information on metrics. Thereby this study is emphasised on the development of the new methodology which is challenging to measure the particle number of nanomaterials that also facilitates to count the number of aggregates in NM suspension both in environmental and exposure media.

**Specific surface area (SSA)** is another dose metric system used in NM characterisation that has become increasingly recognised as important because of the huge surface area exhibited by NMs. SSA is used when evaluating dose-response relationships of NM in understanding nano-toxicology studies (Oberdorster et al., 2007). The larger surface area of NM results in increased surface effects thereby affecting the surface properties such as electronic structure, reactivity and so on. SSA must have the ability to measure in complex biological media and when particles are dispersed in a liquid medium (Budnyk et al., 2010, Heitbrink et al., 2009). The analytical instrument used to measure the SSA is Brunauer–Emmett–Teller (BET) technique. Surface area has been defined by ISO (ISO, 2012a) as the *“the quantity of accessible surface of a sample when exposed to either gaseous or liquid adsorbate phase. Surface area is conventionally expressed as a mass specific surface area or as volume specific area where the total quantity of area has been normalised either to the sample’s mass or volume”* and that *“Specific surface area is defined as the surface area of a substance divided by its mass, unit [m<sup>2</sup>/g]; or the surface area of a*

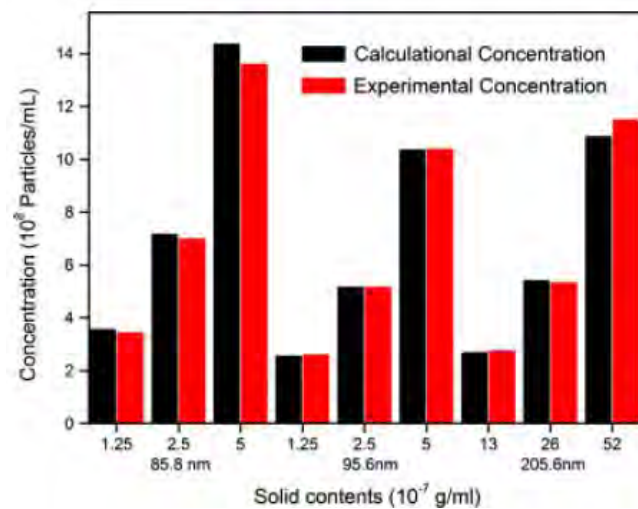
*substance divided by its volume, unit [m<sup>2</sup>/cm<sup>3</sup>].* (Definition taken from (ISO, 2012b)) The research should also consider reporting results in both m<sup>2</sup>/g and m<sup>2</sup>/cm<sup>3</sup>.” (ISO, 2012b).

The following sections are review on some of the published papers related to number concentration metric. The analytical techniques such as NTA, single particle ICP-MS spectroscopy and laser induced breakdown detection (LIBD) are used to measure the NM number. The review of these techniques is as described below.

### **2.1.8 Review on techniques related to particle number concentration**

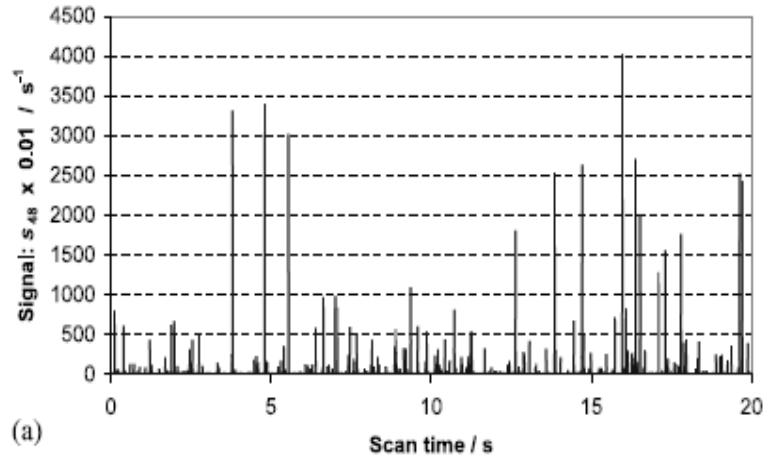
The current research is based on the measurement of particle number in liquid suspensions. The nanoparticle tracking analysis (Boyd et al., 2011, Carr, 2008, Du et al., 2010, Gallego-Urrea et al., 2010) is one such instrument used to measure the particle number where NMs were suspended in liquid. NTA is a new technique that also measures the hydrodynamic size and particle number measurement which was introduced in the year 2004 (Carr, 2008, Du et al., 2010, Haiss et al., 2007a). Whereas, NTA technique as inherent limitations in term of accurate sizing of nanomaterials (NMs), accurate determination of number concentration and the lower particle size limit (Carr, 2012). By using NTA instrument, NMs in suspension can be visualised on an individual basis based on Brownian motion (Malloy and Carr, 2006, Du et al., 2010). While NTA technology comprises of the direct illumination of laser beam on to the surface of the particles in suspension. This can be visualised, sized, counted in real time using the CCD camera, Carr *et al.* (Carr, 2008, Malloy and Carr, 2006) also developed the single particle tracking programme (Halo™ 2.3 NTA), software. The study was carried out by the Du *et al.* (Du et al., 2010) to compare the number concentration of NIST PS nanobeads at different concentration, both by experimentally and mathematically which is shown in the graph (see Figure 2-7). They reported there was a very good agreement between the calculation and experimental method and also stated that accuracy can be increased by controlling the sample concentration. Whereas the size of NMs used in NTA published papers were in the range of

50 to 100 nm. But NTA technique suffer inherent limitations in term of accurate sizing of nanomaterials (NMs), accurate determination of number concentration and the lower particle size limit i.e. 50 to 100 nm (Carr, 2012). NTA provides hydrodynamic diameter measurement for the NMs size similar to DLS instrument (see Section 3.5.1).



**Figure 2-6** Comparison of the measured particle number concentration with mathematical calculation and the experimental concentration of the NIST precision nanobeads (Du et al., 2010).

While single particle ICP-MS spectroscopy is another analytical technique to measure the number concentration. This method was first proposed by McCarthy *et al.* (J. McCarthy, 1993). Each pulse shown in the graph (see Figure 2-7) can be counted as a single particle and the amplification of the each signal is a function of the particle size. (Degueldre and Favarger, 2003a). This transient signal was induced because of the flash of ions in plasma torch, which can be detected and measured by the mass spectrometer detector of SP ICP-MS. This process is a light based technique. Another technique adopted to analyse aerosols is inductive coupled plasma –atomic emission spectroscopy (ICP-AES) (GROW, 1997), which was first proposed by Brochet *et al.* (Brochet U.K, 1998) .



**Figure 2-7** Based on the above signal, particle number concentration can be obtained (Degueldre and Favarger, 2003b).

Figure 2-8 shows the signal obtained by SP-ICP-MS; each pulse is represented as a single particle. Equation below gives the number of NM counted per second which is said to equal to the NM flux that is every NM entering the plasma is counted (Miller, 1924).

$$q_p = \frac{c_p * f_s * \epsilon_n}{60} \quad \text{Eq. 2-5}$$

where:  $c_p$ =nanoparticle concentration in sample ( $\text{mL}^{-1}$ ) ,  $f_s$  is sample flow rate  $\text{mL}/\text{min}$ ),  $p$ = average analyte mass in nanoparticle (g) and  $\epsilon_n$  is nebulisation efficiency.

The process of investigation to calculate the number of NM is still undergoing by integrating DLS with SP-ICP-MS and FFF coupled with SP-ICP-MS. This instrument suffers sensitivity issues when environmental samples are fed to the instrument (Degueldre and Favarger, 2003b). For the measurement of particle number concentration there is a huge limitation in analytical instruments to provide precise measurement. The following section is based on the analytical instruments that can facilitate to measure the NM number concentration.

### 2.1.9 Analytical Instrumentation

The invention of force microscopy by IBM scientists in 1986 (Binnig et al., 1986), is one of the foremost instrumentation to image the NMs. To date the instrumentation such as microscopies and spectroscopies improvised and also facilitate to couple with the various instruments example TECNAI TEM can be coupled with elemental analysis instrument (X-EDS). There are many limitations when considering to image or view the NMs of size range 1-100 nm, such limitations are discussed below.

Analytical techniques such as nanoparticle tracking analysis, ICP-MS and microscopy (Baalousha and Lead, 2012; Boyd et al., 2011; Mitrano et al., 2012) techniques suffer inherent limitations either in term of accurate sizing of NMs, accurate determination of number concentration, the lower size limit or the availability of a standard validated procedure for sample preparation and analysis.(Baalousha and Lead, 2012; Linsinger et al., 2012) Other analytical methods deliver other NM size distributions (*e.g.* intensity for dynamic light scattering (DLS) and mass/volume for field flow fractionation (FFF) that need to be mathematically converted to the required number-based size distribution. This conversion is usually based on a number of assumptions (*e.g.* the NMs are spherical, non-permeable and non-aggregated) and is thus prone to errors, difficult or even impossible if the mass fraction of NMs is not sufficiently large.(Baalousha and Lead, 2007; Baalousha and Lead, 2012; Baalousha et al.

In brief, the analytical techniques such as LIBD-laser induced breakdown detection, FCS, and NTA can measure number particle concentration in suspension and in dynamic mode; however, these techniques do not have the ability to distinguish a target NM in a complex media or in a mixture of NMs of different compositions. NTA and SP-ICP-MS suffer inherent limitations of the lower size limit (*e.g.* typically >10 nm). Therefore, LIBD, FCS and NTA were also ruled out for further investigation.

An ideal technique for the determination of particle number concentration should be able to

- i. Determine an accurate number of NMs irrespective of morphology, density or optical properties of NMs,
- ii. Distinguish aggregates/agglomerates from primary nanoparticles,
- iii. Isolate a target nanoparticle in a complex matrix containing nanoparticles of different composition (e.g. manufactured nanoparticles in a matrices of naturally occurring nanoparticles),
- iv. Measure number concentration at environmentally relevant concentrations ( $\text{ng-}\mu\text{g L}^{-1}$ ) and
- v. Cover the entire nanosize range (e.g. 1-100 nm),
- vi. Provide an accurate measurement of NM dispersion.

However, there is a need for validated analytical tools/methods capable of providing fully quantitative assessment of NM exposure and dose based on the different dose metrics at environmentally/toxicologically relevant concentrations. Thereby this research was a challenge to develop and validate accurately the analytical tool that facilitates the above mentioned points.



## 2.2 Research aims and objectives

This project aims to develop a fully validated method for the quantification of number concentration of engineered NMs in aqueous exposure and environmental systems. To achieve this goal the following sub-objectives are identified:

Aim 1: To synthesize and characterize a range of Ag and Au NMs

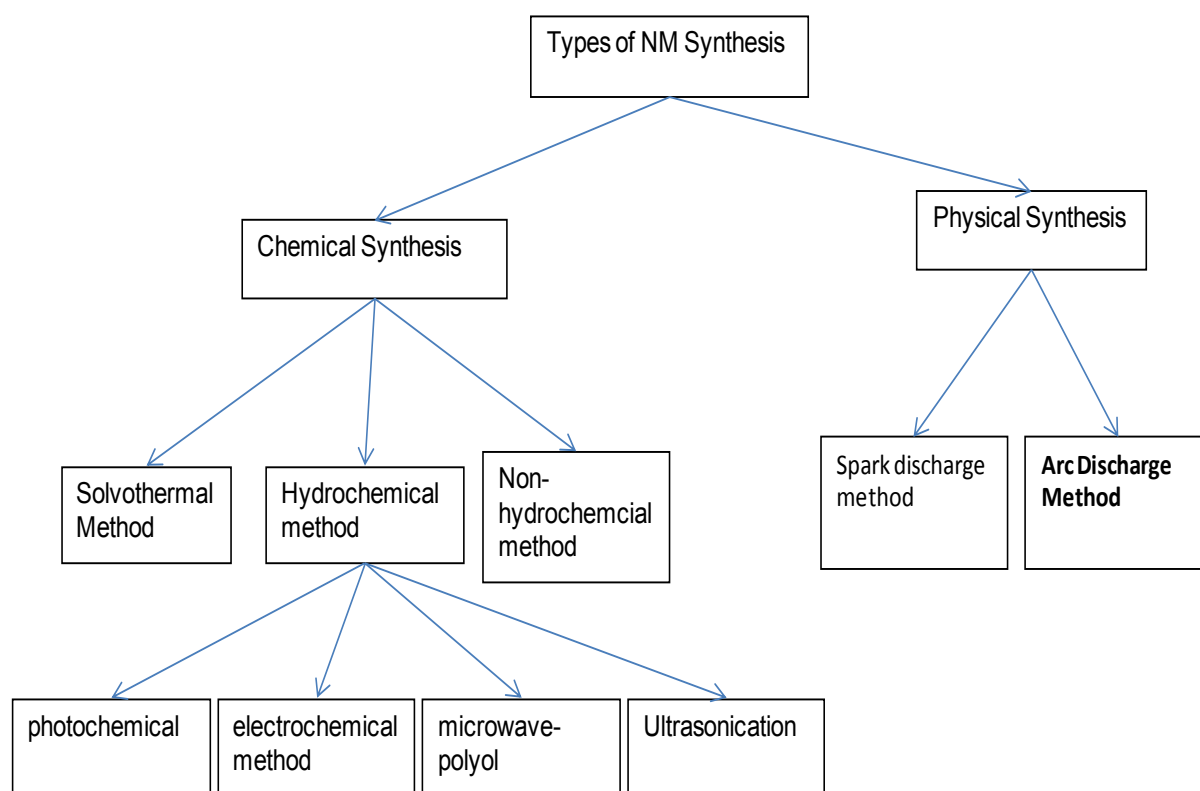
Aim 2: To develop and validate a sample preparation method to enable the quantification of particle number concentration by force and electron microscopy

Aim 3: Demonstrate the applicability of this validated sample preparation method to detect and quantify the number concentration of NMs in complex media at realistic concentrations

## Chapter 3 THEORY OF SYNTHESIS AND CHARACTERISATION OF NMS

### 3.1 Theory for the synthesis of nanoparticles

In this section different types of synthesis are critically reviewed. There are various methods for the synthesis of metal nanoparticles, in general the process of NM synthesis are categorised into (i) chemical methods and (ii) physical methods. which are given in the form of flow chart (see Figure 3-1). Some of these synthesis methods were further discussed.



**Figure 3-1.** Types of NM synthesis

### **3.1.1 Chemical Synthesis Methods**

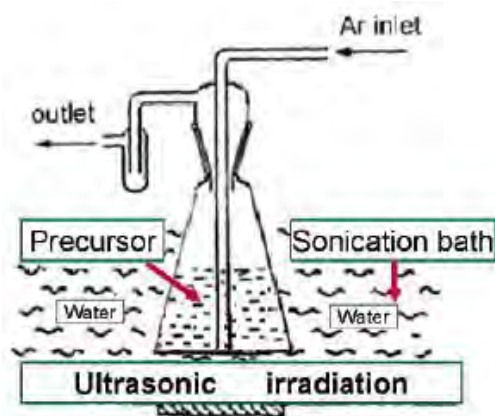
Chemical synthesis is a process of reduction reaction, for example, reducing the precursor such as Chloroauric acid ( $\text{HAuCl}_4$ ) and silver nitrate ( $\text{AgNO}_3$ ) in the presence of reductants. The structure of these NMs can be more easily controlled than physical methods and can be performed by optimizing experimental parameters like temperature, surfactants and solvent compositions. Chemical synthesis may be categorised as follows (i) Solvothermal Method (ii) Hydrothermal method and (iii) Non- hydrochemical method.

#### **3.1.1.1 Hydrochemical Method**

In this hydrochemical method, the chemical reaction takes place in aqueous solution rather than organic or polyol solutions (Franklin Kim, 2002). The hydrochemical method has many advantages in synthesis of metal and other NMs, such as (i) uniform size of NMs (ii) understanding of the growth mechanism and (iii) providing a relatively slow growth rate, which is favourable to control kinetically (Cao et al., 2009, Cao).

#### **3.1.1.2 Ultrasonification method**

A schematic illustration of this method is shown in the Figure 3-2. The procedure adapted by Li *et al.* and synthesised nanoprisms, by added PVP and ethylene glycol solution in a conical flask, stirred by a magnetic stirrer followed by adding gold stock solution to the flask (Li et al., 2006). Subsequently the flask was mounted on a sonification flask and ultrasonically irradiated for a certain time as given in detail by Li *et al.* (Li et al., 2006) . During irradiation, argon gas was utilised to remove the oxygen in the flask.



**Figure 3-2.** Schematic illustration of an ultrasonically irradiated process (Amendola et al., 2008)

### 3.1.1.3 Non-hydrochemical Method

Non-hydrochemical methods are categorised as follows, the: (i) Polyol Reduction Method (Cristina E. Hoppe) and (ii) Template Method (Liu et al., 2009). The Template method is classified further as soft template and hard template. In case of the Polyol reduction method, NPs are synthesised by using polyols such as ethylene glycol, PVP and so on, known as polyol process (Wei et al., 2011).

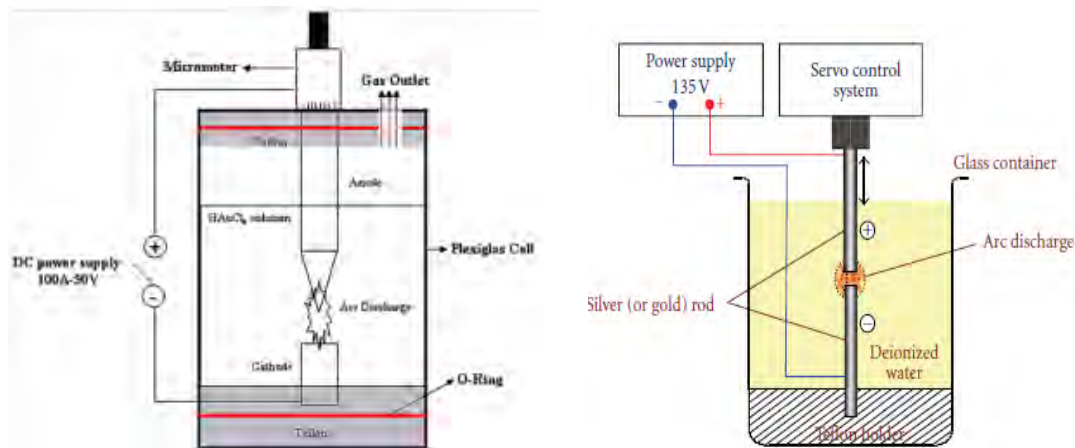
### 3.1.2 Physical Synthesis Methods

Further methods of synthesising nanomaterials are the: (i) arc discharge method (ADM) (ii) chemical vapour deposition (iii) electrodeposition (iv) sol-gel synthesis (Schramm et al., 2012) (v) high energy milling/ball milling (Chen and Liu, 2012) (vi) nanolithography and use of natural nanoparticles. Method (i) and (ii) are similar, separates molecules and atoms are by vaporisation and then allows them to deposit in a controlled manner to form nanoparticles (Ashkarran et al., 2009, Lee and Park, 2007, Tseng et al., 2009, Tien et al., 2010). The schematic set-up of the arc discharge method is shown in the Figure 3-3. (iii) is similar to the first two methods but occurs in solution. In ball milling, nanocrystalline

structures are derived from macro-crystalline structures but the original integrity of the material is retained (Farbod and Khademalrasool, 2011).

### 3.1.2.1 Arc Discharge Method

The arc discharge method consists of mainly two parts – a high current DC power supply and a reactor, which includes two electrodes either Ag or Au (anode, cathode) and a micrometer or servo control system to move the anode towards the cathode, to maintain gap distance between two electrodes. Arc discharge happens between two electrodes when a high voltage is applied. In the case of electrodeposition (Ashkarran et al., 2009) reactors will be immersed in gold solution, when the arc discharge happens between the electrodes the  $\text{HAuCl}_4$  reduces by means of electrons from the plasma zone (Ashkarran et al., 2009).

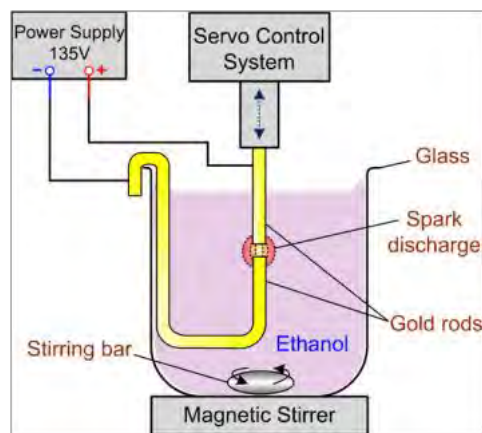


**Figure 3-3.** DC arc discharge system (Lee and Park, 2007, Lung et al., 2007, Ashkarran et al., 2009, Tien et al., 2010)

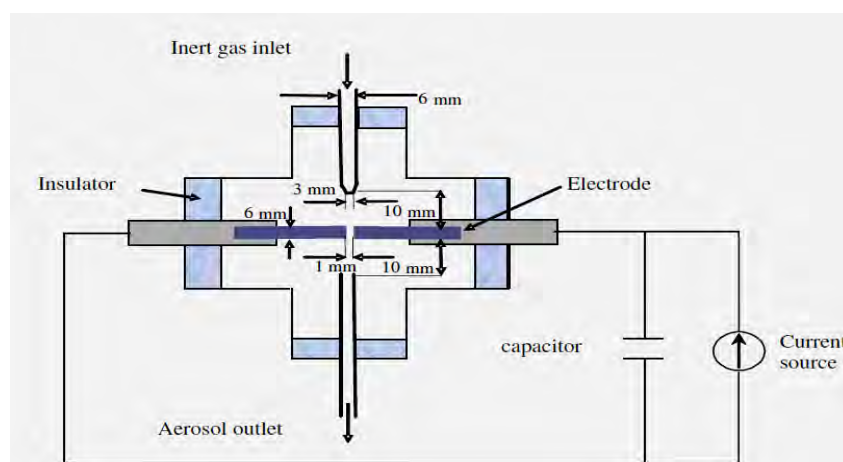
### 3.1.2.2 Spark discharge method

The schematic shown in Figure 3-4 and Figure 3-5 is similar to the arc method, instead of arc between the electrodes, a spark is initiated by gas breakdown. This is one of

the most versatile techniques for the generation of the nanoparticles in the gas phase. Here the electrode material is evaporated in the vicinity of the spark (Ashkarran et al., 2009) and also the vapour cloud is less compared to the evaporation-condensation process. Also, cooling period below the boiling point is quick enough to obtain very high concentration of very small particle forms.



**Figure 3-4.** Schematic of arc discharge method (Tseng et al., 2009)



**Figure 3-5.** Schematic illustration of spark discharge method (Tabrizi et al., 2008, Tabrizi et al., 2009)

### 3.2 Conclusion for Synthesis Procedure

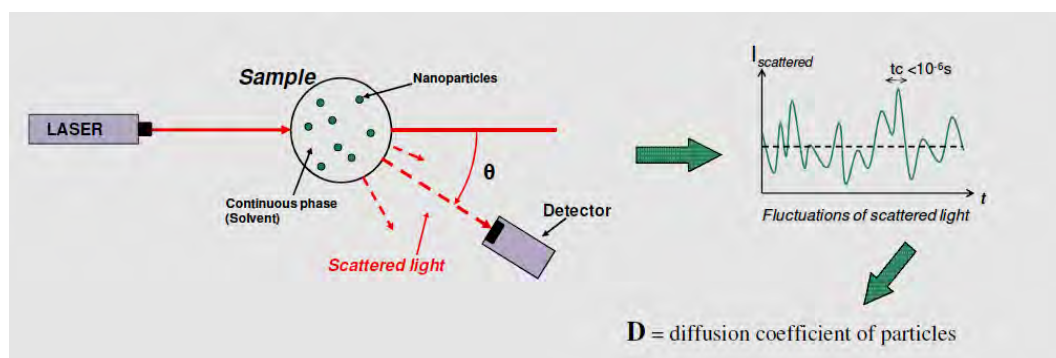
In section 3, both chemical and physical synthesis methods are explained concisely. But for the current research, to measure the particle number concentration, initial work was carried out by synthesising the gold nanoparticles using the wet-chemical approach (Cristina E. Hoppe, Xu et al., 2007, Zhou et al., 2009). This type of synthesis was selected because the gold nanoparticles are extremely stable non-toxic, biocompatible and less polydispersed Au NPs can be easily synthesised in-house. A one-step procedure (Chen and Liu, 2012) was adopted for growth of spherical gold nanoparticles and using poly (N-vinyl-2-pyrrolidone) PVP as a capping agent. PVP is a commonly used protective agent in metal nanoparticles synthesis and easily soluble in water and protects against agglomeration of colloids. This process is known as polyol process (Xu et al., 2007, Sun and Xia, 2002). Here the gold nanoparticles can be easily synthesised approximately by 10 minutes by adding sodium hydroxide as an initiator for the reduction of  $\text{HAuCl}_4$  in the presence of PVP as a capping agent. Using this process, extremely stable and monodispersed NMs can be obtained (Zhou et al., 2009). This is considered to be a green chemistry concept because it doesn't consume energy and reaction time is much less. Investigators of this approach concluded that synthesis is much faster, green chemistry concepts evolved by the not consuming energy and eradication of toxic surfactants (Cristina E. Hoppe, Zhou et al., 2009).

### 3.3 Theory of characterisation Techniques

Some of the different analytical techniques employed in this research for the characterisation of NMs are explained in detail below.

### 3.4 Dynamic Light scattering (DLS)

Dynamic light scattering is also known as photon correlation spectroscopy (PCS), which is a very popular technique to measure the size of the nanoparticles (Hoo et al., 2008). A laser light beam, is directed into a solution containing nanoparticles in liquid media (Pecora, 2000). The light is scattered and then detected at certain angles (Pecora, 2000). The size measurement is based on scattered light fluctuations over time caused by the Brownian motion of nanoparticles (Schmidt and Skinner, 2004). The principle of operation of dynamic light scattering is given shown in the Figure 2-18.



**Figure 3-6.** Principle of operation of dynamic light scattering instrument

The principle of this instrument is shown in the Figure 3-6. A laser passes through the cell via attenuator, the light is scattered and detected by a photomultiplier (detector), which transforms the variation of scattered light intensity to the correlator. The graph shows the intensity of light scattered as a function of time at a given angle (see Figure 3-6) (Miller, 1924). Thereby, the correlation calculations are derived from the fluctuations of scattered



light, which allows the diffusion coefficient  $D$ , of the Brownian particle to be determined. The rate of decay of the correlation function provides the line width of the scattering light (Schmidt and Skinner, 2004, Miller, 1924, Sartor), which is given below in equation 2-1

$$\Gamma = q^2 D_t \quad \text{Eq. 3-1}$$

where  $\Gamma$  is the decay rate.  $D_t$  the translational diffusion coefficient and at the range of angles depending on the wave vector  $q$ . (Schmidt and Skinner, 2004)

$$q = \frac{4\pi n_0}{\lambda} \sin\left(\frac{\theta}{2}\right) \quad \text{Eq. 3-2}$$

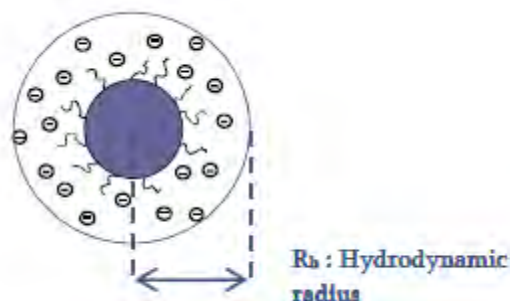
where  $\lambda$  is the incident laser wavelength,  $n_0$  is the refractive index of the sample and  $\theta$  is angle between the detector and the sample cell.

$$D = \frac{K_b T}{6\pi\eta R_h} \quad \text{Eq. 3-3}$$

where  $D$  is the diffusion coefficient of particles,  $K_b$  is the Boltzmann constant,  $T$  is the temperature,  $\eta$  is the dynamic viscosity of the continuous phase and  $R_h$  is the hydrodynamic radius. From this equation the hydrodynamic radius of an object can be determined.

The hydrodynamic size is measured by DLS which gives radius of its dense core and the thickness of any layer of adsorbed molecules on its surface (like polymers, water, surfactants and so on) (Sartor). This hydrodynamic size measurement may give additional

information such as core size and the capping size of NMs when compared to the radius measurement using other techniques like transmission electron microscopy (TEM).

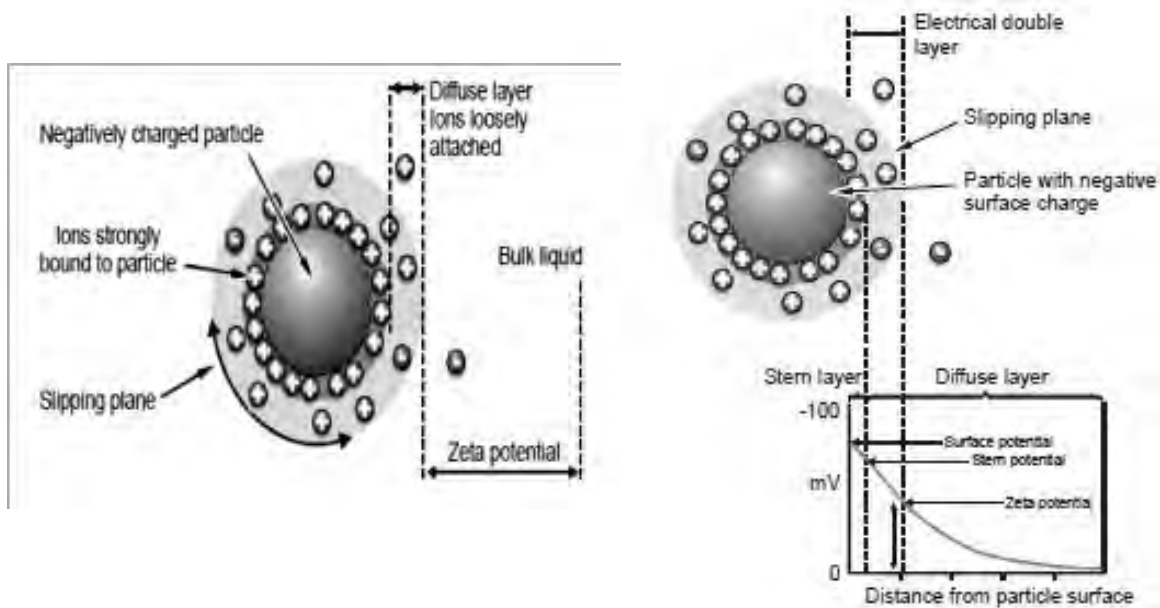


**Figure 3-7.** Hydrodynamic radius of a particle coated with ionic polymer (Pecora, 2000, Sartor).

Although DLS is suitable for size measurements at the nanoscale, in dilute and transparent media, it has a number of limitations while for samples exposed to environment becomes ineffective if the media is opaque (Pecora, 2000). No light transmitted through the complex /opaque media. The natural organic materials NOM or any low heat capacity solvents are very sensitive to the thermal effects induced by the absorption of the laser beam .

### 3.4.1 Electrophoretic Mobility (EPM) and Zeta Potential

Electrophoretic mobility (EPM) is the mobility of the dispersed particles under the influence of an electric field. EPM is measured as the velocity per unit voltage gradient of a particle in a liquid ( $10^{-8} \text{ m}^2 \text{ V}^{-1} \text{ S}^{-1}$ ). Its value is dependent on the charge at the boundary between the atoms moving with the particles and those remaining in the bulk solution. (Jiang et al., 2009, Jérôme F. L. Duval, 2007).

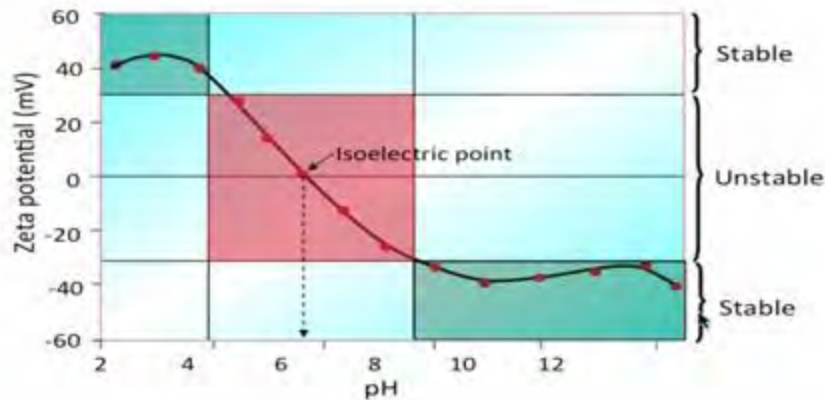


**Figure 3-8** Schematic representation of zeta potential (Jérôme F. L. Duval, 2007).

Zeta potential (V), is a potential that exists between the particle surface and dispersing liquid that determines the particle interaction forces or degree of repulsive or attractive between particles, stability of the NMs depends upon the balance of the repulsive and attractive forces, which exists between the particles as they approach each other. In other words, instability of the particles is mainly due to little or no repulsive force between them, which results in aggregation or flocculation (Carr et al., 2008). Samples are said to stable if they have a large negative or positive zeta potential (Griffiths et al., 2011) that range between  $> +30$  mV or  $> -30$  mV.

As shown in the Figure 3-8, the liquid layer surrounding the particle consists of two parts; Stern region (ions are strongly bounded) and outer diffuse layer (ions are less firmly associated). In the diffuse layer the ions within the boundary move due to gravity, those ions beyond the boundary stay with the bulk dispersant.

### Effect of pH on Zeta Potential



**Figure 3-9.** Effect of pH on zeta potential (Kirby and Hasselbrink, 2004)

The potential that exists at this boundary is the zeta potential. Particles with zeta potentials  $> +30$  mV or  $> -30$  mV are normally considered stable. Zeta ( $\xi$ ) potential can be calculated from EPM based on (Jérôme F. L. Duval, 2007) equation 3-4.

$$v = \frac{\varepsilon E}{\eta} \xi \quad (\text{Eq.3-4})$$

where  $\xi$  is the zeta potential,  $v$  is the measured electrophoretic velocity,  $\eta$  is the viscosity,  $\varepsilon$  is the electrical permittivity of the electrolytic solution and  $E$  is the electric field.

#### 3.4.2 Ultra violet – visible spectroscopy

SPR is a theory to interpret how nanosize metal surfaces interact with incident light. It is measured by Vis spectroscopy. It emerged as a powerful optical detection technique, for the interaction of photons with the surface of NPs which provides the observed light. SPR is defined (Link et al., 2000) as coherent motion of the conduction-band electrons caused by

interaction with an electromagnetic force (EMF) (Mohd Sultan and Johan). For spherical particles, which are those less than 20 nm, this is explained by Mie theory. Link *et al.* provided the theory for larger NPs and other shapes like rod GNPs. As the particle aggregates the absorbance band also increases as well as shifts left to right with larger sizes (Van Hyning and Zukoski, 1998). In this technique, the aggregated particle will display further increases in absorbance and higher wavelength (Mock *et al.*, 2002, Miller and Lazarides, 2005). SPR of gold NPs of particle size 2-50 nm shows an absorption maximum at 520 nm, while silver NPs have a maximum absorption of 400 nm. In spectroscopy, absorbance (A) is defined as:(Mohd Sultan and Johan)

$$A_{\lambda} = \log_{10} (I_0/I) \quad (\text{Eq.3-5})$$

where  $I$  is the intensity of light at a specified wavelength  $\lambda$ , which are passed through the samples i.e. transmitted light intensity and  $I_0$  is the intensity of light before it enters the sample i.e. incident light intensity (Mohd Sultan and Johan). Its unit is given as AU. In UV/VIS spectroscopy absorbance is expressed as ratio of  $(I/I_0)$ , called transmittance (%T) and expressed as a percentage. Therefore, the absorbance  $A$ , based on the transmittance is given as;

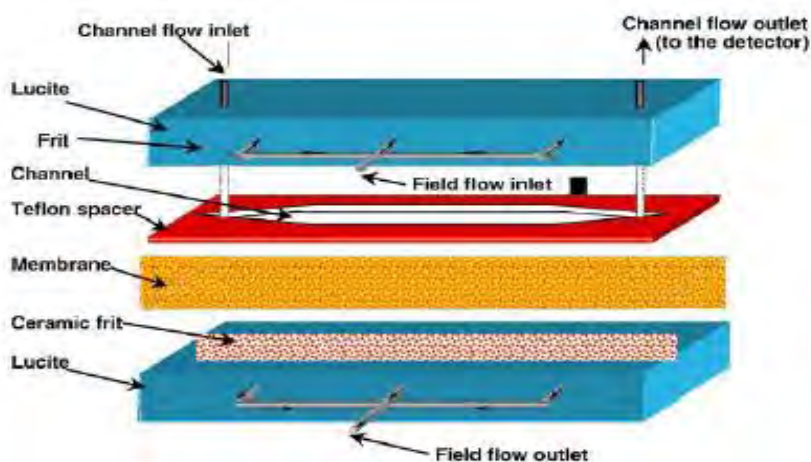
$$A = - \log (\%T) \quad (\text{Eq.3-6})$$

### 3.4.3 Flow field-flow fractionation (F/FFF)

Flow field-flow fractionation is widely used for separation and characterisation for particles and polymers > 1 nm is size (Giddings, 1993). This technique is used in a wide range of research areas and the theory of FFF was proposed by Giddings in 1960s (MYERS, 1976). After the proposal of this technique, different sub-techniques (Giddings, 1993) are categorised such as, flow (F/FFF), sedimentation (SdFFF), thermal (ThFFF),

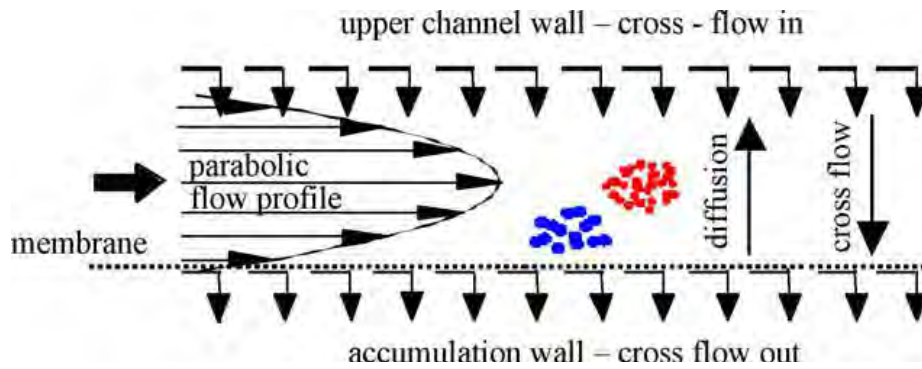
electrical (EIFFF) and gravitational (GrFFF). In this project, the F/FFF technique is utilised. It is again categorised into two types, symmetrical FFF (FIFFF) and asymmetrical FFF (AsFIFFF), whereas, in this study symmetrical FFF is used.

A schematic representation of the F/FFF is shown in the Figure 3-10. It is a symmetrical system which is developed in 1970 (Fraunhofer and Winter, 2004). Separation process in this system occurs in the ribbon-like channel with an applied field (see Figure 3-10). This channel contains the Perspex blocks surrounded by ceramic frits. In order to prevent small particles passing through an ultrafiltration membrane is placed between the frit and channel (Baalousha et al., 2005b). The membrane acts as an accumulation wall that prevents loss of samples through ceramic frits.



**Figure 3-10** Schematic diagram of F/FFF channel (Assemi et al., 2004).

Separation of particles takes place in the channel by a carrier solution, usually a low ionic strength salt solution or surfactant in pure water (Assemi et al., 2004). The selection of carrier solution is of paramount importance in order to minimise sample interactions and maximise separation. Several of them are reported by (Dycus et al., 1995).



**Figure 3-11** Schematic illustration F/FFF separation mechanism.(Giddings, 1993, Assemi et al., 2004, Fraunhofer and Winter, 2004).

When the particles are injected through sample loop at the top of the channel, particles are carried along the parabolic flow profile as shown in the figure above, where the smallest particles move fastest. Immediately after injecting the sample, the sample moves towards the accumulation wall, i.e. when the stop-flow procedure starts where channel remains on but channel flow off (Thang et al., 2001). During the flow, the specific thickness NMs or species spread into different zones depending upon the hydrodynamic diameter and the applied flow field (Koliadima and Karaiskakis, 1990). The smallest particles were carried prior to the larger ones, along the parabolic flow and fractionation starts (Thang et al., 2001). After separation, the sample can be detected by various methods, usually in-line from the channel end. Methods the F/FFF may be coupled with are: (i) UV (most common method of detection). (ii) fluorescence (Hasselov, 2005) (iii) ICP-MS (Stolpe et al., 2005, Lyven et al., 2003, Baalousha et al., 2006), (iv) multi angled laser light scattering MALLS (Baalousha et al., 2005b, Baalousha et al., 2005a) (v) transmission electron microscopy (TEM) (Gimbert et al., 2006, Gimbert et al., 2007, Baalousha et al., 2006) and (vi) AFM (Baalousha and Lead, 2007).

### 3.4.4 Atomic force microscopy (AFM)

Atomic force microscopy evolved from scanning probe microscopy (SPM). SPM is used to visualise and manipulate the atoms and molecules. Three dimensional images can be obtained, which also provides nanometer scale resolution. AFM works by placing a probe on the end of the cantilever. The force between the probe and the end of the cantilever is measured by the simple theory of spring constant (see Figure 3-12). The probe (tip) is at the end of the cantilever (A), the amount of force between the probe and sample depends upon the spring constant or stiffness. This is said to be Hooke's Law (Meyer, 1992):

$$F = - k \cdot x \quad (\text{Eq.3-7})$$

where  $F$  is force in N,  $x$  is the cantilever deflection in metre and  $k$  is spring constant N/m. The force between the tip and the sample can be calculated by maintaining the constant tip-sample separation and by using Hooke's law. Where the spring constant  $k$ , which the beam with constant cross section is given by (Meyer, 1992):

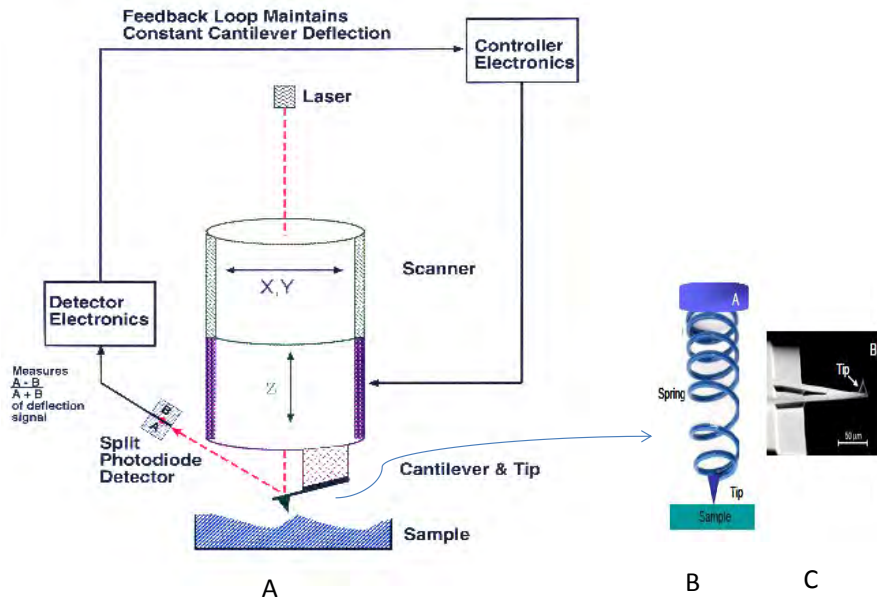
$$k = 3 E I / l^3 \quad (\text{Eq.3-8})$$

where  $E$  is the young's modulus,  $l$  is the length and  $I$  is the moment of inertia. The moment of inertia  $I$ , for the beam of width  $b$  and thickness  $d$  is given by the equation:

$$I = b d^3 / 12 \quad (\text{Eq.3-9})$$

As per the interactions between the tip and sample surface, AFM can be classified as (i) contact mode (repulsive) and (ii) non-contact mode (attractive). The force between the tip and the sample surface is very small, i.e.  $< 10^{-09}$  N. The working principle of AFM in contact mode is shown in the Figure 2-19.





**Figure 3-12** (A) Schematic diagram showing the operating principles of the AFM in the contact mode (picture from digital instruments, CA) (B) Schematic illustration of the cantilever and the distance between the probe and the sample surface, (C) SEM image of the SPM cantilever with the probe. (Picture taken from MikroMasch).(Meyer, 1992)

AFM technique utilises tip or probe scans across the sample surface. The tip-sample position is adjusted based on the set-point determined by the user. After the set-point is given, the tip comes in contact with the sample surface by adsorbed gas layer (Meyer, 1992). Then, scanning of the sample takes place under the action of a piezoelectric actuator (Uchihashi et al., 1994). The laser beam is aimed at the back of the cantilever-tip assembly and reflects off the cantilever surface towards the split photodiode detector, which can detect even a small moment of the deflections in cantilever (Rao et al., 2007). Each deflection (i.e. the distance the scanner moves in the Z-direction) is recorded by the software. The position of the reflected beam on the photodiode detector is monitored by the position sensitive detector (PSD), i.e. a two or four segmented photodiode. A feedback loop maintains the Z-direction movement (i.e. between tip-sample) to the set-point. Otherwise the tip will crash into the sample surface.

### 3.4.5 Transmission electron microscopy (TEM)

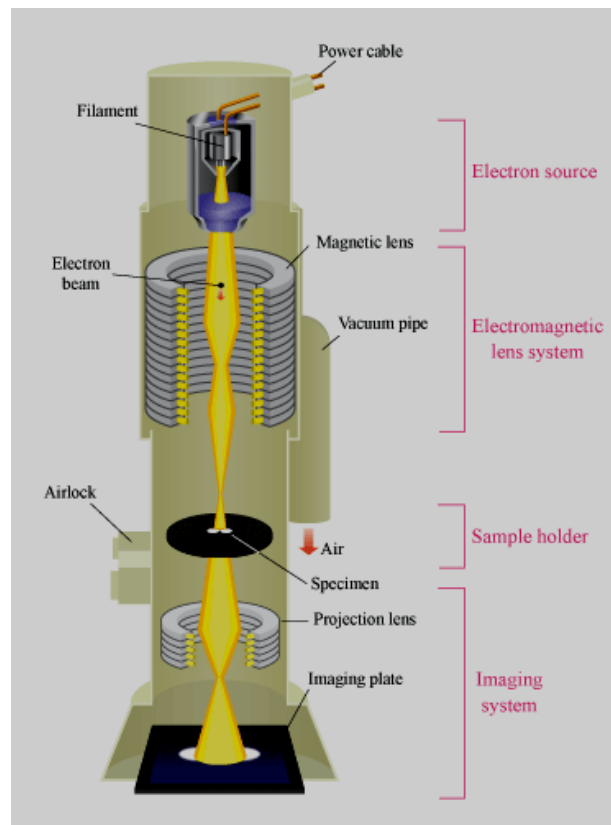
Ernst Ruska, the German engineer was the first to commercially introduce the instrument in the year 1931. Transmission electron microscopy (TEM) provides information on shape, size and imaging of NMs which were produced between the interactions of the samples with the electrons generated by electron gun in the microscopy. The image obtained from this technique also gives shape factor, fractal dimensions and particle size distributions. Furthermore, TEM can be coupled with the energy dispersion X-rays (EDX), electron energy loss spectroscopy (EELS) and which can provide the chemical and elemental information.



**Figure 3-13.** FEI Philips TECNAI F204 (Oxford Instrumentation).

The instrument employed in this research is shown in Figure 3-13, Phillips TECNAI F20, fitted with Oxford Instruments ISIS EDS and Gatan digi PEELS, with a resolution of 0.24 nm and a focal length of 1.77 nm.

The basic principle of instrument operation is shown in the Figure 3-14 below. An electron beam from an electron gun passes through the electromagnetic condenser lens through the sample and through an objective lens and then down to CCD camera. Condenser lens controls the size and intensity of the beam hitting the sample. The objective lens controls the magnification. TEM images show the internal structure of specimen of magnification up to one million times, if the structure is in atomic resolution.



**Figure 3-14.** Schematic illustration of the internal function of TEM (taken from the oxford instruments).

TEM is one of the most powerful and impressive instrumentation with a huge number of advantages they are as follows:

- Having wide range of applications that can used in different scientific, industrial and educational departments
- Images have very high resolution 0.24 nm and can obtain higher quality images

- TEM provides surface analysis, shape of NM measurements, size measurements and structure.
- When coupled with X-EDS can obtain the elemental analysis.

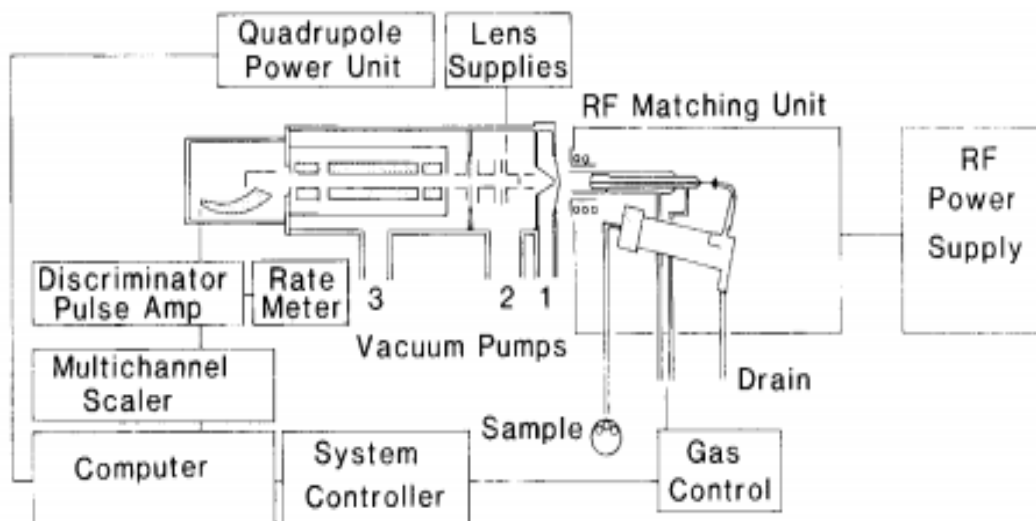
In this investigation, TEM is used very extensively to image the NMs and measure the nanoparticle number concentrations.

#### **3.4.6 Nanoparticle tracking analysis (NTA)**

NTA is used for sizing, counting, visualizing and measuring the particle number concentration. The particles to be viewed are suspended in liquid and they move under Brownian motion. Smaller particles move faster than the larger particles. Through the application of Stokes equation, particle size can be calculated and also the particle concentration can be estimated using the software provided.

#### **3.4.7 Inductively coupled plasma mass spectrometry (ICP-MS)**

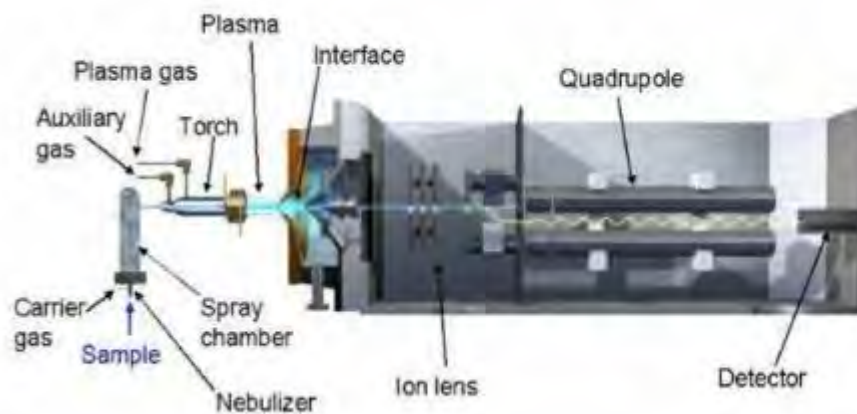
Inductively Coupled Plasma Mass Spectrometry (ICP-MS) is used to measure the mass concentration of the NMs in suspension and measures almost all the elements in the periodic table. It also detects both metallic ((Hirner et al., 2006)) and non-metallic (Ammann, 2007) elements at concentrations as low as 10 ppt and is very widely used to measure the mass concentration of NMs and utilized in many fields such as environmental and life sciences, geochemistry, archaeology and so on (Gurunathan et al.). The diagram shown below was the first ever developed ICP-MS in the year 1992. Later in the year 2014, ICP-MS is improved or enhanced its specification to quantify single particles which is said to be single particle ICP-MS.



**Figure 3-15.** Schematic illustration of the ICP-MS instrument which was first introduced in the year 1983 (Jarvis and Jarvis, 1992)

The first introduction of the ICP-MS instrument and made commercially available is shown in the above Figure 3-15, which was first introduced in 1983, later version on this technique continually improvised. Figure 3-16 shows the recently improvised version of the ICP-MS in 2012. Some of the vital components of the ICP-MS are sample introduction system, ICP torch and radio frequency (RF), quadrupole mass filter and detector, Vacuum system, electrostatic analyser ESA, coil, and interface (see Figure 3-16). NM samples are introduced into the spray chamber where the ions are generated. The plasma source ionises the all most all the elements in the periodic table, an interface system will transfer all the ions from corrosive high temperature and high pressure surrounding from the argon plasma (as an excitation source ionises the sample) into the mass spectrometry analyser having room temperature under low pressure (where mass spectroscopy selectively transmits sample / analyte ions into ratio of mass/charge) to the detector (Allabashi et al., 2009). The mass analyser filter gives the ratio of mass/charge, the separation of ions obtained on the basis of mass/charge ratio (Gurunathan et al.). In order to obtain the mass concentration of the element (which is the sample used) the principle is the electrical signal

from the detector (de Wit et al., 1993) is compared with a signal given by a certified reference material used to calibrate the system (Zeisler et al., 2006). This is used in the studies to measure the mass concentration of the synthesised NMs which can be used to correlate or cross verify with the measurement of particle number. But ICP-MS technique limits the use if the samples having complex media such as natural organic materials and exposure media.



**Figure 3-16.** A diagram showing the cross section of the different components of modern ICPMS (de Wit et al., 1993)

## **Chapter 4 MATERIALS AND METHODOLOGY**

### **4.1 Chapter summary**

In this research, synthesis of good quality of NMs was of paramount importance for the quantification of particle number. Gold nanoparticles were selected since they are electron dense, easily distinguishable from many backgrounds, easy to synthesis, cost-effective and as well as can control the size and shape. Gold nanoparticles were synthesised with two different coating such as citrate and polyvinyl pyrrolidone (PVP). The process of synthesis of gold NMs is given in the first section. These NMs were characterised and quantified for number measurements using different spectroscopic and microscopic techniques. The second section of this chapter describes the different techniques used to characterize the physicochemical properties such as size of the NMs and the mass concentration measurements of NMs.

The third section presents the sample preparation techniques for the microscopic studies. The methods include AFM and TEM techniques which is the most challenging part of the study. This technique required further development of sampling methods to allow for the measurement of particle number. The method developed in this work is detailed in this section and is referred to as the improvised/ enhanced method. Thereby, third section is emphasised on improvised method. This improvised sampling technique validation was performed by using microscopies by counting NMs present in pure water media (simple media).

The fourth section of this study is based on the process of adding different environmentally relevant media to the synthesized nanoparticles. The last section presents

the validation and the imaging methodology of the substrates by AFM and TEM techniques for quantitative measurement of particle number and size.

## 4.2 Synthesis of gold nanoparticles

Gold nanoparticles (AuNMs) were synthesised in-house by chemical method of synthesis, according to the methods described elsewhere (Wraycahen et al., 1995, Greenwood et al., 1995, Zhou et al., 2009, Baalousha et al., 2010, Hitchman et al., 2013). Two separate AuNM suspensions were produced; either coated with polyvinylpyrrolidone (PVP<sub>10</sub>-AuNMs) or citrate (cit-AuNMs) and was used in this study to validate a fully quantitative sample preparation protocol for particle number concentration using TEM. The two NMs (cit-AuNMs and PVP-AuNMs) were selected to represent charge- and sterically-stabilised NMs, respectively.

### 4.2.1 Materials

The chemicals used for the synthesis of gold NMs have been purchased from Sigma-Aldrich are as follows: tetrachloroauric acid (HAuCl<sub>4</sub>·3H<sub>2</sub>O), poly(*N*-vinyl-2-pyrrolidone) with the average molecular weight of 10 000 g/mol (PVP<sub>10</sub>), trisodium citrate dihydrate HOC(COONa)(CH<sub>2</sub>COONa)<sub>2</sub>·2H<sub>2</sub>O and NaOH. These chemicals were analytical grade, and used without further purification. The water used for all reactions and preparations was ultra-high purity water with a resistivity of > 18.2 MΩ cm at 25<sup>0</sup> C. All glassware used for the synthesis immersed for 24 hours in aqua regia (3 parts HCl: 1 part HNO<sub>3</sub>), later rinsed with UHPW and air dried. Substrates for the microscopies such as Carbon coated copper grids for TEM sample preparation and mica sheets 11mm x 11mm x 0.15 mm for AFM was purchased from the Agar Scientific, UK.



#### 4.2.2 **Synthesis of Au NMs capped with citrate**

The synthesis of Au NMs by citrate reduction of  $\text{HAuCl}_4 \cdot 3\text{H}_2\text{O}$  was according to the procedure followed by Turkevich (Turkevich, 1951b) later modified by Frens (Frens, 1973) and others. A 100 ml stock solution of 25 mM Hydrogen tetrachloroaurate was prepared using ultra high purity (UHP) water, of which one ml was further diluted in 99 ml of UHP water. The diluted solution of  $\text{HAuCl}_4$  was heated to boiling point while stirring vigorously and then 4 ml of trisodium citrate stock solution (concentration of citrate stock solution - 25 mM) was added quickly. Further heating was carried out for approximately 15 minutes until the colour of the solution changed from pale yellow to deep red. Finally the solution is kept at room temperature. The purification of the samples was carried out during sample preparation by washing the NM containing substrate after ultracentrifugation and later dried under room temperature (for detailed see Section 4.5).

#### 4.2.3 **Synthesis of Au NMs capped with polymer (PVP<sub>10</sub>)**

Au NMs with a PVP coating were synthesised using two different synthesis methods such as, hot and cold method. In case of the hot method, the mixture of gold and PVP solutions was heated to the temperature of 70 °C. While for the cold method procedure; synthesis of AuNMs was carried out at room temperature. The procedures are explained in detail below.

##### 4.2.3.1 **Hot process**

For the preparation of the Au NMs by the hot process method, the 100 ml stock solution of 25 mM Hydrogen tetrachloroaurate was prepared using ultra high purity (UHP) water, of which one ml was further diluted in 99 ml of UHP water. The diluted solution of

HAuCl<sub>4</sub> was heated to boiling point while stirring vigorously and then the solution of PVP<sub>10</sub> was added as summarised in Table 4-1 and heated at 70 °C for 3.5 hours. After cooling, the solution was washed with water in the ratio of 3:1 and centrifuged for 10 minutes at 4000 rpm. Eventually, these NMs were dispersed in water and filtered with 100 nm filter paper. For these studies, the hot process was ruled out for the further experimentation due to the aggregation and polydispersity of NMs.

#### 4.2.3.2 Cold process

The cold process of synthesis of NMs was given in detailed in the published papers (Zhou et al., 2009). In this process the Au NMs were synthesised without the use of the reducing agent, reducing energy consumption, with less reaction time and retaining control of size. As shown in the Table 4-1, three different sizes of PVP capped Au NMs were synthesised. Briefly, PVP-Au NMs were synthesized by adding an aqueous solution of tetrachloroauric acid (100 ml of 5 mM) to a solution of 2.5 mM PVP with vigorous stirring at room temperature (30 minutes at 21<sup>o</sup> C). 100ml of 0.1M sodium hydroxide (NaOH) solution was then added to initiate the reduction of the gold ions to form Au NMs.

In this method, colour changes occur faster when compared to the hot process, the colour of the solutions have changed from yellow to wine red in 10 minutes to obtain wine red colloid dispersion. In order to get different sizes of AuNMs, the ratio of gold precursor to capping agent was altered as shown in Table 4-1. The cold process resulted in monodispersed NMs, easy to synthesis and very stable. Thereby, AuNMs synthesised with cold process were used for the further sampling and quantification. The purification of the samples was carried out during sample preparation by washing the NM containing substrate after ultracentrifugation and later dried under room temperature (for detailed see Section 4.5).

**Table 4-1** Concentrations of the reactant used for the synthesis of AuNMs capped with PVP

Size of Nanoparticles Synthesised (Instrument Used – TEM) (~nm)	Method of Synthesis	HAuCl <sub>4</sub> ml/(mM)	PVP (mM)	Molar ratio of HAuCl <sub>4</sub> : Capping agent	Temperature (°C)	Reducing agent
25±3.8 (0.46) <sup>b</sup>	Hot	100 ml 5 mM	180 ml 2.78 mM	1 : 6.46	70	--
20±3.3 (0.50) <sup>b</sup>	Hot	20 ml 2.58 mM	180 ml 2.78 mM	1 : 9.70	70	--
10±2.8 (0.28) <sup>b</sup>	Cold	100 ml 5 mM	200 ml 1 mM	1 : 0.40	21	NaOH
15±3.6 (0.35) <sup>b</sup>	Cold	100 ml 5 mM	200ml 0.5 mM	1 : 0.10	21	NaOH
50±4.4 (0.29) <sup>b</sup>	Cold	100 ml 5 mM	200ml 0.25 mM	1 : 0.05	21	NaOH

<sup>b</sup> ( ) coefficient of variation = standard deviation/mean

#### 4.3 Multi-method approach used to characterise the synthesised gold nanoparticles

The synthesised NMs were fully characterised by using a number of analytical and imaging techniques such as

- (i) TEM, Tecani F20 (NM diameter),
- (ii) AFM XE100 (NM height),
- (iii) DLS (z-average Z-dh hydrodynamic diameter),
- (iv) NTA (number average hydrodynamic diameter),
- (v) UV-vis spectroscopy (plasmon resonance),

The measurements are presented in Table 4-1 in results section. The mass concentration of AuNMs in the stock solution was determined by ICP-MS (Agilent 7500cs instrument) as described in our published AFM paper (M. Baalousha<sup>§\*</sup>, 2014).

The following sections give a detailed explanation how these measurements were carried out, including the related sample preparation of all the above techniques.

#### **4.3.1 Hydrodynamic and zeta potential measurement with dynamic light scattering (DLS)**

The instruments used for this research include the Malvern Instruments, Nano ZS, model number ZEN3500, which measures the particle size, molecular weight and zeta potential. Disposable polystyrene cuvettes were used, where the sample must be pipetted carefully into cuvette. A standing operating procedure (SOP) was developed, obtaining consistency in this method. 5-10 measurements were performed to obtain the size of the NMs.

Zeta potential measurement was performed using the same Malvern instrument Nano ZS. Quartz glass cuvettes were used. Initially, before placing the sample for measurement, instrument calibration was performed with either pure water (which should result in a value close to zero), or with the standard solution (Malvern) of known zeta potential with at least 5 to 10 measurements. The equipment was calibrated before application to samples.

#### **4.3.2 Nanoparticle Tracking Analysis (NTA)**

The NTA used in this project is the LM20 from nanosight. The working of this instrument is given in the previous section. The gold nanoparticles are used for measuring both the size and the particle number concentration. The NTA 2.2 Software programme at a maximum video rate of 30 fps was used. Videos with a resolution of 640×480 pixels were captured. The chamber was cleaned prior to each measurement with ethanol and DI-water to ensure that any contaminants that may affect the measurement were removed. The O-ring was regularly checked to ensure no cross contamination occurred. Camera and shutter settings were set manually for each sample. The sample was injected into the cell to measure the parameters. With the same experimental setting, ten measurements were performed. The average of the ten measurements was taken as the final result.

#### **4.3.3 Ultraviolet -Visible spectroscopy**

The sample used for measuring SPR was poured on a cuvette. Before the sample was placed in the instrument, a baseline of the instrument was corrected using pure water. After obtaining the baseline, the cuvette containing the sample was placed inside the instrument. The absorbance obtained was plotted against wavelengths 200-800 nm or a selected region of interest.

#### **4.4 Mass concentration of gold with Inductively Coupled Plasma Mass spectrometry (ICP-MS)**

The mass concentration of Au NMs (both citrate and PVP capped) in the stock solution was determined by ICP-MS (Agilent 7500cs instrument, Wokingham, UK). One mL of stock suspension of Au NMs was diluted with 5mL ultrahigh purity water (UHPW, 18 MU cm<sub>-1</sub>) and 1.25 mL of concentrated aqua regia to achieve 20% aqua regia (Sigma Aldrich, Dorset, UK) to solubilise the gold NMs. The solution was then diluted 10 times to achieve 2% aqua regia acid in the suspension, which is suitable for ICP-MS analysis. The samples were further diluted 100 times in 2% aqua regia before analysis to match the calibration range of

ICP-MS, which is 0–100 ppb. The initial concentration of both citrate and PVP capped NMs are given in results section. The dissolved fraction of Au NMs was determined by performing ultrafiltration (stirred ultrafiltration cell, Millipore, UK) using a 1 kDa regenerated cellulose membrane (Millipore, UK) and measured by ICP-MS. The percentage of the dissolved gold ions was generally <1%.

#### 4.5 Sample preparation

The most critical and challenging part of this research was the sample preparation method for microscopic techniques such as AFM and TEM. Both of these techniques are primarily limited by sample preparation rather than by the capability of microscopy techniques techniques to count and measure the size of NMs. Different preparation techniques have been employed in the literature to prepare samples for microscopy analysis (AFM and TEM) including adsorption, drop deposition and ultracentrifugation (Balnois and Wilkinson, 2002b). Only a few studies have applied this method (Hasselov, 2005, Boyd, 1994, Wu et al., 1990a, Wu et al., 1990b, Baalousha, 2009). These methods are widely applied qualitatively, but have never been validated for quantitatively measurement of particle number concentration from a suspension of NMs. These widely adopted sample preparation methods suffer from a number of issues when used for number concentration analysis such as poor statistical power, requiring the counting of large number of NMs to compensate for the following:

- (i) Low and inconsistent recovery of NMs on the sample substrate and
- (ii) A non-uniform distribution of NMs on the sample substrate.

The adsorption method is a passive method and depends largely on the diffusion of NMs to the substrate as well as the interaction between the NMs and the sample substrate,

and thus the medium physicochemical properties. Hence, the adsorption method interrogates the smallest fraction of NMs with higher diffusion and those NMs that bind strongly to the AFM substrate (Domingos et al., 2009). Thereby this method was ruled out. The drop deposition method is known to induce aggregation artefacts due to reasons such as locally-increased salt concentrations on drying (Domingos et al., 2009b).

The ultracentrifugation method is an active method that forces all NMs in the suspension onto the substrate; however, losses of NMs may occur after centrifugation due to the release of NMs from the substrate or during the essential washing process if the NMs are not strongly attached to the substrate (Baalousha et al., 2014a). Without substantive washing, severe artifacts can occur in case of AFM, which may result in analysis artifacts and bias. These artefacts are discussed by Baalousha *et al.*, (Baalousha and Lead, 2013a). An issue with AFM is the contact of the tip of the AFM cantilever with the substrate. This is not a problem with TEM imaging.

This work has developed a fully quantitative sampling method that allows for the measurement of the size and number of NMs and its aggregates (i.e., determined as the number of primary NMs within aggregates) at environmentally realistic concentrations. The application of the developed method has demonstrated the concentration-dependent aggregation of NMs for low NM concentrations. To develop such capability it has been necessary to:

- a) Develop a validated sample preparation method to enable the measurement of NM number concentration, and
- b) To demonstrate the applicability of this validated sample preparation method to detect and quantify the number concentration of Au NMs both in simple and complex media at realistic concentrations (e.g. 1-20  $\mu\text{g L}^{-1}$ ).

To obtain quantitative measurements it is of paramount importance to recover the NMs suspended in the solution onto the substrate (AFM and TEM). After reviewing potential methods reported in the literature, a selection of methods has been explored. The most promising methods have been further developed and modified. Sample preparation protocols were tested to quantitatively measure NM number concentration from aqueous suspensions. An improved method was later developed which is referred to as the improvised sampling technique. While in this study, the first two methods (stated below) were tested to quantitatively to measure NM number concentration from aqueous suspensions. Such methods are listed below:

- (i) Drop deposition and
- (ii) Ultracentrifugation (Santschi et al., 1998, Baalousha, 2009, Johnston et al., 2007, Boyd, 1994, Wu et al., 1990a, Wu et al., 1990b).
- (iii) Ultracentrifugation with PLL functionalisation of the substrate - improvised sampling technique

These methods were imaged using both AFM and TEM technique which is explained in detail in the following section.

#### **4.5.1 Drop Deposition Method**

##### **4.5.1.1 TEM sample preparation with drop deposition method**

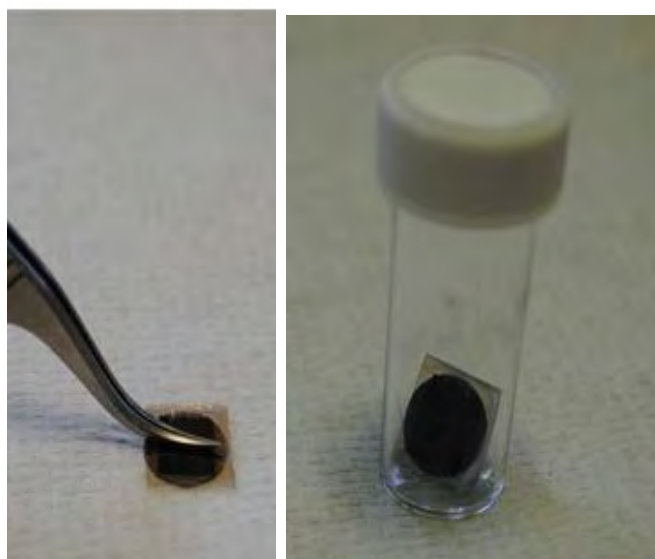
The necessary equipment required for drop deposition is pipette to drop small volumes of NMs (10  $\mu$ L), ultrapure water, diluted NMs or samples, TEM grid, UK and specimen tweezers. A small drop of NMs that is 20  $\mu$ l of various concentrations (see results section) of Au NMs was placed on the carbon coated TEM grids (purchased from Agar Chemicals, 1x S160-3 Carbon films on 3mm 300 mesh grids type). The droplet on the TEM



grid was allowed evaporate, under ambient air conditions. Later TEM imaging was carried out.

#### 4.5.1.2 **AFM sample preparation with drop deposition method**

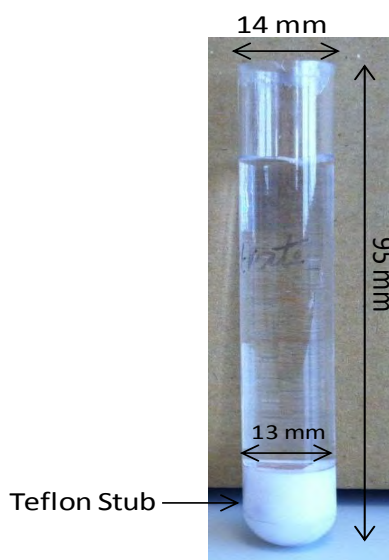
The AFM equipment required the following to scan the AFM images; metal discs as shown in Figure 4-1, mica sheet cut in ~ 1 cm squares, tweezers and a pipette to drop small volume on the pipette. The mica sheet was firmly attached to the metal disc using double sided tape. The sample was then dropped on to the mica until it barely covers the whole surface (10-20  $\mu$ L is usually enough), without making the sample pours over the edge of the mica. Let the sample adsorb to the mica surface during 5 min. Later, wash off un-adsorbed nanoparticles, salts and other components of the sample matrix. The droplet on the AFM grid was allowed to evaporate, under ambient air conditions. The AFM sample was then stored in a closed container until further image analysis using AFM technique.



**Figure 4-1** AFM method of sample preparation

#### 4.5.2 Ultracentrifugation Method for both TEM and AFM substrates

For the ultracentrifugation sampling technique the substrates for microscopy (either mica sheet for AFM or TEM grid) were prepared by suspension of NMs (11.1 ml) using Beckman ultracentrifugation tube shown in the Figure 4-2. The substrate (either TEM or AFM substrates) placed on the Teflon stub, where the NMs will be precipitated by the ultracentrifugation at 150000 g using a Beckman ultracentrifuge (L7-65 Ultracentrifuge, Beckman Coulter Ltd, High Wycombe, UK.) with a swing out rotor SW40Ti on a carbon coated TEM grids. The applied ultracentrifugation force is sufficient to collect all AuNMs larger than 5.0 nm, assuming gold density of  $19.3 \text{ g cm}^{-3}$ . In order to validate the sample preparation protocol for the quantification of number concentration of NMs and to assess the applicability range of this protocol for the NM investigated in this study, two independent replicates of six different concentrations of cit-AuNM and PVP-AuNMs in UHPW in the range of 0.2-100 ppb were prepared for both TEM and AFM analyses.



**Figure 4-2:** Beckman ultracentrifugation tube with Teflon stub to hold TEM grid.

The ultracentrifugation method is an active method that forces all NMs in the suspension onto the substrate. An issue with this method is the loss of NMs (the detailed

explanation regarding the percentage loss of NMs given the results Chapter 6 and Chapter 7) that may occur due to the essential washing process if the NMs were not strongly attached to the substrate. However, washing, is required to prevent artefacts due to salt precipitation and other processes (Baalousha and Lead, 2013a).

The objective of the sample preparation is to get full recovery of the NMs on the substrate, fulfilling the main research aims for quantifying the number of NMs. The number of NM count recovered by this method is discussed in the results chapter. The technique was been modified allowing for the full recovery of NMs on the substrate. This method is explained in the following section.

#### **4.5.3 Ultracentrifugation with surface functionalisation of the substrate**

In order to obtain the full recovery, enhance the retention and distribution of the NMs on the substrates two methods were examined;

- (i) Surface of the substrate was functionalised with a positively charged poly-L-lysine PLL polymer (Sigma Aldrich, Dorset, UK), and
- (ii) Addition of  $\text{CaCl}_2$  (Maitra et al., 1999) to the NM suspension before ultracentrifugation, which was used only for AFM.

Functionalisation using PLL was carried out for both AFM and TEM substrates. For TEM grids, the surface of the grid were covered with a drop of 0.1% poly-L-lysine (Huang et al., 2001) for 15 minutes followed by rinsing three consecutive times in UHPW to remove excess poly-L-lysine, after which the TEM grids were left to dry overnight under ambient air conditions in a covered Petri dish. Following ultracentrifugation, the TEM grids were washed thoroughly by immersing them three consecutive times in UHPW for 30 seconds each, then the TEM grids were left to dry under ambient air conditions before ultracentrifugation of the

suspensions of NM. A similar procedure was followed for AFM by using freshly cleaved mica substrates.

The second method of sampling technique used for AFM was the addition of  $\text{CaCl}_2$  (Yamashita et al., 2002, Maitra et al., 1999) to the NM suspension prior to ultracentrifugation. The addition of  $\text{CaCl}_2$  was mainly to obtain the uniform distribution of NMs on the substrate and also for strong attachment of NMs to the mica sheet in case of AFM technique, possibly due to the bridging by  $\text{Ca}^{2+}$  of the negatively charged mica surface on the partially negatively charged mica sheet (Baalousha and Lead, 2013b). Therefore, addition of the divalent cations to the sterically stabilized NMs combined with the ultracentrifugation may be used to improve the uniformity of the NMs distribution on the AFM substrate. PVP-Au NM samples were prepared in 10 mM  $\text{CaCl}_2$ , whereas cit-AuNMs were prepared in 100–300 mM  $\text{CaCl}_2$  on a bare AFM substrate. The higher concentration of  $\text{CaCl}_2$  used for PVP-AuNMs compared with cit-AuNMs is due to the higher colloidal stability of PVP-Au NM suspensions compared to cit-AuNMs (Hitchman et al., 2013).

#### 4.6 Simple and complex media

In Simple media the sampling approach was validated using citrate- and PVP- coated Au NMs in pure water, which demonstrated an even distribution of NM on the TEM grid and high NM recovery (See results chapter 5 and Chapter 6, for 80-100%) at environmentally relevant NM concentrations (*ca.* 0.20-100  $\mu\text{g L}^{-1}$ ).

Whereas the applicability of the sampling method to complex environmental conditions was then demonstrated by detecting and quantifying number particle concentration of citrate- Au and PVP Au NMs spiked in three different media at

environmentally NM relevant concentrations of 1 to 20  $\mu\text{g L}^{-1}$ . The three different complex media used were as follows:

- (i) EPA synthetic soft water,
- (ii) 5 mg SRFA in one litre of EPA soft water and
- (iii) Natural surface water sample was collected from the Vale Lake.

Both citrate and PVP capped Au NMs were diluted at different concentrations using the above three media. These findings are key to improve the understanding of NM environmental behaviors, fate, effects and dose; and were only enabled by the novel fully quantitative sampling method. TEM analysis was performed by coupling with the X-EDS with all the three complex media mentioned above (see in results sections). The preparation of the above three different media is given in detail below.

#### 4.6.1 EPA synthetic soft water

Preparation of EPA synthetic soft water was followed using the protocol mentioned in EPA methods for measuring the acute toxicity of effluents (Environmental Protection Agency Office of Water (4303T): Washington, 2002). This method takes into account the hardness of the water, its pH and its alkalinity. The Table 3-2 below shows the chemical material quantities of different hardness of synthetic freshwater that have been used.

**Table 4-2** Preparation of synthetic freshwater after using reagent grade chemicals<sup>1</sup>

	Reagent Added (mg/L) to deionised water				Approximate Final Water Quality		
	NaHCO <sub>3</sub>	CaSO <sub>4</sub> . C <sub>2</sub> H <sub>2</sub> O	MgSO <sub>4</sub>	KCl	pH	Hardness	Alkalinity
Very soft	12.0	7.5	7.5	0.5	6.4-6.8	10-13	10-13

Soft	48.0	30.0	30.0	2.0	7.2-7.6	40-48	30-35
Moderately Hard	96.0	60.0	60.0	4.0	7.4-7.8	80-100	57-64
Hard	192.0	120.0	120.0	8.0	7.6-8.0	160-180	110-120
Very hard	384.0	240.0	240.0	16.0	8.0-8.4	280-320	225-245

<sup>1</sup>Taken in part from Marking and Dawson (1973).

The procedure for the preparation of synthetic softwater is described below.

- (i) The reagent grade chemical (such as NaHCO<sub>3</sub>, MgSO<sub>4</sub> and KCl) added to the deionised water (measurements are in (mg/L)<sup>2</sup> as mentioned in the protocol or given same in the Table 4-2 above).
- (ii) After 24 hours of aeration of these chemicals, the solution of CaSO<sub>4</sub>.C<sub>2</sub>H<sub>2</sub>O was prepared (also in (mg/L)<sup>2</sup> as mentioned in the protocol) and added to the above mentioned chemicals. Later, the mixtures were stirred using magnetic stirrer.

#### 4.6.2 Suwannee river fulvic acid (SRFA)

SRFA was purchased from International Humid Substances Society, USA. A 5mg L<sup>-1</sup> SRFA was prepared by dissolving 5 mg SRFA in one litre of EPA soft water (Environmental Protection Agency Office of Water (4303T): Washington, 2002). EPA softwater was prepared by dissolving 48 mg of sodium bicarbonate (NaHCO<sub>3</sub>), 2 mg potassium chloride (KCl), 30 mg of calcium sulphate (CaSO<sub>4</sub>), and 30 mg of Magnesium sulphate (MgSO<sub>4</sub>) in 1 L of ultrahigh purity water (R=18 MΩ). The final solution pH was 6.8.

#### **4.6.3 Natural Surface Water/Lake Water**

Natural surface water sample was collected from the Vale Lake, a site close to Birmingham, United Kingdom. The samples were collected in autumn (27<sup>th</sup> November 2013). All sampling bottles were high density polyethylene, rinsed with dilute nitric acid, UHWP and the sample water, all of which were discarded. Water conductivity 481  $\mu\text{s}$ , dissolve oxygen 62.3 % at 6.66 mg/L, pH 7.48 and insitu temperature was 6<sup>o</sup> C were measured at the time of sampling, samples were filtered (Nuclepore track-Etch membrane, 0.45  $\mu\text{m}$  purchased from Whatman) in the laboratory within 2 hours of sampling. Small volumes were filtered at low flow rates, minimizing the impacts of filtration.

#### **4.7 Imaging NMs for size and number concentration measurements from both TEM and AFM analysis**

##### **4.7.1 Imaging for number measurements by TEM**

All TEM analyses were performed using TECNAI F20 Field Emission gun (FEG) TEM coupled with an x-ray Energy Dispersive Spectrometer (X-EDS) from Oxford Instruments. Qualitative X-EDS analysis was performed to determine particle elemental composition. For imaging NMs on the substrate, different areas on each grid were randomly imaged 30 images being investigated for each TEM grid. The number of NMs in each image was counted by using image J software.

For TEM analysis in results section presents the analysis of images of NMs using the three different methods of sample preparation such as drop, ultracentrifugation and substrate functionalisation with ultracentrifugation. The different media used for the TEM analysis were:

- (i) Ultra-high purity water, - simple media
- (ii) EPA synthetic soft-water, - complex media
- (iii) SRFA-EPA – complex media
- (iv) Natural lake water – complex media.

#### **4.7.2 Imaging for size Measurements by TEM and AFM**

For each sample, a minimum of 2000 NMs was used to calculate the size and shape using Digital Micrograph software (Gatan Inc, Pleasanton, CA, USA) and image J analysis software, which are sufficient to produce a representative number particle size distribution (Baalousha et al.). The measured sizes were then classified into intervals of 0.5 nm to construct particle size distribution histograms.

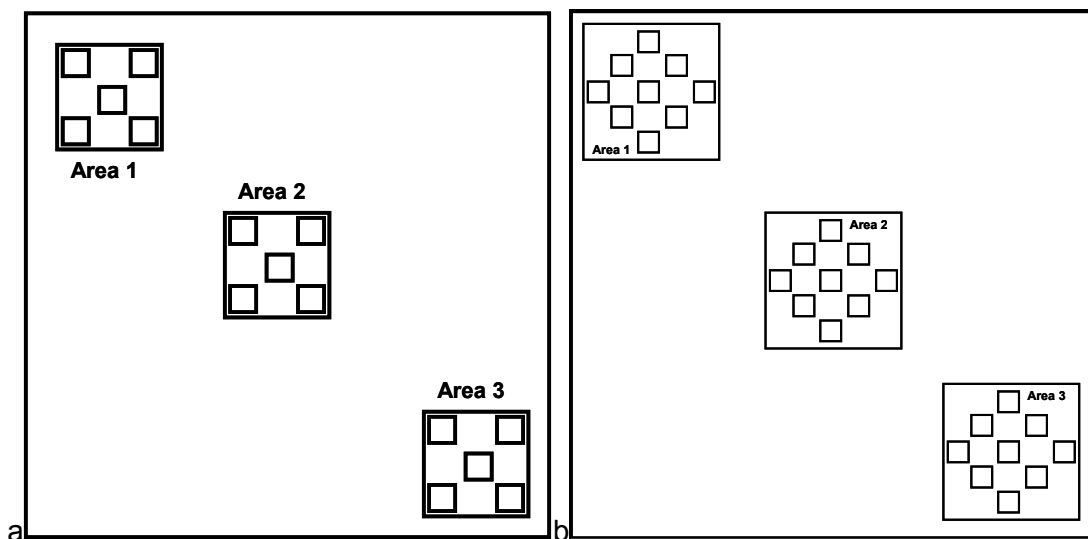
AFM analyses were performed using an XE-100 AFM (Park systems Corp., Suwon, Korea). The measurements were carried out in true non-contact mode using a silicon cantilever with a typical spring constant of 42 N m<sup>-1</sup> (PPP-NCHR, Park systems Corp., Suwon, Korea). All scans were performed under ambient conditions, which have been shown to produce accurate sizes, despite loss of most, but not all water (Balnois and Wilkinson, 2002a). 18, 22 Images were recorded in topography mode with a pixel size resolution of 256 x 256 and a scan rate of 0.5–1.0 Hz. Three different areas on each substrate were investigated and 5–9 images were collected from each area as described in Figure 4-3, resulting in 15–27 images being investigated for each substrate. On average, the time taken for AFM analyses per sample was about 2 hours. The scanned area per image varied between 1 mm x 1 mm to 5 mm x 5 mm depending on the sample concentration and the number of NMs on each image to facilitate NM counting.



For the particle number measurements by AFM technique, two methods of sample preparation were followed such as:

- (i) Sampling technique by surface functionalization of the substrate with a positively charged poly-L-lysine polymer (Sigma Aldrich, Dorset, UK) and later followed by ultracentrifugation and drying process as explained in detail in Section 3.5.3 as well as
- (ii) Addition of  $\text{CaCl}_2$  to the NM suspension before ultracentrifugation given in detail in Section 3.5.3.

These methods were utilised for the fully qualitative and quantitative measurement of the particle number number. The results (see Section 5.2) obtained from this above two sampling techniques is also published (M. Baalousha<sup>§\*</sup>, 2014).



**Figure 4-3** Areas and images scanned by AFM for each sample. Three areas at different locations on the AFM substrate and (a) 5 and (b) 9 images were collected by area, resulting in collecting 15-29 images for each sample.

### **4.7.3 Height Measurements by AFM**

Height measurements of NMs were performed using the transect analysis using the XEI data processing and analysis software of the microscope (Park Systems Corp., Suwon, Korea). For each sample, a minimum of 200 height measurements were performed, which are sufficient to produce a representative particle size distribution (Boyd et al., 2011). The measured heights were then classified into intervals of 0.5 nm to construct particle size distribution histograms, which was fitted with a log-normal distribution function as described elsewhere (Boyd et al., 2011).

### **4.7.4 Validation of the AFM and TEM sample preparation for number concentration measurements**

The above sections emphasised on the process of sampling and imaging using AFM and TEM technique. The improved sampling technique has been validated using the following criteria:

- (i) Uniformity of NM distribution on the substrate between images,
- (ii) The % recovery of NMs on the substrate compared to the concentration of NMs in suspension and
- (iii) The correlation of number concentration measured by TEM/AFM vs. mass concentration in suspension (linearity).

The uniformity of NM distribution on the substrate was evaluated by comparing the number of particles counted at different areas (see Figure 4-3), which was performed by calculating the coefficient of variation of the number of NMs per  $\mu\text{m}^2$  on the images collected at different location on the grid ( $CV = \sigma/\text{mean}$  of number NMs per  $\mu\text{m}^2$  on the different

images). Low CV values indicate uniform distribution of NM on the substrate. The number of NMs in each image was counted by using image J software, ( $N_{counted/image}$ ) and the number of NMs ( $NM L^{-1}$ ) in suspension ( $N_{suspension}$ ) was calculated from counted number of NMs in each TEM image using Eq.4.1

$$N_{suspension} = \frac{N_{counted/image}}{V_{image}} \quad \text{Eq.4.1}$$

Where  $V_{image}$  is the volume of suspension above each TEM image (in litres), which can be calculated according to Eq.4.2

$$V_{image} = A_{image} h \quad \text{Eq.4.2}$$

Where  $A_{image}$  is the area of each image and  $h$  is the height of water column on top of the image.

The mass of NMs ( $M_{recovered}$ ) in suspension can be calculated from the number of NMs in suspension (calculated in Eq.1) according to Eq.4.3

$$M_{recovered} = N_{suspension} v \rho \quad \text{Eq.4.3}$$

Where  $v$  is the volume of the average NM,  $\rho$  is the density of the NMs and  $N_{suspension}$  is the number of NMs in the suspension (calculated from Eq. 4.1).

The total centrifuged mass of NMs ( $M_{centrifuged}$ ) in the centrifuged volume ( $V_{centrifuged}$ ) can be calculated according to Eq.4.4

$$M_{centrifuged} = C_{suspension} V_{centrifuged} \quad \text{Eq.4.4}$$

Where  $C_{suspension}$  is the concentration of NMs in the centrifuged suspension.

Equation 4.4 assumes that Au NMs are insoluble/colloidal form and monodisperse, which is confirmed by the dissolution analysis and the narrow size distribution of the NMs used in this study.

The recovery of NMs on the TEM grid can be calculated according to Eq.4.5 assuming that the NMs are insoluble and spherical (shape factor for citrate and PVP-Au NMs See results sections).

$$\%recovery = \frac{M_{recovered}}{M_{centrifuged}} 100\% \quad \text{Eq.4.5}$$

The following assumptions are embedded in the calculation of the recovery: (i) no losses of NMs to the containers during storage, dilution and ultracentrifugation and (ii) all counted NMs are single entities and no interactions occurred between the NMs.

#### 4.7.5 Number of images required for representative measurement of number concentration.

The number of images required to obtain a representative measurements of NM number concentration was assessed by quantifying the mean number concentration and standard deviation of the mean as a function of the number of images analyzed (Baalousha et al., 2014a). To determine the minimum number of images required to obtain accurate and statistically representative particle number concentration of the entire suspension of NMs, we investigated the stability of the calculated mean number concentration and standard deviation of the mean ( $\sigma_{mean}$ , Eq.4.6) on subpopulations of the scanned images (n=2-27 images) (Baalousha, 2012, Boyd and Cuenat, 2011).

$$\sigma_{mean} = \frac{\sigma}{\sqrt{n}} \quad \text{Eq.4.5}$$

## **Chapter 5 Nanoparticle Characterisation using multi-method approach**

### **5.1 Introduction**

Nanoparticle analysis and characterisation is of paramount importance to know the physical and chemical properties by using robust analytical approaches (Herrmann, November 2012). Environmental risk assessments of engineered nanomaterials were necessary through very extensive characterisation of NM and their aggregates (Hasselov et al., 2008, Stolpe et al., 2005). Thereby, wide characterisation is performed and discussed in terms of NM size measurement such as NM height, diameter, hydrodynamic diameter, size distribution using various analytical method and later NM size measurements were compared. While electron microscopy and atomic force microscopy, with respect to imaging plays a vital role in determination of the shape and size of NM. It was proved in little research work that the toxicity can be shape dependent (Pal et al., 2007, Schaeublin et al., 2012). Furthermore, physicochemical properties of NM are a prerequisite to obtain a quantitative analytical methodology / protocol to determine the NM particle number either in simple or complex media. Which in turn considered that the measurement of particle number is more appropriate for dose-response relationship (explained in Chapter 2) (Oberdorster et al., 2007).

## 5.2 Results and discussion

This chapter is devoted to the discussion of the characterisation and synthesis results using different analytical approaches such as transmission electron microscopy (TEM), atomic force microscopy (AFM), dynamic light scattering (DLS), nanoparticle tracking analysis (NTA), inductively coupled plasma mass spectrometry (ICP-MS) and ultraviolet–visible spectroscopy (UV-vis). The AuNMs of different size and capping were synthesised in-house using different synthesis method as described in Chapter 4 and Section 4.2 and its following subsections. To characterise the in-house synthesised gold nanoparticles special attention were given to obtain the good quality of the product of the synthesis method by comparing the physicochemical properties in terms of size distribution, shape of the particle, monodispersity and solubility. The gold nanoparticles synthesised were characterized using a multi-method approach (Domingos et al., 2009a, Baalousha, 2012b, Baalousha, 2012a) and the key physicochemical properties discussed in this chapter are as follows:

- (i) Size measurement of nanoparticle using TEM, DLS, NTA, and AFM
- (ii) Shape Factor using TEM
- (iii) Zeta potential and
- (iv) UV-vis.

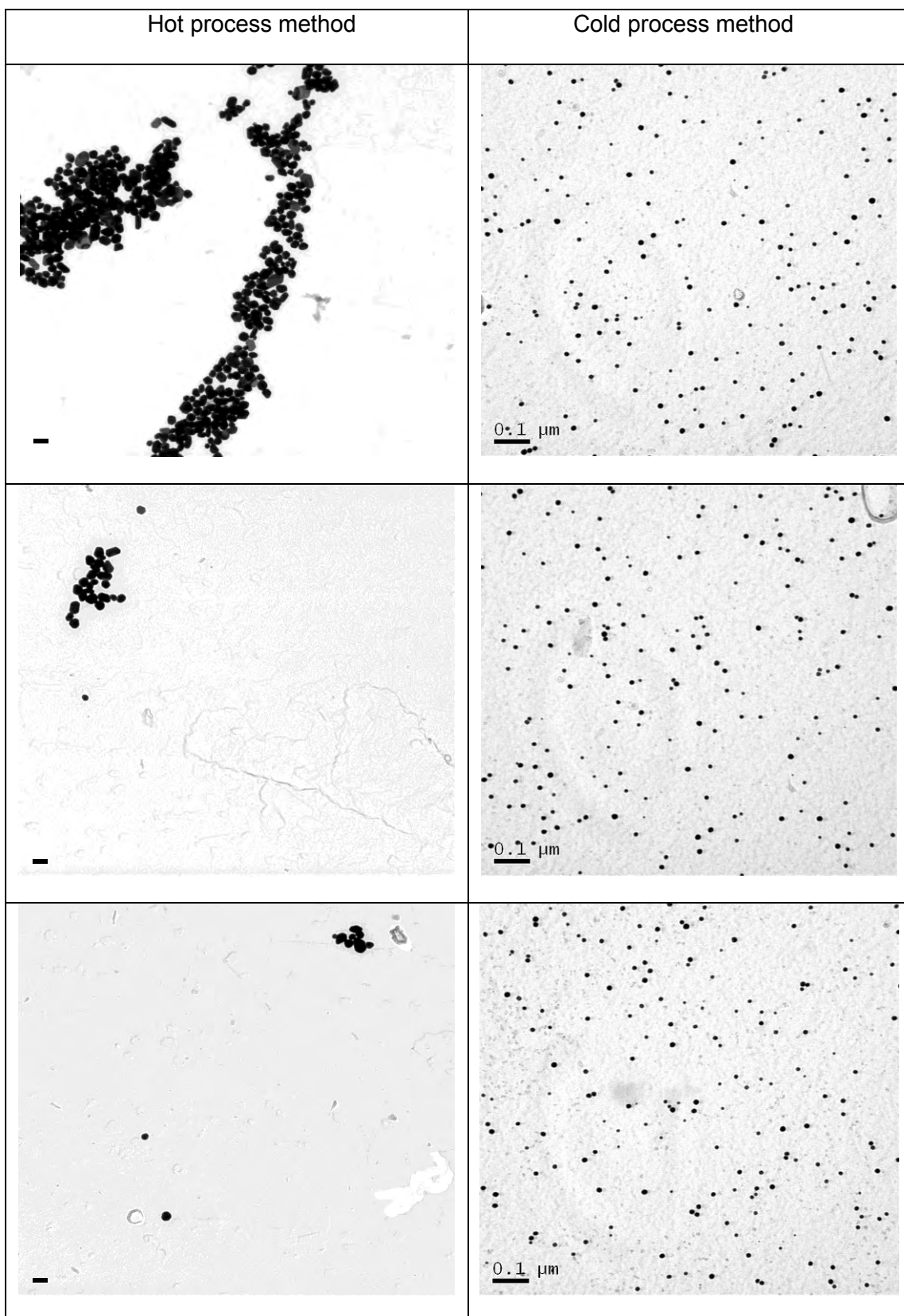
The above initial characterisations were performed to test how the NMs behave when exposed to the environmental relevant conditions. As prepared, suspensions of the gold NMs were later added to the three realistic environmental conditions such as lake water, synthetic soft water and SRFA to observe the unwanted matrix effects or changes to the samples.

The section below gives in detail the characterisation of NMs using various analytical approaches. Later chapters are related to the fully quantitative measurement of NMs by using techniques AFM and TEM.

### **5.3 Synthesis and growth of gold NMs**

Gold NMs were synthesised in-house using two different capping agents such as: citrate and PVP. Synthesis of these NMs is given in detail in Chapter 4 and Section 4.2. As shown in Table 4-1, different sizes of PVP capped Au NMs were synthesised by utilising two different methods of synthesis. The two different methods used were called the cold method and the hot method (section 4.2.3). By the cold method synthesis very well dispersed PVP capped Au NMs were prepared without any aggregation when compared to the hot method. The TEM and AFM micrograph shows the Au NMs dispersion by both hot and cold process. As seen in the Figure 5-1 below, the Au NMs by hot method were aggregated while by cold method NMs are very well dispersed without any aggregation. The requisition of this project is to obtain a very well dispersed Au NMs i.e. without aggregation and with uniform NM size distribution.

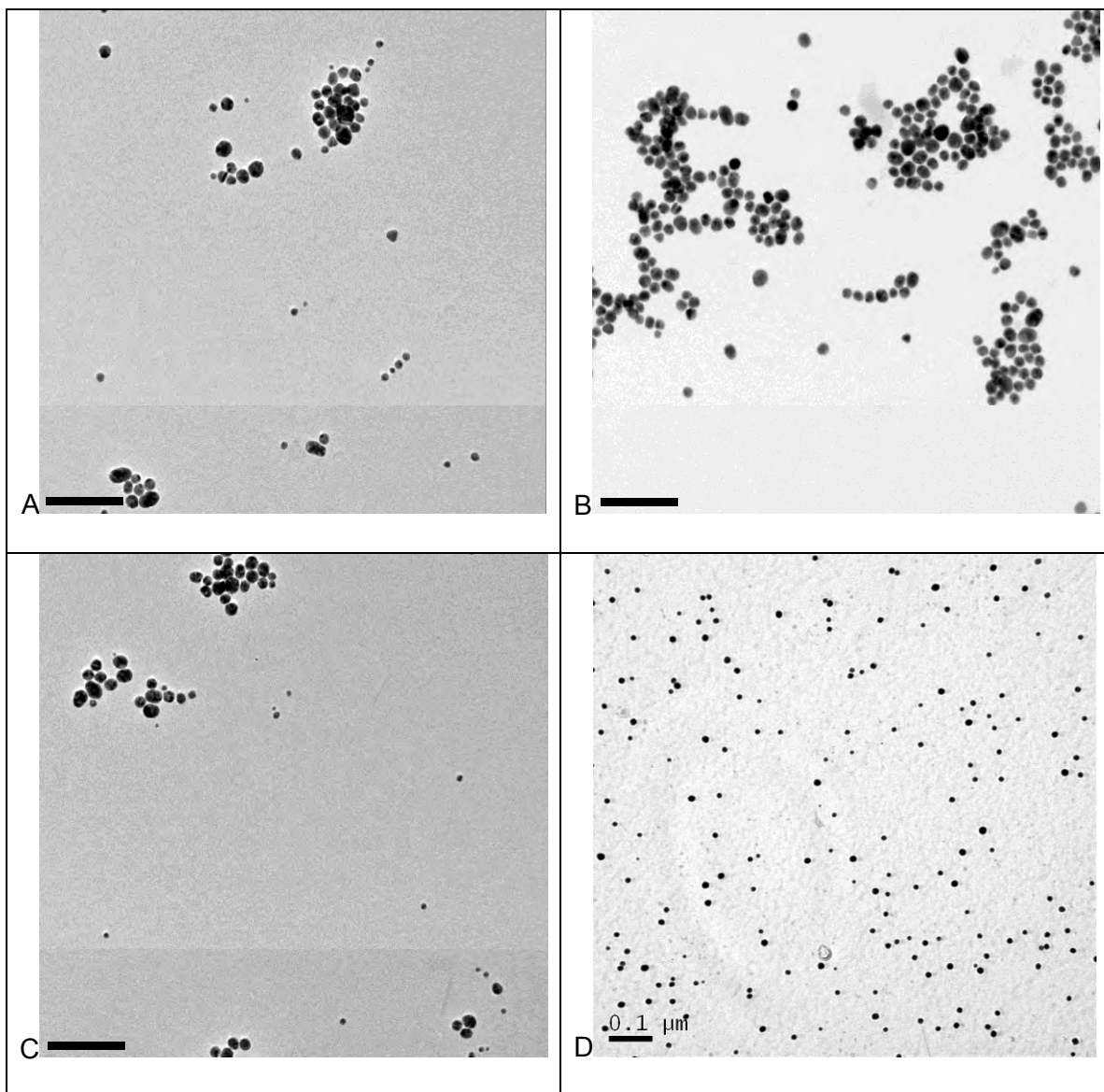




**Figure 5-1** A typical TEM Images of PVP capped Au NMs synthesised by two different synthesis processes such as: (a) hot process and (b) cold process.

Figure 5-1 shows the typical TEM micrographs obtained by two different synthesis methods as described in Chapter 4 and Section 4.2. i.e. hot and cold method of synthesis. Both the hot and cold method of gold NMs synthesised in-house capped with PVP. The hot method of synthesis resulted in the aggregation and not uniformly dispersed (See Chapter 3 and its subsections for the synthesis NMs by hot process) on the substrate as shown in the Figure 5-1(a). In this work, synthesis of Au NMs without any aggregation is a prerequisite in this investigation and to have very well monodispersed Au NMs for the initial analysis for the purpose of dose metric measurement i.e. particle number measurement. The PVP capped gold NMs synthesised by cold method approach were non-aggregated (see Figure 4-1(b)) and used for the further characterisation to analyse the uniformity in distribution, monodispersity, size distribution, spherical and various other analysis using analytical techniques such as DLS, Uv-vis and so on is explained in the further sections.

Similarly for the synthesis of citrate capped gold NMs, the process of synthesis was given in detail in Chapter 4 and in Section 4.2.2. The citrate capped NMs were synthesised in-house by chemical synthesis method (Turkevich, 1951b, Gurunathan et al., Ferns, 1973). Citrate capped Au NMs were synthesised by trial and error method until non-aggregated NMs were obtained.



**Figure 5-2** TEM Images of citrate capped Au NMs synthesised by trial and error method using chemical synthesis processes, images (A, B and C) are aggregated and (D) non-aggregated.

The above TEM micrograph shows the initial synthesis of NMs which were aggregated and polydispersed in Figure 5-2 (A, B and C). But the prerequisite of the investigation is to obtain the monodispersed NMs without any aggregation. By the trial and error method and continuous synthesis of citrate gold NMs finally achieved the non-aggregated and monodispersed NMs, the synthesis of the monodispersed (See Figure 5-2D) citrate capped NMs is given in detailed in Chapter 3 and in Subsection 4.2.3.

Furthermore, various sizes of NMs synthesised by trial and error method is given in Table 4-1. The PVP capped gold NMs having size  $10\pm 2.8$  nm selected for the further characterisation and measurement of particle number. Whilst, citrate capped gold NMs capped having size of  $15\pm 3.3$  nm. The wine red colour of the solution indicates the stability of the citrate capped Au NMs (Faraday, 1857, Frens, 1973, Turkevich, 1951a). These gold NMs were characterised for various physicochemical properties explained in upcoming sections.

## **5.4 Characterisation of Au NMs capped with citrate and PVP**

The physicochemical properties of the synthesised AuNMs were characterised by utilising various analytical techniques both microscopies and spectroscopies (Baalousha and Lead, 2013a, Baalousha, 2012a, Baalousha, 2012b). The microscopies and spectroscopies used for this study are explained in detail in the Chapter 3 and in Section 3.5. Some of the physicochemical properties that were measured are size, shape, surface plasmon resonance, monodispersity and surface charge.

### **5.4.1 In-house synthesised NMs used for characterisation**

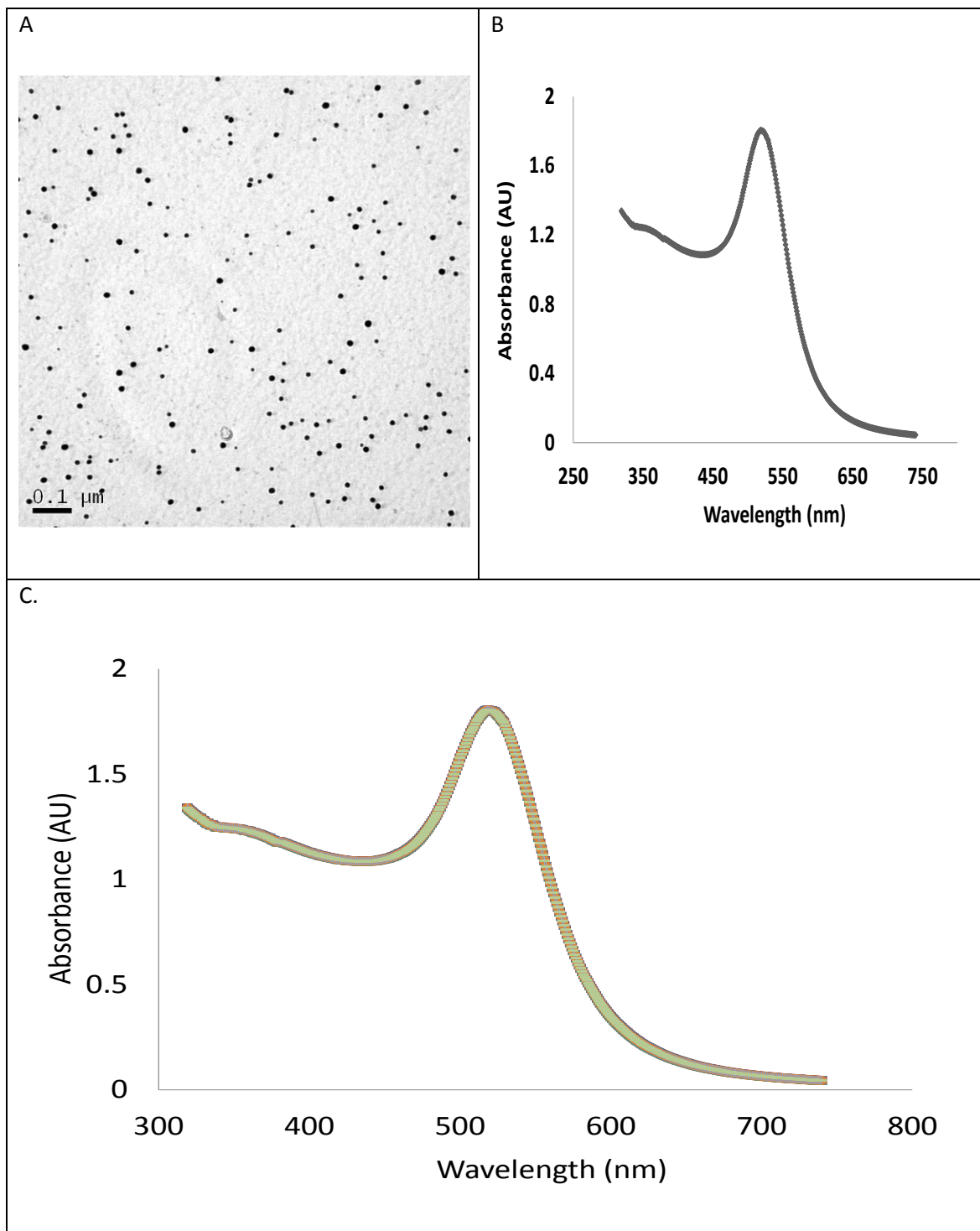
In this research, chemical process of synthesis is identified as the appropriate to synthesise Au NMs after critical reviews (see Chapter 3) of different types of synthesis. By trial and error method of chemical synthesis, Au NMs coated with citrate and PVP were synthesised. PVP Au NMs with cold process (see Table 4-1) of chemical synthesis having three different sizes were synthesised. Au NMs capped PVP having size of  $10\pm 2.8$  nm used

for the particle number measurement and citrate capped Au NMs of size  $15\pm 3.3$  nm used for measurement of particle number.

The process of synthesis of citrate capped Au NMs is given in detail earlier in chapter 4 and in section 4.2. The AuNMs capped with citrate having a size of  $15\pm 3.3$  nm will be used for the particle number measurement. The wine red colour (see Figure 5-3) of the solution indicates the stability of the citrate capped AuNMs (Faraday, 1857, Frens, 1973, Turkevich, 1951a).

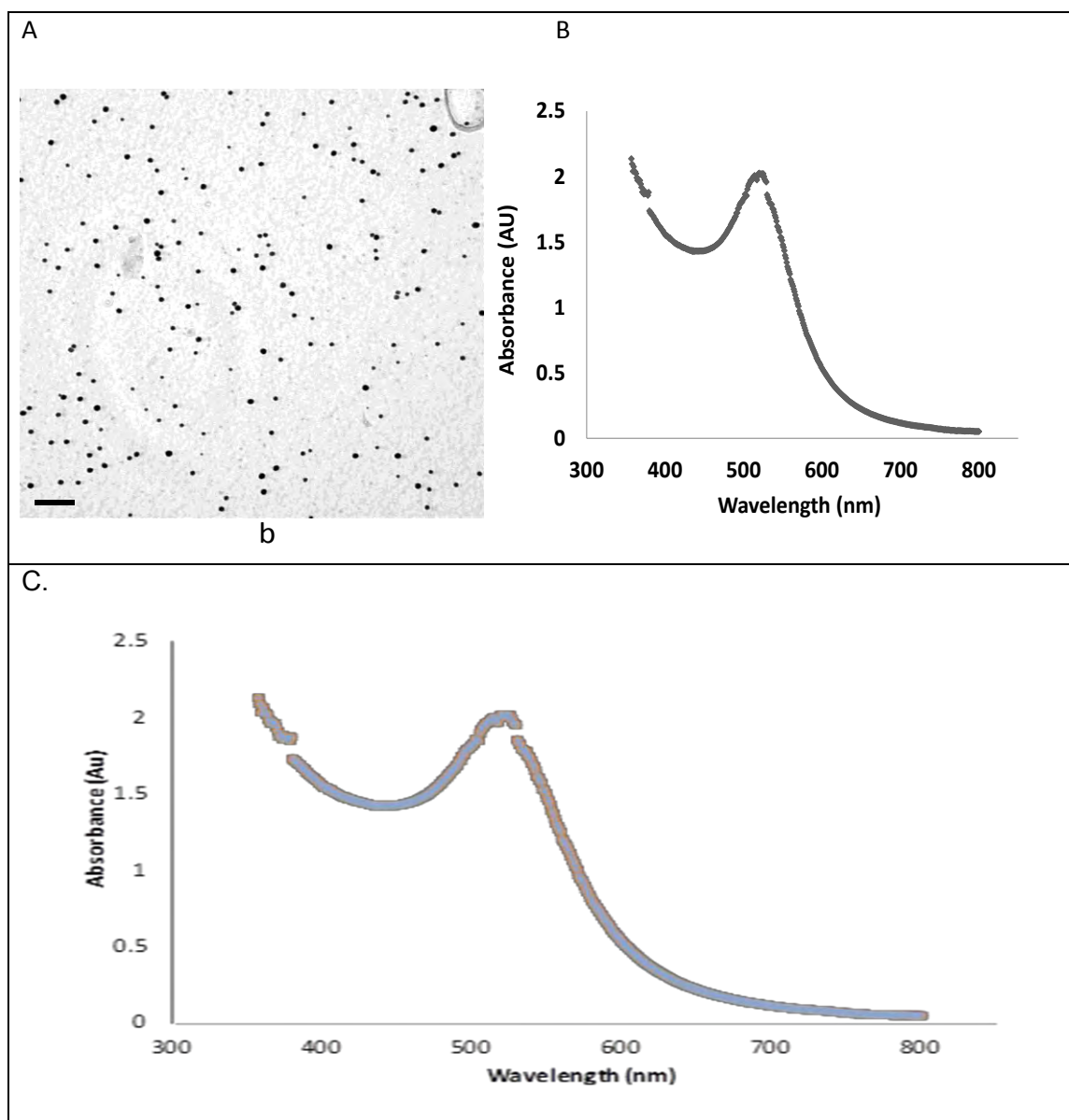
#### **5.4.2 Wavelength measurement by Ultraviolet-visible Spectroscopy (Uv-vis)**

For the in-house synthesised PVP capped Au NMs (size  $10\pm 2.8$  nm) using cold method process and citrate capped Au NMs (size of  $15\pm 3.3$  nm), UV-vis spectroscopy is used to analyse the presence of gold nanoparticles and its dispersity. Experimental procedure to measure the sharp absorbance peak i.e. a measure of wavelength ( $\lambda_{\max}$ ) where the absorbance (A) reaches to its peak value (Haiss et al., 2007b). Formation of gold NMs can be affirmed by measuring the UV-vis absorbance which shows the NMs localised surface plasmon behaviours (Frederick, 1976) and the colour changes from yellow to ruby red during synthesis of gold nanoparticles (the process of synthesis was given in the Chapter 4 and Section 4.2) indicates the formation of the gold NMs in the suspension (Mohd Sultan and Johan).



**Figure 5-3:** (A) UV-vis measurements of AuNMs citrate coated, (B) absorbance spectra of citrate coated AuNMs having 519 nm and (C) the stability test was carried out quarterly for 24 months having absorbance peak of 519 nm.

The experimental procedure to measure the absorbance peak was given in detail in methodology Chapter 4 and in subsection 4.5.3. The above Figure 5-3 shows the synthesised citrate-Au NMs have a single UV-vis absorbance peak centered at 519 nm, indicating that the suspensions of NMs are stable and free of aggregated NMs. Since spectra shows the single sharp peak and absence of other peaks indicates the monodispersity of the AuNMs. Stability test was carried out quarterly for 24 months, the NMs were found to be stable having absorbance peak 519 nm.



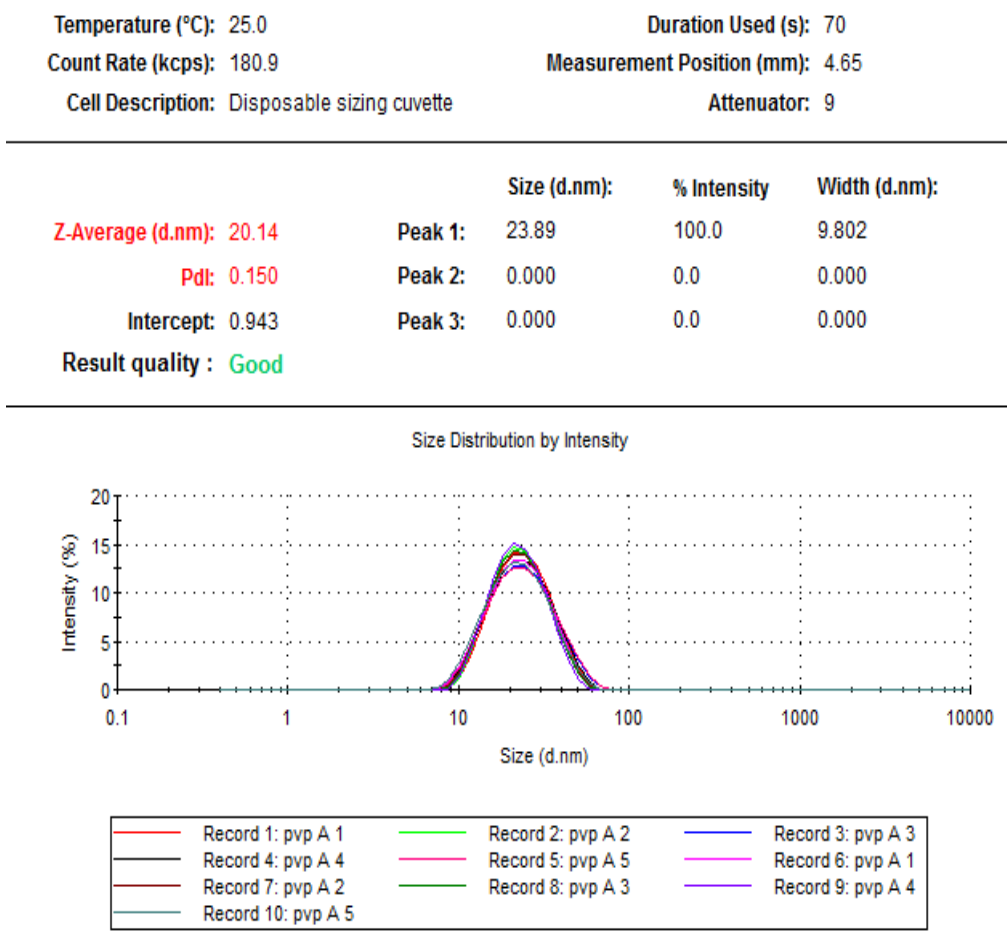
**Figure 5-4** (A) UV-vis measurements of AuNMs PVP coated (B) absorbance spectra of PPV coated AuNMs having 525 nm and (C) the stability test was carried out quarterly for 24 months having absorbance peak of 525 nm

The above Figure 5-4, shows the synthesised PVP capped Au NMs also have a single UV-vis absorbance peak centered at 525 nm, indicating that the suspensions of NMs are stable and free of aggregated NMs (Amendola et al., 2008). Since spectra shows the single sharp absorbance peak and absence of other peaks indicates the monodispersity of the Au NMs. Stability test was carried out quarterly for 24 months, the NMs were found to be stable having absorbance peak 525 nm.

#### **5.4.3 Z-average Hydrodynamic Diameter (Z-dh) and zeta potential**

DLS technique measures the size of the nanoparticles which is the core size of the NM plus the size of the capping agent i.e. said to be hydrodynamic diameter (z-average). The detail experimental procedure for the measurement of size of NMs i.e. hydrodynamic diameter of NMs by DLS technique was given in the Chapter 4 in Section 4.5.





**Figure 5-5** DLS diagram illustrates the hydrodynamic size distribution by intensity of PVP capped AuNMs, obtained by repeating the measurements for the purpose of accuracy.

The Figure 5-5 shows the size distribution spectra of the PVP capped NM. The single narrow peak curve of intensity shows the monodispersity of NMs. The hydrodynamic diameter (z-average) of PVP-Au NMs is  $20.14 \pm 2.6$  (see Table 5-1) and having low polydispersity index of 0.15 respectively. To compare the size distribution with other techniques such as AFM, TEM and NTA see Table 5-4. Zeta potential measures the electric charge on the surface of the NMs. Surface charge of PVP-Au NMs i.e. zeta potential of  $-8.3 \pm 1.6$ . PVP-Au NMs are sterically stabilized.

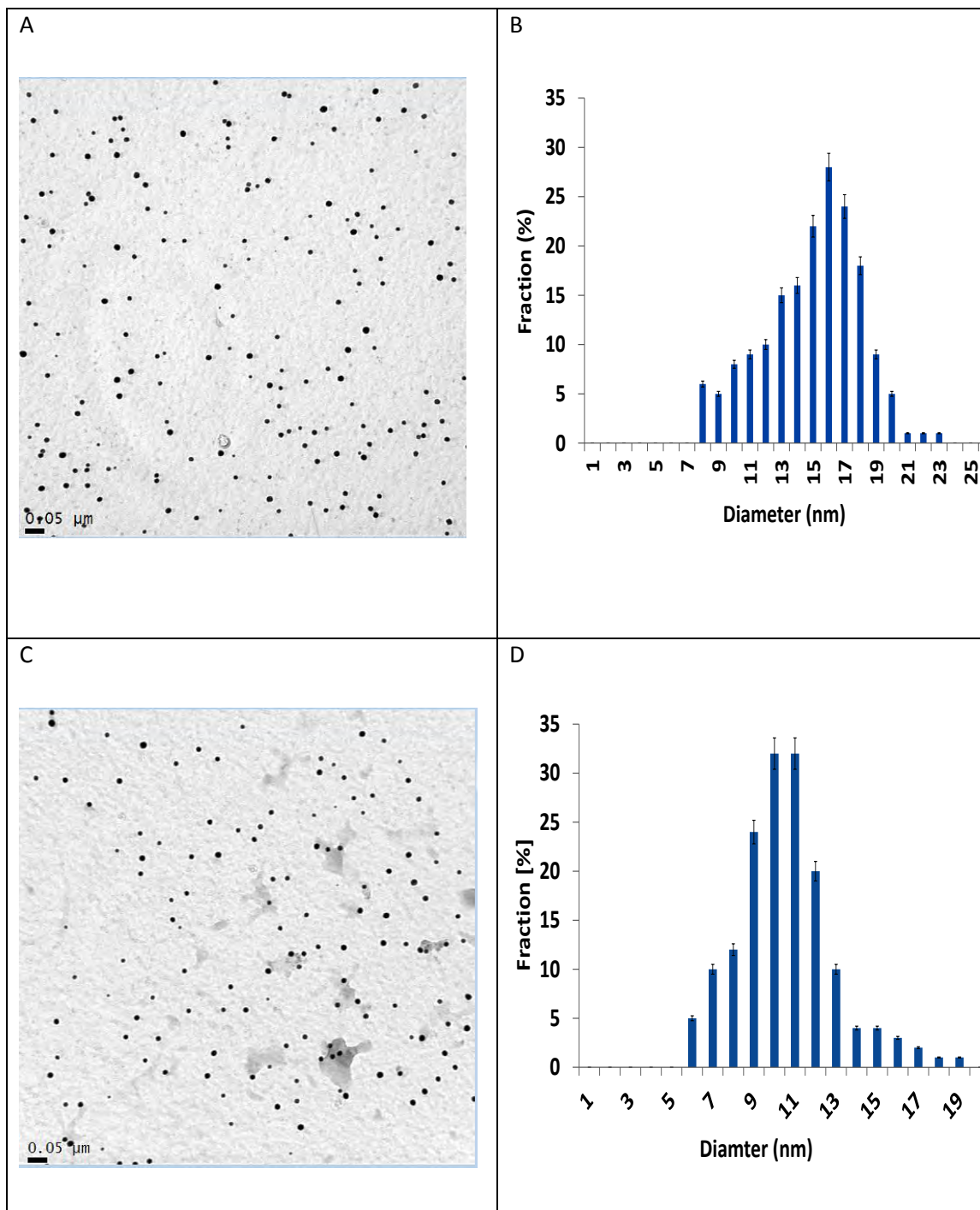


Figure 5-6, shows the size distribution spectra of the citrate capped NM respectively. The hydrodynamic diameter (z-average) of cit-AuNMs  $20.78 \pm 1.8$  and having low polydispersity index of 0.17. To compare the size distribution with other techniques see Table 5-1. While the zeta potential measures the electric charge on the surface of the NMs. Surface charge of Cit-Au NMs have a high surface charge (zeta potential =  $-43 \pm 1.3$  mV). Cit-Au NMs are charge stabilized.

#### **5.4.4 Particle spherical diameter measurement by TEM**

For the measurement of particle size, the NMs in the suspensions needed to be dried on to the substrate later imaging by TEM were performed. Transmission electron microscopy (TEM) imaging is more preferred method to measure the core size of the particle since gold cores look distinctively darker than the capping agents as well as when NMs added to environmental relevant conditions (Leppard, 2008). The reason for the darkness of the core is higher electron densities (Wang, 2000). The procedure / sampling technique to dry the NMs on the substrate for the purpose of TEM imaging is given in detail in Chapter 4 and in Section 4.3, various sampling technique methods were also described in methodology chapter.

To obtain higher accuracy in the measurement of NM size, total of 40 TEM images were utilised and approximately 2000 NMs diameter were measured. The size of NMs was measured by using Gatan Digital Micrograph (available from TEM - Tecani Philips F20 oxford instrumentation) and Image J software. Table 5-1 shows the particle spherical diameter measurement by TEM technique, for both citrate and PVP capped Au NMs.



**Figure 5-7:** Particle size distribution as measured by transmission electron microscopy: (A and B) Citrate capped Au NMs ( $15\pm 3.3$ ) and (C and D) PVP capped Au NMs ( $10\pm 2.8$ ). To obtain higher precision in the size measurement nearly 2000 particles are considered for measuring diameter of the particle using  $\sim 40$  images.

**Table 5-2: Particle spherical diameter measurement by TEM**

Coating of AuNMs	Equivalent spherical diameter (nm) TEM	Range of NMs (nm)	% NMs <15nm based on measured sizes b TEM
Citrate	15±3.3 (0.22)b	8-23	83%
PVP	10±2.8 (0.28)b	6-18	95%

b () coefficient of variation = standard deviation/mean

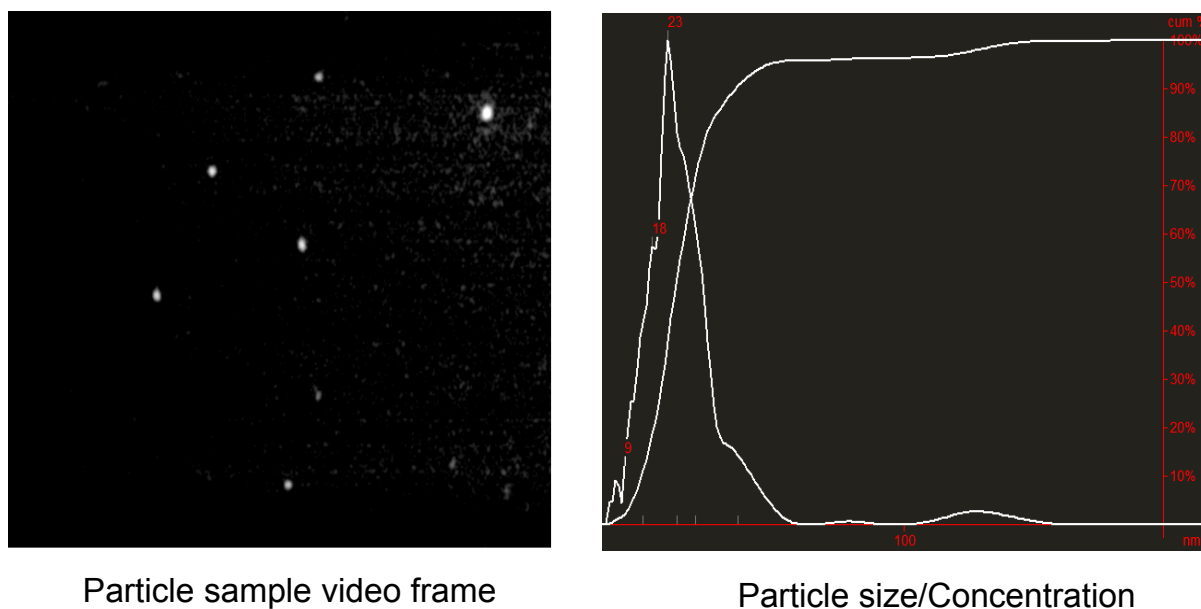
TEM: Transmission Electron Microscopy

The number size distribution of the citrate capped Au NMs and PVP capped Au NMs measured by TEM together with the fitted distribution functions are shown in Figure 5-7. The number average size of citrate capped Au NMs and PVP capped Au NMs was found to be around 15.0±3.3 nm (with a range 8-23 nm) and 10.0±2.8 nm (with a range 6-18 nm) (see Table 4-2), respectively. The coefficient of variation was about 0.22 and 0.28 for cit-Au NMs and PVP capped Au NMs respectively, suggesting that the two suspensions of NMs have relatively low polydispersity.(Baalousha et al., Baalousha and Lead, 2013b) Both NMs contain a high% of NMs smaller than 15 nm; 83% and 95% for cit-Au NMs and PVP-Au NMs, respectively. Also, both NMs are spherical (Figure 5-12). The larger sizes measured by DLS can be attributed to the weighting (intensity based for DLS) and the permeability of the NMs, in particular the PVP-Au NMs(Baalousha, 2012).

#### **5.4.5 Hydrodynamic diameter measurement by NTA**

The NM suspension will be injected to the NTA chamber specially designed optical flat (see methodology Chapter 4) integrated to optical microscope and computer (Carr et al., 2011), where Brownian motion can be visualised on the computer screen with the help of the

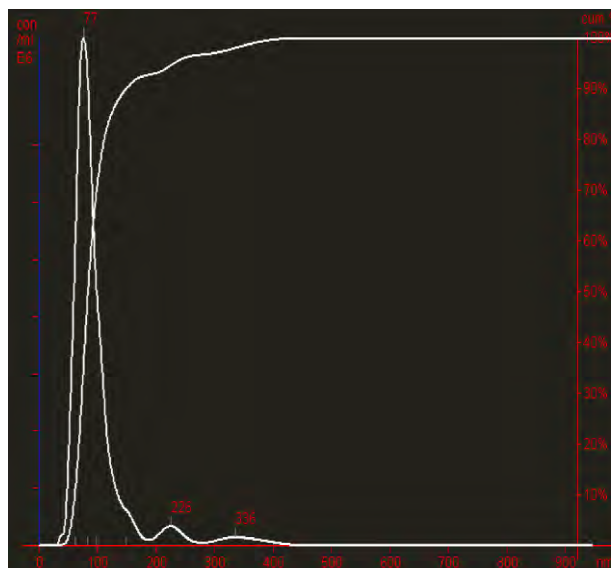
NTA software. NM suspension with very low concentration needed to be injected to the optical chamber to visualise the non-aggregated NMs. In this investigation, NM stock solution was diluted to 100,000 times for both citrate and PVP capped Au NMs and then injected to the optical chamber of NTA instrument. Experimental procedure to measure the hydrodynamic diameter of NMs was given in detail in methodology Chapter 4 and in subsections 4.5.2. The NTA software allowed capturing the still images of the moving NMs as seen in the Figure 5-8 and Figure 5-9 for citrate capped and PVP capped Au NMs respectively.



**Figure 5-8** Particle sample video frame and its size representation obtained from the NTA technique for citrate capped AuNMs having size range of 23 nm.



Particle sample video frame



Particle size/Concentration

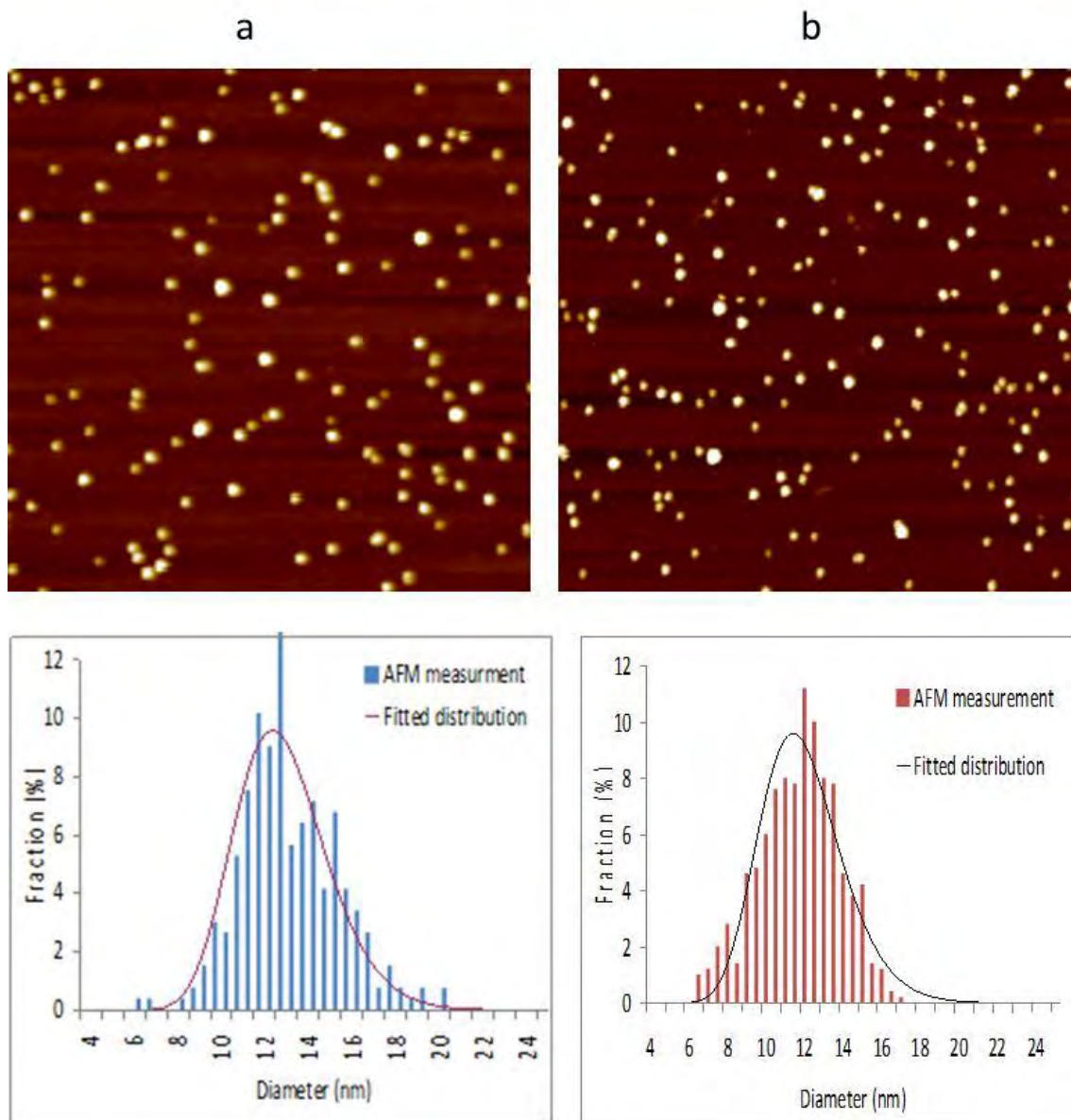
**Figure 5-9** Particle sample video frame and its size representation obtained from the NTA technique for citrate capped Au NMs having size range of 77 nm.

The number average hydrodynamic diameter measured by NTA was generally higher than the z-average hydrodynamic diameter measured by DLS and the number average diameter measured by TEM for citrate Au NMs is 23 nm (Figure 5-8) and for PVP-Au NMs is 77 nm. This is likely due to the lower size detection limit of NTA (*ca.* 10-15 nm for Au NMs) (Carr, 2012), which induces a bias toward larger size as the NMs studied in this article contains a significant fraction of NMs < 15 nm (Table 5-4).

#### **5.4.6 Particle height measurement by (AFM)**

To measure the height of NM using AFM technique, NMs in the suspension have to be dried on the substrate. The sample preparation technique was given in detail in methodology Chapter 4 and in subsection 4.3.3. Figure 5-10 (a and b) shows the micrograph obtained by the AFM technique for both citrate and PVP capped Au NMs respectively. The height of the particle is measured by the AFM (Park Systems Corp., Suwon, Korea) using software provided by the AFM instrument called XEI data processing and analysis software where the line profile panel of XEI software displays the cross-sectional height profile of the particle. For each sample, a minimum of 200 NMs height measurements were performed, which are sufficient to produce a representative particle size distribution (Baalousha, 2012). Table 5-2 shows the particle spherical diameter measurement by AFM technique, for both citrate and PVP capped Au NMs.





**Figure 5-3.** Particle size distribution as measured by atomic force microscopy (A) Cit-Au NMs ( $13.3 \pm 2.1$ ) and (B) PVP-Au NMs ( $12.2 \pm 2.2$ ) nm.

**Table 5-3:** Particle height measure using AFM technique

Coating of Au NMs	Range of NMs (nm)	Particle height (nm) AFM
PVP	6.5-17	$12.2 \pm 2.2(0.18)$ b
Citrate	6.5-21	$13.3 \pm 2.1(0.16)$ b

b ( ) coefficient of variation = standard deviation/mean

AFM Atomic force microscopy

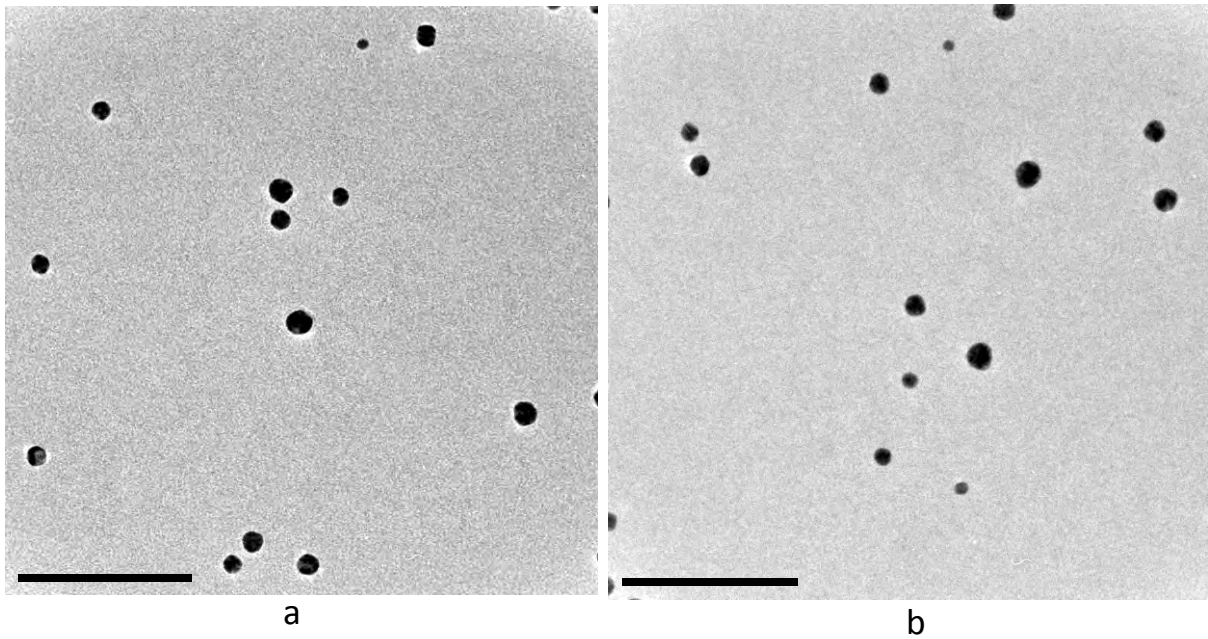
The height of particle obtained by the AFM technique i.e. number size distribution of the cit-Au NMs and PVP-Au NMs together with the fitted distribution functions are shown in Figure 5-10. The average size of cit-Au NMs and PVP-Au NMs was found to be around  $13.3 \pm 2.1$  (with a range 6.5-21 nm) and  $12.2 \pm 2.2$  (with a range 6.5-17 nm), respectively. The coefficient of variation was about 0.16 and 0.18 for PVP-Au NMs and cit-Au NMs respectively, suggesting that the two suspensions of NMs have relatively low polydispersity (Baalousha and Lead, 2013b). The size of NM, having varied between 1-10 nm, said to be nanocluster resulting in narrow size distribution, these have special properties (Qin et al., 2014) hence these particles have technological interests especially in microelectronics, data storage and so on.

#### 5.4.7 Particle shape factor

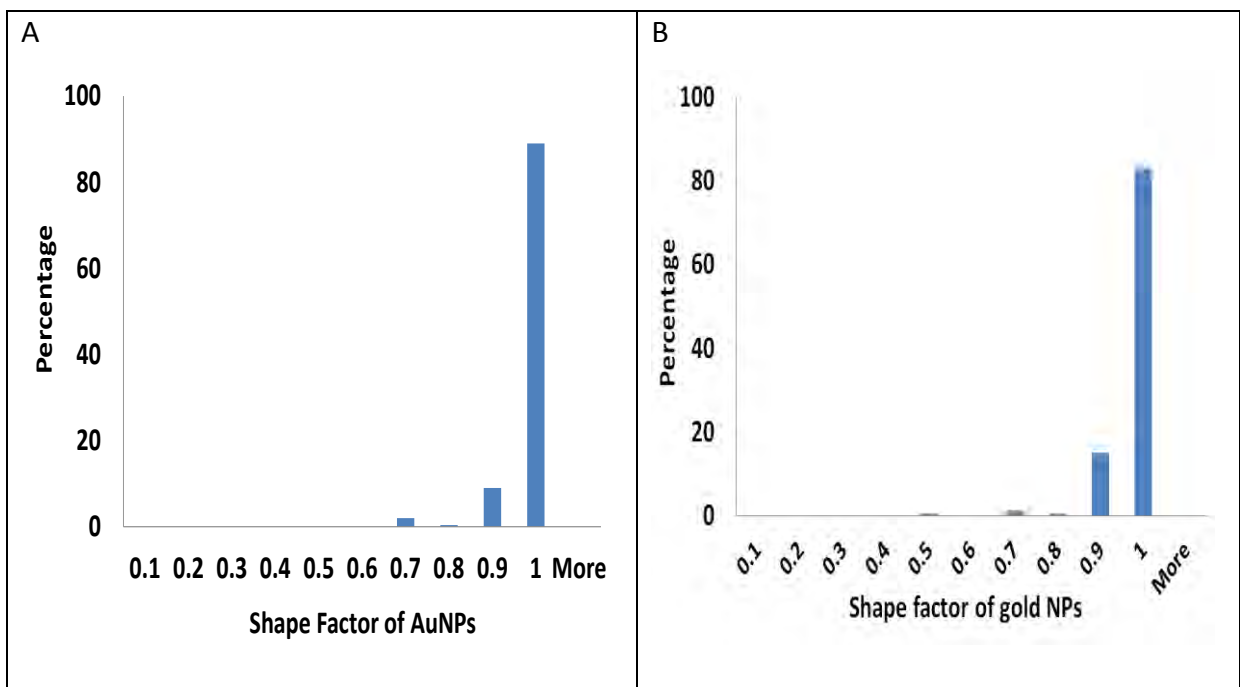
Shape of the particles is very important for toxicity studies (Pal et al., 2007) but less known about its effect on environmental processes. Particle shape can be measured by the circularity factor, C (Fernandez-Garrido et al., 2014) which can be defined by the equation 5-1.

$$C = \frac{4\pi A}{P^2} \quad \text{Eq.5-1}$$

where, A and P are the area and perimeter of the NM respectively. If the particle is spherical then the circularity factor will be 1. Suppose if it's less than one i.e. (0.17-0.54) then the NM shape will be more elongated. For square and triangle the circularity factor will be 0.80 and 0.61 respectively. As per the synthesised NMs in this study the Au NMs both citrate and PVP capped represent spherical when imaged by TEM technique as shown in the Figure 5-11. Approximately >95% of NM synthesised have a shape factor of 1 (see below Figure 5-12), so the shape of the Au NMs synthesised are spherical.



**Figure 5-4.** TEM image of the synthesised Au NMs showing highly spherical and monodispersed



**Figure 5-5** Shape factor of (a) cit-Au NMs and (b) PVP-Au NMs calculated from the micrograph of TEM image of approximately 1500 NMs from 30 images.

For the measurement of shape of the NMs, total of 1500 NMs were considered from 30 images obtained from TEM technique. The software used to measure the shape of NMs was image J analysis. The graphical representation shows the percentage of NMs circular/spherical. As explained above, the maximum percentage (> 95%) of NMs i.e. have circularity factor 1. As per the calculation using the Equation 5-1, about 97.8 % of PVP capped NMs and 96.8 % of citrate capped NMs were having circularity factor of 1. Therefore, the in-house synthesised NMs are spherical in shape.

#### **5.4.8 Mass concentration measurement by ICP-MS**

The process of sample preparation technique for the ICP-MS measurements explained given in detail in methodology Chapter 4 and Section 4.6. The initial concentration measurements of Cit-Au NMs and PVP-Au NMs were  $101.6 \pm 3.2$  and  $167.6 \pm 3.2$  mg L<sup>-1</sup>. The dissolved fraction of AuNMs was determined following ultrafiltration (stirred ultrafiltration cell, Millipore, UK) using 1 kDa regenerated cellulose membrane (Millipore UK) and measured by ICP-MS. The percentage of dissolved gold ions was < 1%.

#### **5.4.9 Comparison of the sizes of NMs measured using different techniques**

The size measurements results of various analytical techniques were summarised in the Table 5-4 below. As shown in the Table 5-4, the DLS and NTA measured particle size will be always higher than the TEM and AFM techniques. DLS and NTA measurements were calculated from the 10 replicates while for TEM and AFM, approximately 2000 NMs were measured from 30 images using image J software. But NTA size measurements were random for each replicates due to lower size detection limit of the instrument (particles < 20 nm unable to detect) (Malloy and Carr, 2006).

**Table 5-4** Physicochemical properties of citrate and PVP coated AuNMs measured by different analytical techniques

Coating of AuNMs	Z-dh (nm) (polydispersity index) DLS	Zeta Potential (mV) DLS	Equivalent spherical diameter (nm) TEM	Particle height (nm) AFM	% NMs <15nm based on measured sizes b TEM	Number average Hydrodynamic diameter (nm) NTA	Wavelength of maximum Uv-vis absorbance
Citrate	20.78±2.6 (0.17)a	-43±1.3	15±3.3 (0.22)b	12.2±2.2(0.21)b	83%	23	519
PVP	20.14±1.8 (0.15)a	-8.3±1.6	10±2.8 (0.28)b	13.3±2.1(0.19)b	95%	53.25	525

a ( ) polydispersed index, b ( ) coefficient of variation = standard deviation/mean

Z-dh: Z-average Hydrodynamic Diameter

DLS: Dynamic Light Scattering

NTA: Nanoparticle Tracking Analysis

TEM: Transmission Electron Microscopy

AFM: Atomic Force Microscopy

Uv-vis: Ultraviolet-visible Spectroscopy

## 5.5 Characterisation of PVP Ag NMs

This section relates the detection and quantification of particle number concentration of silver nanoparticles. The synthesised silver nanoparticles of 5.54 mg/L were received from the Center for Environmental Nanoscience and Risk, University of South Carolina, USA, and exposure media from the Oregon State University, Sinnhuber Aquatic Research Laboratory (OSU/SARL), USA. In collaboration, toxicology experiments were performed whilst the measurement of particle number concentration was performed as part of this thesis.

The initial characterisation of Ag NMs capped with PVP is necessary to establish any transformations under environmental exposure conditions. It was deemed necessary to first fully characterise the physicochemical properties of the NMs as received. In order to achieve this, a multi-method approach was adopted to quantify the NM properties (Domingos et al., 2009a). Table 5-5 below summarised the results obtained by the characterisation of PVP capped Ag NMs. The following discussion is related to the NM characterisation.

**Table 5-5.** Physicochemical properties of PVP coated Ag NMs measured by different analytical techniques

Coating of AgNMs	Z-dh (nm) (polydispersity index) DLS	Zeta Potential (mV) DLS	Equivalent spherical diameter (nm) TEM	% NMs <15nm based on measured sizes by TEM	Wavelength of maximum Uv-vis absorbance
PVP	31.14±1.8 (0.25)a	-8.3±1.6	19.4±6.8 (0.38)b	81%	425

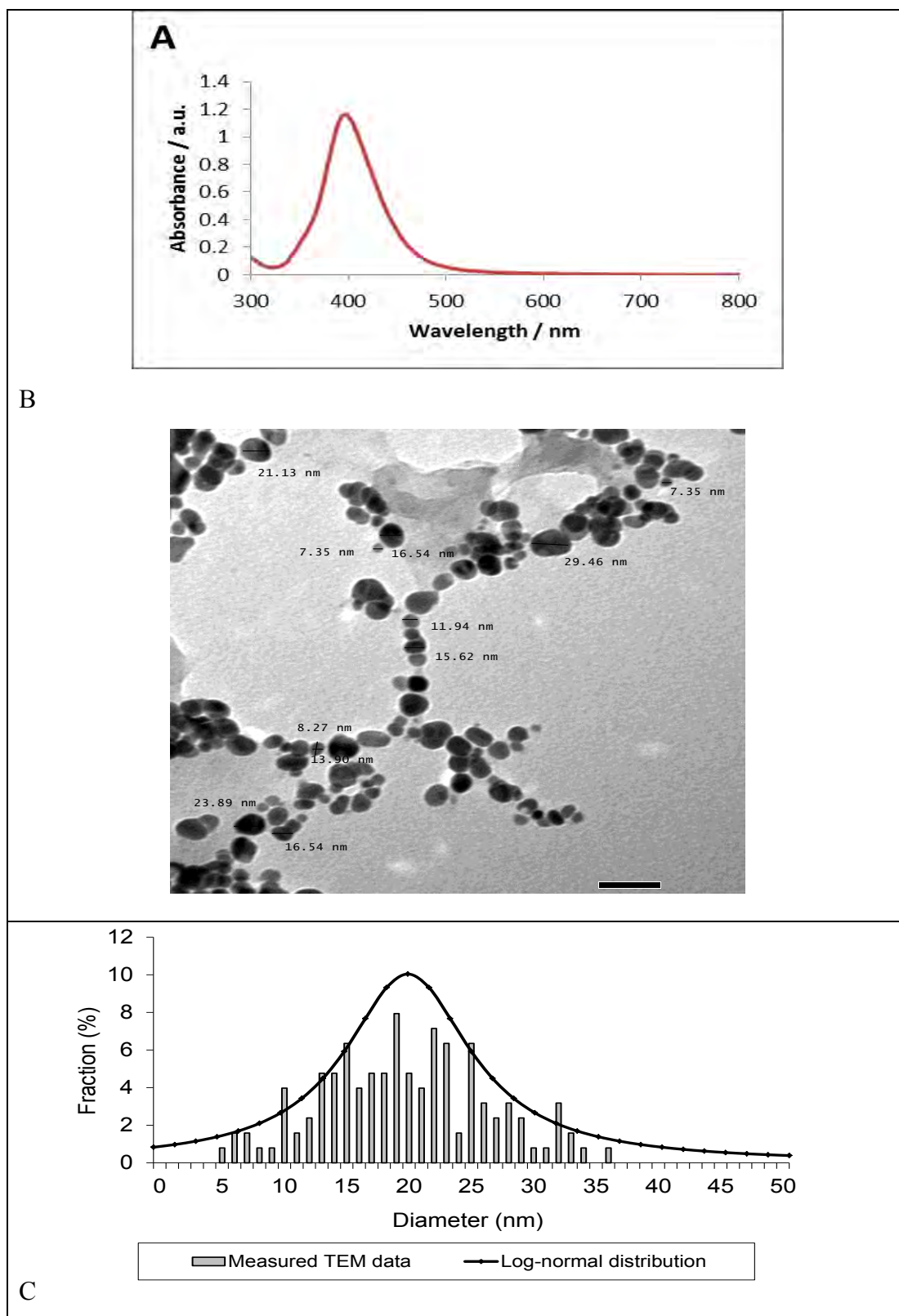
a ( ) polydispersed index, b ( ) coefficient of variation = standard deviation/mean

Z-dh: Z-average Hydrodynamic Diameter

DLS: Dynamic Light Scattering

TEM: Transmission Electron Microscopy

Uv-vis: Ultraviolet-visible Spectroscopy

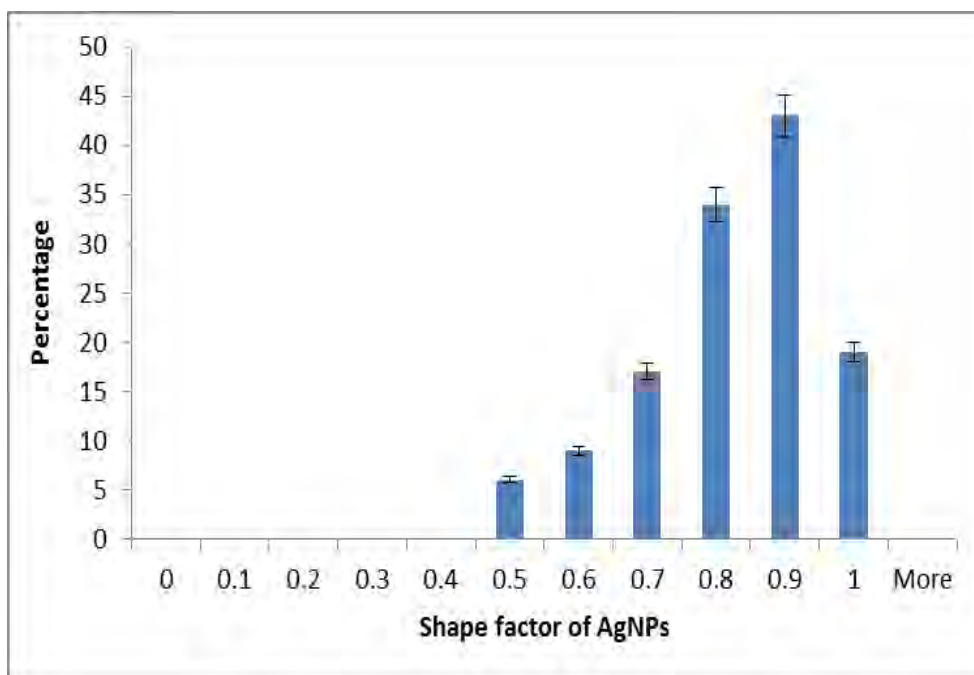


**Figure 5-13.** (A) UV-vis measurements of AgNMs PVP coated having peak absorbance Particle of 425 nm. (B and C) size distribution as measured by transmission electron microscopy of AgNMs ( $19.4 \pm 6.8$  nm) suspended in UHPW and ultracentrifuged on poly-l-lysine functionalized TEM substrate.

Firstly, spherical diameter of the Ag NMs the TEM imaging was carried out. TEM facilitates the accurate diameter of NM (Nowack and Bucheli, 2007), explained in detail further. The PVP capped Ag NMs were ultracentrifuged by forcing the NMs to retain on surface by PLL functionalisation of the substrate i.e. improvised sampling technique protocol validated previously for the Au NMs. The substrate was imaged on different parts of the TEM grid by TEM technique and used nearly 20 images for the size measurements. Figure 5-13 (A) shows the uv-vis spectra of Ag NMs having the absorbance peak at 425 nm. The stability test of Ag NMs was not required since the characterisation and particle number measurements were carried out by freshly prepared Ag NMs.

Figure 5-13(B) shows the micrograph of transmission electron microscopy of PVP capped Ag NMs. The size of the Ag NMs was of the individual NMs was measured, about 2000 NMs were measured from a set of TEM images to obtain the accurate range of NM size. The size distribution of NMs from the electron micrographs were analysed using the imaging software Image J. The number size distribution of the PVP capped Ag NMs measured by TEM together with the fitted distribution functions are shown in Figure 5-13(C). The number average size of PVP capped Ag NMs was found to be around  $19.4 \pm 6.8$  nm (with a range 5-35 nm). The coefficient of variation was about 0.38 for PVP-AgNMs respectively, suggesting that the suspensions of NMs have relatively high polydispersity.(Baalousha et al., Baalousha and Lead, 2013b) Both NMs contain a high% of NMs falls in the range of 4 - 25 nm. Hence, Ag NMs are polydispersed having wider range of NMs.

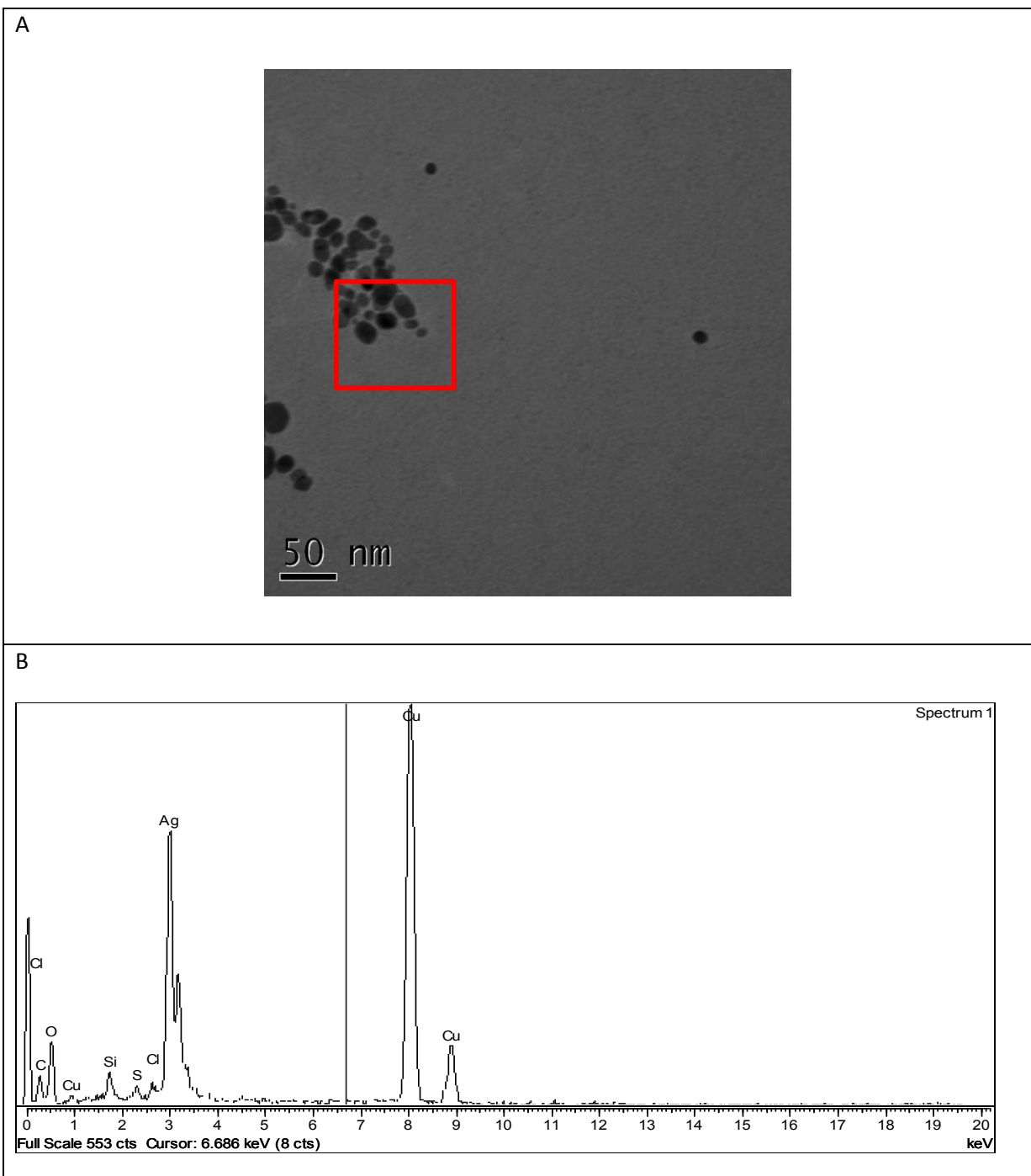




**Figure 5-14.** Shape factor of Ag NMs calculated from the micrograph of TEM image of approximately 2000 NMs.

While the shape of NMs is vital part of the physicochemical characterisation since the particle shape is very significant to the toxicity studies (Asharani et al., 2008, Bar-Ilan et al., 2009). The above Figure 5-14 shows the graphical representation of the percentage of NMs having a range of shape factor (0.5 to 1) The shape factor was calculated by using the formula circularity factor, C (Fernandez-Garrido et al., 2014) (detailed in Section 5.3.7). The average shape factor for Ag NMs was found to be  $0.773 \pm 0.127$ . Therefore, as per the standards stated (Lead et al., 1999) the shape of the NMs was slightly elongated.

Energy Dispersive X-ray Spectroscopy gives an elemental composition of NM as synthesised is shown in Figure 5-15 for the micrograph. This confirms the presence of Ag NMs in the suspension. The elemental composition obtained from this analysis is given in the Table 5.6.



**Figure 5-15** EDX spectra of Ag NMs obtained from the Tecnai Philips F20 TEM

**Table 5-6** Elemental analysis for NMs as obtained by EDX

Element	Carbon	Oxygen	Silicon	Sulphur	Chlorine	Copper	Silver
Weight / %	1.51	2.77	1.04	0.34	0.08	41.34	62.55

## 5.6 Conclusion

The main objective of this chapter is to synthesise the very well monodispersed nanoparticles having good quality and to perform characterisation. Gold nanoparticles with two different capping agent PVP and citrate were synthesised. Also range of sizes of NMs was synthesised. Characterisation of these nanoparticles is a prerequisite prior to the exposure to the realistic environmental conditions. Physicochemical properties of synthesised particles needed to be known so that the fate and behaviour of the NMs after exposure can be compared to its original properties.

After critical review for the synthesis of NMs, wet chemical method, identified as the ideal method to obtain the monodispersed NMs. To measure the physicochemical properties of these NMs range of different techniques both spectroscopies and microscopies were employed. In brief, physicochemical properties analysed for the in-house synthesised citrate and PVP capped Au NMs were as follows:

- i. size measurements by techniques such as NTA, DLS, TEM and AFM,
- ii. concluded the NMs are spherical in shape by TEM imaging and the small variation in the shape of NMs plays a key role when penetrates to human cell (Schaeublin et al., 2012) may be toxic. But less known effects in environmental relevant conditions.
- iii. from ICP-MS it is confirmed that 99.2% of gold ions were converted into NMs and percentage dissolved gold ions found to be < 1%
- iv. while from DLS technique identified the NMs were more stable by surface charge measurements and monodispersed by obtaining sharp observance peak as well as stability test was performed quarterly for 24 months and

- v. monodispersity is also calculated using TEM by identifying 95% and 83 % of the NMs < 15 nm for PVP-Au NMs and cit-Au NMs respectively.

Both Au NMs coated with citrate and PVP were fully characterised, extremely good quality will be used for the measurement of particle number concentration. In order to measure the particle number, these NMs will be added to the ultra high purity water (UPHW) (simple media) and also exposed to the realistic environmental conditions (complex media) to know their fate and behaviour analysed.

Hence fully quantitative assessment of the measurement particle number will be presented both in simple and complex media in the following upcoming chapters.

## **Chapter 6 Number concentration measurement of citrate and PVP AuNMs by simple media using AFM technique**

### **6.1 Chapter Summary**

This chapter presents results and discussion of particle number measurement of citrate Au NMs and PVP capped Au NMs by using the technique atomic force microscopy (AFM). As previously stated in Section 4.3, sampling technique is a critical part and has been limited by the sample preparation rather than by the capability of microscopy techniques to count and measure the size of NMs. After analysing many techniques provided in literature, in this study ultracentrifugation is considered as appropriate sampling techniques. Also ultracentrifugation technique is improvised and enhanced by surface functionalisation see Section 4.3.3. In this chapter both the functionalised and non-functionalised substrates were imaged by AFM and the recovery of NMs obtained by these substrates is shown as an evident to look at the difference between the sampling techniques employed. The analysis of two different types of substrate functionalisation carried out was (i) ultracentrifuged with substrate functionalisation by Poly-L-lysine (PLL) polymer and (ii) addition of  $\text{CaCl}_2$  to the NM suspension before ultracentrifugation. These two techniques were employed to obtain the uniform distribution between the images, as well as NM retention and recovery on the substrate were also considered to be very important for the particle number measurement. Image analysis was carried out to obtain uniformity of distribution between the images explained in detail.

The first section of this chapter is related to the distribution of nanoparticles on the substrate. While the second section presents the percentage recovery of NMs on the substrate and later sections on correlation between with the particle number concentration and the known mass concentration measured by ICP-MS.

Lastly, particle number measurements of the NMs and the number of images required for the measurement of the particle number is presented in detail. The results

obtained from this chapter have been published in Environmental Science: Processes and Impacts on 25 February 2014. This paper is attached at the end the thesis in Appendix B.

## 6.2 Distribution of NMs on the AFM substrate

Distribution of NMs on the substrate is the uniformity of the NMs arrangement between the set of 30 images scanned per substrate. Total six substrates were prepared each having a different concentration of NMs ranging from higher concentration to lower concentration (33.5-670.5 ppb, See Figure 6-1). The number of NMs on each substrate is a concentration dependent. The higher concentration of NM suspension must have higher number of NMs on the substrate having uniform distribution between the images and vice versa. This is further explained in detail in methodology Chapter 4 and in subsection 4.7.5.

Distribution of NMs on the substrate was analysed with different sample preparation techniques and different media. The sample preparation and different media analysed are as follows:

- (i) Non- functionalisation of substrate - means without treating substrate with PLL. Precipitation of Au NMs with simple media (adding Au NMs ultra-high purity water) by ultracentrifugation method of sampling technique.
- (ii) Adding  $\text{CaCl}_2$  to the NM suspension before ultracentrifugation
- (iii) PLL functionalisation of substrate - means treating substrate with PLL before ultracentrifugation, Au NMs suspended in UHPW and
- (iv) PLL functionalization sampling method with complex media i.e. adding Au NMs to natural surface water, Suwannee river fulvic acid and EPA synthetic soft water.

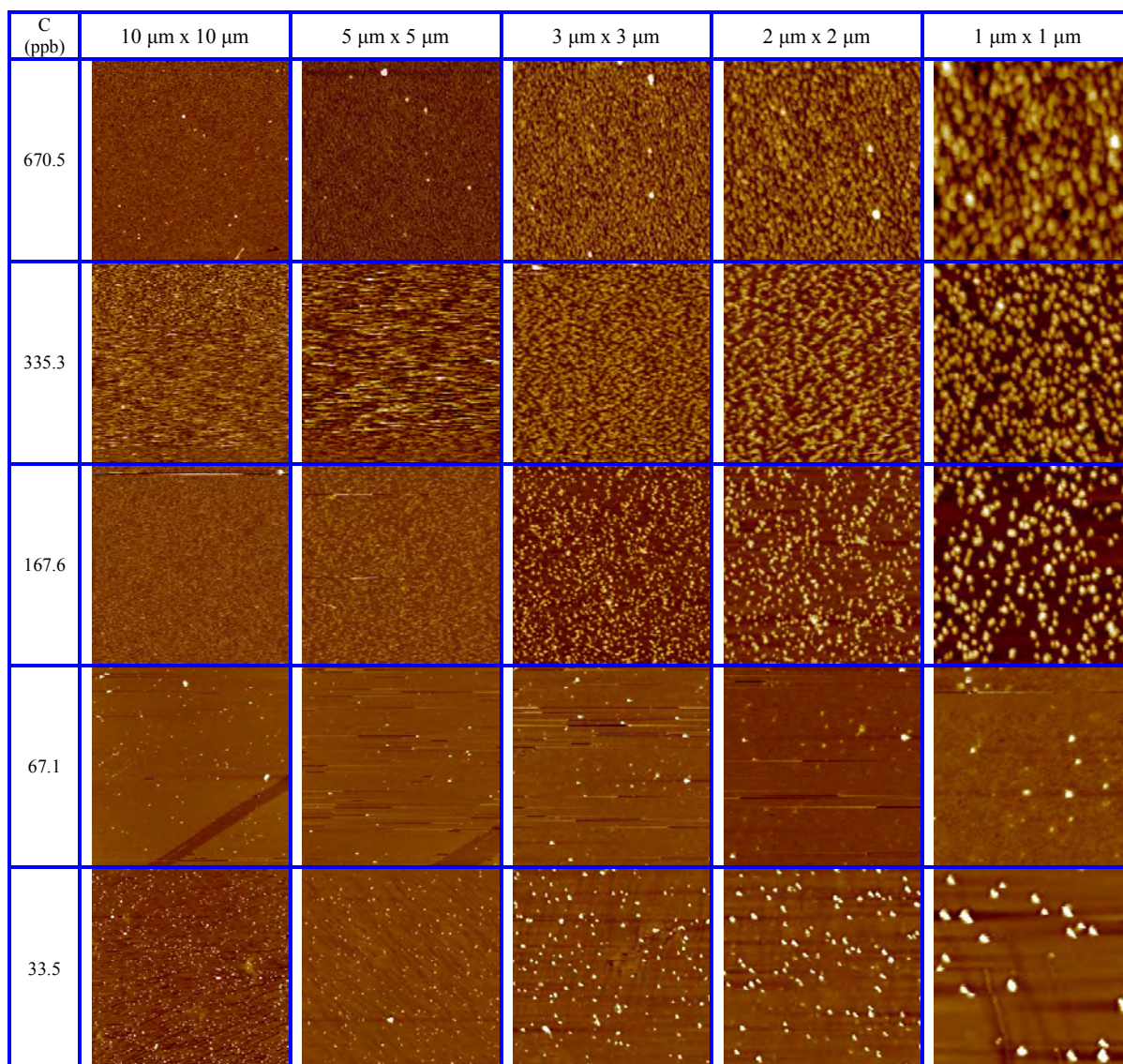
By employing above mentioned sampling techniques with different media, substrate for AFM imaging was prepared. The distribution of NMs on the substrate was imaged and given in detail in the following sections.

### **6.3 NM suspension on non-functionalised substrate**

AFM images of PVP capped Au NMs and citrate capped Au NMs suspended in ultra-high purity water (UHPW) at the range of concentrations is shown in the Figure 6-1, Figure 6-2 and Figure 6-3 respectively. The AFM substrates were not functionalised by PLL.

#### **6.3.1 PVP capped Au NMs on non-functionalised substrate**

Five AFM substrates were prepared each having different NM concentration as explained in the methodology Chapter 4 and in subsections 4.3.2. As shown in the Figure 6-1, shows the distribution of PVP capped Au NMs having different concentration such as the 670.5 ppb, 335.3 ppb, 167.6, 67.1 and 33.5 ppb. The distribution of PVP capped Au NMs at concentrations such as 670.5 ppb, 335.3 ppb and 167.6 ppb are found to be overloaded. On further dilution of the samples to 67.1 ppb and 33.5 ppb, the distribution of NMs found to be non-uniform or random distribution. In some areas, no NMs were observed and in other areas high number of NMs and aggregates were observed. This suggests that the NMs were not attached strongly to the AFM substrate and detached from and re-deposited during substrate washing resulting in losses of NMs at some areas and aggregation of NMs at other areas.

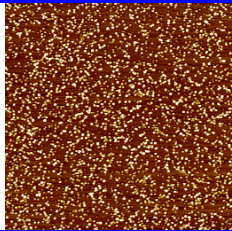
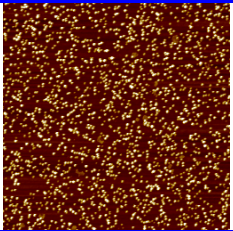
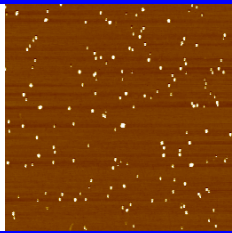
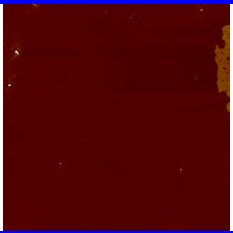
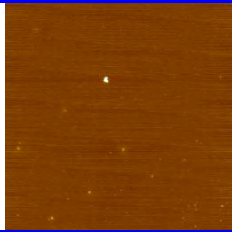
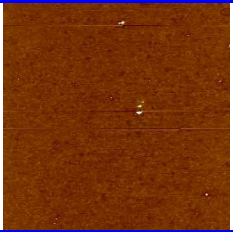

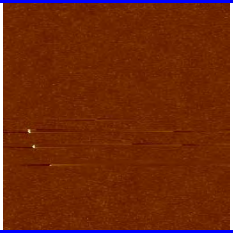
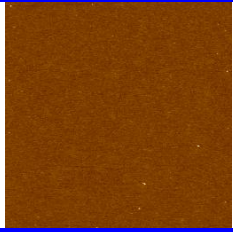


**Figure 6-1** AFM micrographs of PVP capped Au NMs suspended in UHPW and ultracentrifuged on freshly cleaved non-functionalised mica substrate at different concentrations of Au NMs (33.5-670.5 ppb).

The uniformity of NM distribution on the substrate is crucially important to avoid the bias in counting the number of NMs. If an area of low/high number of NMs is imaged and used to calculate number particle concentration in the ultracentrifuged suspension that results in the inaccurate particle number measurements. Thereby, the uniformity in the distribution of NMs between the different images is more vital for further analysis for the quantification of particle number. Further dilution were carried out, different



concentration diluted were 16.8, 3.4 and 1.7 ppb to have additional analysis on the distribution of NMs with the ultracentrifugation method of sample preparation without surface functionalisation.

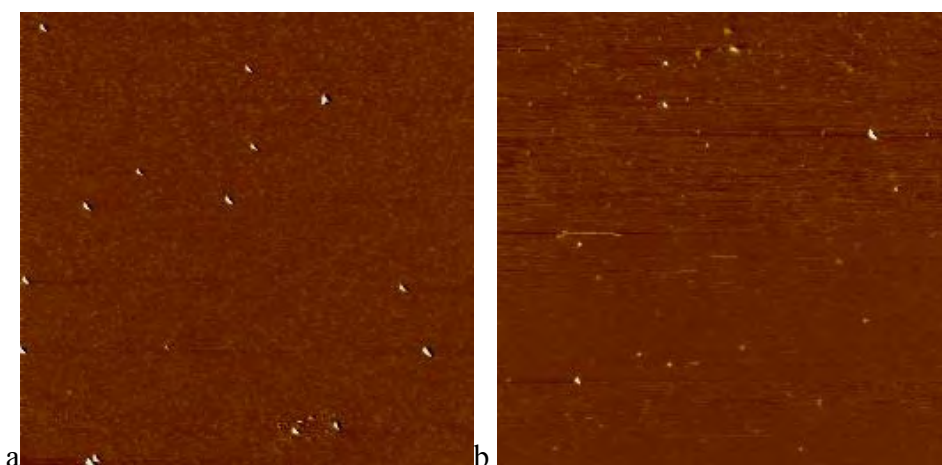
C (ppb)	Batch 2	Bach 3
67.1		
33.5		
16.8		
3.4		
1.7		NA

**Figure 6-2** AFM micrographs (5  $\mu\text{m}$  x 5  $\mu\text{m}$ ) of PVP capped Au NMs suspended in UHPW and ultracentrifuged on freshly cleaved non-functionalised mica substrate at different concentrations of Au NMs (1.7-67.1 ppb).

NA: not analysed

Similarly in Figure 6-2, shows the distribution of PVP capped Au NMs further diluted at different concentration where the distribution of NMs were still found to be non-uniform and few NMs were aggregated. While at the concentration of 33.5 ppb, large population of NMs were found in batch 2 while none of the NMs were seen in batch 3 (see Figure 6-2), for the same concentration (33.5 ppb) the distribution of NMs quantitatively varied between the images. Furthermore analysis was carried out for the citrate capped Au NMs having ultracentrifugation method of sampling technique without surface functionalisation.

### 6.3.2 Citrate capped Au NMs on non-functionalised substrate



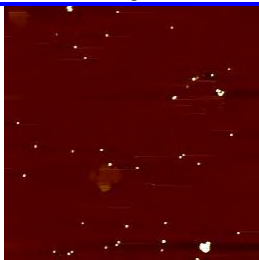
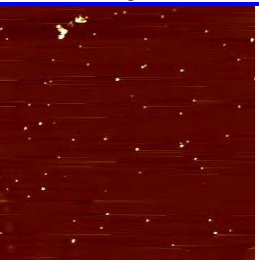
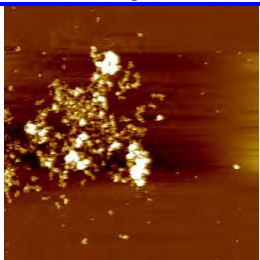
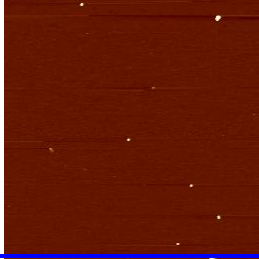

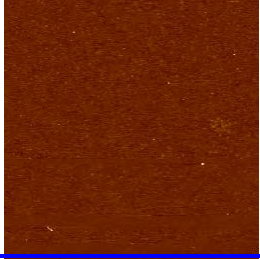

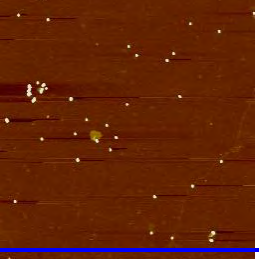
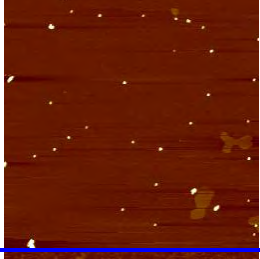
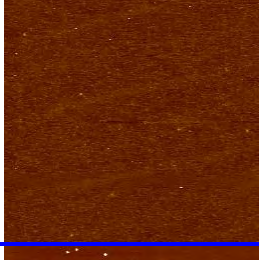
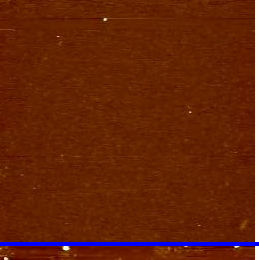
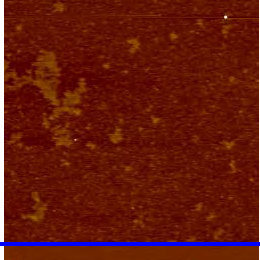
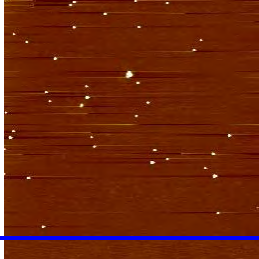
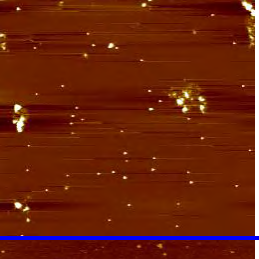
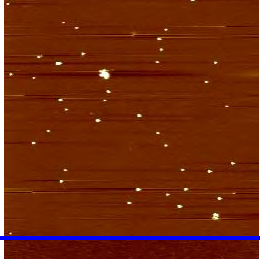
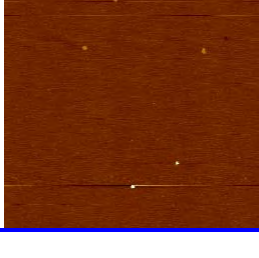
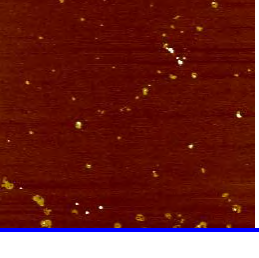
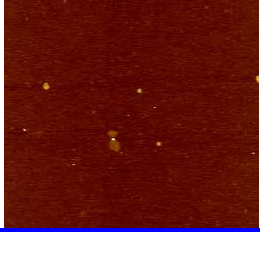
**Figure 6-3** AFM micrographs (5  $\mu\text{m}$  x 5  $\mu\text{m}$ ) of Cit-AuNMs in ultrahigh purity water (UHPW) prepared on freshly cleaved non-functionalised mica substrate at different concentrations (a) 101.6 ppb Au and (b) 40.64 ppb Au.

Further Figure 6-3 shows the AFM images for citrate capped Au NMs having non-uniform distribution between the images. Mainly due to the losses of NMs on the substrate or to the AFM tip interaction on the surface of the substrate while scanning. To prevent the loss of NMs or further particle interaction once sorbed, it is vital to functionalise the substrate surface to retain/adhere the NMs during the process of ultracentrifugation. This process is explained in detail in methodology Chapter 4 in the Section 4.3.3.

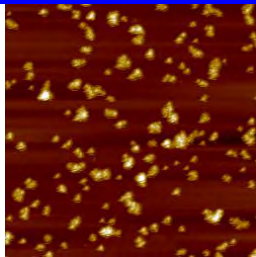
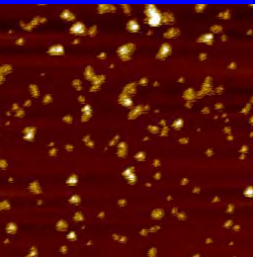
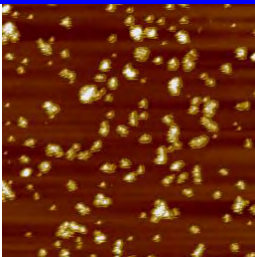
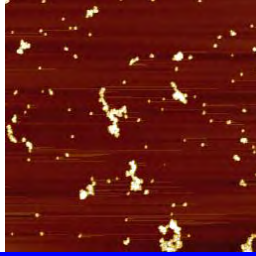
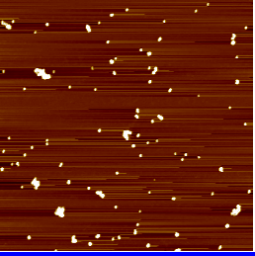
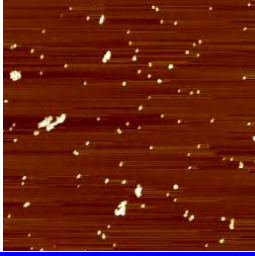
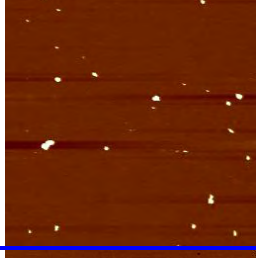
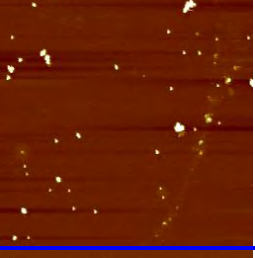
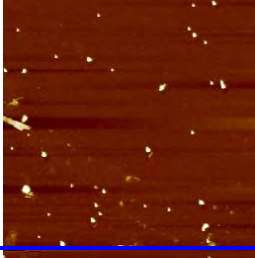
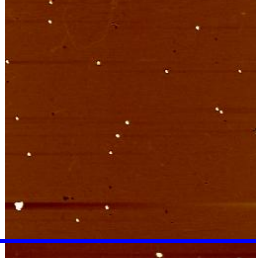
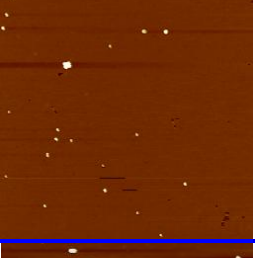
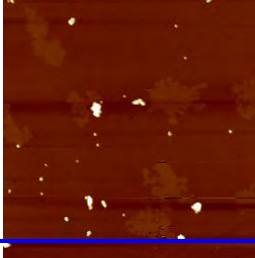
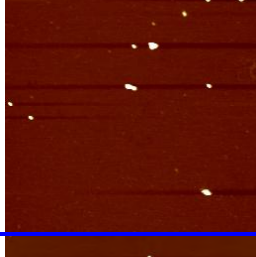
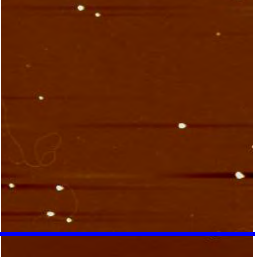
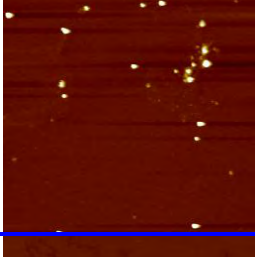



The following section is based on the discussion on the uniformity in NM distribution on the substrate by adding  $\text{CaCl}_2$  to the NM suspension before ultracentrifugation and its results explained in next section.

### **6.3.3 Adding $\text{CaCl}_2$ to the NM suspension before ultracentrifugation**

The procedure followed for the sample preparation by adding  $\text{CaCl}_2$  to NMs is given in detail in Chapter 4 and in Section 4.3.3. The AFM micrographs of citrate capped Au NMs suspended in  $100\ \mu\text{M}$ ,  $\text{CaCl}_2$  and ultracentrifuged on the non-functionalised mica substrate. At different concentration of Au NMs from 1 ppb to 203.2 ppb is shown in the Figure 6-4, for  $100\ \mu\text{M}$   $\text{CaCl}_2$  and ultracentrifuged on a freshly cleaved mica substrate. From these images it was found that for citrate coated NMs at higher concentration of  $\text{Ca}^{2+}$  ions results in improved distribution but not for all the images, still  $\text{Ca}^{2+}$  ions resulted in aggregation and therefore not been investigated. The reason for the improved distribution by the addition of  $\text{CaCl}_2$  is likely due to the bridging of  $\text{Ca}^{2+}$  of the negatively charged mica surface and negatively charged PVP coating. At higher concentration 203.2 ppb and 101.6 ppb found be randomly distributed between the images and also aggregation was observed on few images. Again at lower concentration at 10.2 ppb, NM distribution was not uniform and less NMs were observed between the images but at further more lesser concentration 2 ppb, the number NMs found to be more when compared to the 10.2 ppb. Therefore, the addition of  $100\ \mu\text{M}$   $\text{CaCl}_2$  to NM samples resulted in the non-uniform NM distribution between the images. Similarly, the distribution of NMs were analysed by adding higher concentration of  $200\ \mu\text{M}$   $\text{CaCl}_2$  to the NMs.

C (ppb)	Image 1	Image 2	Image 3
203.2			
101.6			
20.3			
10.2			
2.0			
1.0			

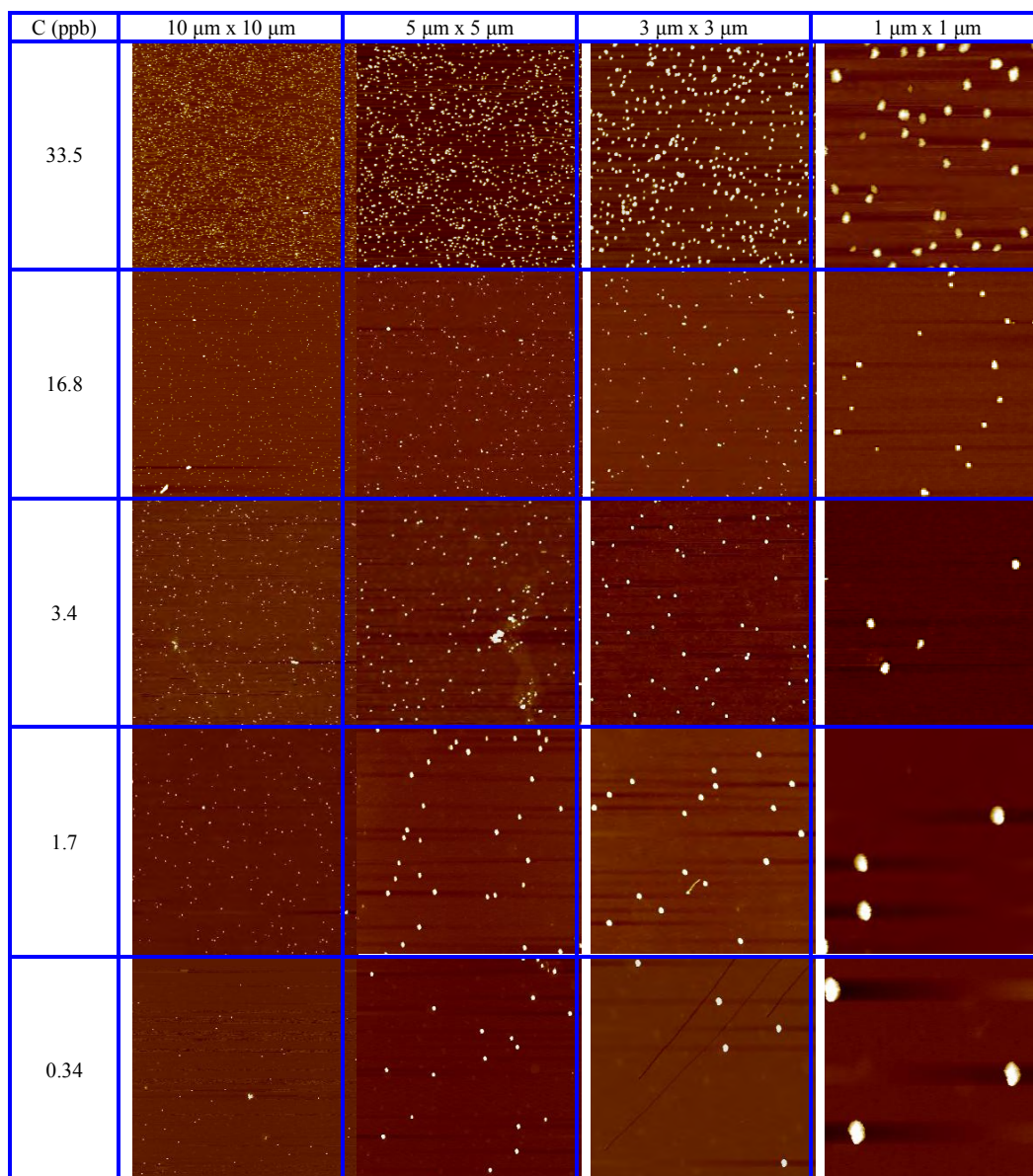
**Figure 6-4** AFM micrographs (5  $\mu\text{m}$  x 5  $\mu\text{m}$ ) of Cit-AuNMs suspended in 100  $\mu\text{M}$   $\text{CaCl}_2$  and ultracentrifuged on freshly cleaved non-functionalised mica substrate at different concentrations of AuNMs (1-203.2 ppb) expressed as ppb Au.

C (ppb)	Image 1	Image 2	Image 3
203.2 2um x 2um			
101.6 3um x 3um			
20.3 3um x 3um			
10.2 3um x 3um			
2.0 3um x 3um			
1.0 3um x 3um			

**Figure 6-5** AFM micrographs (5  $\mu\text{m}$  x 5  $\mu\text{m}$ ) of Cit-AuNMs suspended in 200  $\mu\text{M}$   $\text{CaCl}_2$  and ultracentrifuged on freshly cleaved non-functionalised mica substrate at different concentrations of AuNMs (1-203.2 ppb) expressed as ppb Au.

Further addition of 200  $\mu\text{M}$ ,  $\text{CaCl}_2$  to citrate capped Au NMs and ultracentrifuged on a non-functionalised freshly cleaved mica substrate, Figure 6-5 shows the images at different concentration of Au NMs from 1 ppb to 203.2 ppb. From these images it was found that for citrate coated NMs at higher concentration of  $\text{Ca}^{2+}$  ions results in improved the distribution of NMs (see Figure 6-5) but not for all the images when compared with the 100  $\mu\text{M}$ ,  $\text{CaCl}_2$ , still  $\text{Ca}^{2+}$  ions resulted in aggregation. At higher concentration that is, of 203.2 ppb and 101.6 ppb NMs were randomly distributed between the images and also aggregation was observed on few images. But at lower concentration from 20.3 ppb to 1.0 ppb, NM distribution was improvised between the images. Therefore, the addition of 200  $\mu\text{M}$   $\text{CaCl}_2$  to NMs resulted in the uniform NM distribution when between the images when compared to 100  $\mu\text{M}$   $\text{CaCl}_2$  but still may be loss of NMs which is quantitatively analysed in later discussions.

For the PVP AuNMs the addition of 10 mM  $\text{CaCl}_2$  ultracentrifuged on bare AFM resulted in uniformity in the NM distribution between the images (see Figure 6-6). The uniformity in distribution between the images is possibly due to the bridging by  $\text{Ca}^{2+}$  of the negatively charged mica surface and the partially negatively charged PVP coating (Baalousha and Lead, 2013b). Therefore, addition of divalent cations to sterically stabilized NMs combined with ultracentrifugation can be used to improve the uniformity of NM distribution on the AFM substrate. But at 10 mM  $\text{CaCl}_2$  ultracentrifuged on non-functionalised AFM as shown in Figure 6-8, still few aggregates were present.



**Figure 6-6** AFM micrographs of PVP-Au NMs (5  $\mu\text{m}$  x 5  $\mu\text{m}$ ) suspended in 10 mM  $\text{CaCl}_2$  and ultracentrifuged non-functionalised mica substrate at different concentrations of Au NMs (0.34-33.5 ppb) expressed as ppb Au.

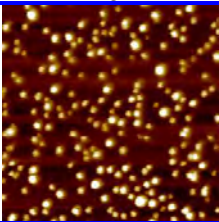
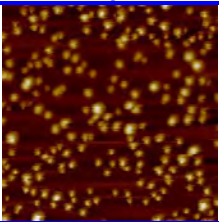
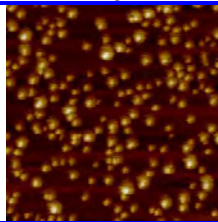
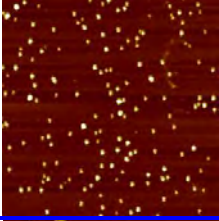
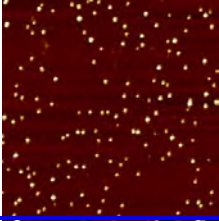
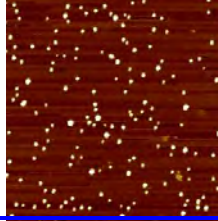
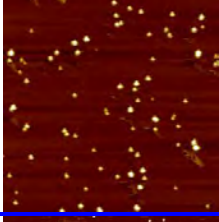
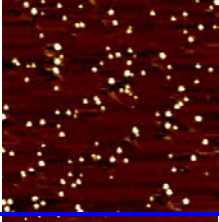
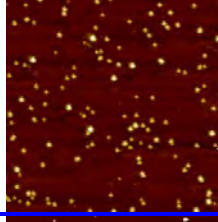
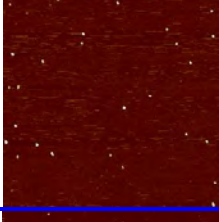
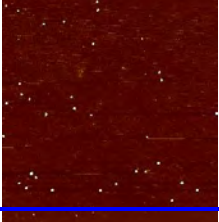
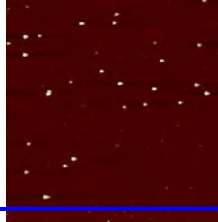
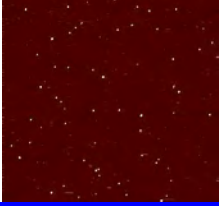
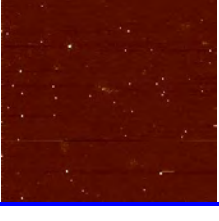
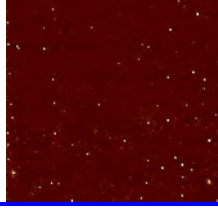
Additionally, overloading of NMs were observed on AFM micrograph (Figure 6-4 and 6-5) at concentration  $>100$  ppb for the NMs investigated in this study. This overloading depends on the size and the density of the NMs being investigated, because for a given concentration of NMs in suspension, the number of NMs increases with the decrease in NM density and size. Further analysis is performed at concentrations  $< 100$  ppb for the NMs, this investigation is beneficial since it allows low concentration measurements to be performed

which are more representative of likely exposure scenarios from the environment, consumer goods and the workplace and allows more realistic toxicology experiments to be performed. Further distribution analysis carried out with NMs suspended on PLL functionalised substrate.

#### **6.3.4 PLL functionalised Au NMs suspended in UHPW**

The sampling technique for PLL functionalisation AFM substrate is explained in the Chapter 4 and in Section 4.3.3. Five AFM substrates having five different concentrations from 1.0 ppb to 101.6 ppb were prepared for the imaging by AFM technique. A total of 30 images per substrate were taken. The Figure 6-7 below shows the AFM images of citrate capped Au NMs in UHPW ultracentrifuged on poly-L-lysine functionalised substrate. For each concentration as seen in Figure below three images were shown. Higher concentration has higher population of NMs when compared to subsequent further lower concentration. Qualitatively when compared from image to image per concentration, NM distributions were seen to be uniform between images. The uniformity in the NM distribution between images will be explained further quantitatively. The uniformity in the distribution of NMs between the images were seen, presumably due to the strong and immediate attachment of the NMs to the AFM substrate following ultracentrifugation, preventing further particle interaction once sorbed. The strong attachment of the NMs is mainly due to the charge attraction between the negatively charged citrate capped Au NMs and the positively charged functionalized substrate (Basic Coulombs law,(R. P. Feynman, 1964)). Qualitatively, distribution of NMs on the substrates both non-functionalised  $\text{CaCl}_2$  and PLL functionalised is explained in further sections below.

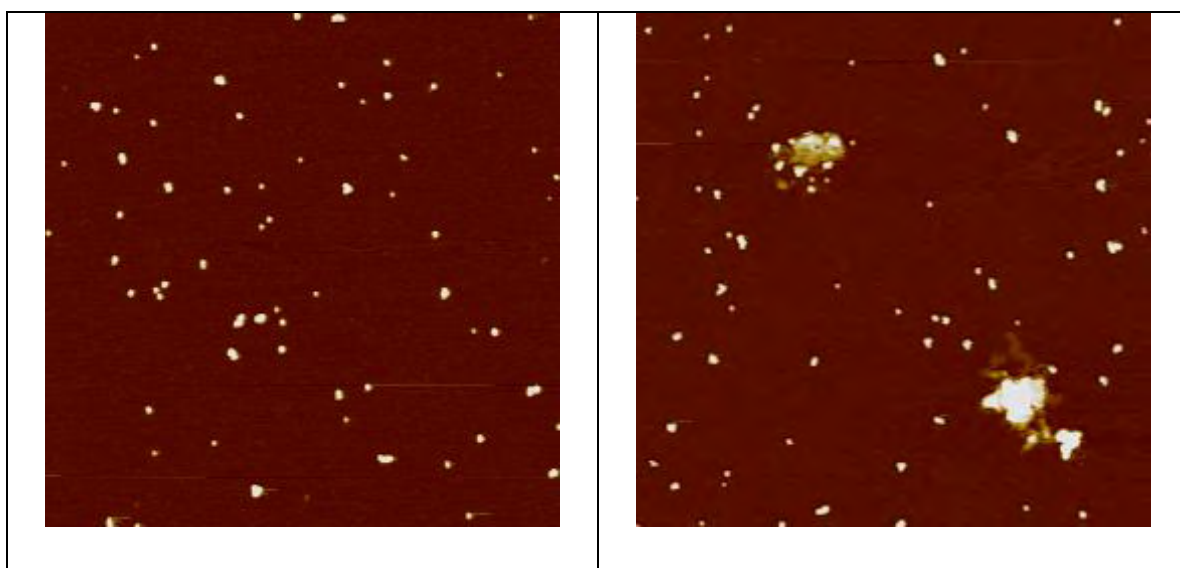


C (ppb)	Image 1	Image 2	Image 3
101.6 1 $\mu$ m x 1 $\mu$ m			
20.3 2 $\mu$ m x 2 $\mu$ m			
10.2 3 $\mu$ m x 3 $\mu$ m			
2.0 3 $\mu$ m x 3 $\mu$ m			
1.0 5 $\mu$ m x 5 $\mu$ m			

**Figure 6-7** AFM micrographs (5  $\mu$ m x 5  $\mu$ m) of Citrate capped Au NMs in UHPW and ultracentrifuged on poly-L-lysine functionalized mica substrate at different concentrations of Au NMs (1.0-101.6 ppb).

The Au NMs added to natural organic materials (that in complex media) suspended on PLL functionalised substrate were also analysed. But unable to image due to the tip interaction with the substrate caused the damaged the tip and distortion in the signalling which provided a poor quality of images. Thereby, scanning the organic contained substrate

by AFM technique leads to blurring of the image. Hence, the artifacts by AFM technique of imaging organic or complex media contained sample will lead to distortion in the scanning that may be due to various reasons such as artifacts related to the tip, type of sample or interaction between the samples. So, AFM technique is ruled out for NMs suspended complex media.



**Figure 6-8** AFM micrographs (5  $\mu\text{m}$  x 5  $\mu\text{m}$ ) of PVP capped Au NMs in UHPW and ultracentrifuged on poly-L-lysine functionalized mica substrate at concentration of 1 ppb.

Quantitatively, the distribution of citrate capped Au NMs and PVP capped Au NMs in UHPW ultracentrifuged on non functionalised AFM substrate was found to be not uniform since coefficient of variation  $CV > 0.2$ , Figures 5-4 and 5-5 and Table 6-1. and therefore has not been investigated. For PVP capped Au NMs, the addition of 10 mM  $\text{Ca}^{2+}$  ions resulted in uniform distribution of the NMs on the AFM substrate shown in Figure 6-6, having  $CV < 0.2$ , Table 6-1, but still aggregation is seen on the substrate as shown in the Figure 6-8. The distribution of citrate capped Au NMs in UHPW ultracentrifuged on functionalized AFM substrate was seen to be more uniform between the images (Figure 6-7,  $CV < 0.2$ , Table

S2), due to the strong attachment of the NMs to the substrate. In the next section is based on the discussion of the strong attachment of NMs on the substrate and also to look at how much percentage NMs suspended in UPHW has been precipitated on the non functionalised and functionalised substrate. Therefore further analysis is given on the recovery of NMs on the substrate.

## **6.4 Recovery of NMs**

To obtain the percentage recovery, the number of NMs on the substrates was counted. Percentage recovery is the ratio of the number of NMs on each substrate to the number of NM in suspension. The recovery of NMs on the AFM substrate was assessed by (i) ignoring NM size polydispersity (*e.g.* using the mass calculated in Eq.4 in Section 4.7.5 and (ii) considering NM size polydispersity (*e.g.* using the mass calculated in Eq.4 in Section 4.7.5). Accounting for size polydispersity results in a higher recovery (~25-70%, Table 5-1), indicating the importance of accounting for NM polydispersity when considering the size distribution and calculation of NM mass from microscopy techniques (Baalousha and Lead, 2013b). The samples studied here have very low polydispersity (CV is about 0.16 and 0.18). Samples with higher polydispersity will result in larger uncertainties in the calculated recoveries. Thus, the discussion below takes into account NM polydispersity when calculating NM recovery.

**Table 6-1:** Recovery of Cit- and PVP-AuNMs by ignoring and considering size polydispersity. The Citrate and PVP AuNMs prepared by Ultracentrifugation on a mica substrate functionalized by poly-L-lysine. The PVP-AuNMs were prepared by ultracentrifugation on a non-functionalised mica substrate from 10 mM CaCl<sub>2</sub> suspension.

Concentration of Cit-AuNMs (ppb)	PLL B1 <sup>a</sup> (%)	PLL B1 <sup>b</sup> (%)	Concentration of PVP-AuNMs (ppb)	10 mM CaCl <sub>2</sub> -B1 <sup>a</sup> (%)	10 mM CaCl <sub>2</sub> -B1 <sup>b</sup> (%)
101.6	63.8	70.9	67.1	30.2	33.2
20.3	61.1	64.1	33.5	36.7	40.3
10.2	48.5	52.3	16.8	23.7	26.0
2.0	59.3	66.0	3.4	33.8	37.1
1.0	65.7	68.9	1.7	27.3	30.0
			0.34	41.2	45.3

NA : Not Available

a: Ignoring polydispersity

b: Considering polydispersity

For Au NMs samples in UHPW ultracentrifuged on the non functionalised AFM substrate, recovery was very poor and was in the range of 0 to 0.5% for citrate-Au NMs and 4 to 45% for PVP-Au NMs. For citrate coated NMs, the addition of 100-200 μM Ca<sup>2+</sup> ions resulted in an increased recovery (1-27%) compared to that in UHPW and higher number concentrations of NMs, but also resulted in formation of aggregates of NMs (Figure 6-4 to Figure 6-6).

**Table 6-2** Recovery of Citrate and PVP coated Au NMs given in brief on non functionalised, on addition of CaCl<sub>2</sub> and PLL functionalised substrates

Citrate capped Au NMs	Recovery (%)	PVP capped Au NMs	Recovery (%)
Non functionalised AFM substrate ultracentrifuged	0-0.5	Non functionalised AFM substrate ultracentrifuged	0-3
100-200 μM CaCl <sub>2</sub> added to Au NMs and ultracentrifuged on Non functionalised substrates	1-27	10 mM CaCl <sub>2</sub> added to NMs followed by ultracentrifugation on Non functionalised substrates	26-45
PLL substrate	48-71	PLL substrate	30-45

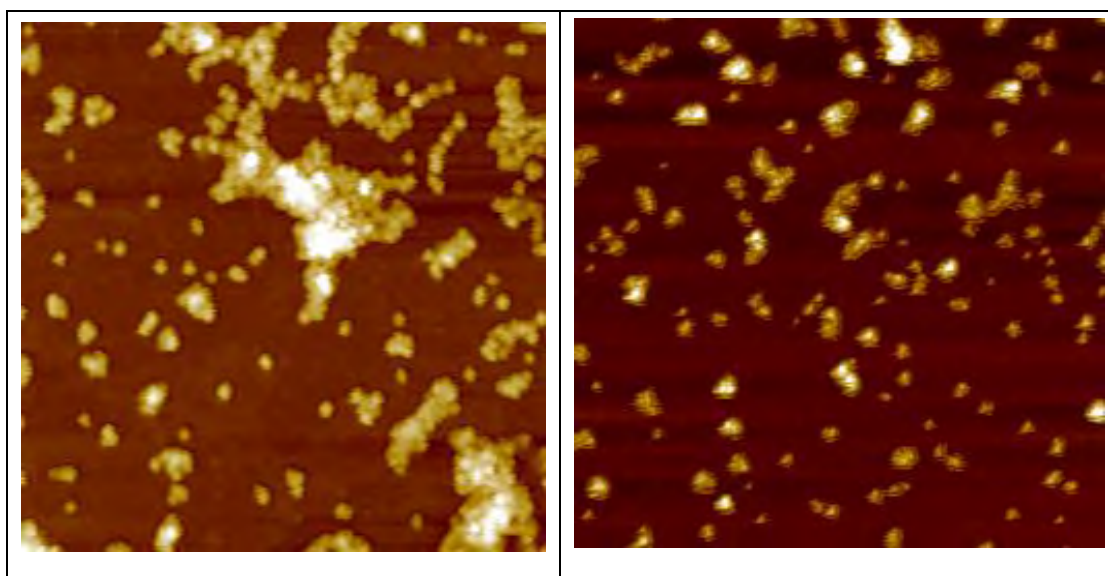
The addition of 10 mM CaCl<sub>2</sub> to PVP-Au NMs followed by ultracentrifugation on bare mica substrate resulted in an increased recovery of the NMs (26-45%, Table 6-2) and about an order of magnitude higher number concentration compared to those prepared in UHPW.

The functionalisation of the AFM substrate with PLL resulted in higher recovery of citrate Au NMs (48-71% Table 5-1). The reason to have higher recovery in case of the citrate NMs on PLL functionalised is mainly due to the higher potential of attraction between NMs and the substrate. Citrate NMs has a higher negative charge measured by zeta potential of -43 mV and the zeta potential for PVP capped Au NMs of -8.3 mV. Thereby, the citrate Au NMs were likely to be more strongly attracted to the positively charged poly-L-lysine functionalised AFM substrate when compared with the PVP Au NMs.

The lower recovery for PVP capped Au NMs compared to the citrate capped Au NMs is due to the presence of aggregates of PVP-Au NMs (Figure 6-8) without washing, which were not accounted for in the recovery calculations. The number of the aggregates represents about 35% of the counted particles; however, it is impossible to estimate the number of NMs within the aggregates by AFM, due to limitation of the technique. Some of

the aggregates contained of 2 to 3 NMs, but other larger aggregates contain unknown number of NMs (Figure 6-8). While with washing results in PVP Au NMs losses the retention on the mica substrate even after functionalisation of the mica, which result in the loss of NMs may be as said before the zeta potential is less compared to citrate NMs. Thereby, results in the less recovery compared to the citrate NMs. Recovery data in brief, is given in the Table 6-2.

These results from the recovery of NMs suggests that by treating or functionalising the surface of the substrate with positively charged polymer is the method of choice to electrostatically stabilise NMs that leads to the higher recovery. While the other choice is the sterically stabilise the NMs by the addition of divalent cations  $Ca^{2+}$  to enhance NM-substrate interactions.



**Figure 6-9** AFM micrographs (5  $\mu\text{m}$  x 5  $\mu\text{m}$ ) of PVP-Au NMs suspended in UHPW and ultracentrifuged on poly-l-lysine functionalized mica substrate not washed.

For PVP-capped Au NMs, the percentage recovery of NMs was for between non-functionalised substrate was found to be between 0% to 3% (see Table 6-2)., while for 10 mM  $CaCl_2$  suspended in NMs the percentage recovery was between 26% - 45 % , the

percentage range decreased when compared to non-functionalised Au NMs. But for the PLL functionalised substrate, were the substrate was washed after ultracentrifugation was found to be 30%-45%. The aggregation and non uniformity of NMs on the substrate may be due to misplacement of the NM on the mica grid due to the surface charge of the mica when reacts with the polymer (Rojas, 2002). The AFM tip interaction also influences the dislocation of the NMs due to electrostatic force between the tip and the sample surface.

## **6.5 Particle number measurement of NMs**

To validate the sampling technique at different NM concentrations, the particle number concentration was calculated at a range of concentrations, which is needed to be investigated and also required to assess the range of applicability of the sample preparation method.

Table 6-3 provides particle number concentration data for citrate-capped Au NMs prepared by three different techniques. Calculating the NM per  $\mu\text{m}^2$  on the sample surface, for five different NM concentration. Particle number on non functionalised substrate was found to be having higher CV represents non uniform distribution of NMs (CV= 0.22 and 0.46), thus less number of NMs of  $0.4\pm 0.1$  to  $1.1\pm 0.5$ , particles per  $\mu\text{m}^2$  for 101.6 ppb.

**Table 6-3** Number of NMs counted per  $\mu\text{m}^2$  of AFM substrate for cit-AuNMs

Concentration (ppb Au)	UHPW-B1 CV	UHPW-B2 CV	100 $\mu\text{M}$ $\text{CaCl}_2$ CV	200 $\mu\text{M}$ $\text{CaCl}_2$ CV	Poly-l-lysine CV
101.6	0.4 $\pm$ 0.1 (0.22)	1.1 $\pm$ 0.5 (0.46)	ND	23.8 $\pm$ 3.8 (0.16)	200.7 $\pm$ 20.5 (0.10)
20.3	NC	NA	1.5 $\pm$ 0.3 (0.24)	4.2 $\pm$ 1.4 (0.34)	38.3 $\pm$ 3.2 (0.08)
10.2	NA	NA	ND	2.6 $\pm$ 0.7 (0.27)	15.2 $\pm$ 0.9 (0.06)
2.0	NA	NA	1.7 $\pm$ 0.4 (0.31)	1.4 $\pm$ 0.4 (0.27)	3.2 $\pm$ 0.6 (0.18)
1.0	NA	NA	ND	0.9 $\pm$ 0.3 (0.34)	1.6 $\pm$ 0.2 (0.12)

The number in the brackets is the coefficient of variation of the number of NM per  $\mu\text{m}^2$  of the substrate

NA: Not analysed

ND: not detected/not sufficient number of particles to be counted

OL: overloading

CV: coefficient of variation

While by the addition of 100  $\mu\text{M}$   $\text{CaCl}_2$  (CV= 0.16 and 0.34), as per the above table approximately 1.6 $\pm$ 0.3 particle per  $\mu\text{m}^2$  for 20 ppb. For 200  $\mu\text{M}$   $\text{CaCl}_2$  added to NMs slightly improved particle number 4.2 $\pm$ 1.4 particle per  $\mu\text{m}^2$  for 20 ppb. Particle number on PLL-functionalised substrate was found to be having lower CV represents uniform distribution of NMs (CV= 0.06 and 0.18), thus more number of NMs of 200.7 $\pm$ 20.5 to 1.6 $\pm$ 0.2, particles per  $\mu\text{m}^2$  for 101.6 ppb to 1 ppb respectively.



**Table 6-4:** Number of NMs counted per  $\mu\text{m}^2$  of AFM substrate for PVP-Au NMs

Concentration (ppb Au)	UHPW -B1 CV	UHPW -B2 CV	UHPW -B3 CV	10 mM CaCl <sub>2</sub> CV	PLL CV
670.5, 335.3 and 167.6	Overloading	NA	NA	NA	NA
67.1	ND	147.4±7.8 (0.05)	68.6±43.5 (0.63)	83.6±11.5 (0.14)	98.5±8.3 (0.08)
33.5	19.4±4.8 (0.25)	7.3±1.8 (0.26)	ND	50.8±4.5 (0.09)	68.1±5.3 (0.17)
16.8	NA	ND	ND	16.4±2.1 (0.13)	28±1.4 (0.09)
3.4	NA	ND	NA	4.7±1.7 (0.15)	6.9±0.4 (0.10)
1.7	NA	ND	NA	1.9±0.3 (0.14)	3.1±0.2 (0.11)
0.34	NA	ND	NA	0.6±0.2 (0.33)	1.6±0.1 (0.24)

The number in the brackets is the coefficient of variation of the number of NM per  $\mu\text{m}^2$  of the substrate

NA: Not analysed

ND: not detected/not sufficient number of particles to be counted

CV: coefficient of variation

Similarly, the number of NMs counted per  $\mu\text{m}^2$  of AFM substrate for PVP capped Au NMs was found to be similar to citrate capped as given in the Table 6-5. The particles per  $\mu\text{m}^2$  for PLL functionalised were found to be higher when compared to the non functionalised grid.

**Table 6-5** Number concentration (particle.L<sup>-1</sup>) of cit-Au NMs in diluted samples

Concentration (ppb Au)	UHPW-B1 CV	UHPW-B2 CV	100 µM CaCl <sub>2</sub> CV	200 µM CaCl <sub>2</sub> CV	Poly-L-lysine CV
101.6	5.90 x 10 <sup>09</sup> 0.22	1.34 x 10 <sup>10</sup> 0.46	ND	2.84 x 10 <sup>11</sup> 0.16	2.67 x 10 <sup>12</sup> 0.10
20.3	NC	NA	1.75 x 10 <sup>10</sup> 0.24	5.00 x 10 <sup>10</sup> 0.34	5.09 x 10 <sup>11</sup> 0.08
10.2	NA	NA	ND	3.12 x 10 <sup>10</sup> 0.27	2.02 x 10 <sup>11</sup> 0.06
2.0	NA	NA	1.99 x 10 <sup>10</sup> 0.24	1.73 x 10 <sup>10</sup> 0.27	4.20 x 10 <sup>10</sup> 0.18
1.0	NA	NA	ND	1.04 x 10 <sup>10</sup> 0.34	2.17 x 10 <sup>10</sup> 0.12

NA: Not analysed

ND: not detected/not sufficient number of particles to be counted

OL: overloading

Table 6-5 represents particle number concentration (particle L<sup>-1</sup>) of citrate capped AuNMs in diluted samples. Five different concentrations is shown in the table from 101.6 to 1.0 ppb. The number of particles per litre in PLL functionalised substrate was found to be higher when compared to the non-functionalised sampling techniques. Higher concentration NM suspension have higher particle.L<sup>-1</sup> (2.67 x 10<sup>12</sup> particle.L<sup>-1</sup>) with lower CV (0.10) confirming uniform distribution between the images. As the mass concentration decreases from 101.6 ppb to 1.0 ppb, the particle number also decreases (2.67 x 10<sup>12</sup> to 2.17 x 10<sup>10</sup> particle.L<sup>-1</sup>).

**Table 6-6** Number concentration (particle.L<sup>-1</sup>) of PVP-AuNMs in diluted samples

Concentration (ppb Au)	UHPW -B1 CV	UHPW -B2 CV	UHPW -B3 CV	10 mM CaCl <sub>2</sub> CV	PVP (washed) CV
670.5, 335.3 and 167.6	Overloading	NA	NA	NA	NA
67.1	ND	1.76 x 10 <sup>12</sup> 0.05	8.21 x 10 <sup>11</sup> 0.63	1.11 x 10 <sup>12</sup> 0.14	1.48 x 10 <sup>12</sup> 0.13
33.5	2.50 x 10 <sup>11</sup> 0.25	9.43 x 10 <sup>10</sup> 0.26	ND	6.75 x 10 <sup>11</sup> 0.09	6.13 x 10 <sup>11</sup> 0.18
16.8	NA	ND	ND	2.17 x 10 <sup>11</sup> 0.13	3.10 x 10 <sup>11</sup> 0.10
3.4	NA	ND	NA	6.22 x 10 <sup>10</sup> 0.15	5.65 x 10 <sup>10</sup> 0.12
1.7	NA	ND	NA	2.51 x 10 <sup>10</sup> 0.14	2.04 x 10 <sup>10</sup> 0.14
0.34	NA	ND	NA	7.58 x 10 <sup>09</sup> 0.33	7.64 x 10 <sup>09</sup> 0.22

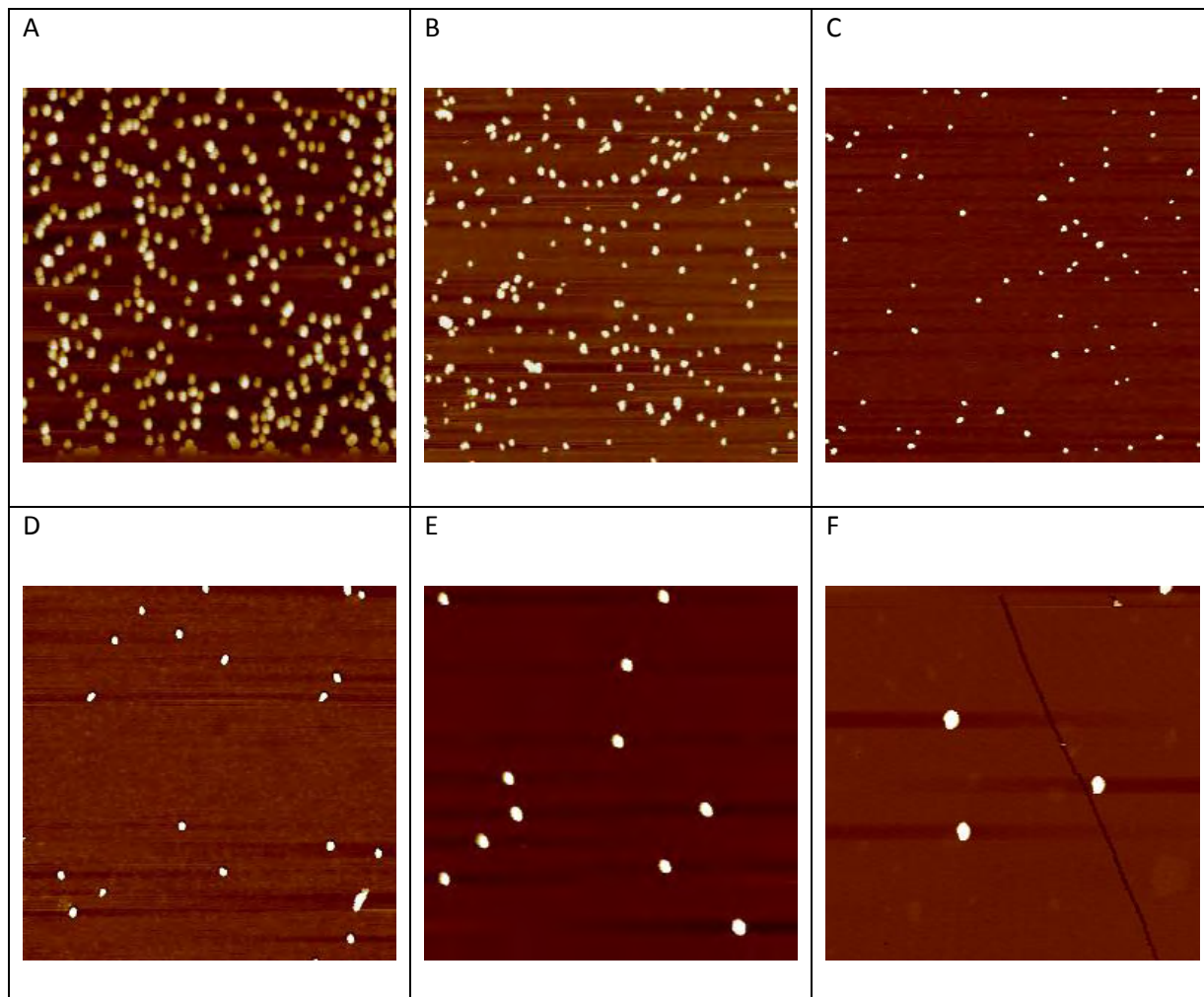
NA: Not analysed

ND: not detected/not sufficient number of particles to be counted

CV: coefficient of variation

Similarly, Table 6-6 represents particle number concentration (particle.L<sup>-1</sup>) of PVP capped Au NMs in diluted samples. Six different concentrations are shown in the table from

167.0 to 0.34 ppb. The number of particles per litre in PLL functionalised substrate was found to be higher when compared to the non-functionalised sampling techniques. At very high concentration of > 67.1 ppb, NMs are overloaded.



**Figure 6-10** Representative atomic force microscopy images of PVP-AuNMs suspended in 10 mM  $\text{CaCl}_2$  showing a uniform distribution of PVP-AuNMs on non-functionalised AFM substrate and the decrease of the number of NMs recovered with the decrease in NM mass concentration in ppb (a) 67.1, (b) 33.5, (c) 16.8, (d) 3.4, (e) 1.7 and (f) 0.34. All images are  $2 \mu\text{m} \times 2 \mu\text{m}$ .

As the concentration of NM decreases from 67.1 ppb to 0.34 ppb, the particle count also decreases  $1.48 \times 10^{12}$  to  $7.64 \times 10^9$  particle. $\text{L}^{-1}$ . As the NM concentration decreases for

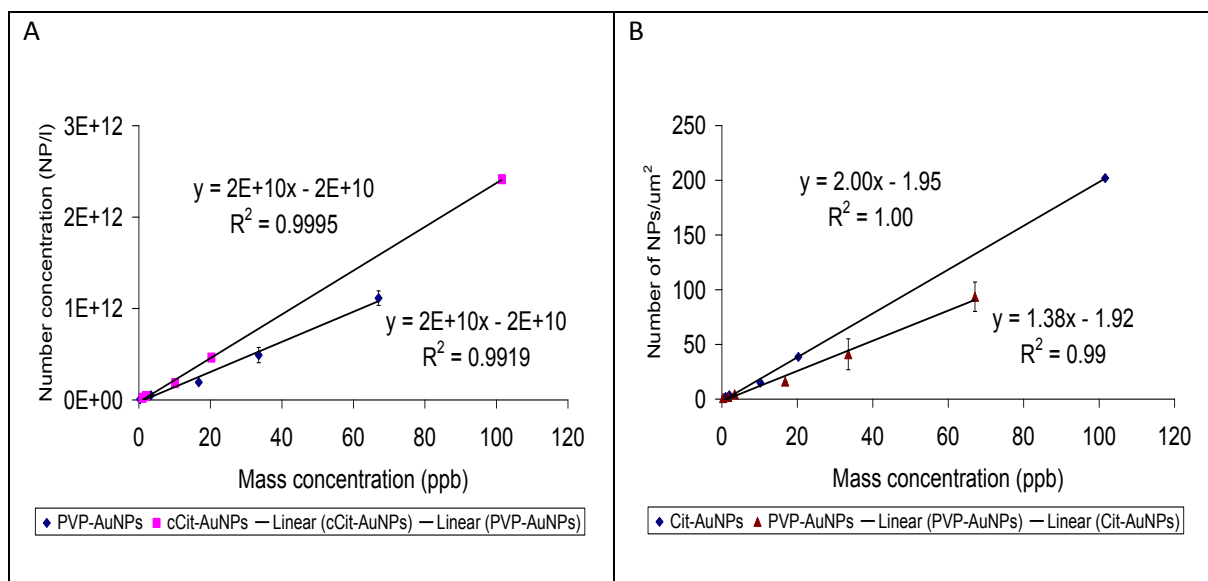
the range of concentrations (67.1 ppb to 0.34 ppb), particle count also decreases, this can be visualised by typical AFM micrograph shown in the Figure 6-10. The next step is to look at the correlation between the NM suspended at the range of concentration with respect to particle count.

## **6.6 Correlation between the mass and number concentration**

The comparison was carried with the known mass concentration (by analytical instrument) and measured particle number. The mass concentration of in-house synthesised NMs i.e. the citrate capped Au NMs and PVP capped Au NMs was measured by the ICP-MS. The measurement of the mass concentration by ICP-MS was explained in detail in Chapter 5 (characterisation of NMs results and discussion) and in Section 5.4.8. . The initial concentration measurements of Cit-Au NMs and PVP-Au NMs were  $101.6 \pm 3.2$  and  $167.6 \pm 3.2$  mg L<sup>-1</sup> respectively. The particle number concentration measured for various concentrations was given in previous Section 5.4.

For non-functionalised mica substrates for both citrate and PVP NMs, as expected the recovery data was very poor (in the range of just 0 to 0.5% and 0-3% respectively), the correlation between mass and number concentrations is not possible to assess.

Similarly, for the citrate capped Au NMs of 100 and 200  $\mu$ M CaCl<sub>2</sub> ultracentrifuged on substrate and also for 10 mM PVP capped Au NMs with non-functionalisation and PLL functionalised substrate due to the absence of NMs on substrates (see Table 6-2) as seen in the recovery data, it is not possible to assess the correlation between the mass and number concentration. The reason may be PVP-Au NMs in UHPW ultracentrifuged on poly-l-lysine functionalized surface, presumably because of the inconsistent losses of NMs at different concentrations due to the weak attachment of the NMs to the AFM substrate.



**Figure 6-11** Correlation between the mass and number concentration of NMs (a) NM/l in diluted suspension and (b) NM/ $\mu\text{m}^2$  on the mica substrate. Cit-AuNMs was prepared by ultracentrifugation on a poly-l-lysine functionalized mica substrate and PVP-Au NMs in 10 mM  $\text{CaCl}_2$  was prepared by ultracentrifugation on a non-functionalised mica substrate. All number concentrations represent average and standard deviation of two independent replicates.

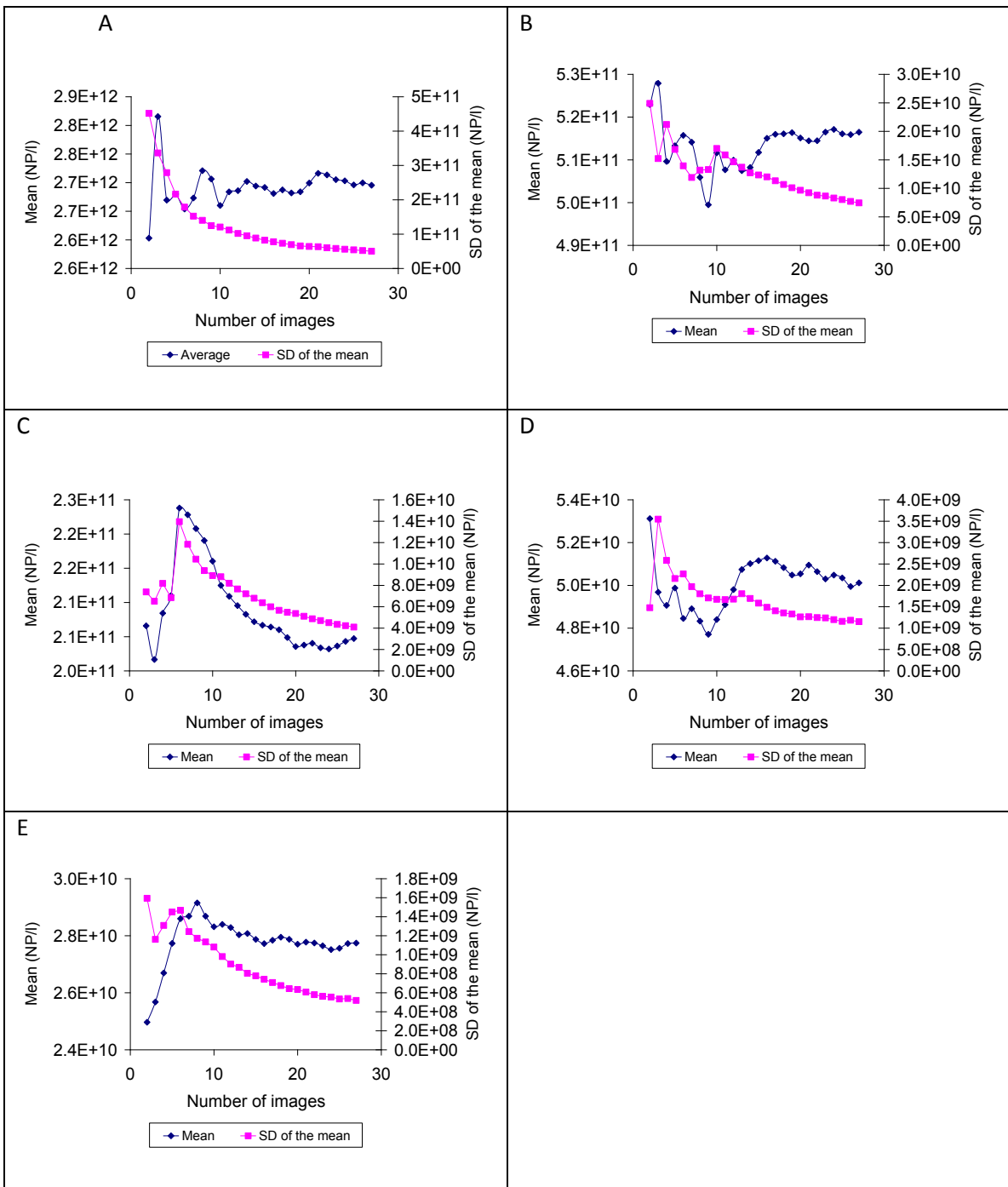
Similarly, for PVP-Au NMs, the addition of 10 mM  $\text{CaCl}_2$  and ultracentrifugation on bare (non-functionalised substrate) mica substrate resulted in better correlation ( $r^2 = 0.992$ , Figure 6-11) between number and mass concentrations. The number of NMs counted per  $\mu\text{m}^2$  of the mica substrate for cit-AuNMs ultracentrifuged on poly-l-lysine functionalized mica and for PVP-AuNMs in 10 mM  $\text{CaCl}_2$  ultracentrifuged on bare mica substrate also shows a good correlation with the mass concentration (Figure 6-11b and Table 6-3 to Table 6-6) and suggests that the sample preparation method is applicable within the concentration range of 0.34-100 ppb for the NMs investigated in this study. Lower concentrations will result in higher uncertainty and variability because of the low number of NMs present on the AFM substrate (Figures 6-6 and 6-7, Table 6-3 and Table 6-6) or will require collecting more images to count sufficient number of NMs, in particular for sizing purposes. Higher

concentrations will result in overloading (particle-particle interaction, Figures 6-5 and 6-6) of the AFM substrate and therefore it becomes impossible to obtain true counts of the NMs and to calculate NM recovery on the AFM substrate. The concentration range of 0.34-100 ppb is applicable for AuNMs of approximately 12-13 nm in diameter. However, the range of concentrations will depend on the size and composition (density) of the NMs.

As previously explained in Section 4.7, scanning of a substrate is carried out randomly over the entire surface. The number of NMs on each scanned image is counted. Thereby, it is necessary to know the number of images required to count the NMs, in order to measure the particle number concentration per substrate.

## **6.7 Number of images required for representative measurement of particle number**

To identify the number of images required to count NMs, two samples were tested for comparison with uniformly distributed NMs on the substrate with respect to non-uniformly distributed NMs on the substrate. Since Citrate Au NMs in UHPW by ultracentrifugation on a PLL functionalised substrate as well for PVP 10 mM CaCl<sub>2</sub> suspended in Au NMs by ultracentrifugation method on non functionalisation mica are uniformly distributed between the images (see Figure 6-14) compared with non-uniform (see Figure 6-14) distribution of NMs between images of a substrate, with the 300 µM CaCl<sub>2</sub> prepared by ultracentrifugation on a non functionalised AFM substrate.



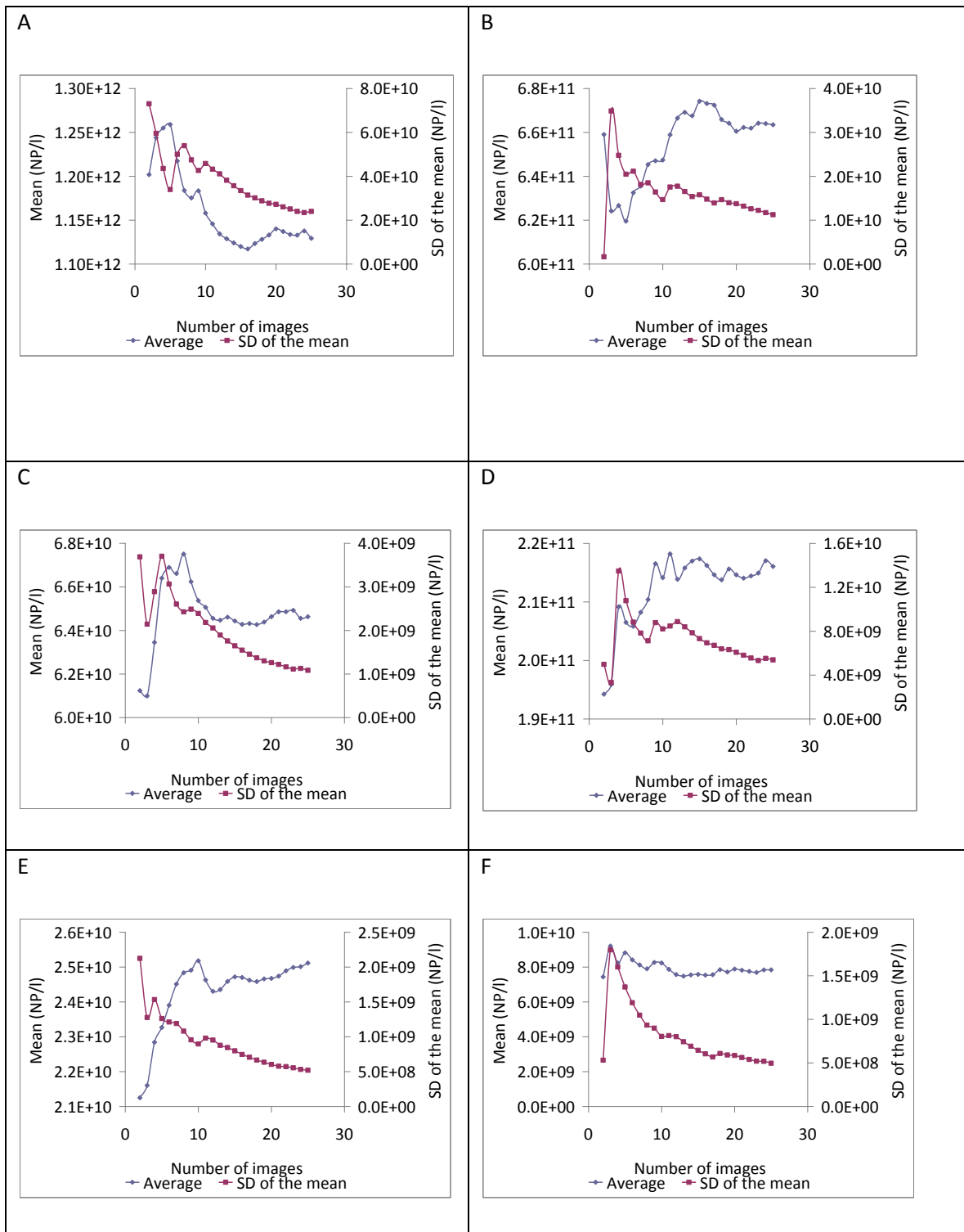
**Figure 6-12** Dependence of the calculated mean number concentration and standard deviation of the mean on the number of images scanned by atomic force microscopy of the cit-AuNMs prepared by ultracentrifugation at 150 000 g on poly-l-lysine functionalized AFM substrates at different concentrations (ppb): (a) 101.6, (b) 20.3, (c) 10.2, (d) 2.0 and (e) 1.0.

The effect of the number of images on the mean number concentration and standard deviation of the mean for cit-Au NMs in UHPW prepared by ultracentrifugation on a poly-l-

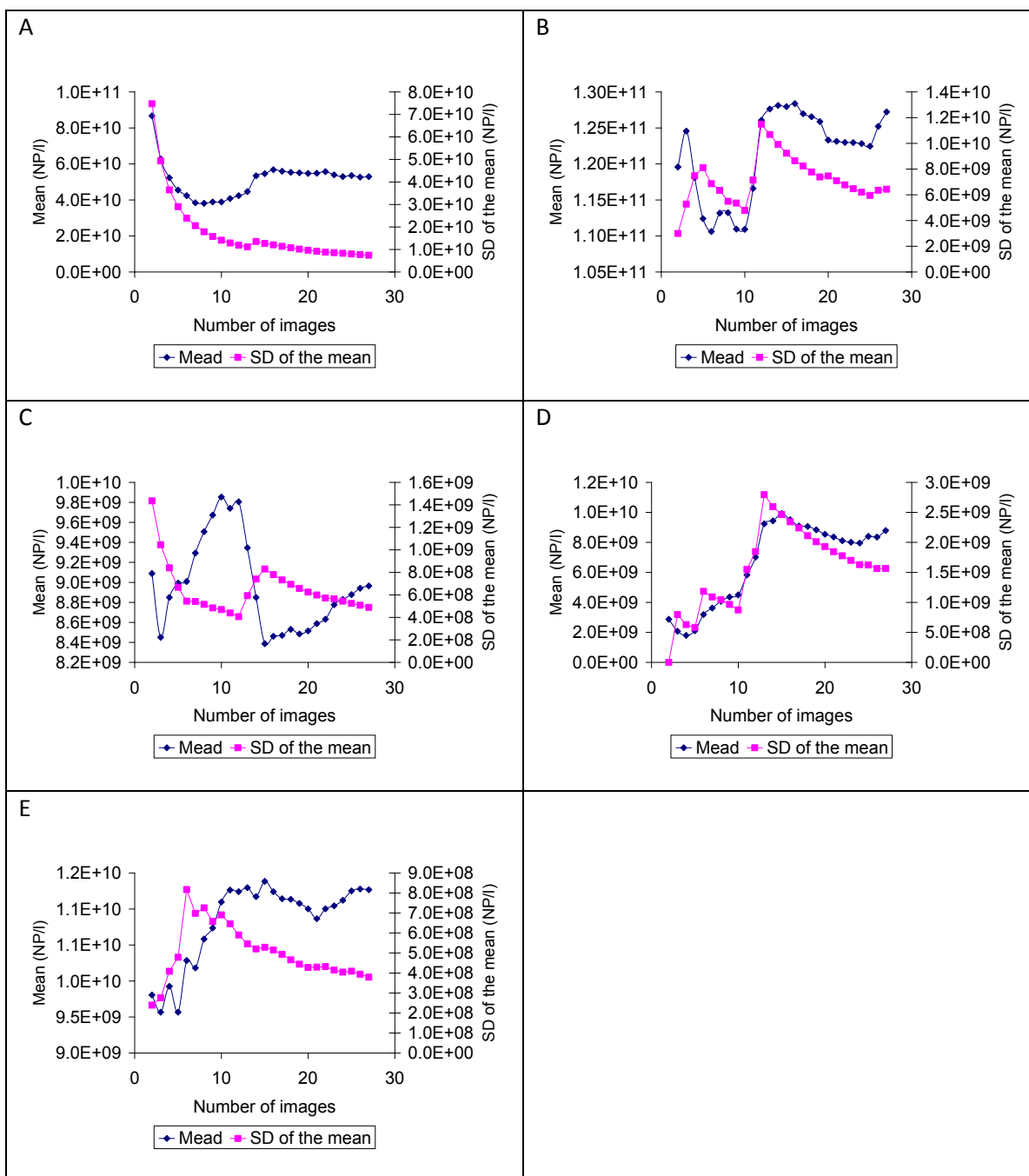


lysine functionalized substrate is shown in Figure 6-12 and for PVP-Au NMs in 10 mM CaCl<sub>2</sub> prepared by ultracentrifugation on non-functionalised mica substrate is shown in Figure 5-13. The mean number particle concentration tends to a stable value for  $\geq 20$  scanned images. The standard deviation of the mean generally decreases with the increase in the number of images and reaches a stable value (see Chapter 4 and Section 4.7.5) at about  $\geq 20$  images. Therefore, 20 images is the required minimum number of images to obtain mean number concentration and standard deviation ( $\sigma$ ) representative of the entire population of NMs.

The mean number concentration and standard deviation of the mean for cit-Au NMs suspended in 300  $\mu$ M CaCl<sub>2</sub> prepared by ultracentrifugation on a non-functionalised AFM substrate and for PVP-Au NMs suspended in UHPW are shown in Figure 6-14. Neither the mean nor the standard deviation tends to a stable value for the number of images scanned for all samples. Therefore, it is impossible to obtain a representative number particle concentration from these samples.



**Figure 6-13** Dependence of the calculated mean number concentration and standard deviation of the mean on the number of images scanned by atomic force microscopy of the PVP-coated AuNMs prepared by adding 10 mM CaCl<sub>2</sub> on a non-functionalised substrate at different concentrations expressed as ppb Au: (a) 67.1, (b) 33.5, (c) 16.8, (d) 3.4, (e) 1.7 and (f) 0.34.



**Figure 6-14** Dependence of the calculated mean number concentration and standard deviation of the mean on the number of images scanned by atomic force microscopy of the cit-coated AuNMs prepared by adding 300  $\mu\text{M}$   $\text{CaCl}_2$  on a non functionalised mica substrate at different concentrations expressed as ppb Au: (a) 101.6, (b) 20.3, (c) 10.2 (d) 2.0 and (e) 1.0.

Therefore, the number of images required for obtaining the representative measurement particle number is > 20 images for AFM techniques. As seen in Figure 6-14, neither the mean number concentration nor standard deviation of the mean is stable for all different range of concentration when compared with the Figure 6-13. In Figure 6-13, the standard deviation of the mean decreases becomes stable after 20 images. Thus minimum of 20 images are to be scanned by analytical instrument to obtain accurate particle number measurement for AFM technique. Stability after 20 images can be attained only if the sampling technique was PLL functionalisation of substrate followed by ultracentrifugation.

## **6.8 Conclusion**

The atomic force microscopy technique enables a full quantitative analysis of NMs at environmentally and toxicologically relevant concentrations that is 0.34-100 ppb for the first time. For the purpose of qualitative analysis, various methods of sampling technique were carried out to improvise the particle number measurement. The method improvised was based on combining substrate functionalisation and ultracentrifugation to ensure high and uniform recovery of NMs on the AFM substrate and quantitative determination of the number of NMs and their number size distribution i.e. forcing the NMs onto the substrate was carried out by surface functionalisation of the substrate while the adding cations to NM suspension.

The quality of the sample preparation method was evaluated using well stabilised in-house synthesised Au NMs coated with citrate and PVP using criteria are as follows:

- (i) full recovery of NMs on the AFM substrate
- (ii) the uniformity of NMs distribution on the AFM substrate and
- (iii) correlation between the mass and the number concentration.

Both citrate and PVP AuNMs were uniformly distributed between the images scanned on the mica substrate, i.e. the coefficient of variation calculated between the number of NMs counted on different area of the substrate was  $<0.20$ . The recovery of NMs on the substrate was fully quantified for the first time and it was up to 71%. Also the number of counted NMs on the substrate was well ( $r^2 > 0.95$ ) correlated with the concentration of NMs in suspension.

The next chapter will investigate the sampling technique proposed and validated by using the transmission electron microscopy. This technique is more powerful in comparison with the AFM. The instrument capability (TEM technique) will enable to overcome the AFM limitations such as determining the number of NMs present within the aggregates and distinguishing between the natural and manufactured NMs when coupled with spectroscopy techniques.

The results obtained from AFM technique was published in 'Environmental Science: Process and Impacts'. The published paper is attached at the end of thesis.

## **Chapter 7 Number concentration measurement of citrate and PVP Au NMs by simple and complex media and Ag NMs with E3 media using TEM technique**

### **7.1 Chapter Summary**

This chapter is related to the results and discussion based on TEM technique. This technique, for the first time fully validated to obtain the accurate measurement of particle number both in simple and complex media i.e. at realistic environmental conditions for gold NMs and in exposure media for silver nanoparticles.

In brief, as said before, the aim of this research was to development of metrology and analytical methods for the detection and quantification of NMs in environmental samples has been identified as one of the most urgent and important research priorities to advance eco-responsible nanotechnology (Alvarez et al., 2009). For an ideal technique, to measure the particle number concentrations especially in complex samples because of the presence of the debris, salts and various other materials less than nanoscale, the following should be able to

- (i) Determine the number of NMs irrespective of morphology, density or optical properties of NMs,
- (ii) Distinguish agglomerates from dispersed NMs,
- (iii) Identify a target NM in a complex matrix containing NMs of different composition (e.g. manufactured NMs in a matrices of naturally occurring NMs),
- (iv) Measure number concentration at environmentally relevant concentrations (e.g. ng- $\mu\text{g L}^{-1}$ ), and
- (v) Cover the entire nanoscale range (i.e. 1-100 nm).

Transmission electron microscopy (TEM) has the potential to meet the requirements outlined above (Baalousha, 2012a, Baalousha, 2012b). However, TEM is primarily limited by sample preparation rather than by the capability of microscopy techniques similar to the AFM. Different preparation techniques have been employed in the literature to prepare samples for microscopy analysis (AFM and TEM) including adsorption, drop deposition and ultracentrifugation (Baalousha, 2012, Baalousha et al., 2005a, Baalousha et al., 2005c, Baalousha, 2012a, Wilkinson et al., 1999a). These widely adopted sample preparation methods suffer from a number of issues when used for number concentration analysis such as poor statistical power, requiring the counting of large number of NMs to compensate for

- (i) Low and inconsistent recovery of NMs on the sample substrate and
- (ii) Non-uniform distribution of NMs on the sample substrate.

Thereby, this chapter gives detailed description of the NMs distribution on the substrate that will be compared with the widely used drop deposition and ultracentrifugation method with the improvised NMs distribution achieved successfully by this study. Moreover, this chapter also gives the elaborate description to meet the requirements of the above stated such as improvised distribution of NMs on the substrate that leads to the accurate measurement of the particle number on the substrate by using TEM technique. Whereas, the FEI Tecnai F20 TEM has a scanning unit STEM integrated, had a bright field and dark field detector that can identify the existence of the particles other than target Au NMs.

This results in the demonstration of the applicability of the validated sample preparation method to detect and quantify the particle number concentration of Au NMs both in simple and complex media at realistic environmental conditions at different concentrations (e.g. 1-20  $\mu\text{g L}^{-1}$ ) using transmission electron microscopy. Also reports on the measurement of particle number of Ag NMs in E3 media. This novel, fully quantitative sampling approach has enabled for the first time measuring the size of NM aggregates and also determined as the number of primary NMs within aggregates at environmentally realistic concentrations, and

demonstrated the concentration-dependent aggregation of NMs at such low NM concentrations.

The first section of this chapter is related to the discussion of the measurement of particle number concentration of cit-Au NMs and PVP Au-NMs in ultra-high purity water (that is called as simple media). While the sample preparation technique adopted for the TEM technique is similar to sampling technique used for AFM, the detailed explanation is given in chapter 4 and Section 4.5.

The second part of the first section of this chapter is the study based on adding Au NMs to the three different complex media at realistic environmental conditions. The three different complex media are as follows:

- (i) EPA synthetic soft water
- (ii) 5 mg/L Suwannee river fulvic acid in EPA soft water and
- (iii) Filtered Natural surface water

The process of adding the Au NMs to the above mentioned complex media is given in detail in Chapter 4 and in Section 4.6. For both the simple and complex media, particle number measurements for five different concentrations were carried out. The five different concentrations were in the range of 1-20  $\mu\text{g L}^{-1}$ . However, the result obtained from this study is explained in detailed. The results obtained from this chapter will be published soon; paper to be published is attached at the end of this thesis in Appendix B.

The above section of this chapter is related to the particle number concentration of gold nanomaterials while the third section is based on the silver nanomaterial. Similar protocol followed to the Ag NMs for the particle number measurements. Analysis carried out by using the Ag NMs both in simple (UHPW) and complex media. The complex media used was E3 media (zebrafish). The Ag PVP NMs was added to E3 media to analyse the fate and



behaviour of the Ag NMs. The measurement of particle number of Ag NMs with and without E3 media is compared in this section. This study was conducted in courtesy with Mr. Michael T. Simonich, Ph.D. Student, (Oregon State University, Sinnhuber Aquatic Research Laboratory, USA). Oregon University was carried out with the toxicity study of the Ag-PVP NMs.

## **7.2 Measurement of particle number concentration by simple media and complex media**

The in-house synthesised gold nanoparticles capped with citrate and PVP were used for the analysis. Measurement of particle number concentration was carried out by adding citrate Au NMs and PVP Au NMs in ultra-high purity water (UHPW) at five different concentrations ranging between 1-20  $\mu\text{g L}^{-1}$ . All TEM analyses were performed using TECNAI F20 Field Emission Gun (FEG) TEM coupled with an X-ray Energy Dispersive Spectrometer (X-EDS) from Oxford Instruments. Qualitative X-EDS analysis was performed to determine particle elemental composition especially in complex media (explained in detail in further sections). Scanning the images on the TEM grid was performed by randomly selecting the different grid area that covers the entire substrate resulting in 35 images being investigated for each TEM grid. The number of NMs in each image was counted by using image J software. To count accurately number of NMs on these substrates, the evaluation of the sample preparation is paramount importance.

Initially, the evaluation of the sample preparation method was performed by using the widely used method such as

- (i) Drop method and
- (ii) Ultracentrifugation method.

These two methods of sample preparation method for the particle number were explained in detail in previous Chapter 4, Section 4.3 and in Subsection 4.3.1 and 4.3.2. and later, the evaluation was carried out for the improvised method of sample preparation i.e..

(iii) Surface functionalisation and ultracentrifugation method.

This method of sample preparation was explained in detail in Chapter 4 and Subsection 4.3.3. In order to obtain the accurate measurement of particle number the few criteria was adopted in this study are as follows:

- (i) NM distribution on the TEM grid between images,
- (ii) The % recovery of NMs on the TEM grid compared to the concentration of NMs in suspension and
- (iii) The correlation of number concentration measured by TEM vs. mass concentration in suspension (linearity).

The uniformity (consistent number of NMs between the grid areas) of NM distribution on the TEM grid was evaluated by comparing the number of particles counted at different areas on the TEM grid, which was performed by calculating the coefficient of variation of the number of NMs per  $\mu\text{m}^2$  on the images collected at different location on the grid ( $\text{CV} = \sigma/\text{mean}$  of number NMs per  $\mu\text{m}^2$  on the different images). Low CV values indicate uniform distribution of NM on the TEM grid.

The number of NMs in each image was counted by using software, MatLab image processing toolbox ( $N_{\text{counted/image}}$ ) and the number of NMs ( $\text{NM L}^{-1}$ ) in suspension ( $N_{\text{suspension}}$ ) was calculated from counted number of NMs in each TEM image using the mathematical modelling see Chapter 4 and in Section 4.7.4.

In the previous chapter it is established that the ultracentrifugation is the most appropriate sample preparation method for microscopy (atomic force microscopy, AFM), providing the most representative number particle size distribution, number average sizes, fully quantitative number particle concentration at environmentally relevant concentrations (0.1-100 ppb) with high recovery (60-80%).

Similarly the validation of surface functionalisation followed by ultracentrifugation method of sample preparation protocol was applied by using TEM technique for simple, environmentally relevant and exposure media. Our unpublished results suggest that AFM does not sufficiently discriminate between the NMs and natural colloids. Below we discuss the quality of the particle number concentration data produced, in simple and complex media in terms of (i) uniformity of NM distribution on the TEM grid, (ii) NM recovery, (iii) number vs. mass concentration correlation and (iv) the minimum number of images required to achieve accurate number particle concentration.

## **7.2.1 Measurement of particle number of Au NMs in simple media by TEM technique**

### **7.2.1.1 Introduction**

Nanoparticles from suspensions was deposited onto a TEM grid prior to analysis and several sample preparation protocols to deposit NMs from suspension onto a TEM grid have been employed in the literature including adsorption, drop deposition and ultracentrifugation. Only a few studies have applied this method (Hasselov, 2005, Boyd, 1994, Wu et al., 1990a, Wu et al., 1990b, Baalousha, 2009). These methods are widely applied qualitatively, but have never been validated to quantitatively measure particle number concentration from a suspension of NMs. At the beginning of this research, the drop method of sample preparation was attempted to have a glance and analyse the NM distribution on the TEM grid and also measurement of particle number was carried out. The process of sample

preparation for drop method carried out in this research was given in detail in Chapter 4 and in Section 4.5.1. Below sections is the discussion pertaining to the quality of the distribution of NMs on the substrate initially by drop deposition method adding UHPW i.e. simple media.

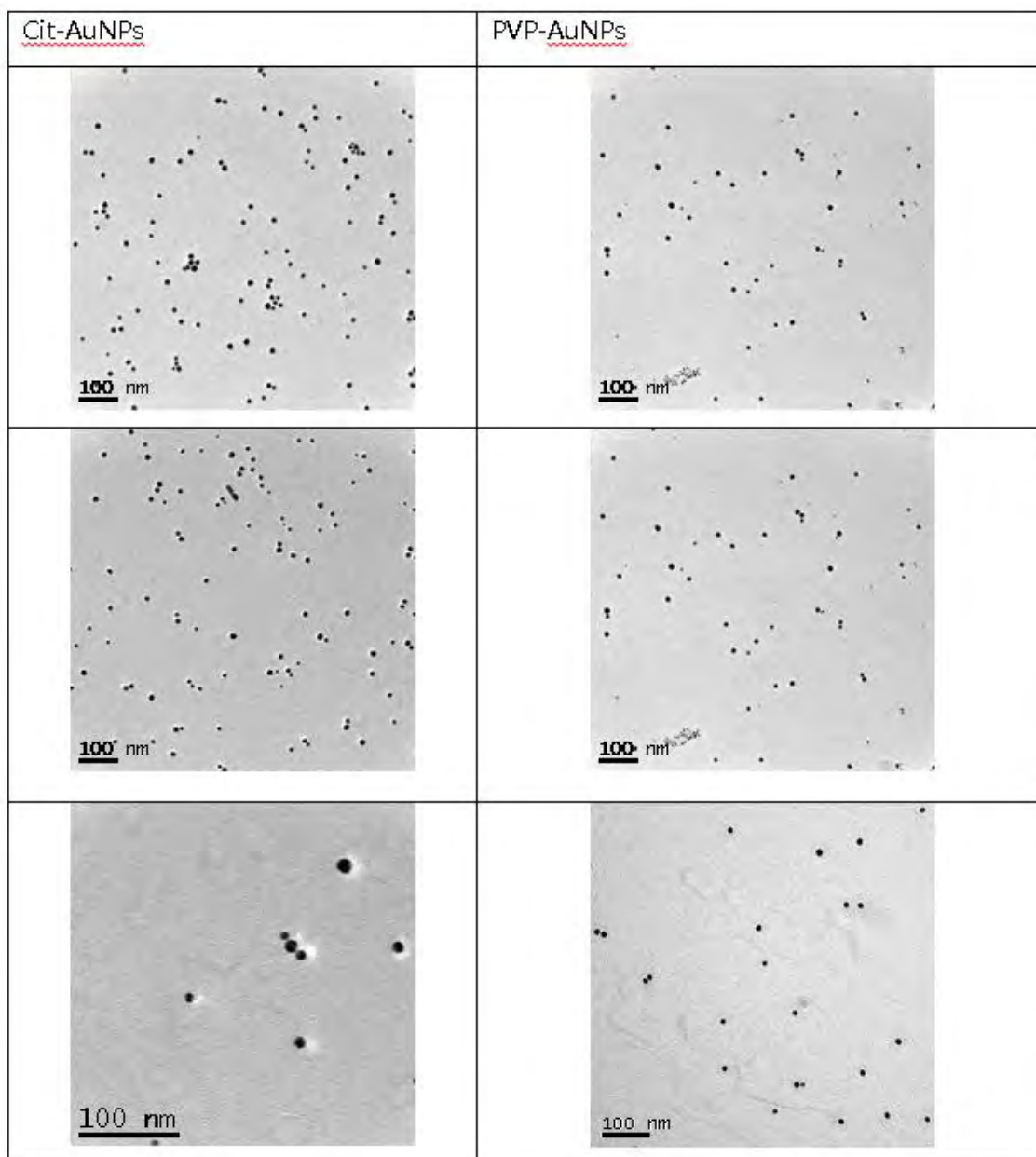
Secondly, the NM distribution on the substrate was analysed for the ultracentrifugation method of sampling techniques. The procedure for sample preparation was given in detail in Chapter 4 and Subsection 4.5.2. The quality of distribution of NMs and the measurement of particle number is given in detail in upcoming sections below.

Third, in order to improvise distribution of NMs and to obtain the good agreement in particle number concentration with respect to the suspension of NMs on the grid, the grid was functionalised with the PLL and NMs were ultracentrifuged on the PLL functionalised grid to obtain good quality of distribution and without any losses of suspended NMs on the grid (sample preparation is explained in detail in Chapter 4.3.3). The distribution of NMs by this improvised sampling technique and their particle number results and discussion is carried out in further sections below.

#### **7.2.1.2 Distribution of NMs in simple media on TEM grids**

Distribution of NMs means the uniformity of NMs on the substrate between the set of images scanned by TEM. The uniformity in distribution of NMs on the substrate depends on the sample preparation technique which was critical part of this investigation. Strong attachment of NMs is a vital part of the research such that all the precipitated NMs on the substrate shouldn't be either misplaced or lost. Also all the NMs from the suspension must be precipitated on the substrate. Uniformity of NMs distribution between images taken at different positions on the TEM grid is essential to obtain representative particle number concentrations and number size distribution, as well as to minimize the number of images required to obtain a representative number particle concentration.

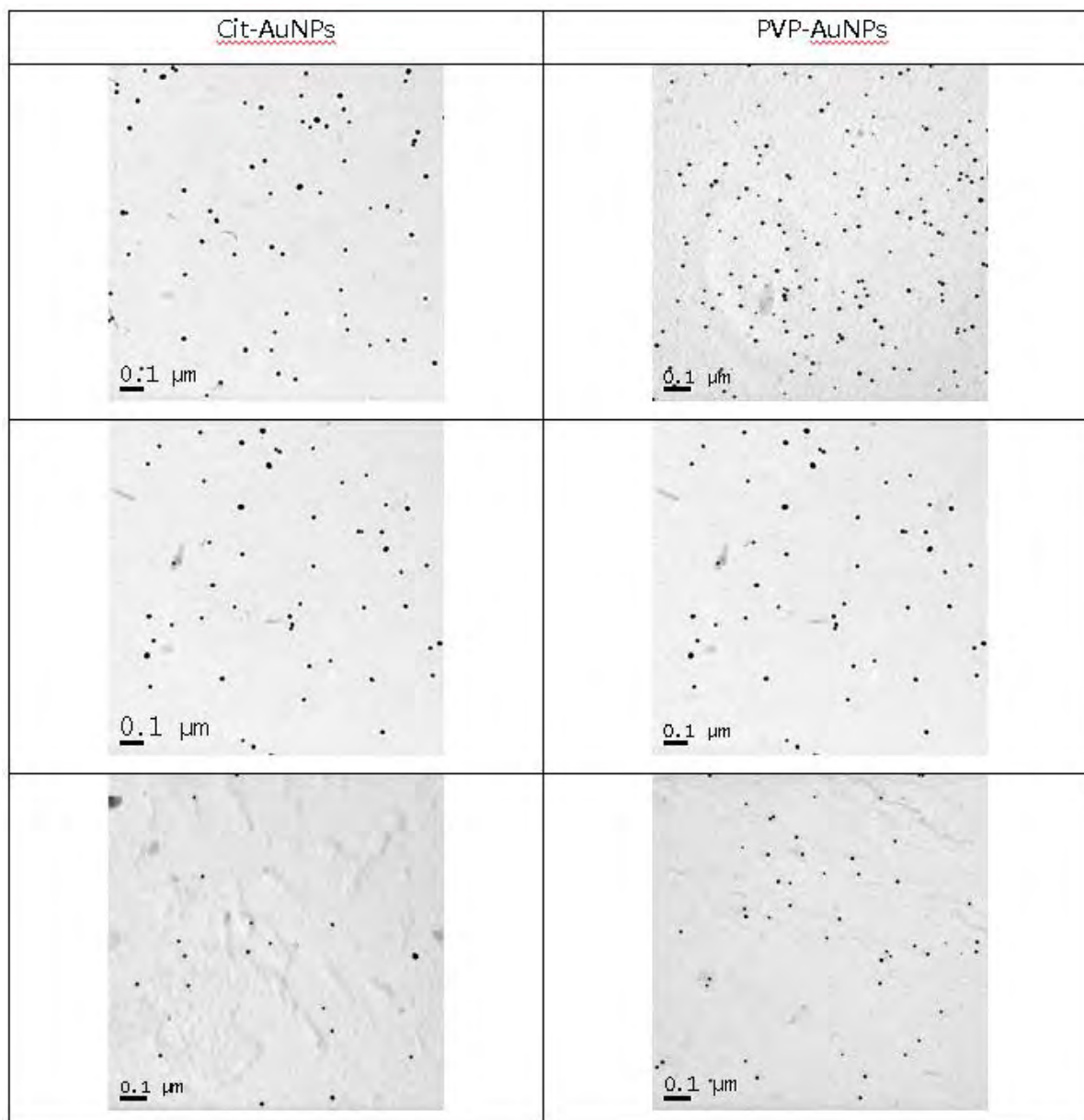
Qualitatively, TEM images of cit-Au NMs and PVP-Au NMs suspended in UHPW and prepared by drop deposition shown in the Figure 7-1 shows a non-uniform distribution of the nanoparticles between images. As shown in Figure 7-1 below for cit-Au NMs having concentration 20.3 ppb which is in the first column the larger NMs were found in the first image when compared with the other two images. Also for the PVP NMs having 16.8 ppb shows the similar distribution when compared with each other i.e. the large disparity in the number of NMs between the images. Since drop deposition sampling technique results lack of uniformity of NM distribution between the images on the TEM grid is likely due to losses and/or displacement of NM on the TEM grid during the washing process. And also the non-uniformity is presumably due to the NMs not attached strongly to the TEM grid that allows the particle movement on the grid surface. The number NMs on each image were also counted and are reported quantitatively. Total of 30 images were taken for each concentration.



**Figure 7-1:** Transmission electron microscopy images of (a) citrate-AuNMs (20.3 ppb) and (b) PVP-AuNMs (15.79 ppb) on bare-TEM grid. Samples were prepared by drop deposition method.

Similarly for the ultracentrifugation method of sample preparation the particle distribution of citrate Au NMs and PVP Au NMs shows the random distribution of NMs between the set of images. Qualitatively, the below Figure 7-2 shows the distribution of NMs the on TEM substrate having the concentration of 9.49ppb for cit Au NMs and 15.79ppb for

PVP Au NMs. Larger disparity in the number of NMs were found when compared from image to image as shown in Figure 6-2 below.

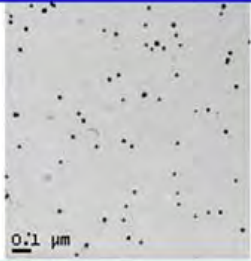
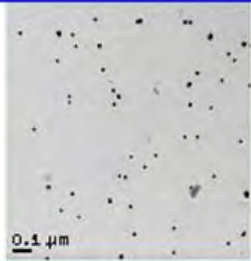
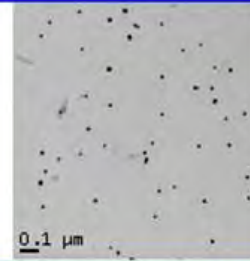
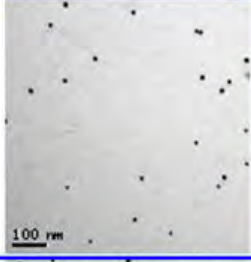
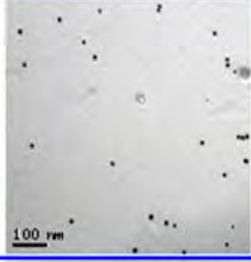
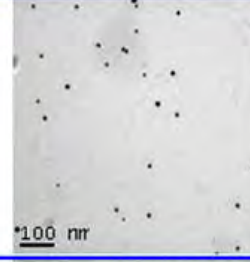
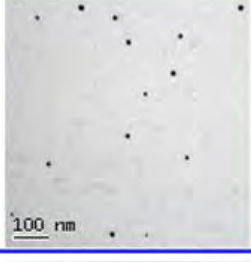
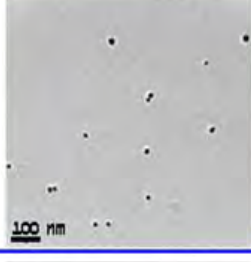
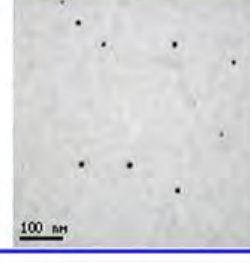
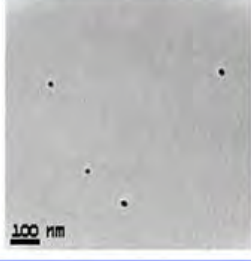

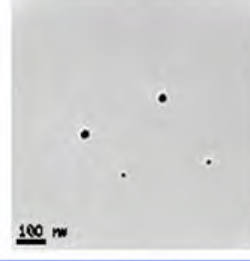
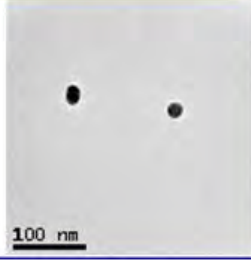
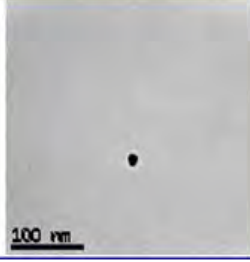
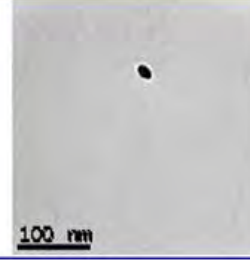


**Figure 7-2:** Transmission electron microscopy images of Citrate- and PVP- capped-AuNMs on bare-TEM grid (a) cit-AuNMs at 9.49 ppb and (b) PVP-AuNMs at 15.79ppb. NMs were suspended in UHPW. Samples were prepared by ultracentrifugation method on non-functionalised TEM grid.

Subsequently, improvised TEM grids were functionalized with a positively charged polymer (poly-L-lysine) to enhance particle attachment to the TEM grid. TEM images of citrate capped Au NMs in UHPW ultracentrifuged on poly-L-lysine functionalized TEM grid (see Figure 7-3 below) show a rather uniform distribution of NMs between the images taken at different positions on the TEM grid. The uniformity between the images is presumably due to the strong attachment of the NMs to the TEM grid following ultracentrifugation, preventing particle movement on the grid surface. As seen in the Figure 7-3, the image of five different concentrations, from higher concentration to lowest concentration i.e. 17.96 ppb to 0.19 ppb was analysed. Optimal grid coverage by citrate capped Au NMs was observed for the concentration range of 17.96 to 0.19 ppb (Figure 7-3), and grid overloading was observed at the highest cit-Au NMs concentration used in this study ( $101.5 \mu\text{g L}^{-1}$ ) (See Figure 7-6a). Optimal coverage indicates no obvious overloading, and subsequent surface aggregation, and sufficient NM numbers per image to enable particle counting within a reasonable time frame.

The comparison between the three different sampling technique can be seen visualized through the representative TEM images. The ultracentrifugation method of sampling with substrate functionalisation gives the best results for the optimal coverage of the NMs on the grid. Similarly, the imaging for the PVP capped Au NMs was also carried out for five different concentrations.

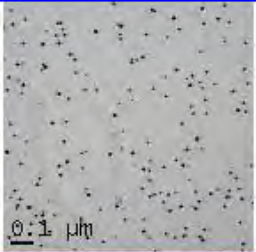
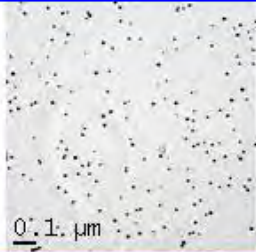
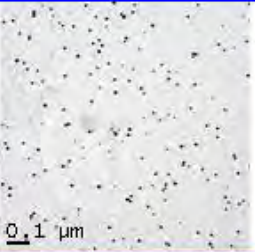
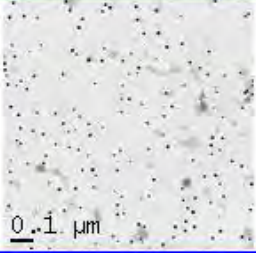
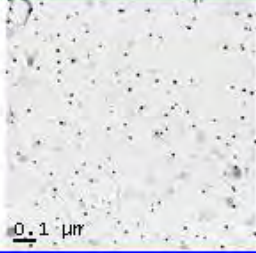
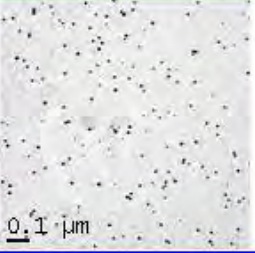

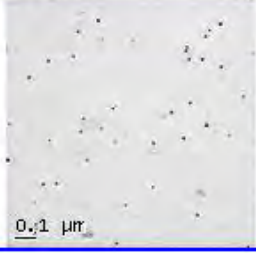
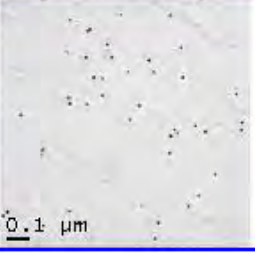
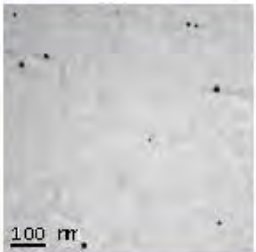
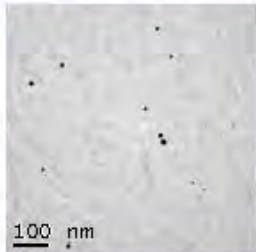
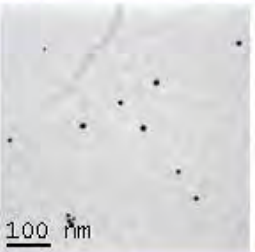
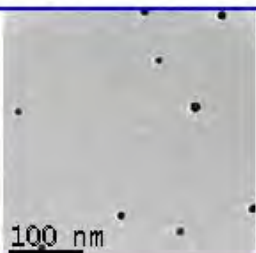
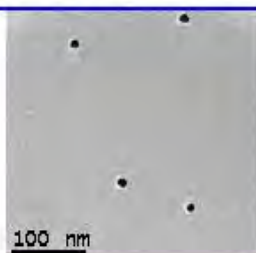
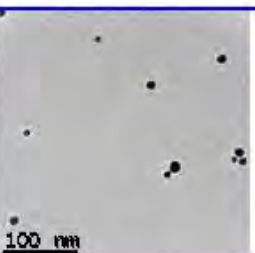


C (ppb)	Image 1	Image 2	Image 3
17.96			
9.49			
1.85			
0.89			
0.19			

**Figure 7-3:** Representative transmission electron microscopy images showing a uniform distribution of Citrate capped-AuNMs on TEM grid that is treated with 0.1% w/v poly-L-lysine and the decrease of the number of NMs recovered with the decrease in NM mass concentration in ppb (a) 17.96, (b) 9.49, (c) 1.85, (d) 0.89 and (e) 0.19. NMs were suspended in UHPW.

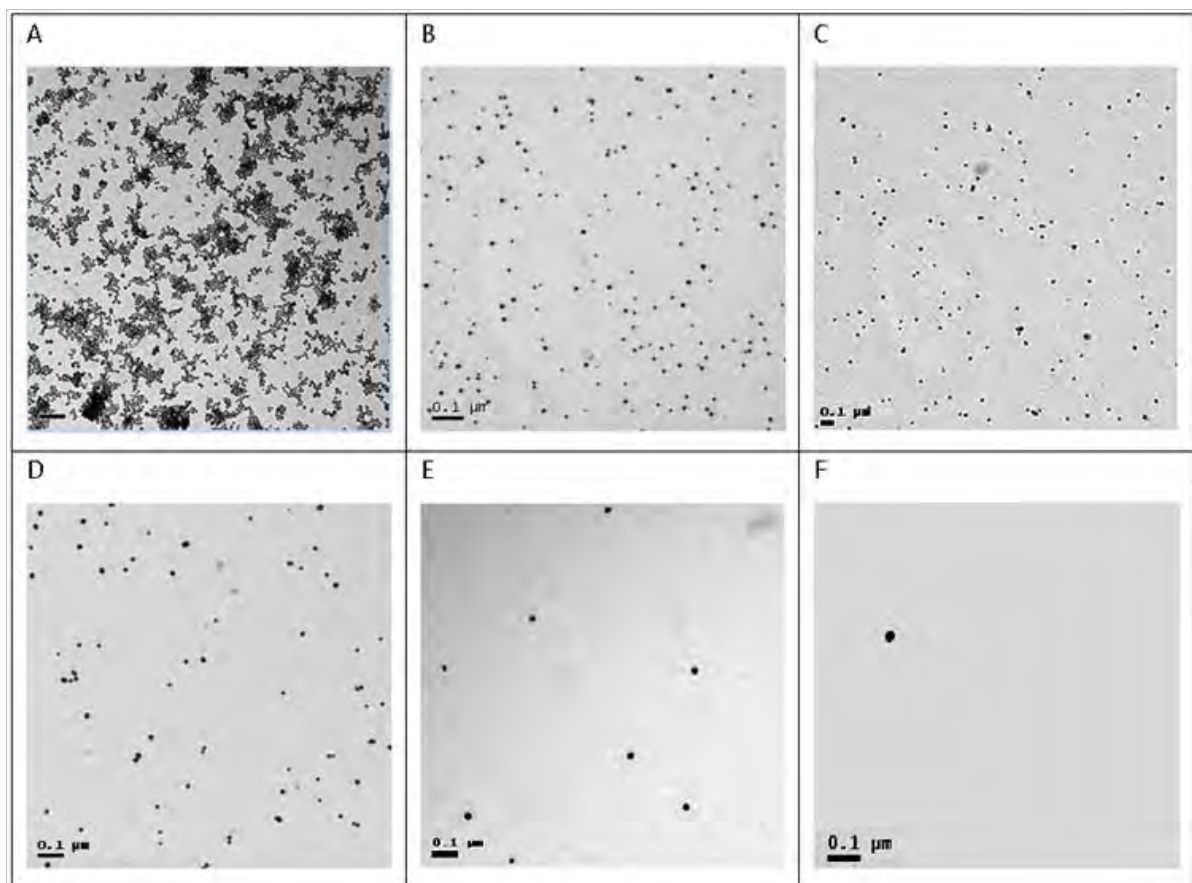
Figure 7-4 shows the TEM images of PVP capped Au NMs in simple media i.e. UHPW, show a reasonable coverage of the TEM grid within the concentration range from 0.34 - 31.38 ppb. For example, the concentration of 15.79 ppb, (in Figure 7-4) the NM distribution between three images (images in second row) were consistent when compared with the images (shown in Figure 7-1 and Figure 7-2 in the first column) by the drop (for same concentration 15.79 ppb) and ultracentrifugation deposition, the distribution of number of NMs varies drastically i.e. the number of particles in some images are more when compared, and in some lesser. This is qualitatively explained with the TEM images whereas quantitatively explanation is given in detail in further sections. This is the first time evaluated with the improvised sampling technique which encompasses active deposition (by ultracentrifugation) and retention (by charge attraction) of NMs on the TEM grid.

Consequently, all subsequent analyses were performed at concentrations in the ranges of 0.20 to 17.96 ppb for cit-Au NMs, and 0.34 to 31.38 ppb for PVP-Au NMs. To compare the distribution with respect to each concentration is explained in the next section.

C (ppb)	Image 1	Image 2	Image 3
31.38			
15.79			
3.34			
1.55			
0.34			

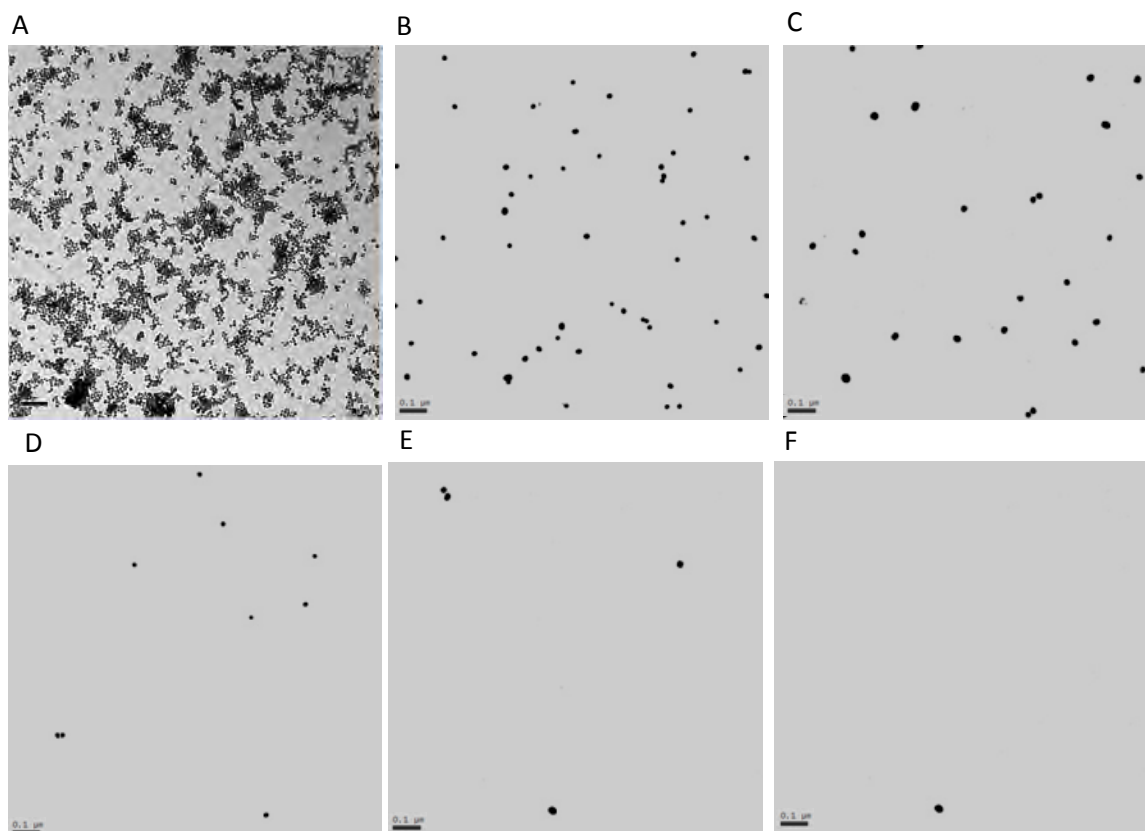
**Figure 7-4:** Representative transmission electron microscopy images showing a uniform distribution of PVP-AuNMs on TEM grid that is functionalized with 0.1% w/v poly-L-lysine and the decrease of the number of NMs recovered with the decrease in NM mass concentration in ppb (a) 31.38, (b) 15.79, (c) 3.34, (d) 1.55 and (e) 0.34. NMs were suspended in UHPW.

Figure 7-5 shows the representative transmission electron microscopy images showing a uniform distribution of citrate coated Au NMs on TEM grid that is treated with 0.1% w/v poly-L-lysine. For the higher concentration the number of NMs was found to be overloaded as shown in Figure 7-4 (A) for 101.5 ppb. As the sample concentration decreases (that is increase in dilution with pure water), the number of NMs also decreases.



**Figure 7-5:** Transmission electron microscopy images showing a uniform distribution of Citrate coated-AuNMs on TEM grid that is treated with 0.1% w/v poly-L-lysine and the decrease of the number of NMs recovered with the decrease in NM mass concentration in ppb (a) 101.5, (b) 17.96, (c) 9.49, (d) 1.85, (e) 0.89 and (f) 0.19. Scale bar in all images is 100 nm. The cit-AuNMs were suspended in UHPW.

Similarly, Figure 7-5 below shows the representative TEM images of PVP capped NMs, showing the distribution of NMs, for the concentration decreasing from higher to lower i.e. from 100 ppb to 0.34 ppb. For the higher concentration it can be seen TEM substrate is overloaded, as the concentration decreases the number of nanoparticles decreased.



**Figure 7-6:** Transmission electron microscopy images showing a uniform distribution of PVP coated-AuNMs on TEM grid that is treated with 0.1% w/v poly-L-lysine and the decrease of the number of NMs recovered with the decrease in NM mass concentration in ppb (a) 101.5, (b) 31.38, (c) 15.79, (d) 9.49, (e) 1.55 and (f) 0.34. Scale bar in all images is 100 nm. The cit-AuNMs were suspended in UHPW.

Quantitatively, the uniformity of NM distribution between the images was evaluated by comparing the number of particles counted at different areas on the TEM grid, which was performed by calculating the coefficient of variation of the number of NMs per  $\mu\text{m}^2$  on the

images collected at different location on the grid ( $CV = \sigma/\text{mean}$  of number NMs per  $\mu\text{m}^2$  on the different images). Low CV values indicate uniform distribution of NM on the TEM grid.

**Table 7-1:** Number concentration (particle  $\text{L}^{-1}$ ) of cit-Au NMs in stock solutions

Concentration ( $\mu\text{g L}^{-1}$ )	NMs in UHPW on non-functionalised TEM grid (drop Method) CV	NMs in UHPW on bared TEM grid (ultracentrifugation Method) CV	NMs in UHPW on PLL functionalised TEM grid CV
101.5	NA	NA	Overloading
20.3	$8.58 \times 10^{12}$ 0.32	$1.05 \times 10^{13}$ 0.31	$2.49 \times 10^{15}$ 0.09
10.2	$6.52 \times 10^{12}$ 0.28	$3.68 \times 10^{12}$ 0.32	$2.55 \times 10^{15}$ 0.13
2.0	NA	NA	$2.90 \times 10^{15}$ 0.10
1.0	NA	NA	$3.02 \times 10^{15}$ 0.37
0.20	NA	NA	$2.79 \times 10^{15}$ 1.00

NA: Not analyzed

UHPW: ultrahigh purity water

CV: coefficient of variation

Thereby quantitatively, the uniformity of NM distribution on the TEM grid was described by the coefficient of variation (CV) of the number of NMs on different images taken at different locations on the TEM grid (Table 7-1). The Table 6-1 shows the different concentration for drop deposition method of sample preparation, the CV was relatively high (0.32 and 0.28 for cit-Au NMs and 0.16 and 0.29 for PVP- Au NMs, respectively). Lower the CV, the stronger the attachment but for drop deposition the CV was found to be higher. Hence, the drop deposition method of sample preparation resulted in the non-uniform distribution of NMs on the substrate between the images. The next step from the drop deposition method is to calculate the percentage of NMs recovered on the substrates.

**Table 7-2:** Number concentration (particle.L<sup>-1</sup>) of PVP-Au NMs in stock solutions

Concentration ( $\mu\text{g L}^{-1}$ )	NMs in UHPW on bared TEM grid (drop method) CV	NMs in UHPW on bared TEM grid (ultracentrifugation) CV	NMs in UHPW on PLL functionalised TEM grid (ultracentrifugation) CV
670.0, 335.0 and 167.5	NA	NA	Overloading
31.38	$2.86 \times 10^{14}$ 0.29	$1.35 \times 10^{15}$ 0.18	$8.82 \times 10^{15}$ 0.05
15.79	$3.46 \times 10^{14}$ 0.16	$3.39 \times 10^{14}$ 0.21	$1.40 \times 10^{16}$ 0.07
3.34	NA	NA	$1.32 \times 10^{16}$ 0.20
1.55	NA	NA	$1.31 \times 10^{16}$ 0.19
0.34	NA	NA	$1.33 \times 10^{16}$ 0.40

NA: not analysed

CV: coefficient of variation

UHPW: ultrahigh purity water

For samples prepared by ultracentrifugation on non-functionalized TEM grid, the CV was also relatively high (0.30-0.32 and 0.18-0.29 for citrate capped and PVP Au NMs, respectively) compared with the CV for samples prepared by ultracentrifugation on PLL-functionalized TEM grids (0.09-0.13 and, 0.05-0.19 for cit-Au NMs ( $2.0\text{-}20.3 \mu\text{g L}^{-1}$ ) and PVP-Au NMs ( $1.7\text{-}33.5 \mu\text{g L}^{-1}$ ), respectively (Table 7-1 and Table 6-2). At very low concentration, a higher CV was observed (CV = 0.4 to 1.0) for cit-Au NMs ( $0.2\text{-}1.0 \mu\text{g L}^{-1}$ ) and (CV = 0.4 to 1.0) for PVP-Au NMs ( $0.34 \mu\text{g L}^{-1}$ ), due to the low number of NMs recovered on the TEM grid of such dilute samples. The higher uniformity of NM distribution on the TEM grid (indicated by the lower CV of the number of TEM detected in different images) is likely due to the strong, possibly irreversible attachment of NMs to the PLL-functionalized TEM grid. Furthermore, these results suggest that best results can be achieved for NM suspensions within the concentration range of  $0.2$  to  $33.5 \mu\text{g L}^{-1}$ , although the CV is higher at the lower concentration essentially because of the poorer counting

statistics. These concentrations are ideal for Au NM in the size range of 10-15 nm. Lower mass concentrations of NM suspensions can be analyzed for smaller NM sizes and for NMs of lower density as, for a constant NM mass concentration, the number of NMs increases with the decrease in particle size and in material density. Analyzing NMs at such low concentrations is beneficial as predicted environmental concentrations of engineered NMs are likely to be in the range of ng -  $\mu\text{g L}^{-1}$ .(Gottschalk et al., 2009, Gottschalk et al., 2013b, Blaser et al., 2008).

### 7.2.1.3 Percentage recovery of NMs by simple media

The percentage recovery of NMs is the the ratio of the number of NM population recovered on the substrate to the number of NM ultracentrifuged as shown in the Equation 6-1 below. For each concentration as shown in the Table 7-3, a TEM grid is prepared and from each grid, 30 images were scanned/taken by TEM. The number of NMs on each image was counted and the percentage of NMs on the entire TEM substrate was calculated with respect to the NM ultracentrifuged. Percentage of recovery is quantified by calculating the ratio of the mass of NM recovered on the TEM grid compared to the mass of NM in suspension or centrifuged.(Baalousha et al., 2014c).

The recovery of NMs on the TEM grid can be calculated according to Eq.7-1 assuming that the NMs are insoluble and spherical (shape factor for cit- and PVP-Au NMs is 0.88 and 0.98, respectively, Table 5-3).

$$R = \frac{M_{recovered}}{M_{centrifugal}} 100\% \quad \text{Eq.7-1}$$



Where: R is the percentage recovery of NMs on the substrate,  $M_{recovered}$  is the total number of NMs on the grid,  $M_{centrifuged}$  is the amount of NMs in suspension ultracentrifuged on the TEM substrate and % recovery is the percentage of NMs recovered on the substrate.

The following assumptions are embedded in the calculation of the recovery:

- (i) no losses of NMs to the containers during storage, dilution and ultracentrifugation and
- (ii) all counted NMs are single entities and no interactions occurred between the NMs.

**Table 7-3: Recovery (%) of cit-Au NMs**

Concentration of Cit-Au NMs ( $\mu\text{g L}^{-1}$ )	Drop deposition	NMs in UHPW Ultracentrifugation on non-functionalised TEM grid	NMs in UHPW Ultracentrifugation on PLL functionalised TEM grid
17.96	2.9	3.5	83.8
9.49	NA	4.2	85.8
1.85	2.5	NA	96.9
0.89	NA	NA	101.5
0.19	NA	NA	93.7
Average			92.3

UHPW: ultrahigh purity water

NA: Not analyzed

As shown in Table 7-3, for both citrate and PVP capped NMs for two different concentrations, percentage recovery was calculated. Low recoveries of 2.9% and 2.5% for citrate coated Au NMs and 2.8% and 2.1% for PVP- coated Au NMs were observed for samples prepared by the drop deposition method. Low recovery was mainly due to the attachment of the NMs on the substrate by drop deposition method. The NMs that were precipitated on the substrate were loosely attached to the substrate. The other reason, may be due to the washing of the substrate that results in the loss of NMs. Hence, enhancement of the NM attachment and the quality of distribution of NMs on the substrate plays a vital role

in the measurement of the particle number. Another important criteria is the number of images required from each TEM grid/substrate to calculate the percentage recovery of the entire grid, that is given in detail in the following subsection.

**Table 7-4** Recovery (%) of PVP capped Au NMs

Concentration of PVP-Au NMs ( $\mu\text{g L}^{-1}$ )	Drop deposition	NMs in UHPW	
		Ultracentrifugation on non-functionalised TEM grid	Ultracentrifugation on PLL functionalised TEM grid
31.38	NA	8.2	53.2
15.79	2.1	6.4	84.5
3.34	2.8	NA	79.7
1.55	NA	NA	79.1
0.34	NA	NA	80.1
Average			75.3

For Au NM samples in UHPW ultracentrifuged on non-functionalized TEM grids, the recovery improved slightly 3.5% and 4.2% for cit-Au NMs and also improved recovery was observed for PVP capped Au NMs upto 8.2%.

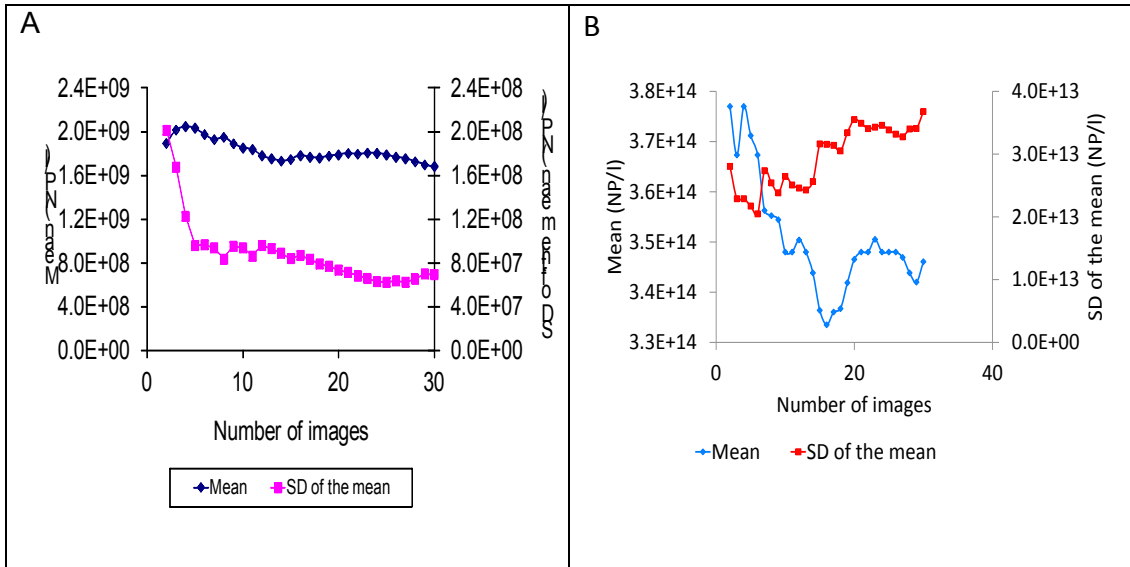
However, for samples prepared by ultracentrifugation on a PLL-functionalized TEM grids, significantly higher recovery was achieved for cit-Au NMs in the range from 83.8% to 101.5%, Table 7-3, and PVP-Au NMs of 53% - 84.5 %, Table 7-4 and Figure 7-6.. The lower recoveries for PVP-Au NMs are likely because of the reduced importance of the charge interactions of PVP-Au NMs (zeta potential =  $-8.3 \pm 1.6$  mV) with the PLL-functionalized TEM grid, compared with that of cit-Au NMs (zeta potential =  $-43 \pm 1.3$  mV) with the PLL-functionalized TEM grid. For higher concentration of PVP-Au NMs ( $31.38 \mu\text{g L}^{-1}$ ), the perceived recovery was relatively low compared with those at lower concentrations ( $0.38$ - $16.8 \mu\text{g L}^{-1}$ ) because of the high number of particles on the TEM grid and the potential overlapping of NMs on the grid. Additionally, higher recoveries (84-101%, for NM concentration in the range  $0.19$  to  $17.96 \mu\text{g L}^{-1}$ ) are achieved for Au NMs by TEM in this

study compared with our previous results on the same NMs by AFM (53-71%) performed under the same conditions.(Baalousha et al., 2014c) This is likely to be due to:

- (i) potential loss of NMs due to tip-NM interactions in AFM analysis, or
- (ii) ability of TEM to distinguish single and aggregated NMs, and the number of individual NMs within aggregated, which was not resolved by AFM analysis due to the better lateral resolution in TEM compared to AFM.

#### **7.2.1.4 Number of images required for representative measurement of particle number**

The number of images required to obtain a representative measurements of NM number concentration was assessed by quantifying the mean number concentration and standard deviation of the mean as a function of the number of images analysed. The quantification of the mean number concentration obtained by counting the NMs of all the images scanned per TEM grid. As explained in the previous Chapter 6 as well as paper published by this research study (Baalousha et al., 2014c) and future upcoming sections (by improvisation in the sampling technique) proves the number of images to be scanned per TEM grid to obtain stable value. That is for cit-Au NMs and PVP-Au NMs prepared by ultracentrifugation on PLL functionalized TEM grid, the mean number concentration (See Chapter 4 and Figure 4.7.5) tends to a stable value for  $\geq 15$  images was observed by AFM analysis. The standard deviation of the mean decreases with the increase in the number of images and reaches a stable value. Therefore, a minimum number of 15 images are required to obtain mean number concentration and a standard deviation ( $\sigma$ ) representative of the entire population of NMs.



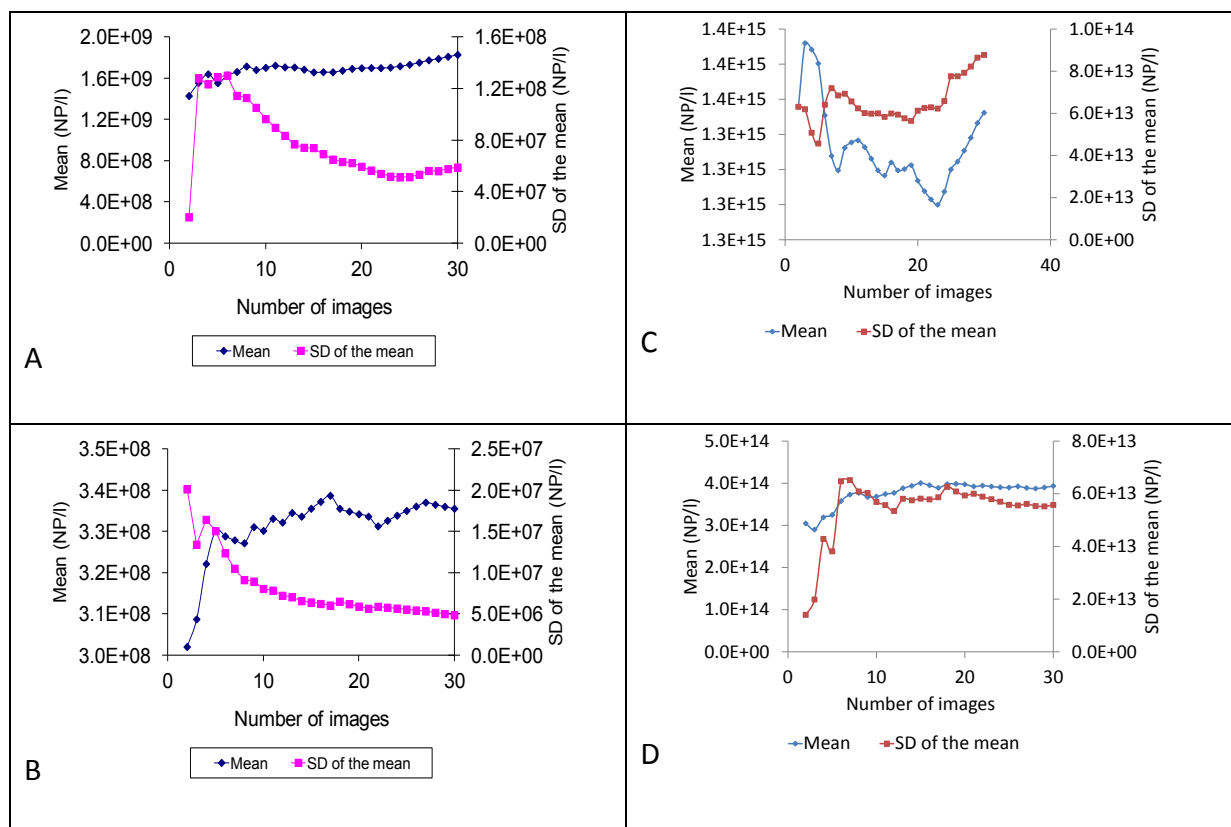
**Figure 7-7:**Dependence of the calculated mean number concentration and standard deviation of the mean on the number of images scanned by transition electron microscopy of the cit-AuNMs prepared by (A) drop deposition (17.96 ppb) and PVP-AuNMs prepared by (B) drop deposition (15.79 ppb).the y axes are not correct here

To determine the minimum number of images required to obtain accurate and statistically representative particle number concentration of the entire suspension of NMs, investigated the stability of the calculated mean number concentration and standard deviation of the mean ( $\sigma_{mean}$ , Eq.7-2) on subpopulations of the scanned images ( $n=2-27$  images).(Baalousha and Lead, 2012; Boyd et al., 2011)

$$\sigma_{mean} = \frac{\sigma}{\sqrt{n}} \quad (\text{Eq.7-2})$$

Figure 7-7 shows the mean number concentration and standard deviation of the mean for cit- Au NMs and PVP-Au NMs prepared by drop deposition method for concentration 17.96 ppb and 15.79 ppb respectively. Neither the mean nor the standard deviation of the mean tend to a stable value for the number of images scanned for all samples, greatly increasing uncertainty. Therefore, drop deposition method of sample preparation results in impossible to obtain a representative measurement of particle number

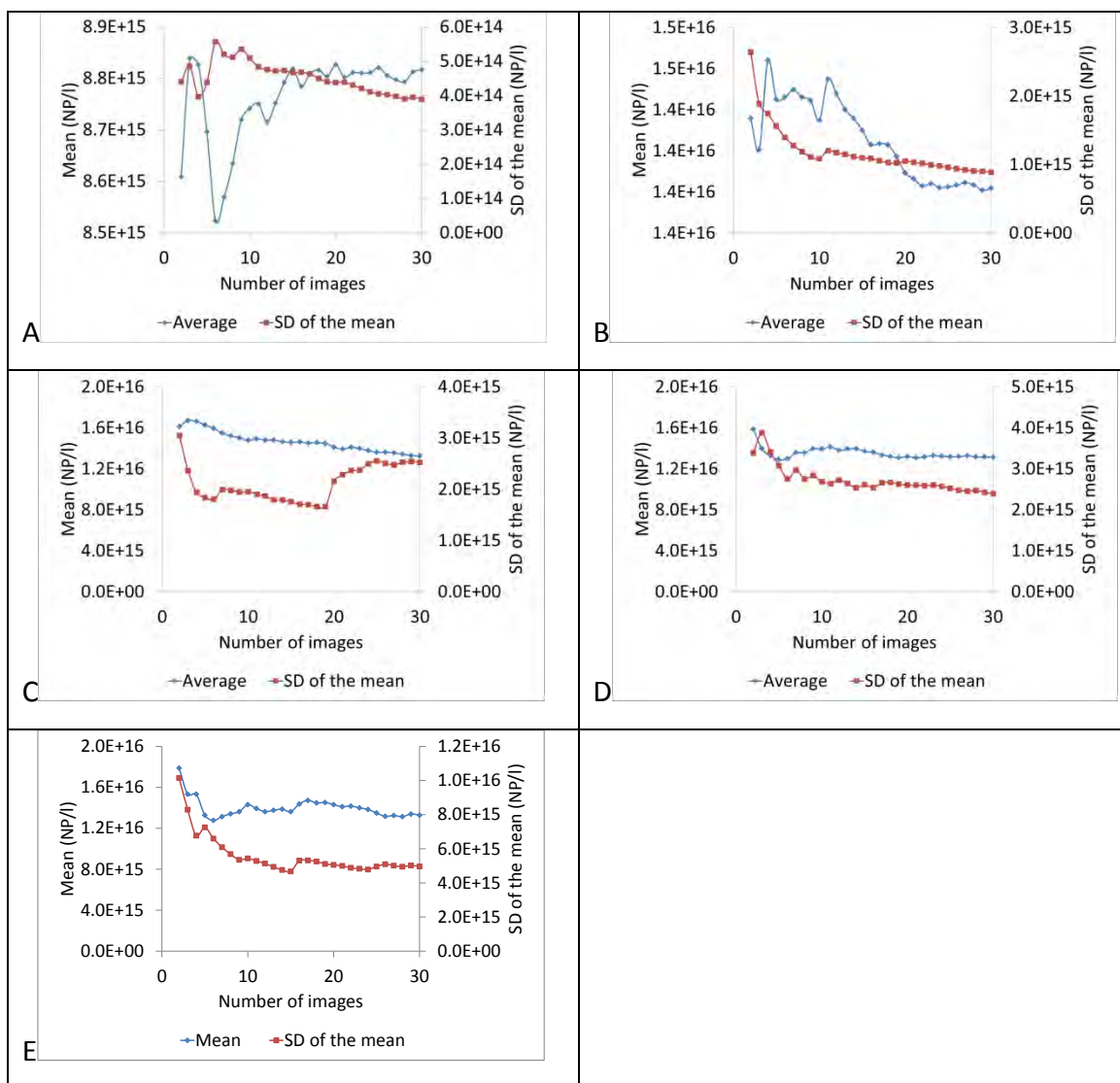
concentration. Thereby, the sample preparation technique must be improved to obtain the optimal coverage of grid for the consistent count the particle number in each image scanned.



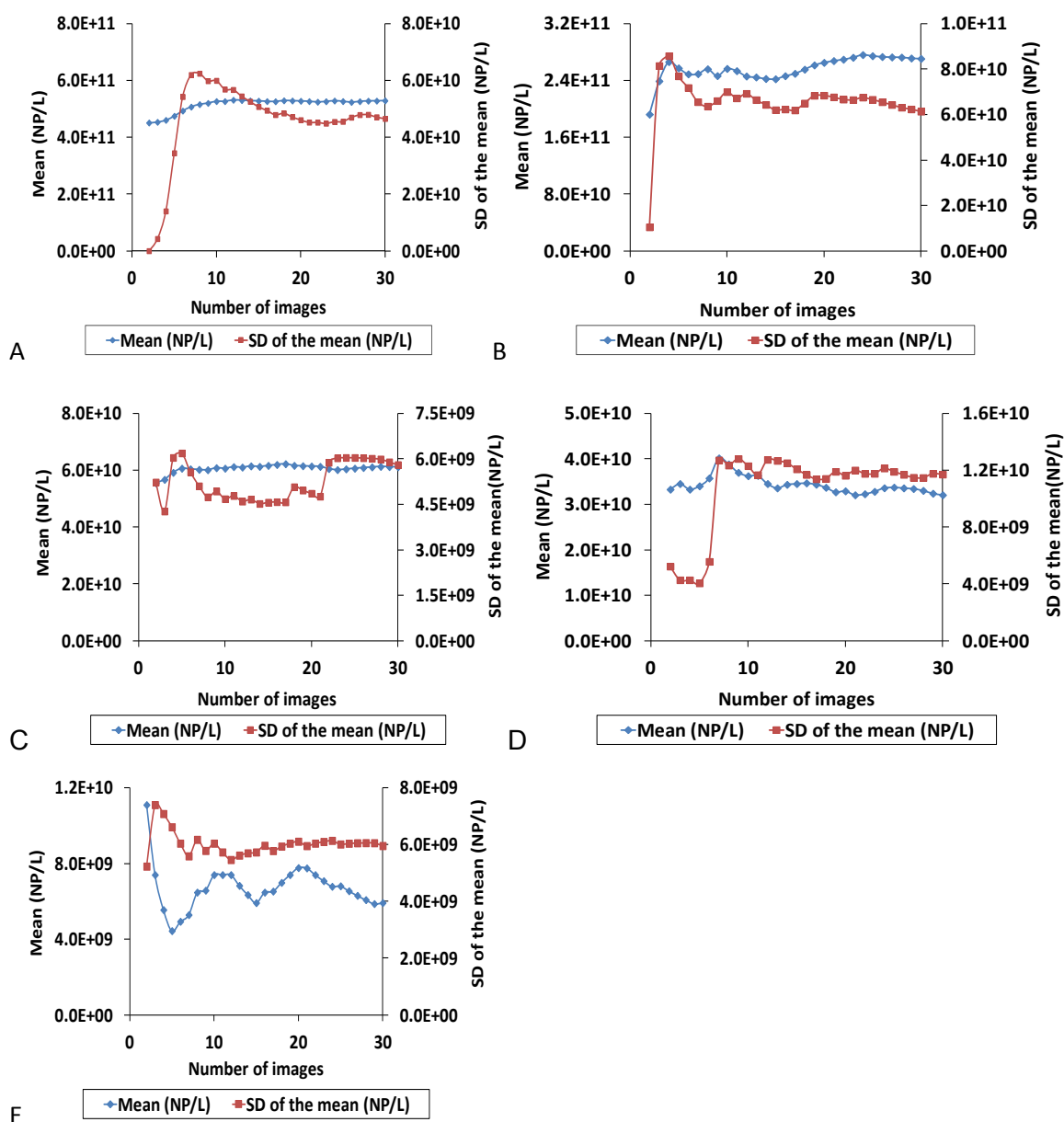
**Figure 7-8:** Calculated mean number concentration and standard deviation of the mean on the number of images scanned by transition electron microscopy of the cit-AuNMs prepared by (A) ultracentrifugation on non functionalised TEM grid (20.3 ppb) and (B) ultracentrifugation non functionalised TEM grid (10.2 ppb); and PVP-AuNMs prepared by (C) ultracentrifugation on non functionalised TEM grid (33.5 ppb) and (D) ultracentrifugation on non functionalised TEM grid (16.8 ppb).

Whereas, for the ultracentrifugation on non functionalised TEM grid, mean number concentration and standard deviation of the mean for citrate capped - Au NMs and PVP capped -Au NMs shown in the Figure 7-8 above. Similar to the drop deposition neither the mean nor the standard deviation tends to a stable value for the number of images scanned

for all samples. Therefore, this method indicates to be modified to obtain the saturated graph eventually for the number of images. It is impossible to obtain a representative number particle concentration from these samples.



**Figure 7-9** Dependence of the calculated mean number concentration and standard deviation of the mean on the number of images scanned by transition electron microscopy of the PVP-AuNMs prepared by ultracentrifugation at 150 000 g on poly-L-lysine functionalized TEM grid at different concentrations (ppb): (a) 31.5, (b) 16.8, (c) 3.4, (d) 1.7 and (e) 0.34.



**Figure 7-10** Calculated mean number concentration and standard deviation of the mean on the number of images analyzed by transmission electron microscopy. TEM samples were prepared by ultracentrifugation of cit-Au NMs at 150 000 g on poly-l-lysine functionalized TEM grid at different concentrations ( $\mu\text{g L}^{-1}$ ): (a) 20.3, (b) 10.2, (c) 2.0, (d) 1.0 and (e) 0.20.

For the improvised sample preparation technique i.e. sample prepared by the poly-L-lysine functionalised TEM grid at different concentrations for the PVP capped and citrate capped Au NMs shown in the Figure 7-9 and Figure 7-10 respectively. The calculated mean number concentration tends to a stable value for  $\geq 15$  images, as was observed for AFM analysis (paper published related to the previous Chapter 6). The standard deviation of the mean decreases with the increase in the number of images and reaches a stable value also at about  $\geq 15$  images. Therefore, for the first time a fully quantitative sample preparation protocol that enables detection and quantification of NM number measurement at low concentration was presented.

#### **7.2.1.5 Correlation between the mass and number concentration**

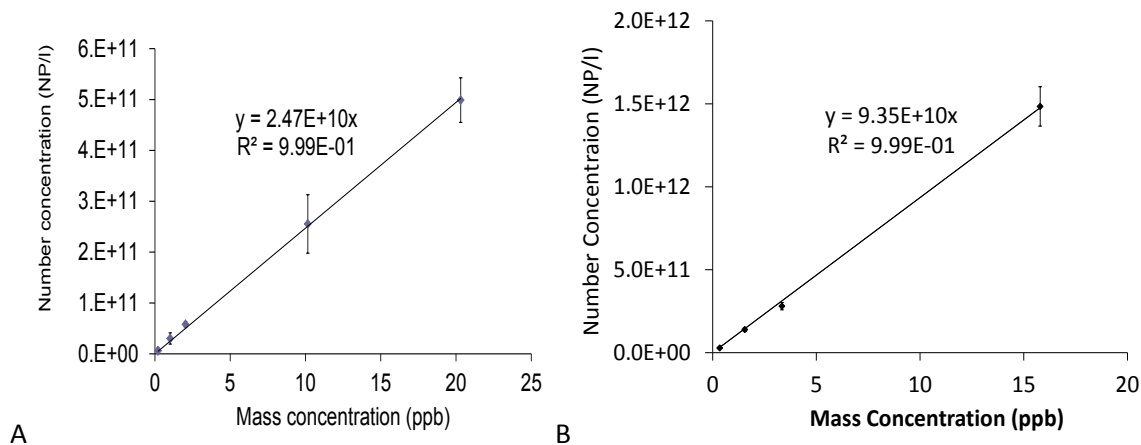
The correlation between the particle number and mass concentration of NMs is important to compare and analyse the applicability of sampling technique to find the lower and upper limit sample concentration. This is explained in detail further. The comparison was carried with the known mass concentration (by analytical instrument) and measured particle number. The mass concentration of in-house synthesised NMs i.e. the citrate capped Au NMs and PVP capped Au NMs was measured by the ICP-MS. The measurement of the mass concentration by ICP-MS was explained in detail in Chapter 5 (characterisation of NMs results and discussion) and in Section 5.4.8.

For the drop deposition method, the correlation between the measured particle number and the mass concentration for cit Au NMs and PVP Au NMs results in the higher uncertainty and variability with greater counting statistics because of the low number of NMs present on the TEM grid, the presence of low NMs i.e. the percentage recovery is shown in Table 7-4. Thereby, the drop deposition method of sampling technique is ruled out for the measurement particle number.

Similarly, for the ultracentrifugation method (without functionalisation of the substrate see Chapter 3, Section 3.3 and Subsection 3.3.2.) of sampling technique the correlation



between mass and particle number concentrations for cit- Au NMs and PVP- Au NMs was ruled out. Because of the lower NM count on the substrate.



**Figure 7-11** Correlation between the mass and number concentration of Au NMs (A) citrate-Au NMs suspended in MQ water, (B) PVP-Au NMs suspended in MQ water. Samples prepared by ultracentrifugation on a poly-l-lysine functionalized TEM grid.

Whilst for the ultracentrifugation method of PLL functionalised substrate (see Chapter 4 and Section 4.3.3) of sampling technique results in the good correlation (Figure 7-11,  $R^2=1.00$ ) between the particle number and mass concentration measurement. These results suggest that the sample preparation method is applicable within the NM concentration range of this is 0.20-17.96 ppb and 0.34-16.8 ppb for cit- Au NMs and PVP- Au NMs investigated in this study. Lower NM concentrations will result in higher uncertainty and variability without greater counting statistics because of the low number of NMs present on the TEM grid (Figures 7-1 and 7-2). However, the lower concentration limit can potentially be reduced, given sufficient time and/or automation to collect higher number of images to improve the statistical confidence in the data.

This research developed and presented for the first time a fully quantitative sample preparation protocol that enables detection and quantification of NM number concentration

for simple media. The methodology was developed to validate the sample preparation method to enable the measurement of NM number concentration by TEM, and also demonstrated the applicability of this validated sample preparation method to detect and quantify the number concentration of Au NMs for the concentrations (e.g. 1-20  $\mu\text{g L}^{-1}$ ). The percentage recovery of NMs on the grid was seen more improved by TEM analysis when compared to the AFM analysis. The sampling approach was validated using citrate- and PVP- coated Au NMs in pure water, which demonstrated an even distribution of NM on the TEM grid and high NM recovery 84-101%. This novel, fully quantitative sampling approach has enabled successfully for the first time measuring the particle number which is applied at environmentally realistic concentrations, explained in detail in the next section. Thus will be proved transmission electron microscopy (TEM) is a vital metrological tool in nanotechnology and as well as environmental nanoscience due to its high spatial resolution and analytical capabilities when coupled to spectroscopic techniques. The following discussion is based on the detailed view on the fate and behavior nanomaterials when added to the realistic environmental media and testing the capability of the analytical tool i.e. TEM to image and detect Au NMs in complex media.

### **7.2.2 Detection and quantification of engineered NMs in environmentally representative complex media**

The applicability of the sampling method to complex environmental samples was demonstrated by detecting and quantifying number particle concentration of Au NMs spiked in the following three different complex media such as

- (i) Synthetic EPA soft water
- (ii) EPA soft water containing 5 mg/L of Suwannee river fulvic acid and as well
- (iii) Filtered lake water / Natural water

All the above mentioned three different complex media at environmentally NM relevant concentrations of 1 to 20  $\mu\text{g L}^{-1}$  used to detect and quantify the number particle. This in turn enabled demonstrated a concentration-dependent aggregation of NM at environmentally relevant NM concentration. In other words, the number of NMs within the aggregates decreased, whereas the number of free NMs increased, with the decrease in NM concentration. These findings are key to improve our understanding of NM environmental behaviors, fate, effects and dose; and were only enabled by the novel fully quantitative sampling method. An ideal technique with realistic environmental samples/complex media should be able to

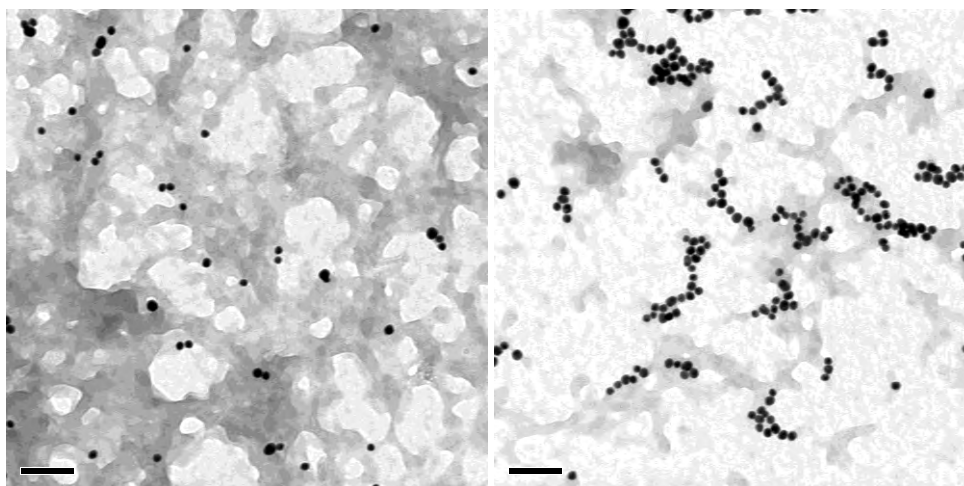
- (i) Determine a true/accurate number of NMs irrespective of morphology, density or optical properties of NMs,
- (ii) Distinguish aggregates/agglomerates from primary nanoparticles,
- (iii) Isolate a target nanoparticle in a complex matrix containing nanoparticles of different composition (e.g. manufactured nanoparticles in a matrices of naturally occurring nanoparticles),

- (iv) Measure number concentration at environmentally relevant concentrations ( $\text{ng-}\mu\text{g L}^{-1}$ ),
- (v) Cover the entire nanosize range (e.g. 1-100 nm),
- (vi) Provides an accurate measurement of NM dispersion.

The protocol used for the detection and quantification of the number of NMs in pure water, similar protocol followed to detect and quantification of Au NMs in complex media. In this investigation, NMs added to the three different environmental samples i.e. said to be NMs in complex media. The following discussion is based on the NMs interactions with the environmental samples. It is a challenge in determining and understanding with the limited analytical techniques and hence in this research is the first time for both improved sampling technique and measurement of particle number concentration in realistic environmental conditions.

#### **7.2.2.1 Au NMs added to SRFA media**

Preparation of SRFA media (EPA soft water containing  $5 \text{ mg L}^{-1}$  Suwannee River fulvic acid) in-house is explained in detail in Chapter 4 in Section 4.6.2. The validated sampling technique (ultracentrifugation on PLL functionalized TEM grids) was applied to detect and quantify the number of cit-Au NMs in SRFA containing EPA soft water spiked with cit-Au NMs ( $1.0$  to  $20.3 \mu\text{g L}^{-1}$  Au). The typical micrographs with x-ray dispersive spectroscopy are presented in a Figure 6-12 and Figure 6-13 respectively. TEM images SRFA media show two distinctive materials.



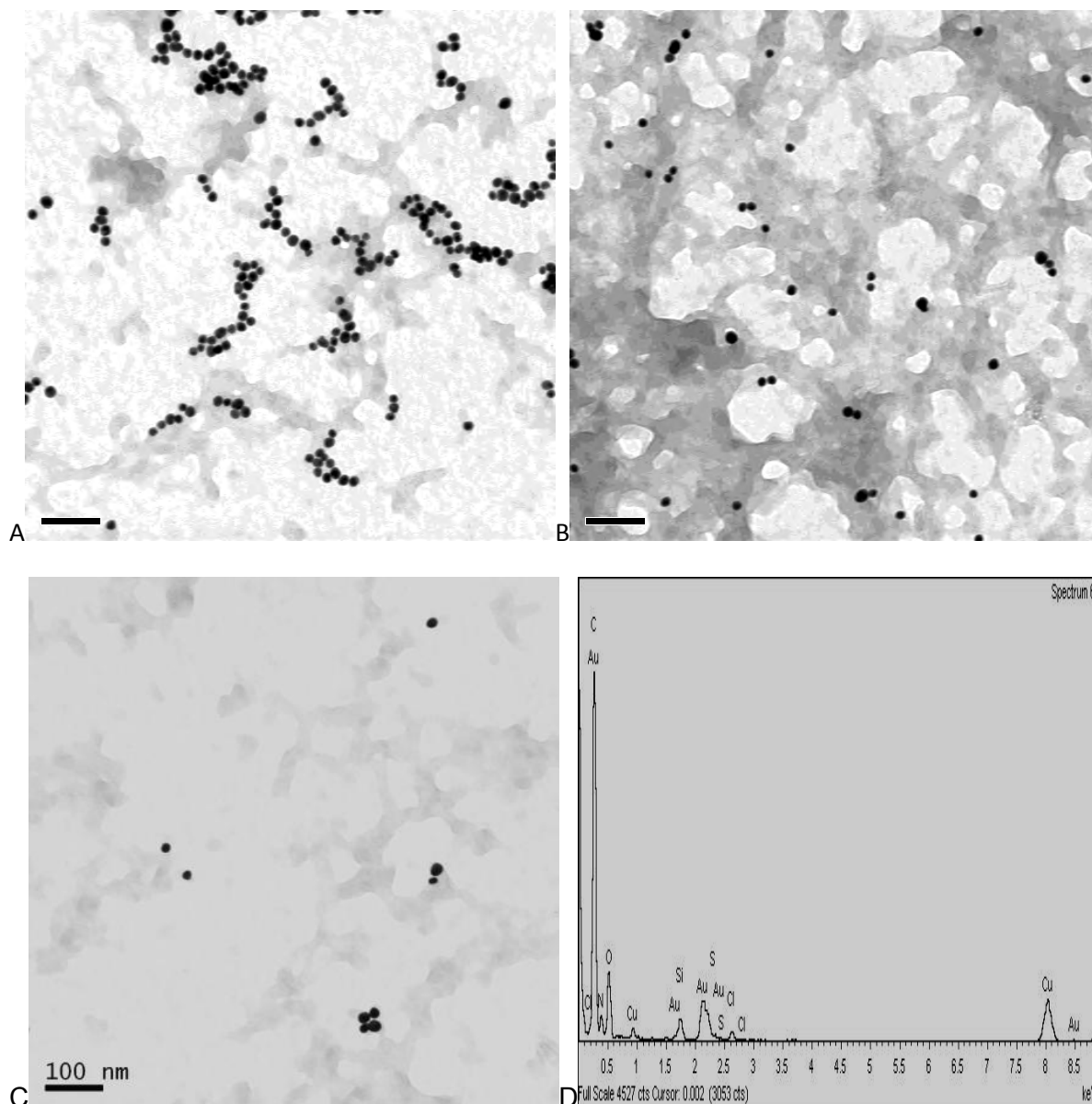
**Figure 7-12** Concentration-dependent aggregation of NMs revealed at environmentally realistic NM concentration by the newly developed fully quantitative sample preparation approach for TEM analysis of NMs (a)  $2.0 \mu\text{g L}^{-1}$  and (b)  $20.3 \mu\text{g L}^{-1}$

The first material was characterized by low contrast and forms a network structure typical of aggregated humic substances, (Leppard, 2008, Wilkinson et al., 1999b, Baalousha et al., 2005c) and the second material is characterized by high contrast and is formed of distinct spherical particles, which were identified by X-EDS as Au NMs (Figure 7-12). Figure 7-12 shows the typical TEM micrograph of two concentrations such as  $2.0 \mu\text{g L}^{-1}$  cit-Au NMs having non aggregated Au NMs while  $20.3 \mu\text{g L}^{-1}$  cit-Au NMs shows the network structure of aggregated particles. Thus the concentration-dependent aggregation of NMs revealed at environmentally realistic NM concentration by the newly developed fully quantitative sample preparation approach for TEM analysis of NMs. As the concentrations of Au NMs decreases, aggregation of NMs also decreases.

The bridging of particles at the higher concentrations of Au NMs may be due to the surface potential of the citrate coated Au NMs. As stated by (Diegoli et al., 2008, Baalousha et al., 2008) zeta potential of NMs less than  $\pm 25 \text{ mV}$  in media having salts and ions is insufficient to prevent coalescence but the highly surface charged NMs have colloidal

stability. Whereas, the zeta potential of the citrate capped nanoparticles in SRFA-EPA media is -43 mV which is high enough to prevent the aggregation but at higher concentration of NMs resulted in the contraction of the electric double layer.

Interestingly at lower concentrations of 1.0 and 2.0  $\mu\text{g L}^{-1}$ , Au NMs occur mainly as individual non-aggregated NMs (Figure 4b and c), whereas at the higher concentration of 20.3  $\mu\text{g L}^{-1}$ , Au NMs occur largely as small aggregates of a few NMs. Figure 7-13 shows a typical TEM micrograph of different concentrations such as 1.0, 2.0  $\mu\text{g L}^{-1}$  and 20.0  $\mu\text{g L}^{-1}$ . From this micrograph it was observed as the concentration of NMs increases from 2.0  $\mu\text{g L}^{-1}$  to 20.0  $\mu\text{g L}^{-1}$  the bridging or chaining of the NMs occur. Figure 7-13 below shows the micrograph of different concentrations and its X-EDS spectra.



**Figure 7-13** Transmission electron microscopy images of cit-Au NMs spiked in synthetic EPA soft water containing 5 mg L<sup>-1</sup> Suwannee River fulvic acid. Mass concentration of cit-Au NMs in µg L<sup>-1</sup> was (A) 20.3, (B) 2.0, (C) 1.0. (D) a representative X-EDS spectrum collected from the dark particles identified as Au NMs. All samples were prepared by ultracentrifugation on poly-l-lysine functionalized TEM grid.

From the above micrographs, 100 % of all observed NMs were either single NMs or aggregates of 1-5 NMs at 1 µg L<sup>-1</sup>, 96% of NMs are either single or aggregates of 1-5 NMs at 2 µg L<sup>-1</sup> and only 38.7% are single NMs or aggregates of 1-5 NMs at 20.3 µg L<sup>-1</sup> and 61.3

% are aggregates that contain higher numbers of NMs at 20.3  $\mu\text{g L}^{-1}$ . These observations are in accord on concentration-dependent aggregation of iron oxide NMs, which was observed at high NM concentrations (e.g. 1-200  $\text{mg L}^{-1}$ ) (Baalousha, 2009). Further it is shown in table below quantitatively the number of NMs in each aggregate. The following explanation is the number concentration (particle  $\text{L}^{-1}$ ) of citrate capped Au NMs in stock solutions in EPA-SRFA media.

**Table 7-5** : Number concentration (particle  $\text{L}^{-1}$ ) of cit-Au NMs in stock solutions

Concentration ( $\mu\text{g L}^{-1}$ )	NMs in UHPW on non-functionalised TEM grid (drop Method) CV	NMs in UHPW on bared TEM grid (ultracentrifugation Method) CV	NMs in UHPW on PLL functionalised TEM grid CV	NM in EPA-SRFA on PLL functionalised TEM grid CV
101.5	NA	NA	Overloading	Overloading
20.3	$8.58 \times 10^{12}$ 0.30	$1.05 \times 10^{13}$ 0.31	$2.49 \times 10^{15}$ 0.09	$2.66 \times 10^{15}$ 0.03
10.2	NA	$3.68 \times 10^{12}$ 0.32	$2.55 \times 10^{15}$ 0.13	$2.81 \times 10^{15}$ 0.19
2.0	NA	NA	$2.90 \times 10^{15}$ 0.10	$3.02 \times 10^{15}$ 0.09
1.0	NA	NA	$3.00 \times 10^{15}$ 0.37	NA
0.20	NA	NA	$2.79 \times 10^{15}$ 1.00	NA

CV: coefficient of variation

NA: Not analyzed

UHPW: ultrahigh purity water

SRFA: Suwannee river fulvic acid

Quantitatively, the measurement of particle number of citrate capped Au NMs shown in the above Table 6-6 at different concentrations. To compare particle number of Au NMs suspended in simple and complex media with different sampling technique such as the drop method and the ultracentrifugation method, without and with functionalization of the TEM substrate shown in the above Table 7-6. The particle number (particle  $\text{L}^{-1}$ ) in EPA-SRFA on PLL functionalised TEM substrate with simple and complex media was found to be in the same range ( $2.49 \times 10^{15}$  to  $3.02 \times 10^{15}$  particle  $\text{L}^{-1}$ ) and the coefficient of verification



(CV) of the number of NMs on different images taken at different locations on TEM grid are also lower between the range (CV - 0.03 to 0.10) for the concentrations 2.0 to 20.3  $\mu\text{g L}^{-1}$ . Thereby the particle number concentration between the simple and complex media was found to be having a good agreement, since no losses of NMs were observed exempting aggregation seen at higher concentration (20.3  $\mu\text{g L}^{-1}$ ) when media is added to Au NMs. But the feasibility of TEM technique integrated with the elemental analysis facility provided to identify the natural materials and the NMs. The X-EDS analysis shows the presence of naturally occurred NMs (which were not counted) and the sorption of elements such as chlorine, silver, nitrogen, aluminium, carbon, copper, and Silicon on the NMs (Figure 7-13 D). While the representative X-EDS spectrum showing the dark particles were identified as Au NMs. At higher concentration that is at 20.3  $\mu\text{g L}^{-1}$ , NMs are aggregating, due to surface charge neutralization between the SRFA-coated Au NMs.(Chen et al., 2007a, Chen et al., 2006, Chen and Elimelech, 2007) or may be SRFA replacing citrate coating on Au NMs.(Diegoli et al., 2008).

**Table 7-6** % number fraction of aggregates containing a certain number of primary NMs in soft EPA water containing 5 mg L<sup>-1</sup> SRFA at a range of NM concentrations ca. 1-20 µg L<sup>-1</sup>. Analysis was performed on 15 images collected at different locations on the TEM grid.

Number of NMs in an aggregate	1.0 µg L <sup>-1</sup>	2.0 µg L <sup>-1</sup>	20.3 µg L <sup>-1</sup>
Single NMs	84.5	85.7	6.9
1-5	15.5	10.2	31.8
6-10	0.0	4.0	12.8
11-15	0.0	0.0	10.6
16-20	0.0	0.0	10.6
21-30	0.0	0.0	11.3
31-40	0.0	0.0	8.0
41-50	0.0	0.0	8.0

The above Table 6-6 shows the percentage number fraction of aggregates containing a certain number of primary NMs in soft EPA water containing 5 mg L<sup>-1</sup> SRFA at a range of NM concentrations ca. 1-20 µg L<sup>-1</sup>. Quantitatively, the number of NMs in an aggregate was counted since the individual NMs in a smaller aggregate were loosely bonded so that each NM in an aggregate can be identified and counted. The image J or Matlab software facilitates to count the number of NMs in an aggregate, suppose if an aggregate appear in larger size it is impossible to count the number of NMs in an aggregate. Analysis was performed on 15 images collected at different locations on the TEM grid. It was seen that about 84.5% and 85.7% of single NMs were seen at lower NM suspensions 1.0 - 2.0 µg L<sup>-1</sup> respectively and about 15.5-10.2% aggregates having 1-5 number of NMs in an aggregate. While at higher NM suspensions it was found only 6.9% of single NMs and remaining NMs were aggregated as mentioned in the Table 6-6 above. Here, it was demonstrated for the first time that NM concentration-dependent aggregation also occur at environmentally

realistic NM concentrations and become nearly negligible at very low NM concentrations (ca. 1-2  $\mu\text{g L}^{-1}$ ). These low, environmentally realistic concentrations are at a level where analytical techniques usually employed to study NM aggregation e.g. DLS, Uv-vis, (Baalousha et al., 2008, Baalousha et al., Lead et al., 1999) fail because of sensitivity and selectivity issues. This presents TEM as a possible mean to investigate NM aggregation at realistic concentrations. The observed NM aggregation is due to NM surface charge neutralization and/or bridging between the SRFA-coated Au NMs.(Chen and Elimelech, 2007, Chen et al., 2006, Chen et al., 2007b). SRFA has been shown previously to replace citrate coating on Au NMs.(Diegoli et al., 2008). The following discussion is on total percentage recovery of citrate capped Au NMs spiked in EPA-SRFA media is shown in the Table 6-8 below.

**Table 7-7** Recovery (%) of cit-Au NMs

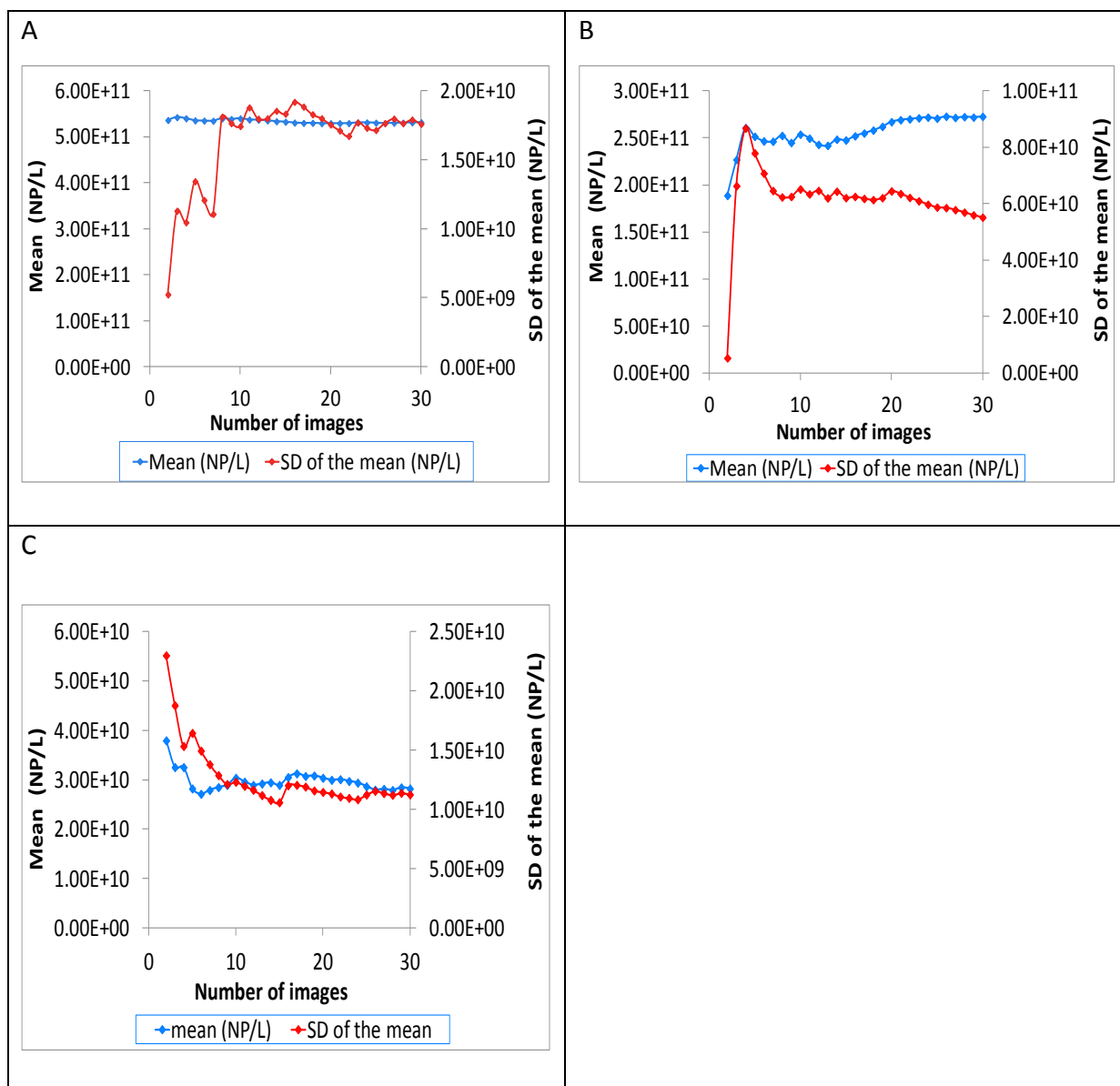
Concentration of Cit-Au NMs ( $\mu\text{g L}^{-1}$ )	Drop deposition	NMs in UHPW Ultracentrifugation on non-functionalised TEM grid	NMs in UHPW Ultracentrifugation on PLL functionalised TEM grid	NMs suspended in EPA water containing 5mg/L SRFA
20.3	2.9	3.5	83.8	81.1
10.2	NA	1.2	85.8	86.0
2.0	NA	NA	96.9	89.07
1.0	NA	NA	101.5	84.05
0.20	NA	NA	93.7	NA
Average			92.3	84.8

UHPW: ultrahigh purity water

NA: Not analyzed

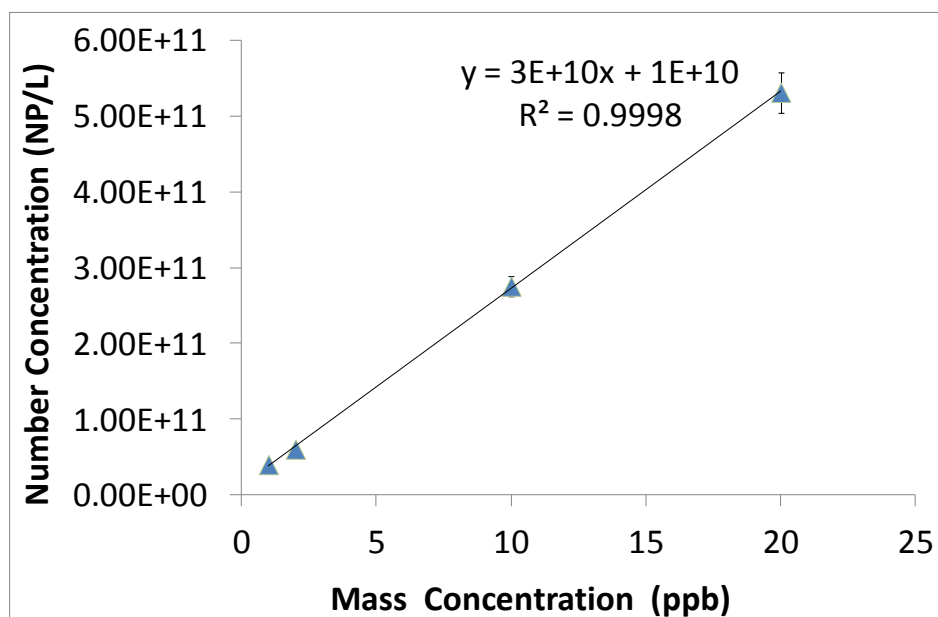
SRFA: Suwannee river fulvic acid

The percentage Au NMs recovered on each TEM substrate at different concentrations is given in the above Table 7-8. The calculations to obtain the percentage recovery are given in Section 4.7.5. The percentage recovery of citrate capped NMs spiked in SRFA-EPA is in the range of 81% to 89% shown in the Table 7-8 for four different concentrations range from 20.0 to 1.0 ppb. It is found to be having good agreement with the recoveries of NMs in simple media/ UHPW which is in the range of 84 to 96%. Thus, this sample preparation protocol can be applied to detect and quantify the number of engineered NM in various media.



**Figure 7-14** Dependence of the calculated mean number concentration and standard deviation of the mean on the number of images scanned by transmission electron microscopy of the cit-Au NMs spiked with EPA soft water containing 5 mg L<sup>-1</sup> Suwannee River fulvic acid prepared by ultracentrifugation at 150 000 g on poly-l-lysine functionalized TEM grid at different concentrations (ppb) : (a) 20.3, (b) 2.0 and (c) 1.0 .

The next step is to identify the number of images required for the representative measurement of particle number. The procedure to calculate the number of images required is explained in detail in Chapter 4 and in Subsection 4.7.5. Figure 7-14 above shows the mean number concentration and standard deviation of the mean in particles per litre of citrate capped Au NMs spiked in EPA-SRFA media, as a function of Au NM concentration. For the NMs in complex media the calculated mean number concentration tends to a stable value after  $\geq 15$  image which is similar to the simple media. Also the standard deviation of the mean decreases with the increase in the number of images and reaches a stable value at about  $\geq 15$  images. Therefore, a minimum number of 15 images are required to obtain mean number concentration and a standard deviation ( $\sigma$ ) representative of the entire population of NMs in EPA-SRFA media. The next step is to verify the correlation between the mass concentrations with the particle number concentration.

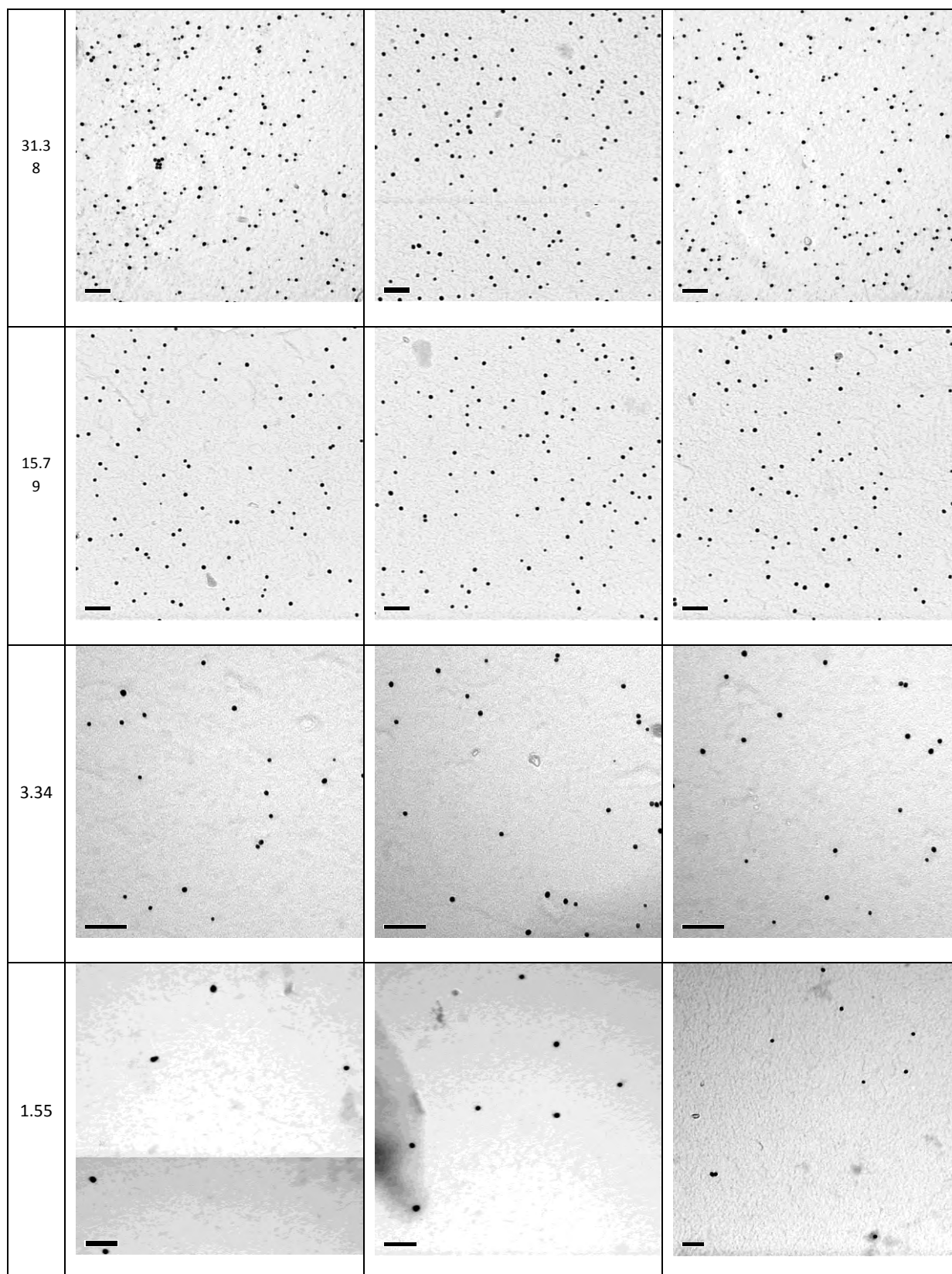


**Figure 7-15** Correlation between the mass and number concentration of citrate capped Au NMs cit-Au NMs spiked with EPA soft water containing 5 mg L<sup>-1</sup> Suwannee River fulvic acid prepared by ultracentrifugation at 150 000 g on poly-l-lysine functionalized TEM grid at different concentrations (ppb).

The applicability of sampling technique to the SRFA-EPA media was analysed and comparison of number concentration with the mass concentration obtained by ICP-MS was performed. Figure 7-15 above shows the correlation of mass and number concentration. Whilst for the ultracentrifugation method of PLL functionalised substrate for the Au NMs EPA-SRFA media is proved from the above graph that results to be having good correlation  $R^2=0.99$  between the particle number and mass concentration measurement. These results suggest that the sample preparation method is also applicable within the NM concentration range of this is 0.20-20.00 ppb for cit- Au NMs added to EPA-SRFA media is investigated in this study. Similarly, further investigation is carried on by adding Au NMs to the synthetic water.

### **7.2.2.2 Au NMs added to the synthetic EPA soft water**

The distribution of NMs on the substrate was validated on the PLL functionalised grid followed by ultracentrifuging the suspension of Au NMs in the EPA synthetic softwater. For the synthetic EPA soft water, the in-house synthesised Au NMs were added to it. The process of making EPA software is given in the Section 4.4.1 in detail. The behaviour of NMs were analysed when added to the EPA softwater and in turn the NMs were quantified for the measurement of particle number similarly as described in the Section 7.2. (i.e. measurement of particle number of Au NMs added in simple media).



**Figure 7-16** Representative transmission electron microscopy images showing a uniform distribution of PVP-AuNMs spiked in EPA soft water on TEM grid that is functionalized with 0.1% w/v poly-L-lysine and the decrease of the number of NMs recovered with the decrease



in NM mass concentration in ppb (a) 31.38, (b) 15.79, (c) 3.34 and (d) 1.55. NMs were suspended in UHPW.

The micrograph of the Au NMs added to the synthetic soft water is shown in the Figure 7-20 below. No changes were observed in the physical state of Au NMs when exposed to synthetic EPA soft water. There were no changes observed in zeta potential, no aggregation or morphology of the particles when compared with the initial characterisation of the Au NMs with UHPW (see Chapter 5, Characterisation results of Au NMs in UHPW). Qualitatively, the distribution of NMs on the substrate in EPA media was evaluated by comparing the representative number of particles counted at different areas on the TEM grid, which was performed by calculating the coefficient of variation (CV).

**Table 7-8** Number concentration (particle.L<sup>-1</sup>) and percentage recovery of PVP Au NMs in EPA soft water in stock solutions

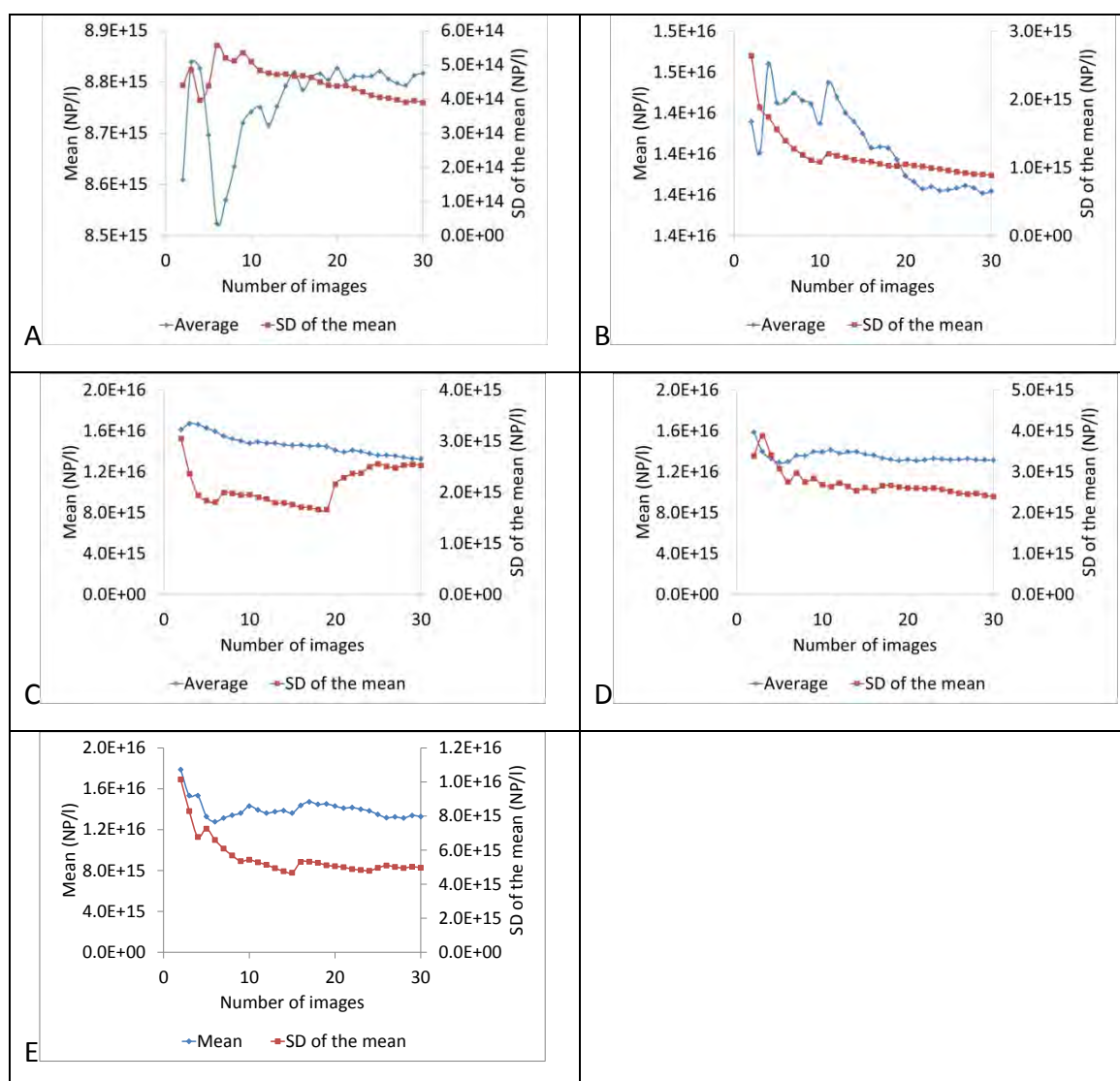
Concentration ( $\mu\text{g L}^{-1}$ )	NMs in UHPW On PLL functionalised TEM grid (ultracentrifugation) CV	NMs in EPA soft water On PLL functionalised TEM grid (ultracentrifugation) CV	% recovery NMs in EPA media Ultracentrifugation on PLL functionalised TEM grid
670.0, 335.0 and 167.5	Overloading	Overloading	NA
31.38	$8.82 \times 10^{15}$ 0.05	$9.23 \times 10^{15}$ 0.08	62
15.79	$1.40 \times 10^{16}$ 0.07	$2.63 \times 10^{16}$ 0.12	78
3.34	$1.32 \times 10^{16}$ 0.20	$1.26 \times 10^{16}$ 0.09	85
1.55	$1.31 \times 10^{16}$ 0.19	$9.83 \times 10^{15}$ 0.15	82
0.34	$1.33 \times 10^{16}$ 0.40	NA	NA

NA: not analysed

CV: coefficient of variation

UHPW: ultrahigh purity water

Quantitatively, the CV of NMs spiked in EPA softwater was low in the range of 0.08-0.15 for the concentrations 0.34-31.38 as shown in the Table 7-11. The measurement of particle number of NMs in EPA soft water was found to be having very good agreement; thereby the PLL functionalised ultracentrifugation method can be applied for the detection, quantification and characterisation of NMs in EPA softwater. The percentage recovery of NMs spiked in EPA soft water were also found to be slightly higher by 2% when compared with the NMs in pure water. At higher NM concentration i.e. at 31.38 ppb the percentage recovery is low due to the high number of particles on the TEM grid and the potential overlapping of NMs on the grid.



**Figure 7-17** Dependence of the calculated mean number concentration and standard deviation of the mean on the number of images scanned by transition electron microscopy of

the PVP-AuNMs prepared by ultracentrifugation at 150 000 g on poly-L-lysine functionalized TEM grid at different concentrations (ppb): (a) 31.5, (b) 16.8, (c) 3.4, (d) 1.7 and (e) 0.34.

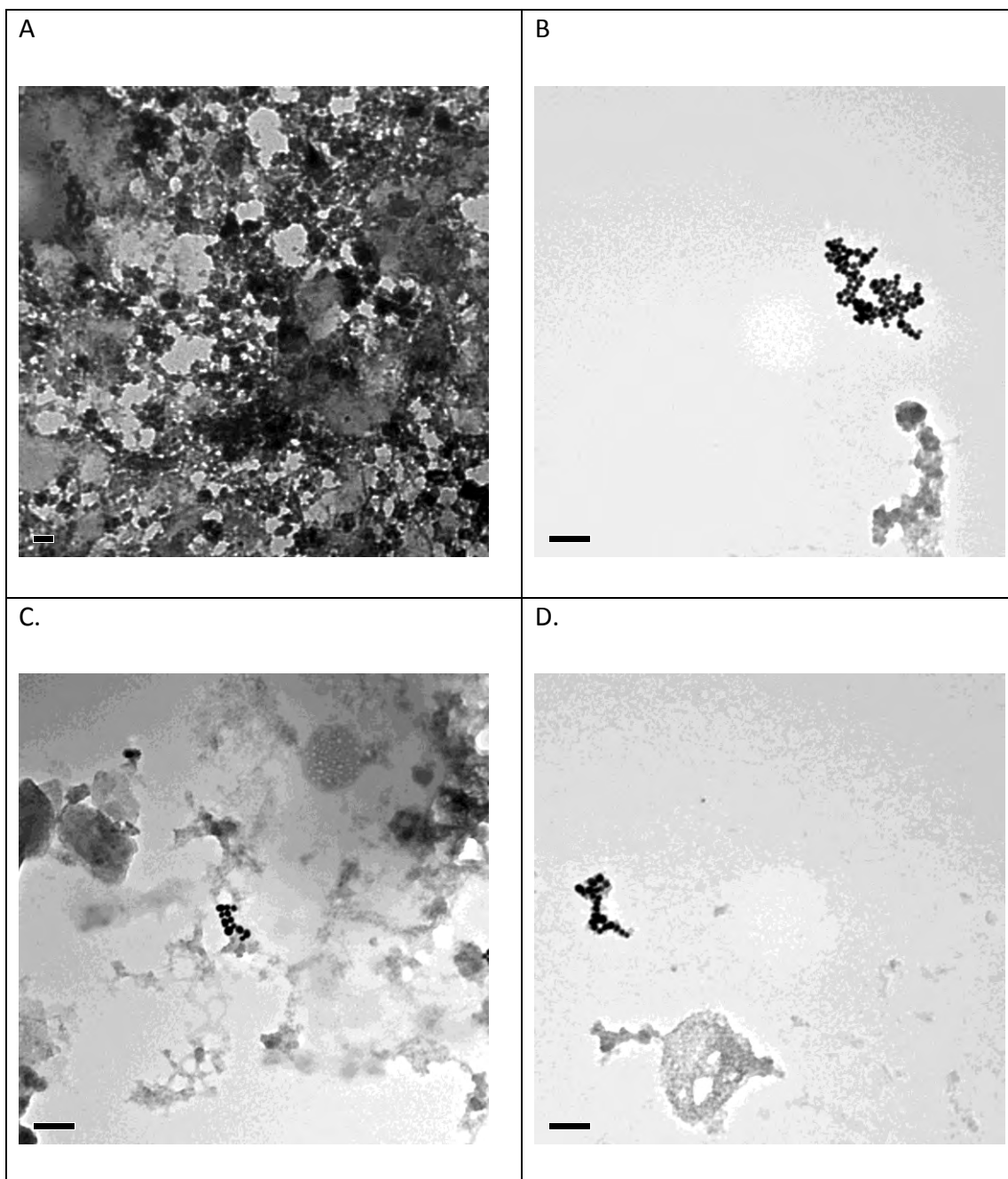
A minimum of 15 images are required to obtain the representative measurement of particle number concentration (statistical calculation is given in the chapter 4 and in Section 4.7.5). The standard deviation of the mean decreases with the increase in the number of images and reaches a stable value also at about  $\geq 15$  images for NM in EPA media. This is graphically shown in the Figure 7-17. Therefore, for the first time fully validated protocol for particle number measurements in simple and complex media was successfully investigated.

#### **7.2.2.3 Au NMs added to lake water/Natural surface water**

AuNMs were added to filtered lake water samples. The process of collection and filtration was explained in detailed in Chapter 4 and Section 4.4.3. In order to validate the sample preparation protocol for the detection and quantification of engineered nanomaterials in natural waters, natural lake water was spiked with PVP capped Au NMs and observed by TEM; the following samples were prepared by ultracentrifugation

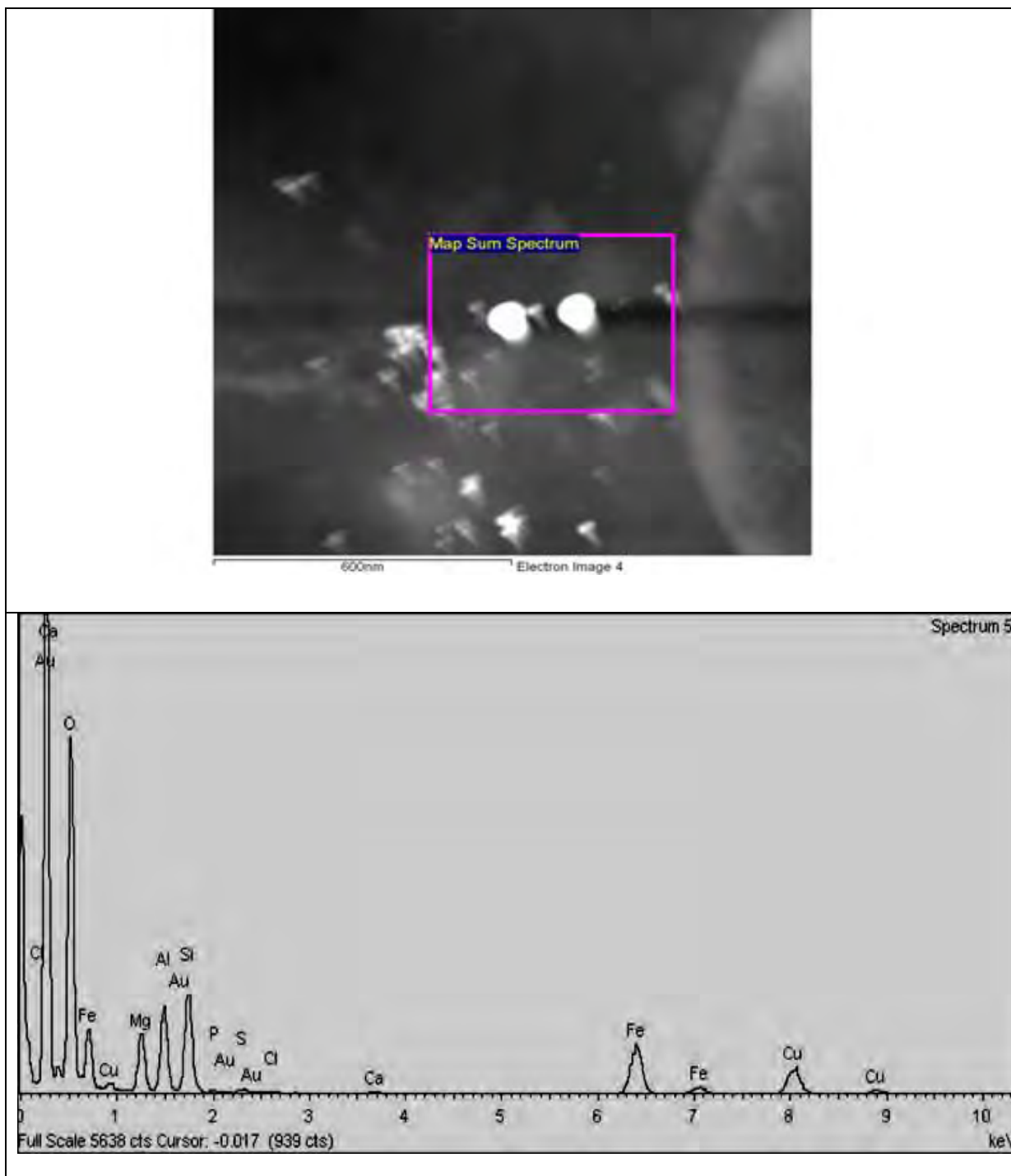
- (i) lake water, (without NMs)
- (ii) lake water spiked with 3.4 and 1.7 ppb PVP capped Au NMs
- (ii) 10 fold dilution of lake water (without NMs) and
- (iv) 10 folds diluted lake water spiked with 3.4 and 1.7 ppb PVP-AuNMs.

X-EDS with TEM was used to confirm the presence of AuNMs. The number of AuNMs/image was counted manually. AuNMs were distinguished by their higher contrast compared to natural nanoparticles and colloids and this was confirmed by X-EDS.

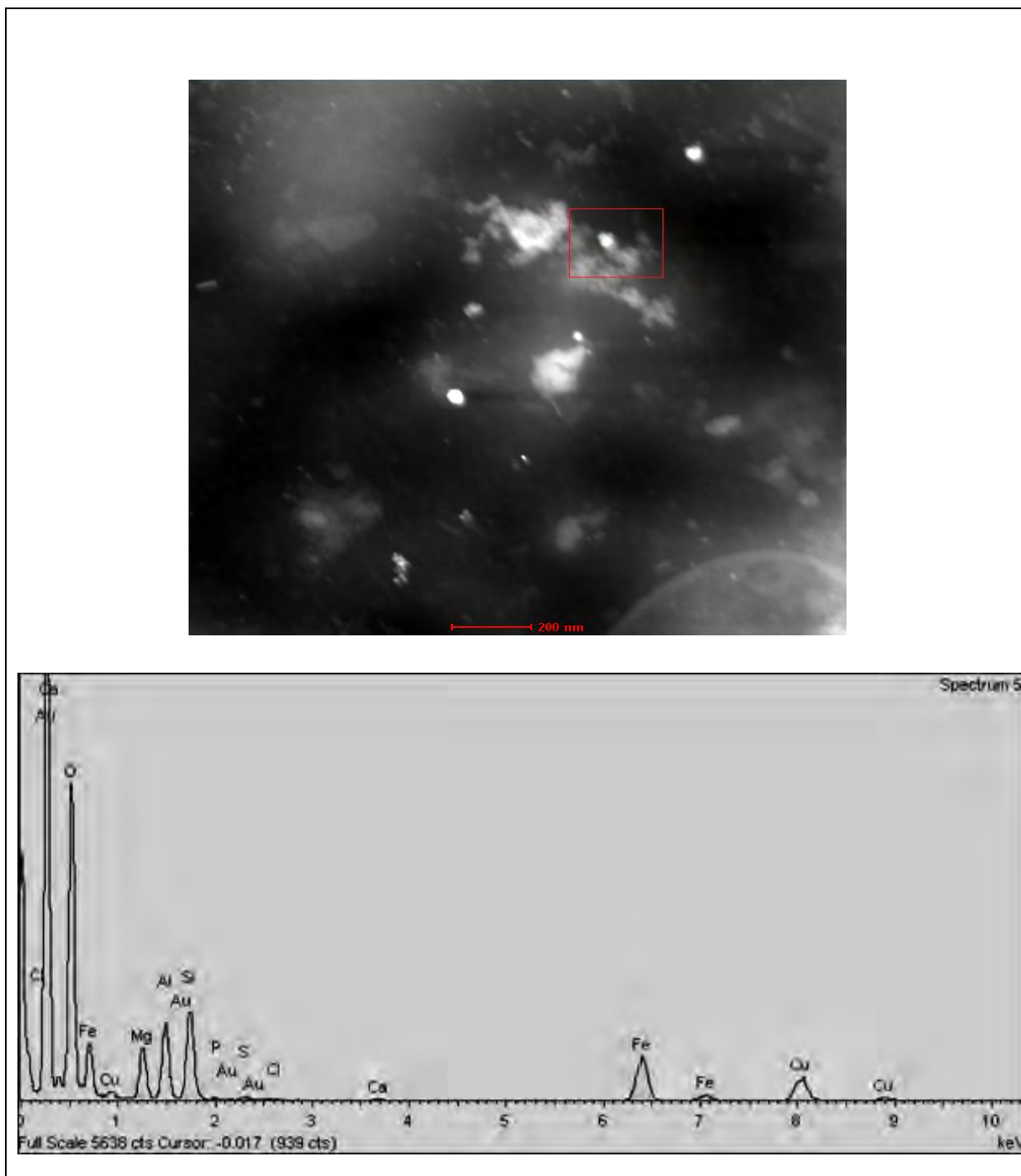


**Figure 7-18** Representative transmission electron microscopy images showing distribution of PVP-AuNMs suspended in complex media (9.1 % of lake water) and UHPW of 90.9 % prepared by ultracentrifugation on poly-l-lysine functionalized TEM grid at the concentration of (A) overloaded with 100% of lake water without NMs, none of NMs visible (B) 10 folds diluted lake water spiked with  $3.4 \mu\text{g L}^{-1}$  of NMs and (c and d) 10 folds diluted lake water spiked with  $1.7 \mu\text{g L}^{-1}$  of Au NMs

Typical TEM micrographs together with the x-ray energy dispersive spectroscopy are presented in Figure 7-18 to Figure 7-19. As shown in the Figure 7-18(a), shows the TEM image of the natural water sample after filtered under 450 nm without NMs resulted in overloading of the natural organic material (NOM). Due to the overloading of the NOM, the visibility of the synthesised NMs is reduced when the TEM analysis was carried out. Thereby, the natural water sample was diluted 10 times in UHPW and further the analysis was performed with the concentration of 3.4 ppb and 1.7 ppb respectively (Figure 6-16 (b) and (c)), AuNMs spiked in lake water. The recovery of NMs after reacting with natural water was found to be more by 3.4 % in comparison to UHPW (Table 7-9).



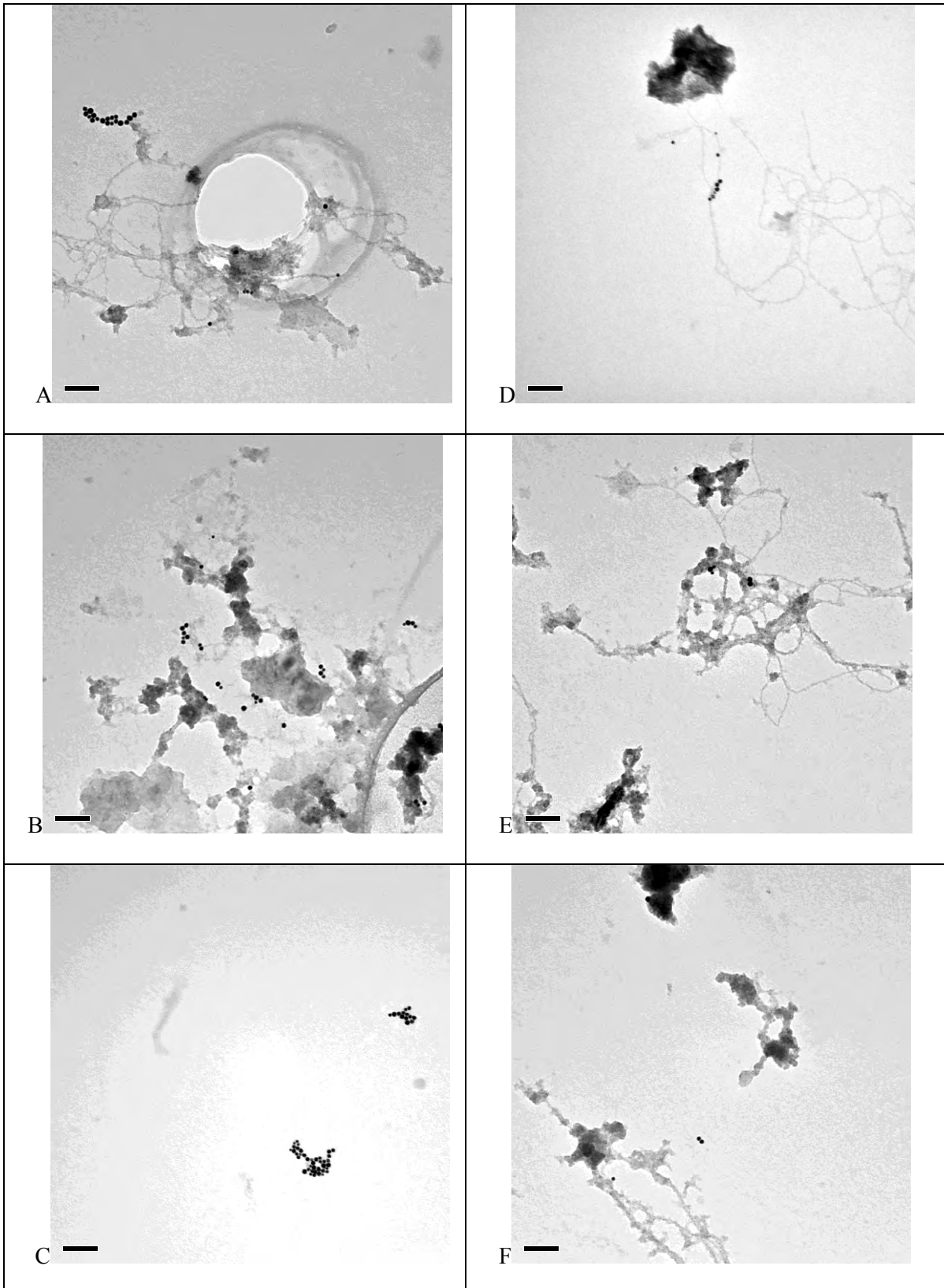
**Figure 7-19** Representative TEM images showing distribution of PVP-AuNMs suspended in complex media (9.1 % of lake water) and UHPW of 90.9 % prepared by ultracentrifugation on poly-L-lysine functionalized TEM grid at the concentration of  $3.4 \mu\text{g L}^{-1}$  and its representative X-EDS spectrum collected from the dark particles identified as Au NMs.



**Figure 7-20** Representative TEM images showing distribution of PVP-AuNMs suspended in complex media (9.1 % of lake water) and UHPW of 90.9 % prepared by ultracentrifugation on poly-L-lysine functionalized TEM grid at the concentration of  $1.7 \mu\text{g L}^{-1}$  and its representative X-EDS spectrum collected from the dark particles identified as Au NMs.

For the NMs spiked in lake water samples X-EDS was performed. Figure 7-19 and Figure 7-20 shows the X-EDS spectrum of the marked area in the micrograph. The X-EDS analysis shows the presence of naturally occurred NMs and the sorption of elements such as calcium, chlorine, silver, nitrogen, magnesium, aluminium, carbon, copper, iron, Silicon and Phosphorous on the NMs (Figure 6-19 (a) and (b)) for the concentration range of  $3.4 \mu\text{g L}^{-1}$  and  $1.7 \mu\text{g L}^{-1}$  respectively.





**Figure 7-19** Representative transmission electron microscopy images showing distribution of cit-AuNMs suspended in complex media (lake water) prepared by ultracentrifugation on

poly-l-lysine functionalized TEM grid at the concentration of 3.4 ppb (A-C) and 1.7 NMs (D-F).

Furthermore images of Au NMs spiked on lake water samples was performed at NM concentrations of  $3.4 \mu\text{g L}^{-1}$  and  $1.7 \mu\text{g L}^{-1}$  shown in the above Figure 7-21. At the concentration of 3.4 ppb when NMs spiked with the natural organic material Au NMs was found to be aggregate more in presence of NOM. But the TEM technique provided an opportunity to count the number of NMs in each aggregate. As NM concentration decreased, number of Au NMs spiked also decreases. But lower NM concentrations will result in higher uncertainty and variability (data see Table 7-9) because of the low number of NMs present on the TEM grid (Figures 7-21 (C) and (F)), or will require the collection of more images to count sufficient number of NMs, which may require automated imaging to acquire a very high number of images. Thus, the lower concentration limit can potentially be reduced to few tens of  $\text{ng L}^{-1}$ . Thus, the method presented here will allow quantitative analysis of low concentrations ( $\text{ng to } \mu\text{g L}^{-1}$ ) of NMs to be performed, which are more representative of likely exposure scenarios from the environment,(Baalousha, 2012a) consumer goods and the workplace and allows more realistic toxicology experiments to be performed. Higher NM concentrations ( $>40 \text{ ppb}$ ) will result in overloading (NM-NM interaction, Figure 7-18) of the TEM grid and therefore it becomes impossible to obtain true counts of the NMs and to calculate NM recovery on the TEM grid. The NM concentration range of 0.2-18 ppb is applicable for Au NMs of approximately 12-13 nm in diameter. For smaller sizes of NMs, lower concentrations of 0.20 ppb are feasible, whereas for larger sizes higher concentrations will be required. Furthermore, the range of NM concentrations will depend on the size and composition (density) of the NMs (see discussion above). The upper concentration range can be extended to higher concentrations by centrifuging smaller volumes of NM suspensions.

**Table 7-9** Number concentration (particle.L<sup>-1</sup>) of PVP-Au NMs in stock solutions

Concentration (µg L <sup>-1</sup> )	NMs in UHPW on PLL functionalised TEM grid (ultracentrifugation) CV	NM in lake water on PLL functionalised TEM grid CV
670.0, 335.0 and 167.5	Overloading	Overloading
33.5	8.82 x 10 <sup>15</sup> 0.05	NA
16.8	1.40 x 10 <sup>16</sup> 0.07	1.51x10 <sup>16</sup> 0.35
3.4	1.32 x 10 <sup>16</sup> 0.20	1.38 x 10 <sup>16</sup> 0.25
1.7	1.31 x 10 <sup>16</sup> 0.19	1.41 x 10 <sup>16</sup> 0.28
0.34	1.33 x 10 <sup>16</sup> 0.40	NA

NA: not analysed

CV: coefficient of variation

UHPW: ultrahigh purity water

The particle number concentration of PVP capped Au NMs in lake water is shown in the Table 7-9. The distribution of NMs on the TEM grid after reacting with the natural materials CV was found relatively high (0.28 and 0.35) when compared with the UHPW. The high CV and particle number is due to the overlapping of the natural organic material and aggregation of synthesised NMs or may be misinterpreting in NM count. But with respect to aggregation, the microscopy allowed identifying each NM and count accurately (Figure 7-20). But the number of NMs in UHPW has good agreement with the particle number in lake water media but 3% higher particle number when compared with the UHPW (See Table 7-9).

**Table 7-10** Recovery (%) of cit-Au NMs and PVP-Au NMs

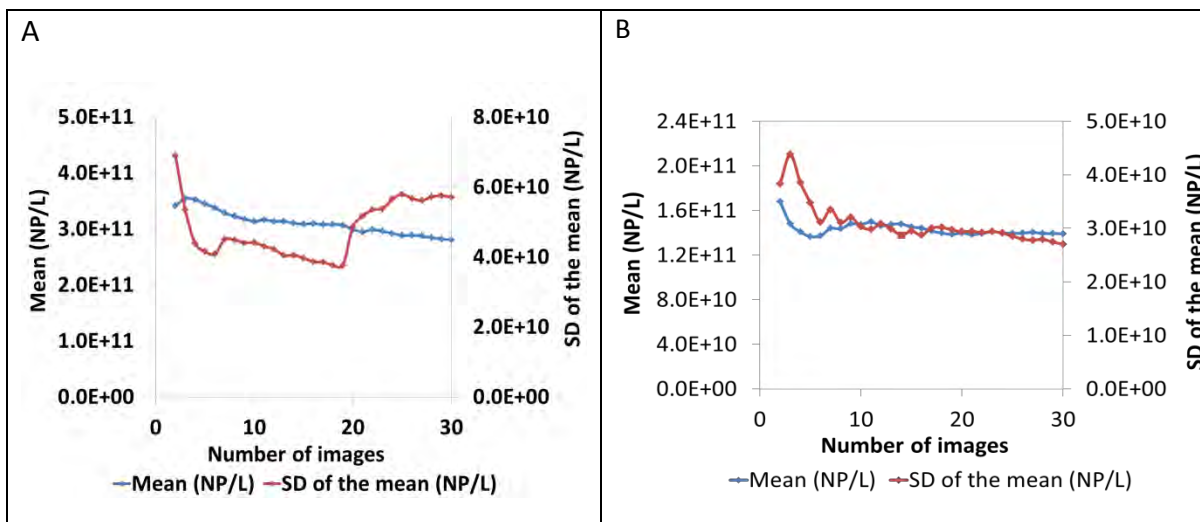
Concentration of PVP-Au NMs ( $\mu\text{g L}^{-1}$ )	NMs in UHPW Ultracentrifugation on PLL functionalised TEM grid	NMs suspended in Lake water
33.5	53.2	NA
16.8	84.5	85.9
3.4	79.7	80.5
1.7	79.1	83.5
0.34	80.1	NA
Average	75.3	82.0

UHPW: ultrahigh purity water

NA: Not analyzed

SRFA: Suwannee river fulvic acid

The recovery of NMs in natural lake water was found to be 80.5 and 86% for PVP-AuNMs (Table 7-10), in good agreement with the recoveries in UHPW. The recovery of PVP Au NMs in UHPW is between 80-85%. Thus, this sample preparation protocol can be applied to detect and quantify the number of engineered NM in natural waters. Further analysis was carried out with the number of images satisfactory for the measurement of particle number concentration for PVP capped Au NMs in natural lake.



**Figure 7-22** Calculated mean number concentration and standard deviation of the mean on the number of images scanned by transmission electron microscopy of the PVP-AuNMs with complex media (9.1% lake water and 90.9% of UHPW+NMs) prepared by ultracentrifugation at 150 000 g on poly-l-lysine functionalized TEM grid at the concentrations of (ppb) : (a) 3.4 and (b) 1.7.

The stability of the calculated mean number concentration and standard deviation of the mean with respect to the number of images was investigated for the Au NMs spiked in lake water is shown in the Figure 7-22. For the higher NM suspensions i.e. at the concentration of 3.4 ppb, the mean number and standard deviation of the mean stabilises after 20 images. Therefore, for higher number of NM suspension and at higher content natural organic matter (NOM) in media, the number of images required was higher ( $\geq 30$  images) when compared with pure water and other less content NOM. Whereas, as the NMs in the suspension decreases i.e. for the concentration of 1.7 ppb after 10 images, the graph was found to be stable. Therefore, the number of images required for the measurement particle number concentration depends upon the type of media NMs suspended and also concentration of NMs suspended in the media.

### 7.2.3 Conclusions

This research study presents for the first time a fully validated sample preparation protocol for the analysis of engineered NMs by TEM in both simple and complex natural aquatic media. The presented sample preparation protocol enables the full quantitative analysis of NMs number concentrations and number size distribution by TEM at environmentally and toxicologically relevant concentrations (*i.e.* 0.2-20 ppb). This method is based on forcing the NMs onto the TEM grid via ultracentrifugation and the NMs strong attachment due to TEM grid functionalization of the TEM grid by a positively charged polymer (poly-L-lysine).

The protocol was validated using well stabilized Au NMs (coated by PVP or citrate) using the following criteria (i) NM recovery on the TEM grid, (ii) distribution of NM on the TEM grid, (iii) correlation between mass and number concentrations. Both citrate- and PVP-Au NMs were uniformly distributed on the TEM grid; that is the coefficient of variation between the numbers of NMs counted on different areas of the grid was  $< 0.20$ . The recovery of the NMs on the TEM grid was quantified for the first time and it was up to 100%. The number of counted NMs correlated well ( $R > 0.95$ ) with the concentrations of NMs in suspension.

The applicability of the protocol to detect and measure the number concentration of NMs in a natural water sample, EPA-SRFA, synthetic EPA was demonstrated where the respective media spiked with Au NMs at different concentrations of range from 0.2-33.5 ppb. Similarly, AuNMs were uniformly distributed on the TEM grid ( $CV < 0.2$ ) and good correlation between number and mass concentrations ( $R^2 \sim 0.9$ ) and high recovery (67-85%) were achieved.

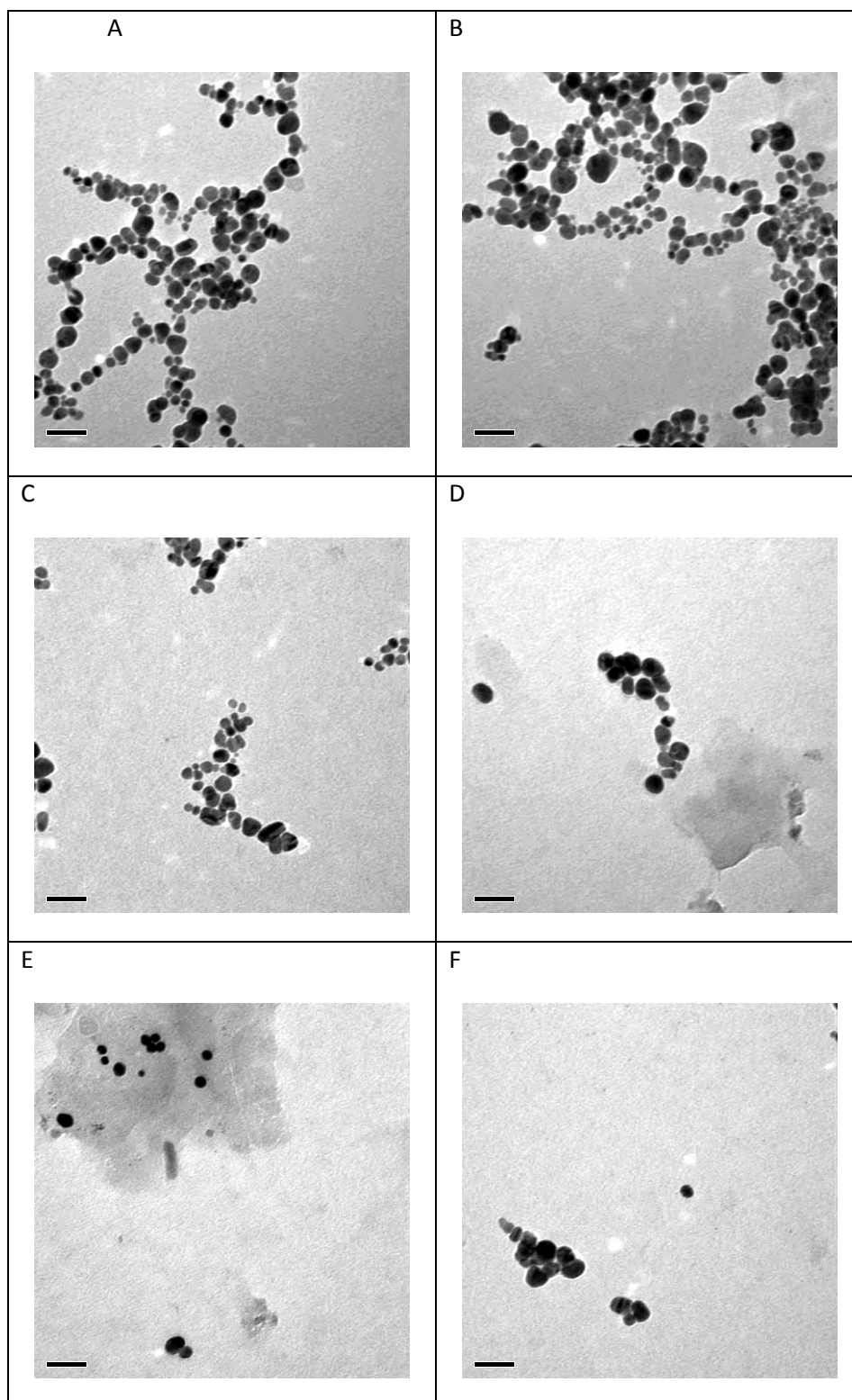
### **7.3 Particle number and size measurement analysis of Ag NMs by simple media (pure water) and complex media (E3)**

This section relates the detection and quantification of particle number concentration of silver nanoparticles. The synthesised silver nanoparticles of 5.54 mg/L were received from the Center for Environmental Nanoscience and Risk, University of South Carolina, USA, and exposure media from the Oregon State University, Sinnhuber Aquatic Research Laboratory (OSU/SARL), USA. In collaboration, toxicology experiments were performed whilst the measurement of particle number concentration was performed as part of this thesis.

Initially, the physico-chemical characterisations of the Ag NMs were performed. Later sections were carried on with the particle number measurements with pure water and with media. The characterisation of the Ag NMs by multi-method was explained in detail in the Chapter 5 and in Subsection 5.5.

#### **7.3.1 Quantifying the particle number of Ag NMs in pure water/simple media**

The distribution of NMs on the substrate between the set of images taken by TEM was found to be uniform. The uniformity in distribution of NMs on the substrate depends on the sample preparation technique which was critical part of this investigation to be validated for the Ag NMs. Uniformity of NMs distribution between images taken at different positions on the TEM grid is essential to obtain representative particle number concentrations and number size distribution, as well as to minimize the number of images required to obtain a representative number particle concentration.



**Figure 7-23** Transmission electron microscopy images showing a distribution of AgNMs on TEM grid previously treated with 0.1% w/v poly-L-lysine and the decrease of the number of NMs recovered with the decrease in NM mass concentration in ppb (a and b) 55.40, (c and d) 11.08, (e and f) 5.54. Scale bar in all images is 50 nm. The AgNMs were suspended in UHPW.



Qualitatively, TEM images of PVP-AgNMs suspended in UHPW and prepared by enhancing the particle attachment to the TEM grid by surface functionalisation followed by ultracentrifugation shown in the Figure 7.23 for three different NM concentrations. For the higher concentration of NM suspension i.e. for Figure 7-23 (a and b), TEM technique allows to count individual NMs but overlapping of NMs might result in inaccuracy in particle number measurement. While for lower NM suspension (Figure 7-23 (c, d, e and f), the TEM allows the more accurate count of NMs. The number NMs on each image were also counted and are reported quantitatively. Total of 30 images were taken for each concentration.

**Table 7-11** Number concentration (particle.L<sup>-1</sup>) and % recovery of Ag NMs in stock solutions

Dilution ppb	NMs in UHPW on PLL functionalised TEM grid (particle/L) CV	% Recovery
554	Overloading	NA
55.4	$7.94 \times 10^{13}$ 0.10	74 %
45.0	$6.96 \times 10^{13}$ 0.12	80%
11.08	$1.25 \times 10^{14}$ 0.27	84 %
8.50	$0.96 \times 10^{14}$ 0.27	82%
5.54	$8.25 \times 10^{13}$ 0.15	80 %
1.10	$3.92 \times 10^{14}$ 0.34	87%

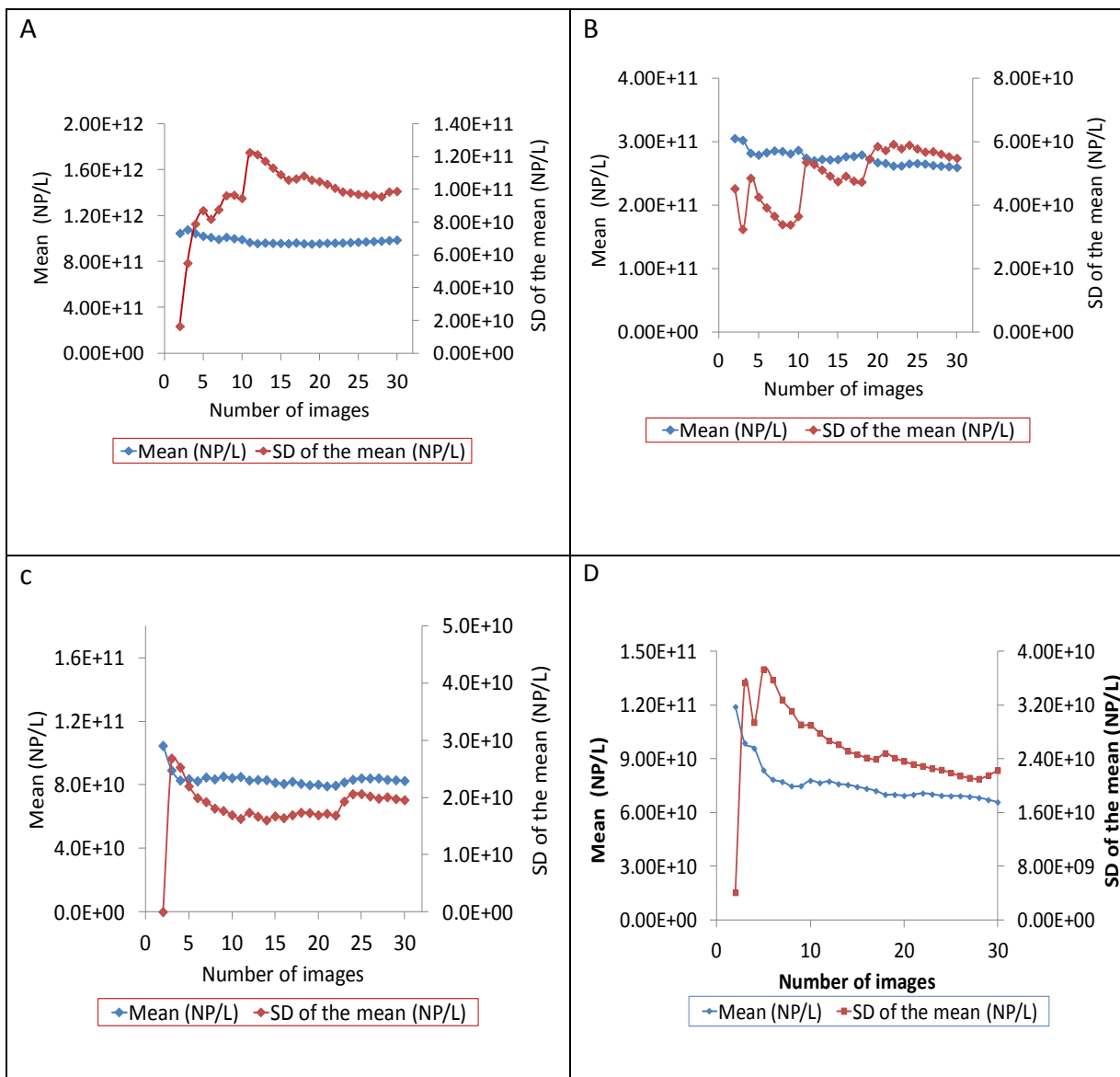
NA: not analysed

CV: coefficient of variation

UHPW: ultrahigh purity water

Quantitatively, the uniformity of Ag NM distribution on the TEM grid is described by the coefficient of variation (CV) of the number of NMs on different images taken at different locations on the TEM grid, the process of imaging and the number of images to be taken was described in Chapter 4 and in Subsection 4.7.5. The Table 7-11 shows the different concentration of NMs, the CV was relatively low (0.10 and 0.27 for PVP- Ag NMs) for higher NM suspension. Hence, sample preparation, resulted in the uniform distribution of NMs on the substrate between the images. The measurement of particle number for different concentrations is shown in the Table 7.11, which is the range of  $7.94 \times 10^{13}$  to  $3.92 \times 10^{14}$  (particles/L). Furthermore, these results suggest that best results can be achieved for NM suspensions within the concentration range of 1.10 to  $55.40 \mu\text{g L}^{-1}$ , although the CV is higher at the lower concentration essentially because of the poorer counting statistics. At higher concentration of 554 ppb the NMs were found to be overloaded, at the concentration of 55.4 ppb the number of NMs counted reduced due to the overlapping or aggregation of NMs when compared to the lower concentration (11.08 and 5.54 ppb).

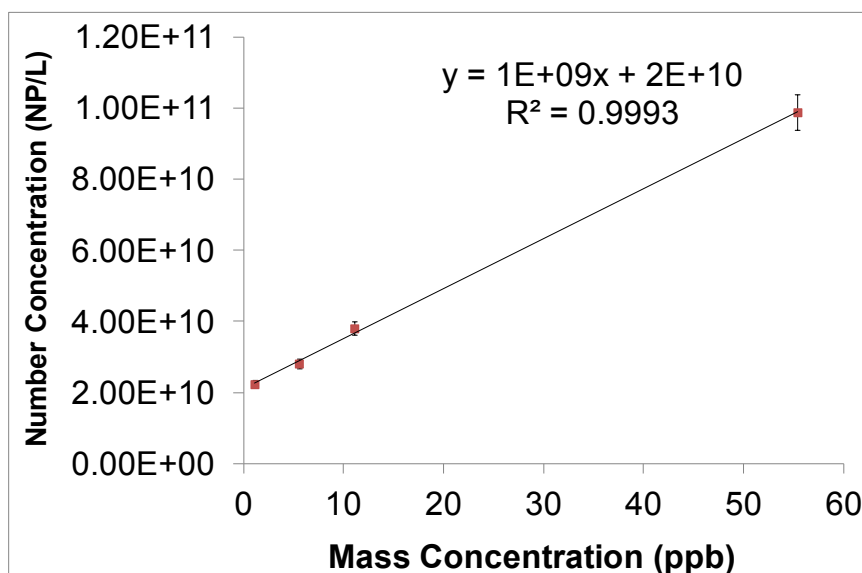
The percentage recovery of Ag NMs is quantified by calculating the ratio of NM recovered on the substrate. The percentage recovery of Ag NMs in pure water is in the range of 74% to 87% (see Table 7.11). For higher concentration of PVP-Ag NMs ( $55.40 \mu\text{g L}^{-1}$ ), the perceived recovery was relatively low compared with those at lower concentrations ( $1.10$ - $11.08 \mu\text{g L}^{-1}$ ) because of the high number of particles on the TEM grid and the potential overlapping of NMs on the grid. Similarly, percentage recovery of PVP capped gold NMs (Table 7.4, at 31.83 ppb observed 53.2% recovery) comparable with the PVP Ag NMs, i.e. in terms of lower recoveries observed at higher NM suspension, essentially because of the poorer counting statistics and higher recoveries at lower NM. Furthermore, these results suggest that best results can be achieved for NM suspensions within the concentration range  $> 30 \mu\text{g L}^{-1}$ .



**Figure 7-20** Calculated mean number concentration and standard deviation of the mean on the number of images scanned by transition electron microscopy of the PVP-AuNMs prepared by ultracentrifugation at 150 000 g on poly-L-lysine functionalized TEM grid at different concentrations in ppb: (a) 55.40, (b) 11.08 (c) 5.54 and (d) 1.10.

The mean number concentration and standard deviation of the mean for cit- and PVP-Ag NMs TEM grid are shown in Figure 7.24. The mean number concentration tends to a stable value for  $\geq 15$  images, as was observed for AFM analysis (Baalousha et al., 2014a). The standard deviation of the mean decreases with the increase in the number of images

and reaches a stable value also at about  $\geq 15$  images. Therefore, a minimum number of 15 images are required to obtain mean number concentration and a standard deviation ( $\sigma$ ) representative of the entire population of PVP Ag NMs.



**Figure 7-21** Correlation between the mass and number concentration of PVP capped Ag NMs in MQ water. Samples prepared by ultracentrifugation on a poly-L-lysine functionalized TEM grid.

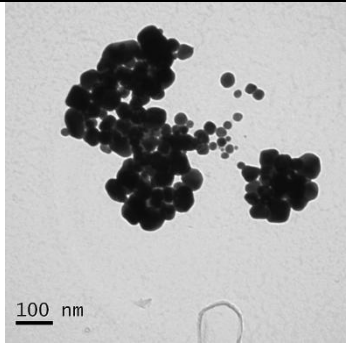
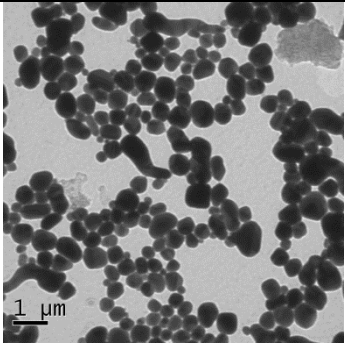
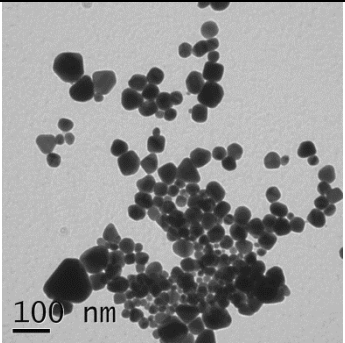
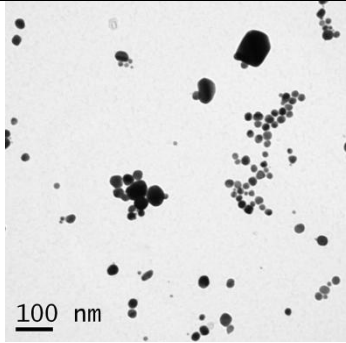
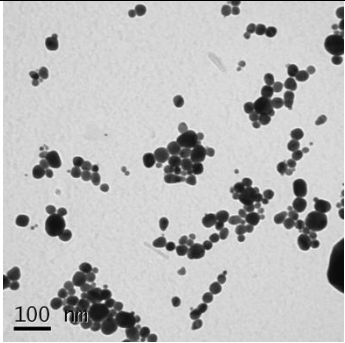
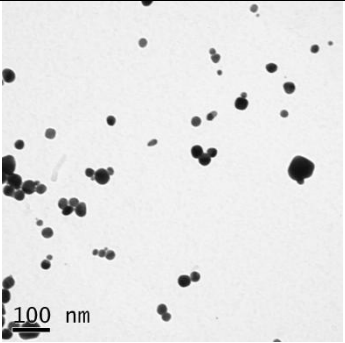
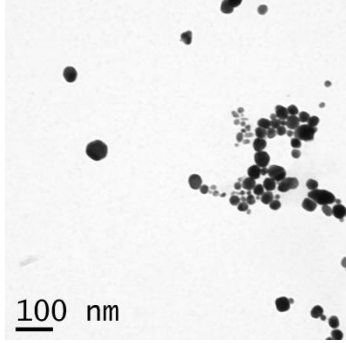
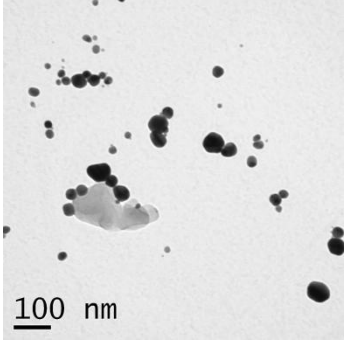
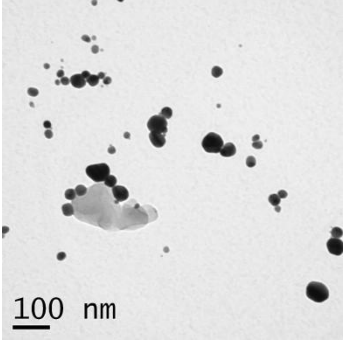
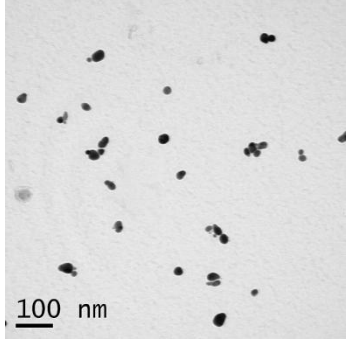
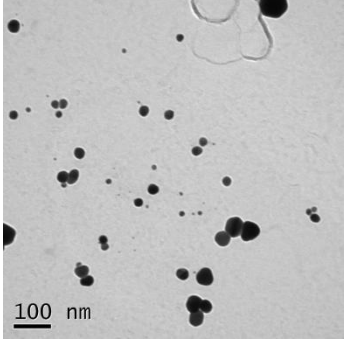
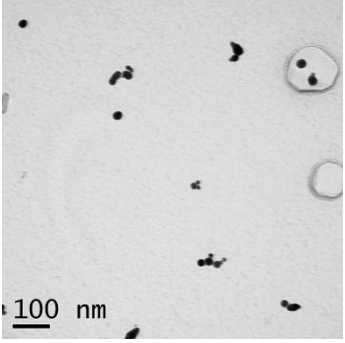
Excellent correlation between mass and number concentrations for PVP- Ag NMs was observed (Figure 7.25,  $R^2=0.99$ ), indicating no preferential NM loss at any concentration. These results suggest that the sample preparation method is applicable within the NM concentration range of this is 1.10 - 55.40  $\mu\text{g L}^{-1}$  for PVP- Ag NMs investigated in this study. These highly characterized engineered Ag NMs will be further analysed by adding in synthetic E3 media (zebrafish media). In order to validate the protocol employed for the measurement particle number of Ag NMs when added to E3 media.

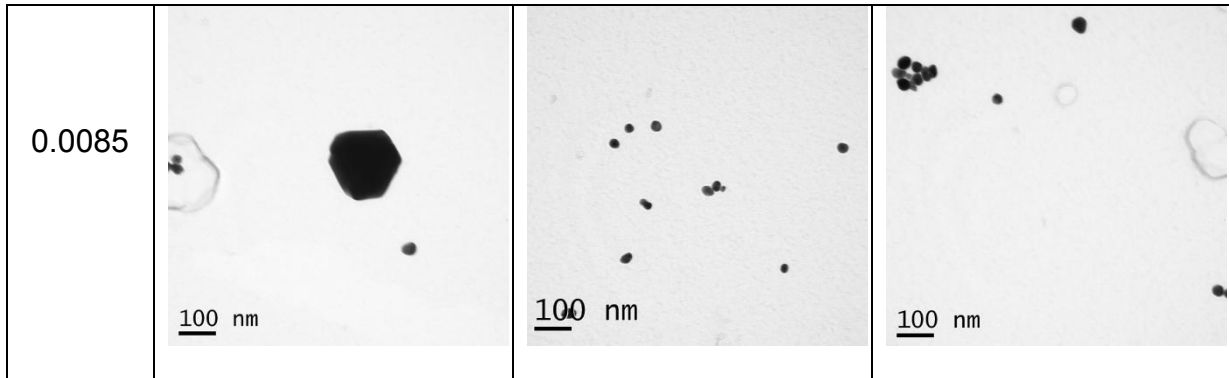
### **7.3.2 Detection and quantification of engineered Ag NMs in E3 media.**

Silver nanoparticles capped with PVP received from (In courtesy with the Sinnhuber Aquatic Research Laboratory (SARL), Oregon State University, USA ) were added to the E3 media to detect and quantify the particle number concentration. E3 media was prepared in the University of Birmingham, the recipe for the preparation or protocol was sent by Aquatic Research Laboratory, Oregon State University. The protocol for the preparation of E3 media is given below.

The E3 medium compositions are described in the toxicology report of SARL lab, for the purpose of comparative studies both number concentration measurements (part of this thesis) and toxicology studies performed by SARL followed similar protocol for the preparation of E3 media. The 5.54 mg/L stock solution of Ag-PVP was diluted in 125  $\mu\text{M}$   $\text{CaCl}_2$  to make 2.22, 0.44, 0.089 and 0.017 mg/L Ag-PVP stocks. These were in turn diluted two folds into E3 medium (5 mM NaCl, 0.17 mM KCl, 0.33 mM  $\text{CaCl}_2$ , 0.33 mM  $\text{MgSO}_4$ ) in the 96-well screening plates to form the final concentrations tested, 2.77, 1.11, 0.22, 0.045, 0.0085 and 0 mg/L Ag-PVP, in 62.5  $\mu\text{M}$   $\text{CaCl}_2$ . The measurement of particle number at these concentrations was carried out by TEM.

The improvised/enhanced method of sampling technique was used to validate and (Chapter 4 and in Section 4.7.4) to detect and quantify the number of PVP Ag NMs in E3 media using TEM analytical technique. The NM concentration for PVP Ag NMs spiked in E3 media were in the range of 0.0 to 2.77  $\text{mg L}^{-1}$  Ag. Typical TEM micrographs together with the x-ray energy dispersive spectroscopy are presented in the following Figure 7-28 and Figure 7-29 respectively.

Dilution (mg/L)	Image A	Image B	Image C
2.77			
1.11			
0.22			
0.045			



**Figure 7-26** Transmission electron microscopy images showing a distribution of PVP Ag NMs on TEM grid that is treated with 0.1% w/v poly-L-lysine, the different concentration imaged were as follows in ppb (a) 2770, (b) 1110, (c) 220, (d) 45, (e) 8.5 ppb in 62.5  $\mu$ M  $\text{CaCl}_2$

Figure 7-26 shows the micrograph of the transmission electron microscopy images for different concentration of PVP capped Ag NMs spiked in E3 media. The different concentration considered for TEM imaging were as follows: 2770 ppb, 1110 ppb, 220 ppb, 45 ppb and 8.5 ppb. At higher suspension Ag NMs, i.e. 2770 and 1110 ppb as seen in the above scanned TEM image is overloaded and a particle number concentration could not be accurately measured. At the dilution of 220 ppb, concentration of NMs are still higher to identify the individual NMs and difficult to predict the number of NMs overlapping even with the help of X-EDS. But at the NM concentration of 45 and 8.5 ppb, the particle number can be quantified to the accurate value.

**Table 7-12:** Number concentration (particle.L<sup>-1</sup>) of AgNMs in both UHPW and E3 media

Dilution (ppb)	NMs in UHPW on PLL functionalised TEM grid (ultracentrifugation) CV	% Recovery	NMs in E3 media on PLL functionalised TEM grid (ultracentrifugation) CV	% Recovery
2770	Overloading	NA	Overloading	NA
1110	Overloading	NA	Overloading	NA
554	Overloading	NA	Overloading	NA
220	NA	NA	5.94x 10 <sup>13</sup> 0.30	29%
55.4	7.94 x 10 <sup>13</sup> 0.10	74 %	NA	NA
45	6.96 x 10 <sup>13</sup> 0.12	80%	9.27 x 10 <sup>13</sup> 0.18	79%
11.08	1.25x 10 <sup>14</sup> 0.17	84 %	2.65 x 10 <sup>14</sup> 0.21	84%
8.5	0.96 x 10 <sup>14</sup> 0.09	82%	3.63 x 10 <sup>14</sup> 0.15	86%
5.54	8.25x 10 <sup>13</sup> 0.15	80 %	NA	NA
1.10	3.92x 10 <sup>14</sup> 0.34	87%	NA	NA

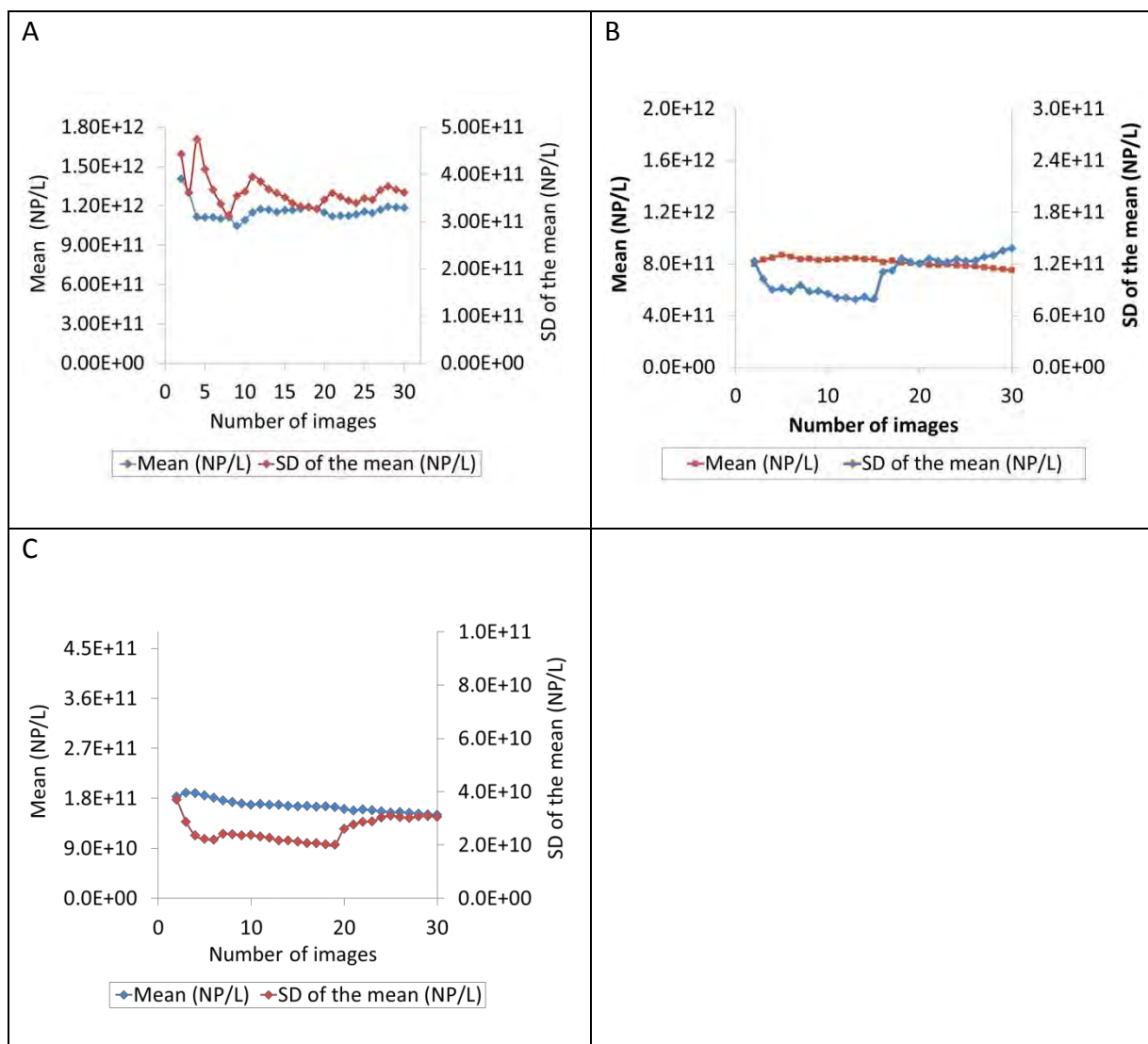
NA: not analysed

CV: coefficient of variation

UHPW: ultrahigh purity water



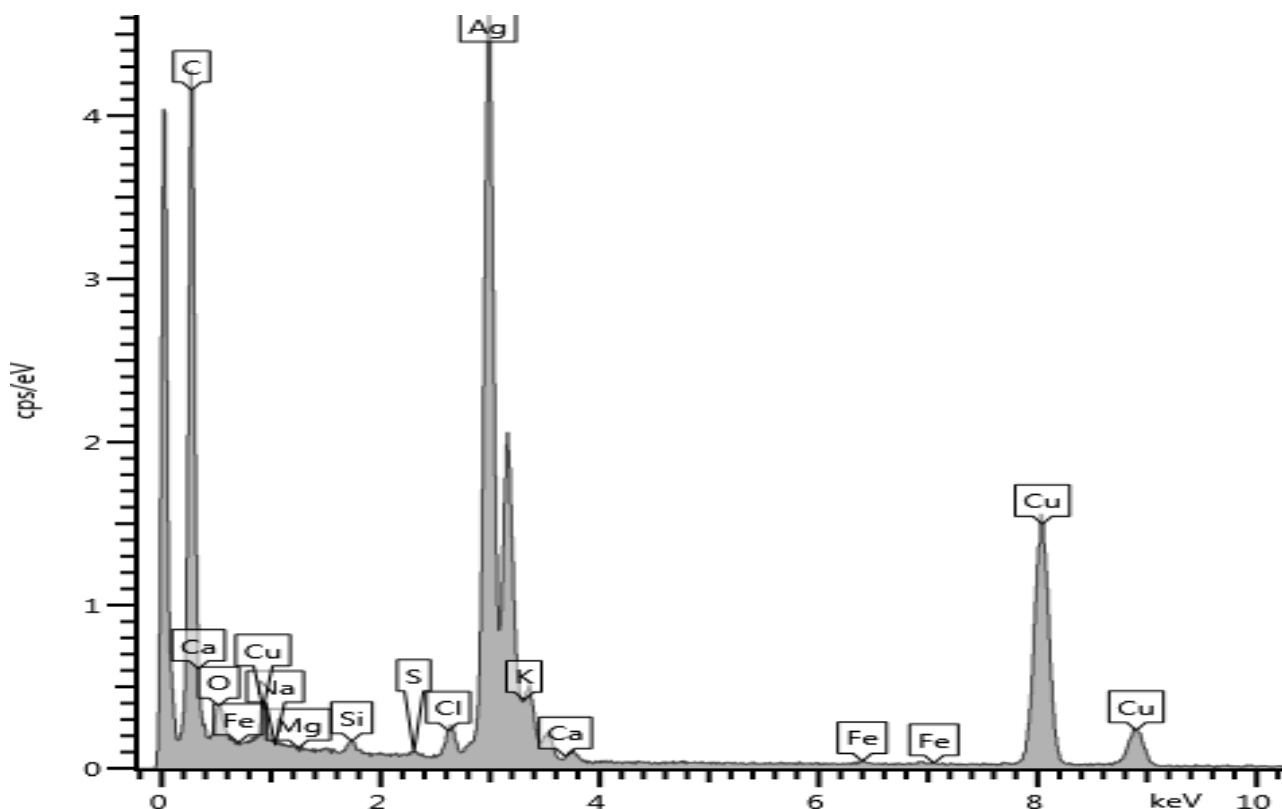
Quantitatively, the measurements of particle number at different concentrations of PVP Ag NMs in E3 media is given in the above Table 7-12. For the quick glance between the NMs in pure water and in media, highlight made in green represents the NMs in pure water while without any colour indication shown in the table represents the NMs in media. At lower concentrations (1.1 and 11.08  $\mu\text{g L}^{-1}$ ), Ag NMs occur mainly as individual non-aggregated NMs (Figure 7-25), whereas at the higher concentration ( $> 45 \mu\text{g L}^{-1}$ ), Ag NMs occur largely as aggregates of a few NMs. At higher concentration (220 ppb) in E3 media the possibility of getting lower percentage of NMs, may be due to the overlapping of NMs and organic materials. But higher advantage at lower concentrations, (NMs in media) since less probability of the NM aggregation was observed. The measurement of particle number at lower concentration of NMs in media is comparatively accurate as stated and proved in the previous section for the Au NMs in various media. Characterizing NMs at low concentrations is beneficial as predicted environmental concentrations of engineered NMs are likely to be in the range of ng -  $\mu\text{g L}^{-1}$ . (Blaser et al., 2008, Gottschalk et al., 2013a, Gottschalk et al.)



**Figure 7-22** Calculated mean number concentration and standard deviation of the mean on the number of images scanned by transition electron microscopy of the PVP-AgNMs in E3 media prepared by ultracentrifugation at 150 000 g on poly-l-lysine functionalized TEM grid at different concentrations : (a) 220 ppb, (b) 45 ppb and (e) 8.5 ppb.

For PVP Ag NMs prepared by ultracentrifugation on PLL functionalized TEM grid, the mean number concentration (Figure 7-27 (b) and (c)) tends to a stable value for  $\geq 20$  images, as was observed for AFM analysis.(Baalousha et al., 2014a). It is proved by the above graphical representation. But at higher concentration (Figure 7-29 (a)) graphical plot shows the non stabilised SD of the mean, because the percentage recovery is 26% and CV is also higher

At higher NM concentration, for example at 220 ppb, only 26% of NMs were recovered. The reason for the loss/unseen synthesised NMs in E3 sample is due to the dissolution or overlapping of natural organic material (Buffle et al., 1998). Identification of the NMs and other natural nanomaterial in E3 is performed by the x-ray energy dispersive spectroscopy.



**Figure 7-8** X-EDS spectrum of PVP Ag NMs

The X-EDS analysis shows the presence of naturally occurred NMs (which were not counted) and the sorption of elements such as calcium, chlorine, silver, nitrogen, magnesium, aluminium, carbon, copper, iron, Silicon and Phosphorous on the NMs. Above Figure 7-28 shows the X-EDS analysis for the Ag NMs in E3 media where some of the elements not seen in X-EDS (magnesium, aluminium, iron, calcium) of Ag NMs in pure water. There was no counting error observed either in identifying or differentiating NOM with Ag NMs.

## 7.4 Conclusion

From the Ag NMs with and without media can be concluded that apart from successfully measuring particle number of gold NMs both in simple and complex media using TEM technique, this studies also facilitates the validation of quantifying the particle number of silver NMs in both simple media and E3 media. Thereby this section enabled the successful validation of the protocol of the measurement of NM particle number at different concentration range from 55.4-1.10 ppb having good correlation between number and mass concentration ( $R^2 \sim 0.99$ ) and high recovery (74-87%) were achieved.

Similarly the applicability of the protocol to detect and measure the number concentration of Ag NMs in E3 media was demonstrated where the respective media spiked with Ag NMs at different concentrations of range from 8.5-45 ppb. Ag NMs having good correlation between number and mass concentrations ( $R^2 \sim 0.9$ ) and high recovery (75-86%) were achieved.

## Chapter 8 Conclusion and future work

This investigation presents for the first time fully validated nanometrologic system for the accurate quantification of particle number concentration both in simple and environmentally-relevant media as well as exposure media. Initial analysis was carried out using atomic force microscopy where this instrumentation allowed to fully quantify the number concentration of NMs in pure water but had a sensitivity issues when environmental relevant samples were considered for the quantifications of the complex media samples. But whereas using an analytical technique transmission electron microscopy integrated with the EDX, along with a developed sample preparation process, quantitative analysis of NMs at environmentally and toxicologically relevant concentrations was performed (see Table 7-1). Various methods of sampling technique was carried out to improvise the particle number measurement and concluded that based on forcing the NMs onto a substrate via ultracentrifugation leads to the accurate quantification of NMs. Forcing the NMs onto the substrate was carried out by surface functionalisation of the substrate while the adding cations to NM suspension. Correlation between mass and number concentrations for cit- and PVP- Au NMs was observed ( $R^2=1.00$ ), indicating no preferential NM loss at any concentration. These results suggest that the sample preparation method is applicable within the NM concentration range shown in the Table 7-2 for cit- and PVP- Au NMs investigated in this study. This is an ultimate sampling technique that can be applied for both simple and complex media and for both gold and silver NMs which is proved in this research for the first time.

The method was validated using well stabilised in-house synthesised monodispersed gold NMs (coated with citrate and PVP) and silver NMs (obtained from Arnold school of public health, Columbia USA) using criteria are as follows:

- i. uniformity in the distribution of NMs between the images on the substrate
- ii. full recovery of NMs on the substrate
- iii. accurate quantification of particle number
- iv. correlation between the mass and the NM concentration.
- v. count number of NMs in an aggregate by differentiating NOMs

Hence the critical and challenging measurement of particle in suspension was succeeded with the analytical high resolution instrumentation transmission electron microscopy integrated with the X-EDS. The particle number measurement is highly useful in toxicology studies (Health & Safety Laboratory, 2011) for the measurement of dose-response curve and to measure the NMs in realistic environmental relevant conditions.

**Table 8-1:** Summary of the NMs added to different media and concentration range validated

Nanomaterials Used	NMs added in the following media	Concentration range methodology validates ( $\mu\text{g L}^{-1}$ )
Citrate capped Au NMs	(a) Pure water	0.20 -20.3
	(b) EPA synthetic water	
PVP capped Au NMs	(c) SRFA+EPA	0.34 -31.38
	(d) Lake/natural water	
PVP capped Ag NMs	(a) Pure water	1.10 - 45.0
	(b) E3 media	

Table 7-1 summarises the different NMs used in this research and adding Au NMs to the four different media and adding Ag NMs to the two different media as stated in the Table facilitated successfully apply the protocol for the concentration range mentioned in table

under various conditions environmental and exposure media. Thereby, the criteria or the aims and objectives speculated in this research was successfully enabled to fully validated for the first time to measure the particle number concentration which was demonstrated for both environmental and exposure media.

For the future analysis the validated protocol can be further analysed using different nanomaterials and by adding NMs different complex media. Further integrating various spectroscopies to the microscopies such as X-EDS to SP-ICPMS.

The sample preparation methodology can be enhanced further to obtain the uniform distribution of NMs on the substrates by the introducing the electrodes into the NM suspension were the NM surface charge get polarised so that eventually gets non aggregated. The other method is substrate polarisation that is placing the substrates on the high voltage electrode and simultaneously introducing the droplet of NM suspension.

## REFERENCES

- AALTO, P., HAMERI, K., PAATERO, P., KULMALA, M., BELLANDER, T., BERGLIND, N., BOUSO, L., CASTANO-VINYALS, G., SUNYER, J., CATTANI, G., MARCONI, A., CYRYS, J., VON KLOT, S., PETERS, A., ZETZSCHE, K., LANKI, T., PEKKANEN, J., NYBERG, F., SJOVALL, B. & FORASTIERE, F. 2005. Aerosol particle number concentration measurements in five European cities using TSI-3022 condensation particle counter over a three-year period during health effects pollution on susceptible subpopulations. *Journal of the Air & Waste Management Association*, 55, 1064-1076.
- AGARWAL, G. S., CHAN, K. W., BOYD, R. W., CABLE, H. & DOWLING, J. P. 2007. Quantum states of light produced by a high-gain optical parametric amplifier for use in quantum lithography. *Journal of the Optical Society of America B-Optical Physics*, 24, 270-274.
- AITKEN, R., HANKIN, S., ROSS, B., TRAN, C., STONE, V., FERNANDES, T., DONALDSON, K., DUFFIN, R., Q CHAUDHRY, TA WILKINS, SA WILKINS, LEVY, L., SA ROCKS & MAYNARD, A. 2009. A review of completed and near completed environment, health and safety research on nanomaterials and nanotechnology (concise report), [www.safenano.org](http://www.safenano.org).
- AL GLOBUS, DAVID BAILEY, JIE HAN, RICHARD JAFFE, CREON LEVIT, RALPH MERKLE & SRIVASTAVA, D. 2000. NASA applications of molecular nanotechnology. *The Journal of the British Interplanetary* volume 51, pp. 145-152, .
- ALLABASHI, R., STACH, W., DE LA ESCOSURA-MUNIZ, A., LISTE-CALLEJA, L. & MERKOCI, A. 2009. ICP-MS: a powerful technique for quantitative determination of gold nanoparticles without previous dissolving. *Journal of Nanoparticle Research*, 11, 2003-2011.
- ALVAREZ, P. J. J., COLVIN, V., LEAD, J. & STONE, V. 2009. Research Priorities to Advance Eco-Responsible Nanotechnology. *Acs Nano*, 3, 1616-1619.
- AMENDOLA, V., MENEGHETTI, M., STENER, M., GUO, Y., CHEN, S., CRESPO, P., GARCÍA, M. A., HERNANDO, A., PENGO, P., PASQUATO, L., MIGUEL, V. R. & ANGELA, I. L. P.-L. 2008. Chapter 3 - Physico-Chemical Characteristics of Gold Nanoparticles. *Comprehensive Analytical Chemistry*. Elsevier.
- AMMANN, A. A. 2007. Inductively coupled plasma mass spectrometry (ICP MS): a versatile tool. *Journal of Mass Spectrometry*, 42, 419-427.
- ASHARANI, P. V., WU, Y. L., GONG, Z. & VALIYAVEETIL, S. 2008. Toxicity of silver nanoparticles in zebrafish models. *Nanotechnology*, 19, 255102.
- ASHKARRAN, A. A., IRAJI ZAD, A., MAHDAVI, S. M., AHADIAN, M. M. & HORMOZI NEZHAD, M. R. 2009. Rapid and efficient synthesis of colloidal gold nanoparticles by arc discharge method. *Applied Physics A*, 96, 423-428.
- ASSEMI, S., NEWCOMBE, G., HEPPLWHITE, C. & BECKETT, R. 2004. Characterization of natural organic matter fractions separated by ultrafiltration using flow field-flow fractionation. *Water Research*, 38, 1467-1476.
- BAALOUSHA, M. 2009. Aggregation and disaggregation of iron oxide nanoparticles: Influence of particle concentration, pH and natural organic matter. *Science of the Total Environment*, 407, 2093-101.
- BAALOUSHA, M., AND J. R. LEAD, 2012. Rationalizing Nanomaterial Sizes Measured by Atomic Force Microscopy, Flow Field-Flow Fractionation, and Dynamic Light Scattering: Sample Preparation, Polydispersity, and Particle Structure: *Environmental Science & Technology*. *Environmental Science & Technology*, v. 46, no. 11, p. 6134-6142.



- BAALOUSHA, M., AND PRASAD, A. & LEAD, J. 2014a. Quantitative measurement of the nanoparticle size and number concentration from liquid suspensions by atomic force microscopy. *Environ Sci Process Impacts*.
- BAALOUSHA, M., HOW, W., VALSAMI-JONES, E., LEAD, J. R., JAMIE, R. L. & EUGENIA, V.-J. 2014b. Chapter 1 - Overview of Environmental Nanoscience. *Frontiers of Nanoscience*. Elsevier.
- BAALOUSHA, M. & JAMIE, R. L. 2011. The dose makes the poison. *Nat Nano*, 6, 329-329.
- BAALOUSHA, M., JU-NAM, Y., COLE, P. & LEAD, J. R. 2010. Characterization of nanoparticle, size, shape, morphology, oxidation state and crystallinity: A multi-method approach. *Geochimica Et Cosmochimica Acta*, 74, A37-A37.
- BAALOUSHA, M., JU-NAM, Y., COLE, P. A., GAISER, B., FERNANDES, T. F., HRILJAC, J. A., JEPSON, M. A., STONE, V., TYLER, C. R. & LEAD, J. R. Characterization of cerium oxide nanoparticles-part 1: size measurements. *Environmental Toxicology and Chemistry*, 31, 983-93.
- BAALOUSHA, M., KAMMER, F. V. D., MOTELICA-HEINO, M., BABOROWSKI, M., HOFMEISTER, C. & LE COUSTUMER, P. 2006. Size-based speciation of natural colloidal particles by flow field flow fractionation, inductively coupled plasma-mass spectroscopy, and transmission electron microscopy/X-ray energy dispersive spectroscopy: Colloids-trace element interaction. *Environmental Science & Technology*, 40, 2156-2162.
- BAALOUSHA, M., KAMMER, F. V. D., MOTELICA-HEINO, M. & LE COUSTUMER, P. 2005a. 3D characterization of natural colloids by FIFFF-MALLS-TEM. *Analytical and Bioanalytical Chemistry*, 383, 549-556.
- BAALOUSHA, M., KAMMER, F. V. D., MOTELICA-HEINO, M. & LE COUSTUMER, P. 2005b. Natural sample fractionation by F1FFF-MALLS-TEM: Sample stabilization, preparation, pre-concentration and fractionation. *Journal of Chromatography A*, 1093, 156-166.
- BAALOUSHA, M. & LEAD, J. 2013a. Characterization of natural and manufactured nanoparticles by atomic force microscopy: Effect of analysis mode, environment and sample preparation: Colloid Surf.A: . *Physicochem.Eng.Asp.*, v. 419, p. 238-247.
- BAALOUSHA, M. & LEAD, J. R. 2007. Characterization of natural aquatic colloids (< 5 nm) by flow-field flow fractionation and atomic force microscopy. *Environmental Science & Technology*, 41, 1111-1117.
- BAALOUSHA, M. & LEAD, J. R. 2013b. Nanoparticle dispersity in toxicology. *Nat Nanotechnol*, 8, 308-9.
- BAALOUSHA, M., MANCIULEA, A., CUMBERLAND, S., KENDALL, K. & LEAD, J. R. 2008. Aggregation and surface properties of iron oxide nanoparticles: Influence of ph and natural organic matter. *Environmental Toxicology and Chemistry*, 27, 1875-1882.
- BAALOUSHA, M., MOTELICA-HEINO, M., GALAUP, S. & LE COUSTUMER, P. 2005c. Supramolecular structure of humic acids by TEM with improved sample preparation and staining. *Microscopy Research and Technique*, 66, 299-306.
- Effect of monovalent and divalent cations, anions and fulvic acid on aggregation of citrate-coated silver nanoparticles*, Directed by BAALOUSHA, M., NUR, Y., RÄJMER, I., TEJAMAYA, M. & LEAD, J. R.
- BAALOUSHA, M., PRASAD, A. & J, L. 2014c. Quantitative measurement of the nanoparticle size and number concentration from liquid suspensions by atomic force microscopy. *Environ Sci Process Impacts*.
- BAALOUSHA, M. E. A. 2012a. Characterisation of cerium oxide nanoparticles - Part 1: Size measurements: *Environ.Toxicol.Chem.*, . v.31, no. 5 983-993.
- BAALOUSHA, M. E. A. 2012b. Charaterization of cerium oxide nanoparticles-Part 2: Nonsize measurements: *Environ.Toxi:Chem.*, . v.31, no.5, 994-1003.
- BAALOUSHA MOHAMMED, HOW WILLIAM, VALSAMI-JONES EUGENIA & R., L. J. 2014. Chapter 1 - Overview of Environmental Nanoscience. *Frontiers of Nanoscience*. Elsevier.

- BALMES, J. R., EISNER, M. D. & GOTWAY, V. C. B. J. M. D. E. E. K. C. L. F. M. A. N. S. S. B. 2015. 74 - Indoor and Outdoor Air Pollution. *Murray and Nadel's Textbook of Respiratory Medicine (Sixth Edition)*. Philadelphia: W.B. Saunders.
- BALNOIS, E. & WILKINSON, K. J. 2002a. Sample preparation techniques for the observation of environmental biopolymers by atomic force microscopy. *Colloids and Surfaces a-Physicochemical and Engineering Aspects*, 207, 229-242.
- BALNOIS, E. & WILKINSON, K. J. 2002b. Sample preparation techniques for the observation of environmental biopolymers by atomic force microscopy. *Colloids and Surfaces A: Physicochemical and Engineering Aspects*, 207, 229-242.
- BAR-ILAN, O., ALBRECHT, R. M., FAKO, V. E. & FURGESON, D. Y. 2009. Toxicity Assessments of Multisized Gold and Silver Nanoparticles in Zebrafish Embryos. *Small*, 5, 1897-1910.
- BAUR, J. & SILVERMAN, E. 2007. Challenges and Opportunities in Multifunctional Nanocomposite Structures for Aerospace Applications. *MRS Bulletin*, 32, 328-334.
- BENJAMIN ARAZI, B. G. U. 2006. Enhancing Security with Nanotechnology.
- BINNIG, G., QUATE, C. F. & GERBER, C. 1986. Atomic force microscope. *Physical Review Letters*, 56, 930-933.
- BISWAS, A., BAYER, I. S., BIRIS, A. S., WANG, T., DERVISHI, E. & FAUPEL, F. 2012. Advances in top-down and bottom-up surface nanofabrication: techniques, applications & future prospects. *Adv Colloid Interface Sci*, 170, 2-27.
- BLASER, S. A., SCHERINGER, M., MACLEOD, M. & HUNGERBHLER, K. 2008. Estimation of cumulative aquatic exposure and risk due to silver: Contribution of nano-functionalized plastics and textiles. *Science of the Total Environment*, 390, 396-409.
- BORUCU, G., OZDEMIR, H., DEMIR, G., YIGIT, S. & OZCAN, H. K. 2010. Quantification of Atmospheric Particle Number Concentration for Selected Children Playgrounds: A Case Study in Istanbul. *Journal of Residuals Science & Technology*, 7, 147-152.
- BOYD, R. D. 1994. Similarities and Differences between Single-Side and Uniform Heating for Fusion Applications .1. Uniform Heat-Flux. *Fusion Technology*, 25, 411-418.
- BOYD, R. D. & CUENAT, A. 2011. New analysis procedure for fast and reliable size measurement of nanoparticles from atomic force microscopy images. *Journal of Nanoparticle Research*, 13, 105-113.
- BOYD, R. D., PICHAIMUTHU, S. K. & CUENAT, A. 2011. New approach to inter-technique comparisons for nanoparticle size measurements; using atomic force microscopy, nanoparticle tracking analysis and dynamic light scattering. *Colloids and Surfaces a-Physicochemical and Engineering Aspects*, 387, 35-42.
- BROCHET U.K, D. W. 1998. *J. Aerosol Sci.* 20, 1525.
- BUDNYK, A. P., DAMIN, A., AGOSTINI, G. & ZECCHINA, A. 2010. Gold Nanoparticle Aggregates Immobilized on High Surface Area Silica Substrate for Efficient and Clean SERS Applications. *Journal of Physical Chemistry C*, 114, 3857-3862.
- BUFFLE, J., WILKINSON, K. J., STOLL, S., FILELLA, M. & ZHANG, J. 1998. A Generalized Description of Aquatic Colloidal Interactions: The Three-colloidal Component Approach. *Environmental Science & Technology*, 32, 2887-2899.
- BUZEA, C., PACHECO, I. I. & ROBBIE, K. 2007. Nanomaterials and nanoparticles: Sources and toxicity. *Biointerphases*, 2, Mr17-Mr71.
- CAO, Q. L. A. Y. Preparation and Characterization of Gold Nanorods. *Pěrez-Juste, J., et al., Coordination Chemistry Reviews*, 2005. 249: p. 1870-1901.
- CAO, Y. C., WANG, Z., JIN, X., HUA, X. F., LIU, M. X. & ZHAO, Y. D. 2009. Preparation of Au nanoparticles-coated polystyrene beads and its application in protein immobilization. *Colloids and Surfaces a-Physicochemical and Engineering Aspects*, 334, 53-58.
- CARR 2012. Nanoparticle Tracking Analysis:A Review of Applications and Usage 2010 – 2012.
- CARR, B. 2008. Nanoparticle tracking system analyzes polydispersed samples. *Laser Focus World*, 44, 83-86.

- CARR, R., HOLE, P., MALLOY, A., SMITH, J., WELD, A. & WARREN, J. 2008. The real-time, simultaneous analysis of nanoparticle size, zeta potential, count, asymmetry and fluorescence. *Nsti Nanotech 2008, Vol 1, Technical Proceedings*, 866-870.
- CARR, R., SIUPA, A., POTTAGE, K., HANNELL, C. & SULLIVAN, J. 2011. The direct, real-time and multi-parameter visualisation and analysis of individual virus and gene delivery nanoparticles by laser microscopy and Nanoparticle Tracking Analysis. *Human Gene Therapy*, 22, A81-A81.
- CHEN, D. & LIU, H. Y. 2012. One-step synthesis of nickel ferrite nanoparticles by ultrasonic wave-assisted ball milling technology. *Materials Letters*, 72, 95-97.
- CHEN, K. L. & ELIMELECH, M. 2007. Influence of humic acid on the aggregation kinetics of fullerene (C60) nanoparticles in monovalent and divalent electrolyte solutions. *Journal of Colloid and Interface Science*, 309, 126-134.
- CHEN, K. L., MYLON, S. E. & ELIMELECH, M. 2006. Aggregation Kinetics of Alginate-Coated Hematite Nanoparticles in Monovalent and Divalent Electrolytes. *Environmental Science & Technology*, 40, 1516-1523.
- CHEN, K. L., MYLON, S. E. & ELIMELECH, M. 2007a. Enhanced aggregation of alginate-coated iron oxide (hematite) nanoparticles in the presence of calcium, strontium, and barium cations. *Langmuir*, 23, 5920-8.
- CHEN, K. L., MYLON, S. E. & ELIMELECH, M. 2007b. Enhanced Aggregation of Alginate-Coated Iron Oxide (Hematite) Nanoparticles in the Presence of Calcium, Strontium, and Barium Cations. *Langmuir*, 23, 5920-5928.
- COLVIN, V. L. 2003. The potential environmental impact of engineered nanomaterials. *Nat Biotech*, 21, 1166-1170.
- CRISTINA E. HOPPE, M. L., IVÁN PARDIÑAS-BLANCO, AND M. ARTURO LÓPEZ-QUINTELA One-Step Synthesis of Gold and Silver Hydrosols Using Poly(N-vinyl-2-pyrrolidone) as a Reducing Agent. *Langmuir*, 2006, 22 (16), pp 7027–7034.
- CUNHA, M. N. V., INÃJICIO, J. O., GRANBERG, F., KARLSSON, O., LEIJON, M., LIU, L. & BELÃJK, S. N. 2015. Molecular Approaches to Recognize Relevant and Emerging Infectious Diseases in Animals. *Veterinary Infection Biology: Molecular Diagnostics and High-Throughput Strategies*. Springer New York.
- DALE, A. L., CASMAN, E. A., LOWRY, G. V., LEAD, J. R., VIPARELLI, E. & BAALOUSHA, M. 2015. Modeling Nanomaterial Environmental Fate in Aquatic Systems. *Environmental Science & Technology*, 49, 2587-2593.
- DARK, M. L. 2006. A photovoltaics module for incoming science, technology, engineering and mathematics undergraduates. *Physics Education*, 46, 303.
- DE WIT, J. C. M., VAN RIEMSDIJK, W. H. & KOOPAL, L. K. 1993. Proton binding to humic substances. 2. Chemical heterogeneity and adsorption models. *Environmental Science & Technology*, 27, 2015-2022.
- DEGUELDRE, C. & FAVARGER, P. Y. 2003a. Colloid analysis by single particle inductively coupled plasma-mass spectroscopy: a feasibility study. *Colloids and Surfaces a-Physicochemical and Engineering Aspects*, 217, 137-142.
- DEGUELDRE, C. & FAVARGER, P. Y. 2003b. Colloid analysis by single particle inductively coupled plasma-mass spectroscopy: a feasibility study. *Colloids and Surfaces A: Physicochemical and Engineering Aspects*, 217, 137-142.
- DIEGOLI, S., MANCIULEA, A. L., BEGUM, S., JONES, I. P., LEAD, J. R. & PREECE, J. A. 2008. Interaction between manufactured gold nanoparticles and naturally occurring organic macromolecules. *Science of the Total Environment*, 402, 51-61.
- DOMINGOS, A. L., TUCCI, S., JR., GARCIA, S. B., DE BESSA, J., JR., COLOGNA, A. J. & MARTINS, A. C. 2009a. Use of a latex biomembrane for bladder augmentation in a rabbit model: biocompatibility, clinical and histological outcomes. *Int Braz J Urol*, 35, 217-24; author reply 225-6.

- DOMINGOS, R. F., BAALOUSHA, M. A., JU-NAM, Y., REID, M. M., TUFENKJI, N., LEAD, J. R., LEPPARD, G. G. & WILKINSON, K. J. 2009b. Characterizing manufactured nanoparticles in the environment: multimethod determination of particle sizes. *Environmental Science & Technology*, 43, 7277-84.
- DONALDSON, K. & POLAND, C. A. 2013. Nanotoxicity: challenging the myth of nano-specific toxicity. *Current Opinion in Biotechnology*, 24, 724-734.
- DONALDSON, K., SCHINWALD, A., MURPHY, F., CHO, W.-S., DUFFIN, R., TRAN, L. & POLAND, C. 2013. The Biologically Effective Dose in Inhalation Nanotoxicology. *Accounts of Chemical Research*, 46, 723-732.
- DU, S. F., KENDALL, K., MORRIS, S. & SWEET, C. 2010. Measuring number-concentrations of nanoparticles and viruses in liquids on-line. *Journal of Chemical Technology and Biotechnology*, 85, 1223-1228.
- DUFFIN, R., TRAN, C. L., CLOUTER, A., BROWN, D. M., MACNEE, W., STONE, V. & DONALDSON, K. 2002. The Importance of Surface Area and Specific Reactivity in the Acute Pulmonary Inflammatory Response to Particles. *Annals of Occupational Hygiene*, 46, 242-245.
- DUFFIN, R., TRAN, L., BROWN, D., STONE, V. & DONALDSON, K. 2007. Proinflammogenic effects of low-toxicity and metal nanoparticles in vivo and in vitro: highlighting the role of particle surface area and surface reactivity. *Inhal Toxicol*, 19, 849-56.
- DYCUS, P. J. M., HEALY, K. D., STEARMAN, G. K. & WELLS, M. J. M. 1995. Diffusion-Coefficients and Molecular-Weight Distributions of Humic and Fulvic-Acids Determined by Flow Field-Flow Fractionation. *Separation Science and Technology*, 30, 1435-1453.
- ENVIRONMENTAL PROTECTION AGENCY OFFICE OF WATER (4303T): WASHINGTON, U. 2002. US.EPA Methods for measuring the acute toxicity of effluents and receiving water to freshwater and marine organisms;EPA-821-R-02-012; U.S. Environmental Protection Agency Office of Water (4303T): Washington, DC, 02.
- FARADAY, M. 1857. The Bakerian Lecture: Experimental Relations of Gold (and Other Metals) to Light. *Phil. Trans. R. Soc. Lond.*,
- FARBOD, M. & KHADEMALRASOOL, M. 2011. Synthesis of TiO<sub>2</sub> nanoparticles by a combined sol-gel ball milling method and investigation of nanoparticle size effect on their photocatalytic activities. *Powder Technology*, 214, 344-348.
- FERNANDEZ-GARRIDO, S., KAGANER, V. M., HAUSWALD, C., JENICHEN, B., RAMSTEINER, M., CONSONNI, V., GEELHAAR, L. & BRANDT, O. 2014. Correlation between the structural and optical properties of spontaneously formed GaN nanowires: a quantitative evaluation of the impact of nanowire coalescence. *Nanotechnology*, 25.
- FERNS 1973. Nature physical science. *Nature Chemistry*.
- FRANKLIN KIM, J. H. S., AND PEIDONG YANG\* 2002. Photochemical Synthesis of Gold Nanorods. *American Chemical Society, J. AM. CHEM. SOC.* 2002, 124, 14316-14317.
- FRAUNHOFER, W. & WINTER, G. 2004. The use of asymmetrical flow field-flow fractionation in pharmaceuticals and biopharmaceuticals. *European Journal of Pharmaceutics and Biopharmaceutics*, 58, 369-383.
- FREDERICK 1976. Correlation of Measurements of Absorbance in the Ultraviolet and Visible Regions at Different Spectral Slitwidths. *Analytical Chemistry*, 48.
- FRENS, G. 1973. Controlled nucleation for the regulation of the particle size in monodisperse gold suspensions. *Nature Phys.Sci.*, .
- GAISER, B., ROSENKRANZ, P., LEAD, J., TYLER, C., JEPSON, M., FERNANDES, T. & STONE, V. 2009. Nanoparticle Risk to the Environment and Human Health. *Inhaled Particles X*, 151.
- GALLEGO-URREA, J. A., TUORINIEMI, J., PALLANDER, T. & HASSELLOV, M. 2010. Measurements of nanoparticle number concentrations and size distributions in contrasting aquatic environments using nanoparticle tracking analysis. *Environmental Chemistry*, 7, 67-81.
- GIDDINGS, J. C. 1993. Field-Flow Fractionation - Analysis of Macromolecular, Colloidal, and Particulate Materials. *Science*, 260, 1456-1465.

- GIDHAGEN, L., JOHANSSON, C., LANGNER, J. & FOLTESCU, V. L. 2005. Urban scale modeling of particle number concentration in Stockholm. *Atmospheric Environment*, 39, 1711-1725.
- GIMBERT, L. J., HAMON, R. E., CASEY, P. S. & WORSFOLD, P. J. 2007. Partitioning and stability of engineered ZnO nanoparticles in soil suspensions using flow field-flow fractionation. *Environmental Chemistry*, 4, 8-10.
- GIMBERT, L. J., HAYGARTH, P. M., BECKETT, R. & WORSFOLD, P. J. 2006. The influence of sample preparation on observed particle size distributions for contrasting soil suspensions using flow field-flow fractionation. *Environmental Chemistry*, 3, 184-191.
- GOTTSCHALK, F., KOST, E. & NOWACK, B. 2013a. Engineered nanomaterials in water and soils: A risk quantification based on probabilistic exposure and effect modeling. *Environmental Toxicology and Chemistry*, 32, 1278-1287.
- GOTTSCHALK, F., ORT, C., SCHOLZ, R. W. & NOWACK, B. 2011. Engineered nanomaterials in rivers - Exposure scenarios for Switzerland at high spatial and temporal resolution. *Environmental Pollution*, 159, 3439-3445.
- GOTTSCHALK, F., SONDERER, T., SCHOLZ, R. W. & NOWACK, B. 2009. Modeled Environmental Concentrations of Engineered Nanomaterials (TiO<sub>2</sub>, ZnO, Ag, CNT, Fullerenes) for Different Regions. *Environmental Science & Technology*, 43, 9216-9222.
- Environmental concentrations of engineered nanomaterials: Review of modeling and analytical studies*, Directed by GOTTSCHALK, F., SUN, T. & NOWACK, B.
- GOTTSCHALK, F., SUN, T. & NOWACK, B. 2013b. Environmental concentrations of engineered nanomaterials: Review of modeling and analytical studies. 181, 287-300.
- GREENWOOD, O. D., BOYD, R. D., HOPKINS, J. & BADYAL, J. P. S. 1995. Atmospheric Silent Discharge Versus Low-Pressure Plasma Treatment of Polyethylene, Polypropylene, Polyisobutylene, and Polystyrene. *Journal of Adhesion Science and Technology*, 9, 311-326.
- GRIFFITHS, D. A., BERNT, W., HOLE, P., SULLIVAN, J., MALLOY, A. & CARR, B. 2011. Single-particle resolution particle size and zeta potential analysis by nanoparticle tracking analysis. *Abstracts of Papers of the American Chemical Society*, 242.
- GROW, T. J. M. A. W. R. 1997. Inductively Coupled Plasma -Atomic Emission Spectrometry. *SPRINGER-VERLAG NEW YORK, INC, 1 / VOL. 2, N O. 1.*
- GSCHWIND, S., FLAMIGNI, L., KOCH, J., BOROVINSKAYA, O., GROH, S., NIEMAX, K. & GUNTHER, D. 2011. Capabilities of inductively coupled plasma mass spectrometry for the detection of nanoparticles carried by monodisperse microdroplets. *Journal of Analytical Atomic Spectrometry*, 26, 1166-1174.
- GURUNATHAN, S., HAN, J., PARK, J. & KIM, J.-H. A green chemistry approach for synthesizing biocompatible gold nanoparticles. *Nanoscale Research Letters* C7 - 248, 9, 1-11.
- HAISS, W., THANH, N. T. K., AVEYARD, J. & FERNIG, D. G. 2007a. Determination of size and concentration of gold nanoparticles from UV-Vis spectra. *Analytical Chemistry*, 79, 4215-4221.
- HAISS, W., THANH, N. T. K., AVEYARD, J. & FERNIG, D. G. 2007b. Determination of Size and Concentration of Gold Nanoparticles from UV-Vis Spectra. *Analytical Chemistry*, 79, 4215-4221.
- HANDY, R., OWEN, R. & VALSAMI-JONES, E. 2008. The ecotoxicology of nanoparticles and nanomaterials: current status, knowledge gaps, challenges, and future needs. *Ecotoxicology*, 17, 315-325.
- HANNAH, W. & THOMPSON, P. B. 2008. Nanotechnology, risk and the environment: a review. *Journal of Environmental Monitoring*, 10, 291-300.
- HARTMANN, N. B., SKJOLDING, L. M., HANSEN, S. F., KJØLHOLT, J., GOTTSCHALCK, F. & BAUN, A. 2014. Environmental fate and behaviour of nanomaterials New knowledge on important transformation processes.

- HASSELLOV, M. 2005. Relative molar mass distributions of chromophoric colloidal organic matter in coastal seawater determined by Flow Field-Flow Fractionation with UV absorbance and fluorescence detection. *Marine Chemistry*, 94, 111-123.
- HASSELLOV, M., READMAN, J., RANVILLE, J. & TIEDE, K. 2008. Nanoparticle analysis and characterization methodologies in environmental risk assessment of engineered nanoparticles. *Ecotoxicology*, 17, 344-361.
- HEALTH & SAFETY LABORATORY, B., UK 2011. Health & Safety Executive NanoAlert Service.
- HEITBRINK, W. A., EVANS, D. E., KU, B. K., MAYNARD, A. D., SLAVIN, T. J. & PETERS, T. M. 2009. Relationships Among Particle Number, Surface Area, and Respirable Mass Concentrations in Automotive Engine Manufacturing. *Journal of Occupational and Environmental Hygiene*, 6, 19-31.
- HERRMANN, J. November 2012. Nanoparticle characterisation instrumentation.
- HIRNER, A., LADWIG, F., STRANSKY, H., OKUMOTO, S., KEINATH, M., HARMS, A., FROMMER, W. B. & KOCH, W. 2006. Arabidopsis LHT1 is a high-affinity transporter for cellular amino acid uptake in both root epidermis and leaf mesophyll. *Plant Cell*, 18, 1931-46.
- HITCHMAN, A., SMITH, G. H., JU-NAM, Y., STERLING, M. & LEAD, J. R. 2013. The effect of environmentally relevant conditions on PVP stabilised gold nanoparticles. *Chemosphere*, 90, 410-6.
- HOO, C., STAROSTIN, N., WEST, P. & MECARTNEY, M. 2008. A comparison of atomic force microscopy (AFM) and dynamic light scattering (DLS) methods to characterize nanoparticle size distributions. *Journal of Nanoparticle Research*, 10, 89-96.
- HUANG, N. P., MICHEL, R., VOROS, J., TEXTOR, M., HOFER, R., ROSSI, A., ELBERT, D. L., HUBBELL, J. A. & SPENCER, N. D. 2001. Poly(L-lysine)-g-poly(ethylene glycol) layers on metal oxide surfaces: Surface-analytical characterization and resistance to serum and fibrinogen adsorption. *Langmuir*, 17, 489-498.
- IQBAL, P., PREECE, J. A. & MENDES, P. M. 2012. Nanotechnology: The “Top-Down” and “Bottom-Up” Approaches. *Supramolecular Chemistry*. John Wiley & Sons, Ltd.
- ISO 2012a. ISO/TR 13014:2012: Nanotechnologies -- Guidance on physico-chemical characterization of engineered nanoscale materials for toxicologic assessment.
- ISO 2012b. ISO/TS 11937:2012(en)Nanotechnologies — Nanoscale titanium dioxide in powder form — Characteristics and measurement.
- J. MCCARTHY, C. D. 1993. characterisation of environmental particles. 247-315.
- JARVIS, I. & JARVIS, K. E. 1992. Plasma spectrometry in the earth sciences: techniques, applications and future trends. *Chemical Geology*, 95, 1-33.
- JÉRÔME F. L. DUVAL 2007. Electrophoresis of Soft Colloids: Basic Principles and Applications. *Environmental colloidal and particles by Kevin J. Wilkinson Ph.D. Jamie R. Lead Ph.D.*, 315-344.
- JIANG, J. K., OBERDORSTER, G. & BISWAS, P. 2009. Characterization of size, surface charge, and agglomeration state of nanoparticle dispersions for toxicological studies. *Journal of Nanoparticle Research*, 11, 77-89.
- JO, G., CHOE, M., LEE, S., PARK, W., KAHNG, Y. H. & LEE, T. 2012. The application of graphene as electrodes in electrical and optical devices. *Nanotechnology*, 23, 112001.
- JOHNSTON, M. E., BOYD, R. D. & MCGRATH, M. 2007. Growth and carcass response to dietary fat for modern lean pigs. *Journal of Animal Science*, 85, 91-91.
- JU-NAM, Y. & LEAD, J. R. 2008. Manufactured nanoparticles: An overview of their chemistry, interactions and potential environmental implications. *Science of the Total Environment*, 400, 396-414.
- KEUNE, H., GUTLEB, A. C., ZIMMER, K. E. & RAVNUM, S. 2012. We’re only in it for the knowledge? A problem solving turn in environment and health expert elicitation. *Environmental Health*.
- KIRBY, B. J. & HASSELBRINK, E. F. 2004. Zeta potential of microfluidic substrates: 1. Theory, experimental techniques, and effects on separations. *Electrophoresis*, 25, 187-202.

- KLABUNDE, K. J. & RICHARDS, R. M. 2001. *Nanoscale Materials in Chemistry, 2nd Edition*, New York, Wiley Interscience.
- KOLIADIMA, A. & KARAIKAKIS, G. 1990. Potential-Barrier Field-Flow Fractionation, a Versatile New Separation Method. *Journal of Chromatography*, 517, 345-359.
- KRYSTEK, P., ULRICH, A., GARCIA, C. C., MANOHAR, S. & RITSEMA, R. 2011. Application of plasma spectrometry for the analysis of engineered nanoparticles in suspensions and products. *Journal of Analytical Atomic Spectrometry*, 26, 1701-1721.
- LEAD, J. 2011. Introduction to a special issue on trace metal speciation - GEOSPEC 2010. *Environmental Chemistry*, 8, 1-1.
- LEAD, J. & SMITH, E. 2009. *Environmental and Human Health Impacts of Nanotechnology*.
- LEAD, J. R., BALNOIS, E., HOSSE, M., MENGHETTI, R. & WILKINSON, K. J. 1999. Characterization of Norwegian natural organic matter: Size, diffusion coefficients, and electrophoretic mobilities. *Environment International*, 25, 245-258.
- LEAD, J. R. & VALSAMI-JONES, E. 2014. Nanoscience and the environment. *Frontiers of Nanoscience*. Elsevier.
- LEAD, J. R. & WILKINSON, K. J. 2006. Environmental Colloids and Particles: Current Knowledge and Future Developments *CURRENT KNOWLEDGE AND FUTURE DEVELOPMENTS*.
- LEE, G. G. & PARK, J. S. 2007. Hydrogen sorption property of Zr<sub>55</sub>V<sub>29</sub>Fe<sub>16</sub> nanopowder synthesized by the plasma arc discharge process. *Materials Transactions*, 48, 1566-1570.
- LEPPARD, G. G. 2008. Nanoparticles in the Environment as Revealed by Transmission Electron Microscopy: Detection, Characterisation and Activities. *Current Nanoscience*, 4, 278-301.
- LI, C. C., CAI, W. P., LI, Y., HU, J. L. & LIU, P. S. 2006. Ultrasonically induced Au nanoprisms and their size manipulation based on aging. *Journal of Physical Chemistry B*, 110, 1546-1552.
- LIANG, A. H., ZHOU, L. P. & JIANG, Z. L. 2011. A Simple and Sensitive Resonance Scattering Spectral Assay for Detection of Melamine Using Aptamer-Modified Nanosilver Probe. *Plasmonics*, 6, 387-392.
- LINK, S., BURDA, C., MOHAMED, M. B., NIKOOBAKHT, B. & EL-SAYED, M. A. 2000. Femtosecond transient-absorption dynamics of colloidal gold nanorods: Shape independence of the electron-phonon relaxation time. *Physical Review B*, 61, 6086-6090.
- LIU, J. K., LUO, C. X., YANG, X. H. & ZHANG, X. Y. 2009. Ultrasonic-template method synthesis of CdS hollow nanoparticle chains. *Materials Letters*, 63, 124-126.
- LOUIE, S. M., MA, R., LOWRY, G. V., JAMIE, R. L. & EUGENIA, V.-J. 2014. Chapter 2 - Transformations of Nanomaterials in the Environment. *Frontiers of Nanoscience*. Elsevier.
- LUNG, J. K., HUANG, J. C., TIEN, D. C., LIAO, C. Y., TSENG, K. H., TSUNG, T. T., KAO, W. S., TSAI, T. H., JWO, C. S., LIN, H. M. & STOBINSKI, L. 2007. Preparation of gold nanoparticles by arc discharge in water. *Journal of Alloys and Compounds*, 434, 655-658.
- LYVEN, B., HASSELLOV, M., TURNER, D. R., HARALDSSON, C. & ANDERSSON, K. 2003. Competition between iron- and carbon-based colloidal carriers for trace metals in a freshwater assessed using flow field-flow fractionation coupled to ICPMS. *Geochimica Et Cosmochimica Acta*, 67, 3791-3802.
- M. BAALOUSHAŞ+\*, A. P. A. J. R. L. 2014. Quantitative measurement of nanoparticle size and number concentration from liquid suspensions by atomic force microscopy. *rsc.li/process-impacts*.
- MADHUMITHA, G. & ROOPAN, S. M. 2013a. Devastated Crops: Multifunctional Efficacy for the Production of Nanoparticles. *Journal of Nanomaterials*, 2013, 12.
- MADHUMITHA, G. & ROOPAN, S. M. 2013b. Devastated crops: multifunctional efficacy for the production of nanoparticles. *J. Nanomaterials*, 2013, 3-3.
- MAITRA, A., KUMAR, P., K, T. & SAHOO, S. K. 1999. Process for the preparation of highly monodispersed polymeric hydrophilic nanoparticles. *US Patent 5874111*.
- MALLOY, A. & CARR, B. 2006. Nanoparticle tracking analysis - The Halo (TM) system. *Particle & Particle Systems Characterization*, 23, 197-204.

- MEREDITH, P., BETTINGER, C. J., IRIMIA-VLADU, M., MOSTERT, A. B. & SCHWENN, P. E. 2013. Electronic and optoelectronic materials and devices inspired by nature. *Reports on Progress in Physics*, 76, 034501.
- MERK, V., REHBOCK, C., BECKER, F., HAGEMANN, U., NIENHAUS, H. & BARCIKOWSKI, S. In Situ Non-DLVO Stabilization of Surfactant-Free, Plasmonic Gold Nanoparticles: Effect of Hofmeister's Anions. *Langmuir*, 30, 4213-4222.
- MEYER, E. 1992. Atomic Force Microscopy. *Progress in Surface Science*, 41, 3-49.
- MILLER, C. C. 1924. The Stokes Einstein law for diffusion in solution. *Proceedings of the Royal Society of London Series a-Containing Papers of a Mathematical and Physical Character*, 106, 724-749.
- MILLER, M. M. & LAZARIDES, A. A. 2005. Sensitivity of metal nanoparticle surface plasmon resonance to the dielectric environment. *Journal of Physical Chemistry B*, 109, 21556-21565.
- MOCK, J. J., BARBIC, M., SMITH, D. R., SCHULTZ, D. A. & SCHULTZ, S. 2002. Shape effects in plasmon resonance of individual colloidal silver nanoparticles. *Journal of Chemical Physics*, 116, 6755-6759.
- MOHD SULTAN, N. & JOHAN, M. R. Synthesis and Ultraviolet Visible Spectroscopy Studies of Chitosan Capped Gold Nanoparticles and Their Reactions with Analytes. *The Scientific World Journal*, 2014, 7.
- MYERS, J. C. G. F. J. F. Y. M. N. 1976. Flow Field-Flow Fractionation: A Versatile New Separation Method. *SCIENCE*, VOL. 193.
- NICHOLS, G., BYARD, S., BLOXHAM, M. J., BOTTERILL, J., DAWSON, N. J., DENNIS, A., DIART, V., NORTH, N. C. & SHERWOOD, J. D. 2002. A review of the terms agglomerate and aggregate with a recommendation for nomenclature used in powder and particle characterization. *Journal of Pharmaceutical Sciences*, 91, 2103-2109.
- NOWACK, B. & BUCHELI, T. D. 2007. Occurrence, behavior and effects of nanoparticles in the environment. *Environmental Pollution*, 150, 5-22.
- NOWACK, B., RANVILLE, J. F., DIAMOND, S., GALLEGRO-URREA, J. A., METCALFE, C., ROSE, J., HORNE, N., KOELMANS, A. A. & KLAINE, S. J. 2012. Potential scenarios for nanomaterial release and subsequent alteration in the environment. *Environmental Toxicology and Chemistry*, 31, 50-59.
- OBERDÄRSTER, G. N., OBERDÄRSTER, E. & OBERDÄRSTER, J. 2007. Concepts of Nanoparticle Dose Metric and Response Metric. *Environmental Health Perspectives*, 115, A290-A290.
- OBERDORSTER, G., OBERDORSTER, E. & OBERDORSTER, J. 2007. Concepts of Nanoparticle Dose Metric and Response Metric. *Environmental Health Perspectives*, 115, A290-A290.
- PAL, S., TAK, Y. K. & SONG, J. M. 2007. Does the antibacterial activity of silver nanoparticles depend on the shape of the nanoparticle? A study of the gram-negative bacterium Escherichia coli. *Applied and Environmental Microbiology*, 73, 1712-1720.
- PECORA, R. 2000. Dynamic Light Scattering: Applications of Photon Correlation Spectroscopy.
- PEDRO J. J. ALVAREZ, \* VICKI COLVIN, ‡ JAMIE LEAD, § AND VICKI STONE 2009. Research Priorities to Advance Eco-Responsible Nanotechnology.
- PICCINNO, F., GOTTSCHALK, F., SEEGER, S. & NOWACK, B. 2012. Industrial production quantities and uses of ten engineered nanomaterials in Europe and the world. *Journal of Nanoparticle Research C7 - 1109*, 14, 1-11.
- QIN, W., LOHRMAN, J. & REN, S. 2014. Magnetic and Optoelectronic Properties of Gold Nanocluster-Thiophene Assembly. *Angewandte Chemie International Edition*, 53, 7316-7319.
- R. P. FEYNMAN, R. B. L., M. SANDS 1964. 'The Feynman Lectures on Physics' Volume I. Addison-Wesley Publishing Co, USA.
- RAO, A., SCHOENENBERGER, M., GNECCO, E., GLATZEL, T., MEYER, E., BRANDLIN, D. & SCANDELLA, L. 2007. Characterization of nanoparticles using Atomic Force Microscopy. *Proceedings of the International Conference on Nanoscience and Technology*, 61, 971-976.
- REPORT, U. G. R. 2007. Characterising the Potential Risks posed by Engineered Nanoparticles.



- ROCO, M. C. 2005a. Environmentally responsible development of nanotechnology. *Environ Sci Technol*, 39, 106A-112A.
- ROCO, M. C. 2005b. Environmentally responsible development of nanotechnology. *Environmental Science & Technology*, 39, 106A-112A.
- ROJAS, O. J. 2002. Adsorption of polyelectrolytes on mica. *Encyclopedia of Surface and Colloid Science*.
- ROSA, A. L., YAN, M., FERNANDEZ, R., WANG, X. & ZEGARRA, E. 2010. Proton-fountain Electric-field-assisted Nanolithography (PEN): Fabrication of polymer nanostructures that respond to chemical and electrical stimuli.
- SAGER, T. M. & CASTRANOVA, V. 2009. Surface area of particle administered versus mass in determining the pulmonary toxicity of ultrafine and fine carbon black: comparison to ultrafine titanium dioxide. *Part Fibre Toxicol*, 6, 1743-8977.
- SANTSCHI, E. M., PURDY, A. K., VALBERG, S. J., VROTSOS, P. D., KAESE, H. & MICKELSON, J. R. 1998. Endothelin receptor B polymorphism associated with lethal white foal syndrome in horses. *Mamm Genome*, 9, 306-9.
- SARTOR, M. DYNAMIC LIGHT SCATTERING.
- SCHAEUBLIN, N. M., BRAYDICH-STOLLE, L. K., MAURER, E. I., PARK, K., MACCUSPIE, R. I., AFROOZ, A. R. M. N., VAIA, R. A., SALEH, N. B. & HUSSAIN, S. M. 2012. Does Shape Matter? Bioeffects of Gold Nanomaterials in a Human Skin Cell Model. *Langmuir*, 28, 3248-3258.
- SCHMIDT, J. R. & SKINNER, J. L. 2004. Brownian motion of a rough sphere and the Stokes-Einstein Law. *Journal of Physical Chemistry B*, 108, 6767-6771.
- SCHRAMM, C., RINDERER, B. & TESSADRI, R. 2012. Sol-gel synthesis and characterization of polyimides based on the reaction of butane-1,2,3,4-tetracarboxylic acid with 3-aminopropyltriethoxysilane. *Journal of Applied Polymer Science*, 125, 1201-1206.
- SEATON, A., SOUTAR, A., CRAWFORD, V., ELTON, R., MCNERLAN, S., CHERRIE, J., WATT, M., AGIUS, R. & STOUT, R. 1999. Particulate air pollution and the blood. *Thorax*, 54, 1027-32.
- SMITA, S., GUPTA, S. K., BARTONOVA, A., DUSINSKA, M., GUTLEB, A. C. & RAHMAN, Q. 2012. Nanoparticles in the environment: assessment using the causal diagram approach. *Environmental Health*.
- STOLPE, B., HASSELLOV, M., ANDERSSON, K. & TURNER, D. R. 2005. High resolution ICPMS as an on-line detector for flow field-flow fractionation; multi-element determination of colloidal size distributions in a natural water sample. *Analytica Chimica Acta*, 535, 109-121.
- STONE, V., HANKIN, S., AITKEN, R., ASCHBERGER, K., BAUN, A. & CHRISTENSEN, F. 2010. Engineered Nanoparticles: Review of Health and Environmental Safety (ENRHES). *ENRHES*.
- STONE, V., HANKIN, S., AITKEN, R., ASCHBERGER, K., BAUN, A., CHRISTENSEN, F., FERNANDES, T., HANSEN, S.F., ARTMANN, N.B., HUTCHINSON, G., JOHNSTON, H., MICHELETTI, G., PETERS, S., ROSS, B., SOKULL-KLUETTGEN, B., STARK, D., TRAN, L. (2010). Engineered Nanoparticles: Review of Health and Environmental Safety (ENRHES). *ENRHES*.
- SUN, Y. G. & XIA, Y. N. 2002. Shape-controlled synthesis of gold and silver nanoparticles. *Science*, 298, 2176-2179.
- TABRIZI, N. S., ULLMANN, M., VONS, V. A., LAFONT, U. & SCHMIDT-OTT, A. 2008. Generation of nanoparticles by spark discharge. *Journal of Nanoparticle Research*, 11, 315-332.
- TABRIZI, N. S., XU, Q., PERS, N. M. & SCHMIDT-OTT, A. 2009. Generation of mixed metallic nanoparticles from immiscible metals by spark discharge. *Journal of Nanoparticle Research*, 12, 247-259.
- THANG, N. M., GECKEIS, H., KIM, J. I. & BECK, H. P. 2001. Application of the flow field flow fractionation (FFFF) to the characterization of aquatic humic colloids: evaluation and optimization of the method. *Colloids and Surfaces a-Physicochemical and Engineering Aspects*, 181, 289-301.
- TIEN, D.-C., CHEN, L.-C., VAN THAI, N. & ASHRAF, S. 2010. Study of Ag and Au Nanoparticles Synthesized by Arc Discharge in Deionized Water. *Journal of Nanomaterials*, 2010, 1-9.

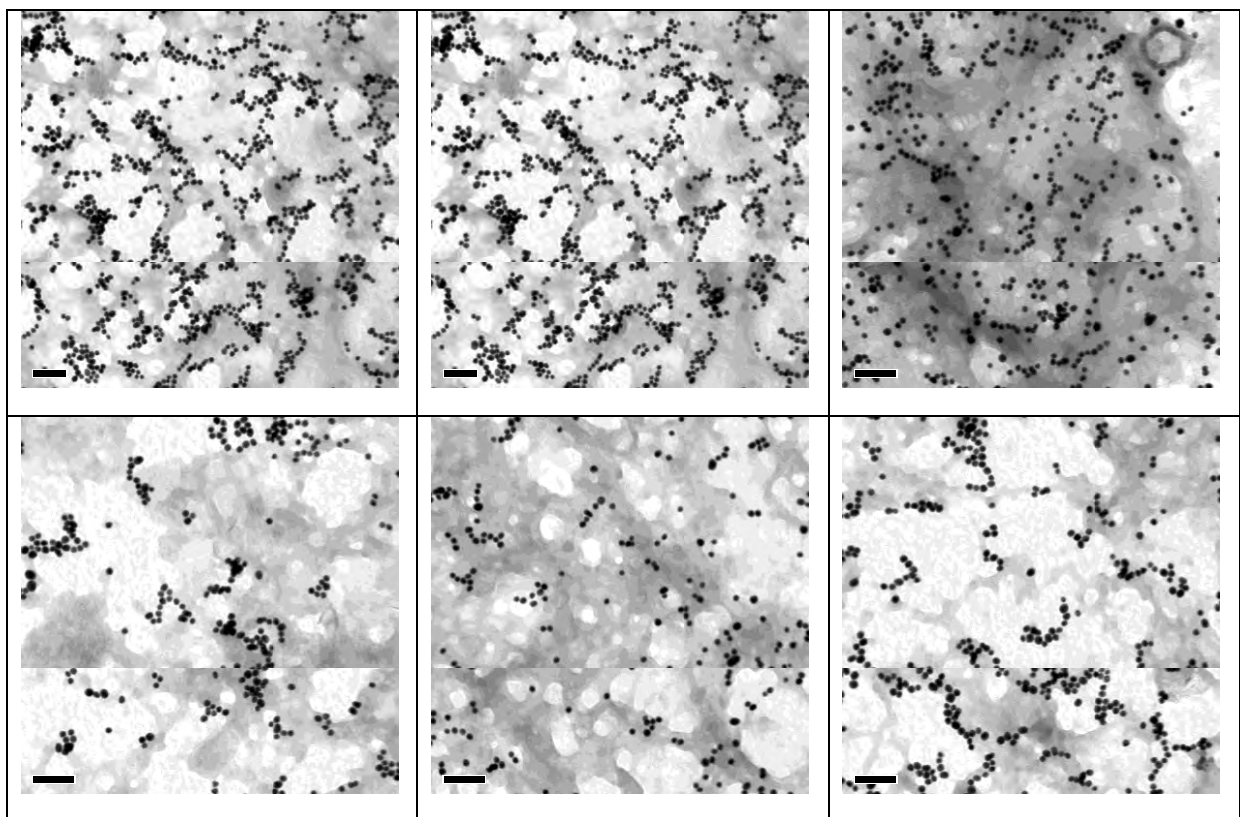
- TIRUVANNAMALAI-ANNAMALAI, R., ARMANT, D. R. & MATTHEW, H. W. T. 2014. *Bottom-up vs. top-down approaches in tissue engineering*.
- TSENG, K.-H., HUANG, J.-C., LIAO, C.-Y., TIEN, D.-C. & TSUNG, T.-T. 2009. Preparation of gold ethanol colloid by the arc discharge method. *Journal of Alloys and Compounds*, 472, 446-450.
- TURKEVICH 1951a. A STUDY OF THE NUCLEATION AND GROWTH PROCESSES IN THE SYNTHESIS OF COLLOIDAL GOLD.
- TURKEVICH, J., P. C. STEVENSON, AND J. HILLIER, 1951b. A study of the nucleation and growth processes in the synthesis of colloidal gold. *Discuss. Faraday Soc.*, v. 11, no. 0, p. 55-75.
- UCHIHASHI, T., OKUSAKO, T., YAMADA, J., FUKANO, Y., SUGAWARA, Y., IGARASHI, M., KANEKO, R. & MORITA, S. 1994. Contact Electrification on Thin SrTiO<sub>3</sub> Film by Atomic-Force Microscope. *Japanese Journal of Applied Physics Part 2-Letters*, 33, L374-L376.
- VAN HYNING, D. L. & ZUKOSKI, C. F. 1998. Formation mechanisms and aggregation behavior of borohydride reduced silver particles. *Langmuir*, 14, 7034-7046.
- WAGNER, S., LEGROS, S., LOESCHNER, K., LIU, J., NAVRATILOVA, J., GROMBE, R., LINSINGER, T. P. J., LARSEN, E. H., VON DER KAMMER, F. & HOFMANN, T. 2014. First steps towards a generic sample preparation scheme for inorganic engineered nanoparticles in a complex matrix for detection, characterization, and quantification by asymmetric flow-field flow fractionation coupled to multi-angle light scattering and ICP-MS. *Journal of Analytical Atomic Spectrometry*.
- WANG, X., LOW, X. C., HOU, W., ABDULLAH, L. N., TOH, T. B., MOHD ABDUL RASHID, M., HO, D. & CHOW, E. K.-H. 2014. Epirubicin-Adsorbed Nanodiamonds Kill Chemoresistant Hepatic Cancer Stem Cells. *ACS Nano*, 8, 12151-12166.
- WANG, Y. & CHOU, S. Y. 1992. Engineering Sub-50 Nm Quantum Effect Devices and Single-Electron Transistors Using Electron-Beam Lithography. *Journal of Vacuum Science & Technology B*, 10, 2962-2965.
- WANG, Z. L. 2000. Transmission electron microscopy of shape-controlled nanocrystals and their assemblies. *Journal of Physical Chemistry B*, 104, 1153-1175.
- WEI, L., XIAO, L. H. & HE, Y. 2011. Synthesis of water soluble silver-nanoparticle-embedded polymer nanofibers with poly(2-ethyl-2-oxazoline) by a straightforward polyol process. *Journal of Materials Research*, 26, 1614-1620.
- WILKINSON, K. J., BALNOIS, E., LEPPARD, G. G. & BUFFLE, J. 1999a. Characteristic features of the major components of freshwater colloidal organic matter revealed by transmission electron and atomic force microscopy. *Colloids and Surfaces a-Physicochemical and Engineering Aspects*, 155, 287-310.
- WILKINSON, K. J., BALNOIS, E., LEPPARD, G. G. & BUFFLE, J. 1999b. Characteristic features of the major components of freshwater colloidal organic matter revealed by transmission electron and atomic force microscopy. *Colloids and Surfaces A: Physicochemical and Engineering Aspects*, 155, 287-310.
- WILSON, W. 2012. (<http://www.nanotechproject.org/HYPERLINK> "<http://www.nanotechproject.org/>") <<http://www.nanotechproject.org/>>. .
- WIMUKTIWAN, P., SHIOWATANA, J. & SIRIPINYANOND, A. 2015. Investigation of silver nanoparticles and plasma protein association using flow field-flow fractionation coupled with inductively coupled plasma mass spectrometry (FIFFF-ICP-MS). *Journal of Analytical Atomic Spectrometry*, 30, 245-253.
- WRAYCAHEN, D., BELL, A. W., BOYD, R. D., ROSS, D. A., BAUMAN, D. E., KRICK, B. J. & HARRELL, R. J. 1995. Nutrient-Uptake by the Hindlimb of Growing Pigs Treated with Porcine Somatotropin and Insulin. *Journal of Nutrition*, 125, 125-135.
- WU, D. D., BOYD, R. D., FIX, T. J. & BURR, D. B. 1990a. Regional Patterns of Bone Loss and Altered Bone Remodeling in Response to Calcium Deprivation in Laboratory Rabbits. *Calcified Tissue International*, 47, 18-23.

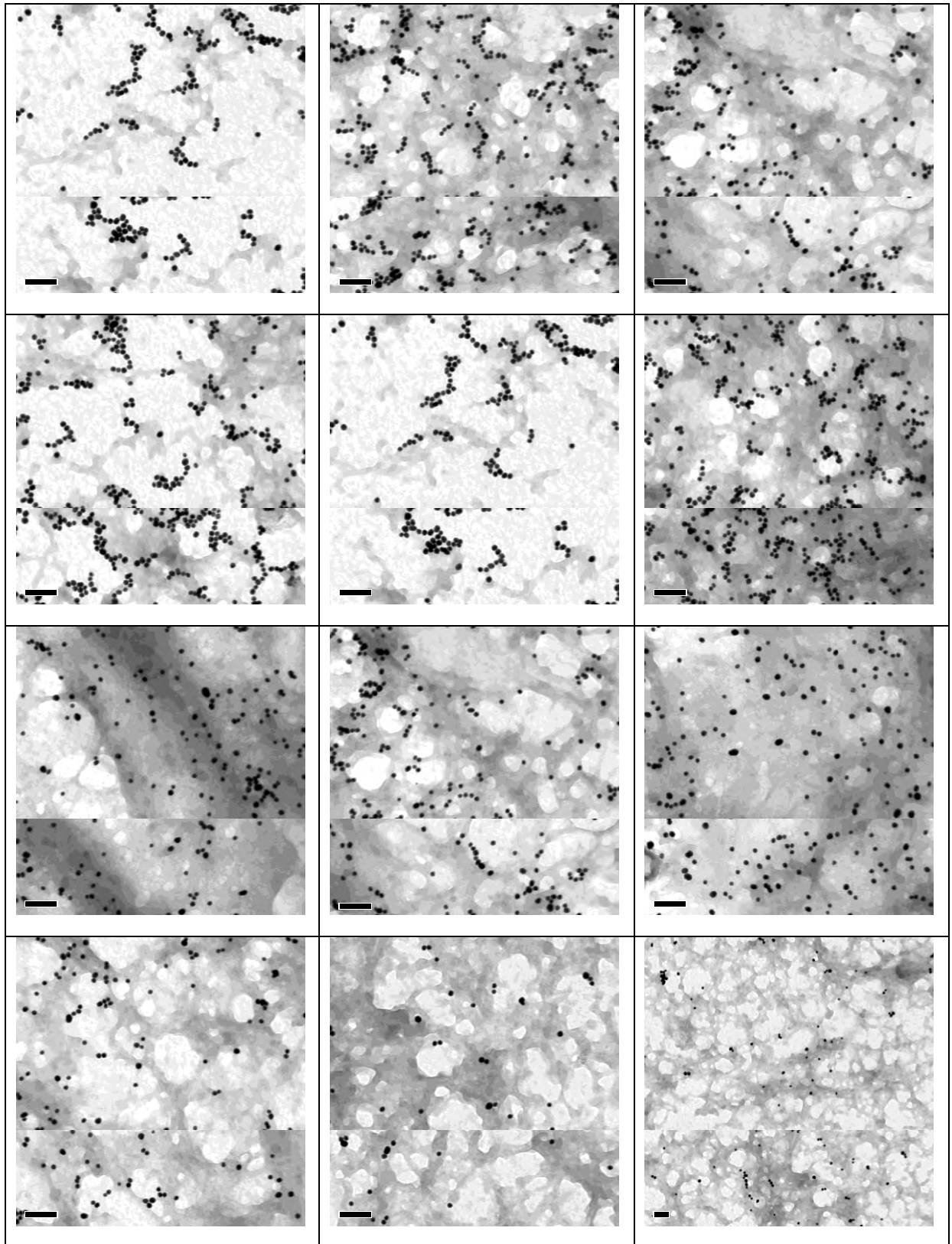
- WU, D. D., BURR, D. B., BOYD, R. D. & RADIN, E. L. 1990b. Bone and Cartilage Changes Following Experimental Varus or Valgus Tibial Angulation. *Journal of Orthopaedic Research*, 8, 572-585.
- XU, R. 2004. ISO International standards for particle sizing. *China Particuology*, 2, 164-167.
- XU, Z. C., SHEN, C. M., XIAO, C. W., YANG, T. Z., ZHANG, H. R., LI, J. Q., LI, H. L. & GAO, H. J. 2007. Wet chemical synthesis of gold nanoparticles using silver seeds: a shape control from nanorods to hollow spherical nanoparticles. *Nanotechnology*, 18.
- YAMASHITA, M., KAMEYAMA, K., YABE, S., YOSHIDA, S., FUJISHIRO, Y., KAWAI, T. & SATO, T. 2002. Synthesis and microstructure of calcia doped ceria as UV filters. *Journal of Materials Science*, 37, 683-687.
- ZHOU, M., WANG, B. X., ROZYNEK, Z., XIE, Z. H., FOSSUM, J. O., YU, X. F. & RAAEN, S. 2009. Minute synthesis of extremely stable gold nanoparticles. *Nanotechnology*, 20.

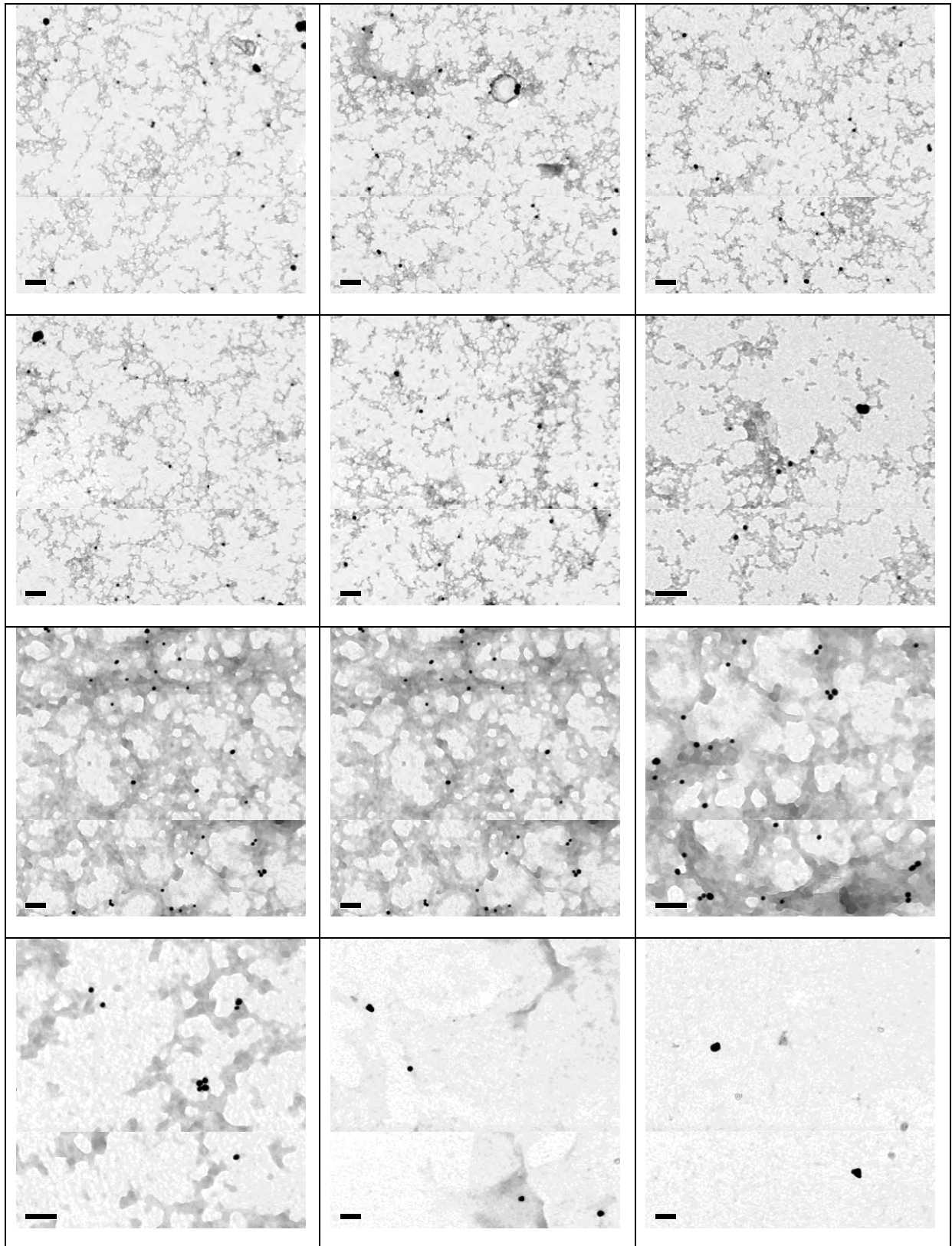
## APPENDIX A

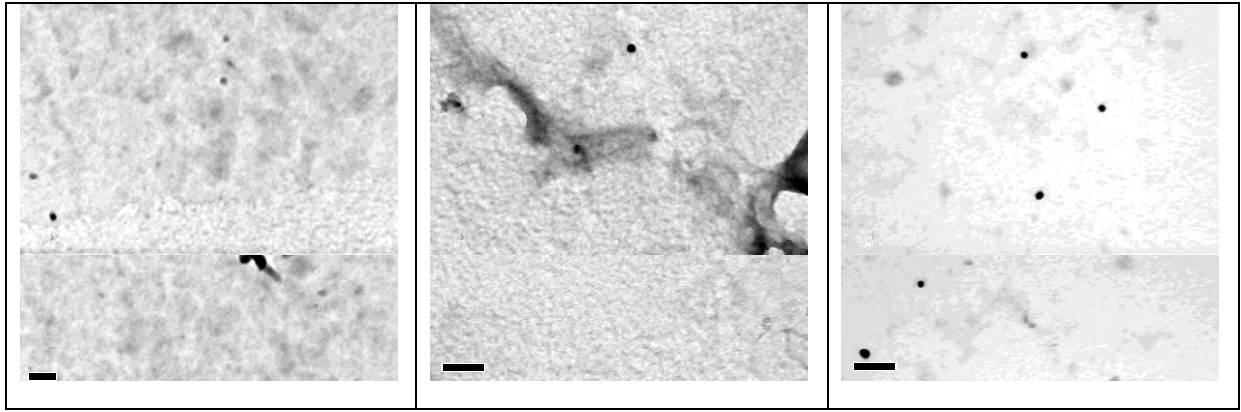
Few TEM images and results

SRFA ARRANGED FROM HIGHER CONCENTRATION TO LOWER

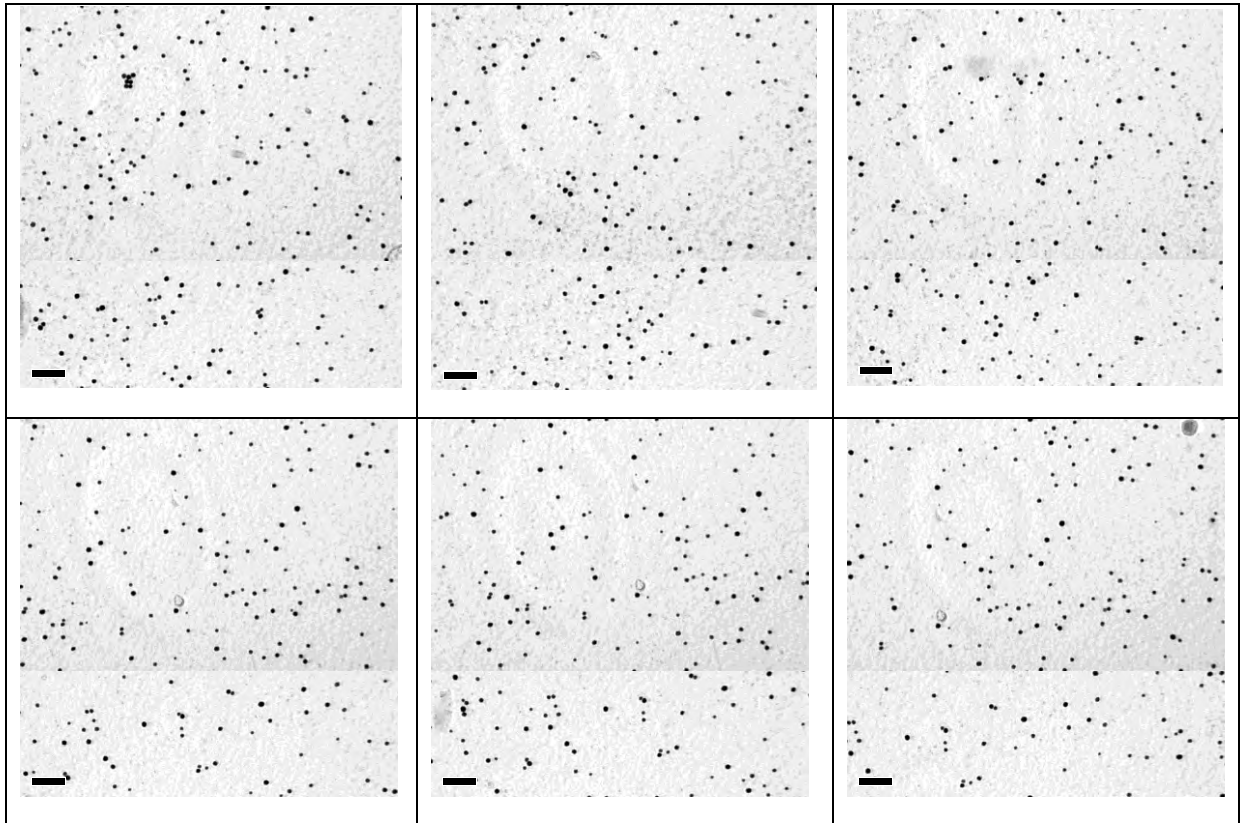


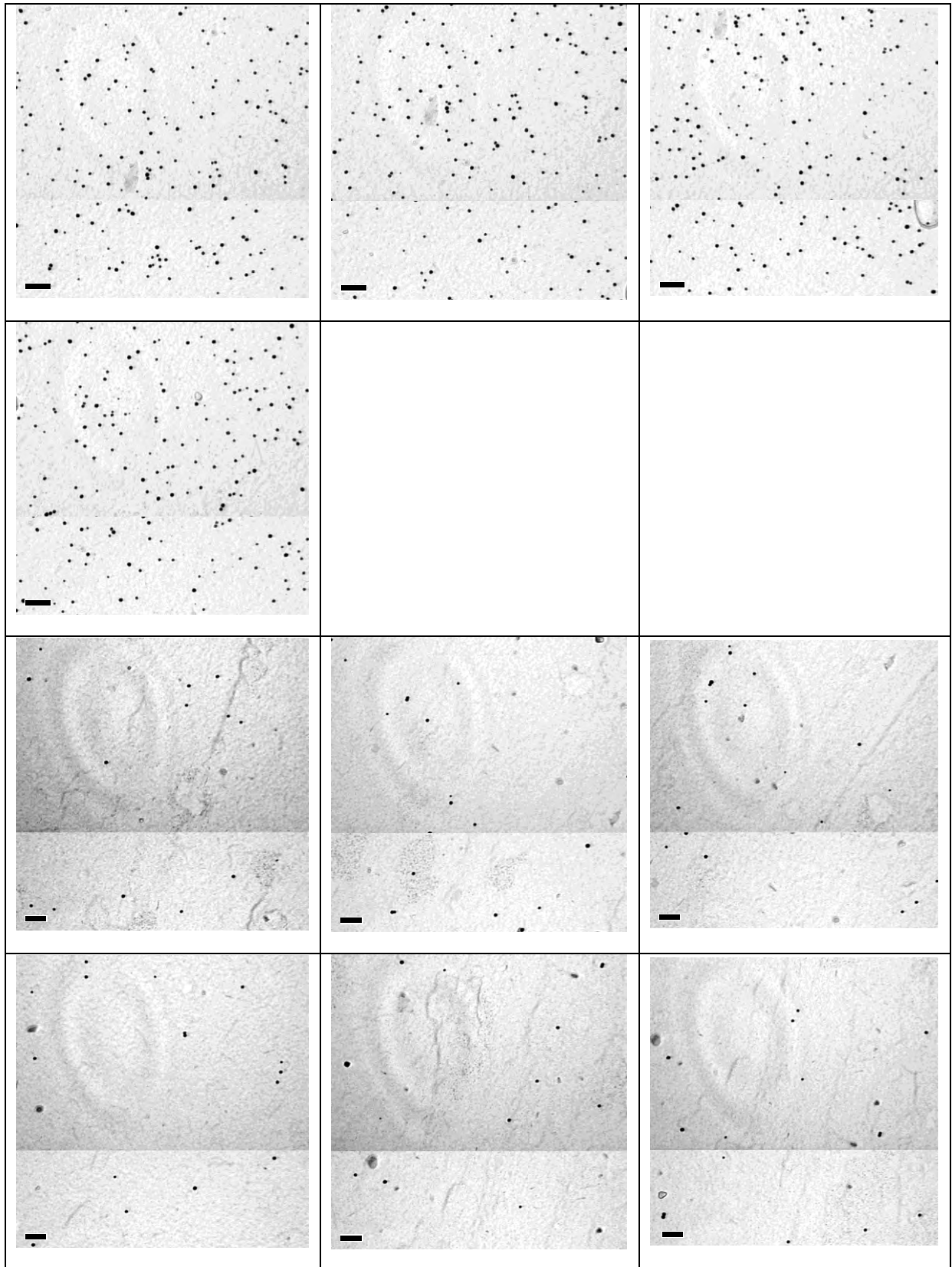


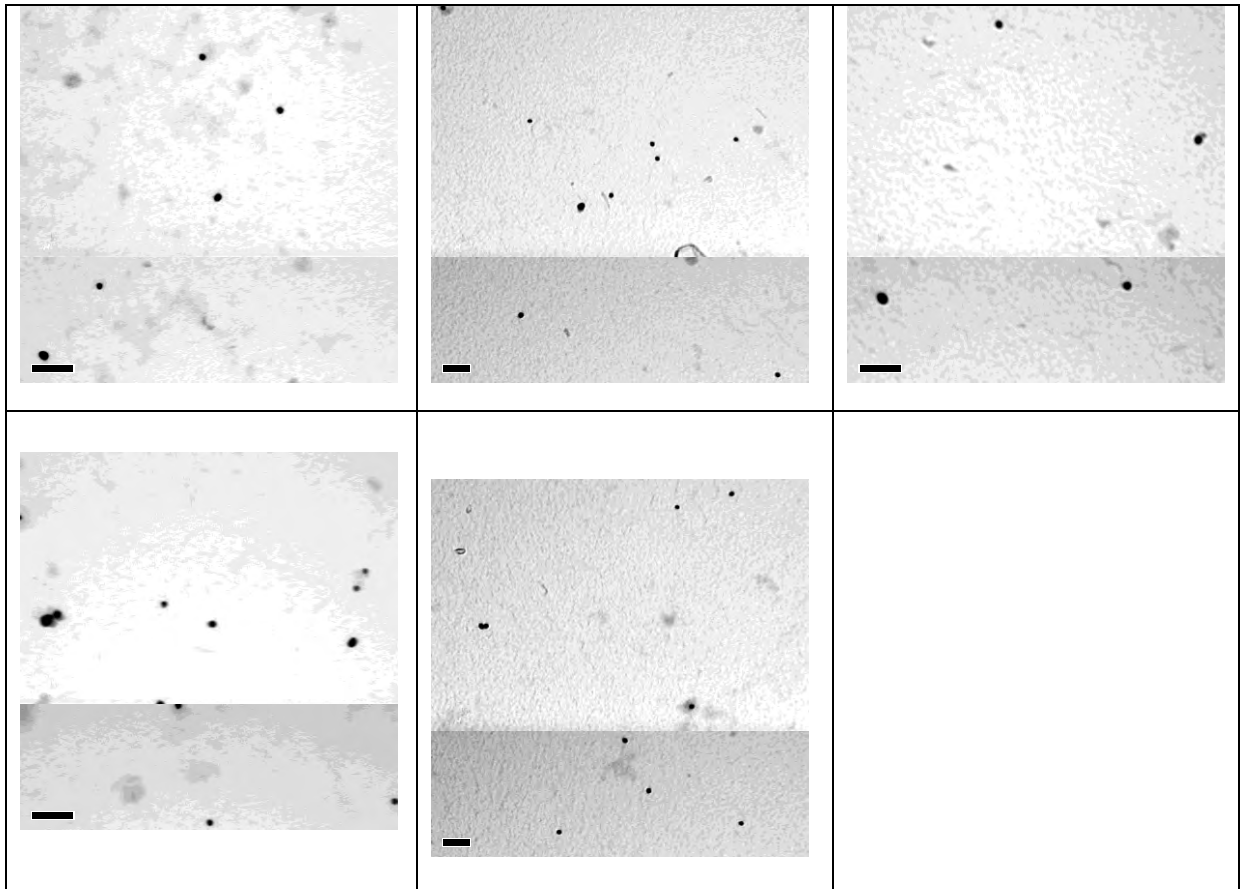




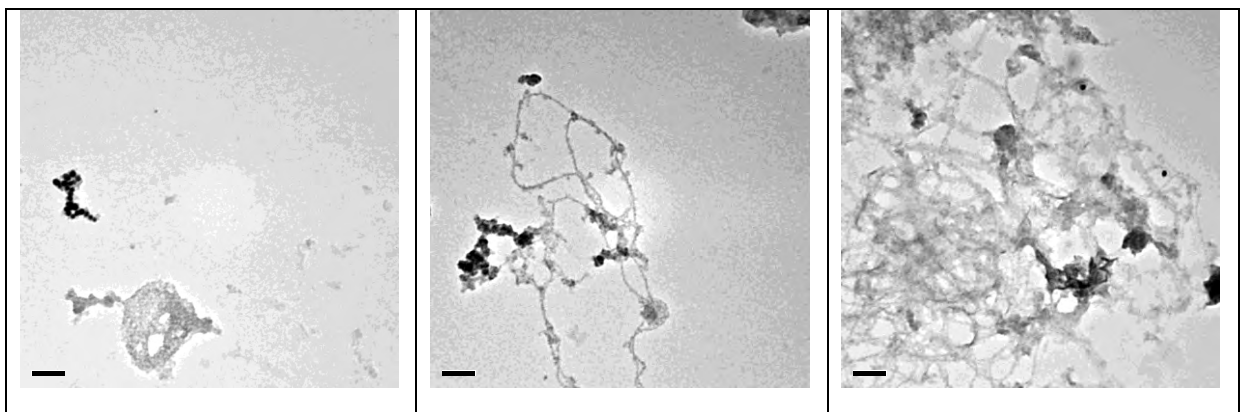
EPA ARRANGED FROM HIGHER CONCENTRATION TO LOWER



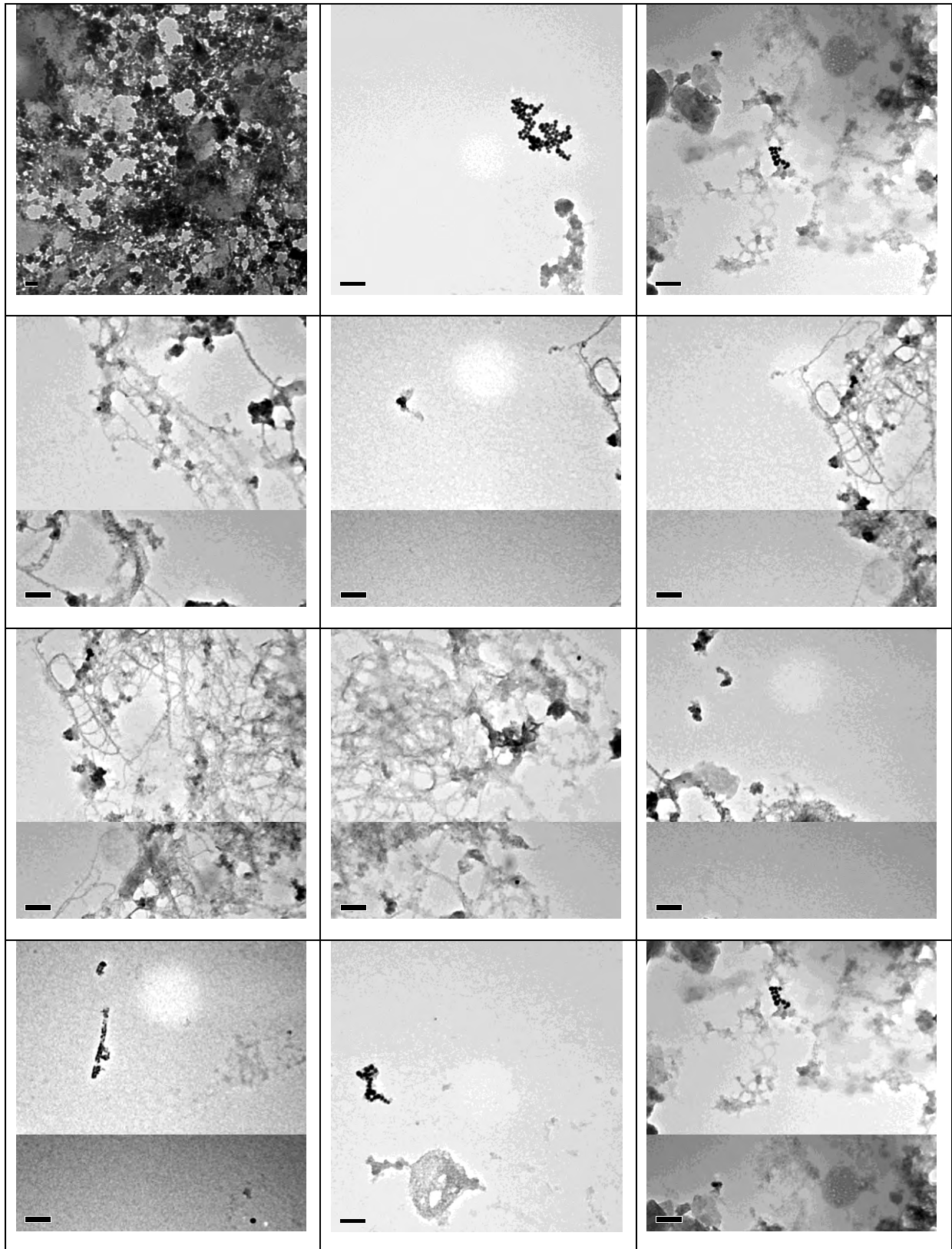




Lake water samples







## APPENDIX B

Published work

Published papers:

Baalousha, M + Prasad, A, Lead J Quantitative measurement of nanoparticle size and number concentration from liquid suspensions by atomic force microscopy –Environmental Science Process and Impacts - Published FEB-2014 – complete results of Chapter 5 and 6-attached at the end.

*A Prasad, M. Baalousha and J. R. Lead* Detection and quantification of engineered nanoparticles by transmission electron microscopy: protocol validation and application to environmental samples – Published – Complete results of Chapter 7

Mohammed Baalousha, Ashwini Prasad, Mithun Sikder, , Jamie Lead and Thomas G Chandler<sup>3</sup>  
Concentration-dependent behaviours of nanoparticles – Published – Results based on Chapter 7



Contents lists available at ScienceDirect

Science of the Total Environment

journal homepage: [www.elsevier.com/locate/scitotenv](http://www.elsevier.com/locate/scitotenv)



## An electron microscopy based method for the detection and quantification of nanomaterial number concentration in environmentally relevant media



A. Prasad<sup>a</sup>, J.R. Lead<sup>a,b,\*</sup>, M. Baalousha<sup>b,\*</sup>

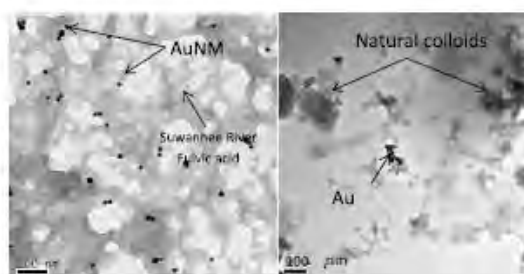
<sup>a</sup> School of Geography, Earth and Environmental Sciences, College of Life and Environmental Sciences, University of Birmingham, Edgbaston, Birmingham B15 2TT, United Kingdom

<sup>b</sup> Center for Environmental Nanoscience and Risk, Department of Environmental Health Sciences, Arnold School of Public Health, University South Carolina, Columbia 29208, SC, United States

### HIGHLIGHTS

- Fully quantitative sampling method for analysis of NMs by TEM is presented
- The method combines ultracentrifugation and TEM grid functionalization
- Initial validation has been performed using AuNMs in pure and synthetic EA waters
- The TEM sampling method enables direct measurement of NM number concentration
- The TEM sampling method enables detection of NMs in complex natural samples

### GRAPHICAL ABSTRACT



### ARTICLE INFO

#### Article history:

Received 2 June 2015  
 Received in revised form 23 July 2015  
 Accepted 24 July 2015  
 Available online 29 August 2015

Editor: D. Barcelo

#### Keywords:

Nanomaterials  
 Transmission electron microscopy  
 Sample preparation  
 Quantitative analysis  
 Particles number concentration  
 Environmental media

### ABSTRACT

Improved detection and characterization of nanomaterials (NMs) in complex environmental media requires the development of novel sampling approaches to improve the detection limit to be close to environmentally realistic concentrations. Transmission electron microscopy (TEM) is an indispensable metrological tool in nanotechnology and environmental nanoscience due to its high spatial resolution and analytical capabilities when coupled to spectroscopic techniques. However, these capabilities are hampered by the conventional sample preparation methods, which suffer from low NM recovery. The current work presents a validated, fully quantitative sampling technique for TEM that overcomes conventional sample preparation shortcomings, and thus enables the use of TEM for measurement of particle number concentration and their detection in complex media at environmentally realistic concentrations. This sampling method is based on ultracentrifugation of NMs from suspension onto a poly-L-lysine (PLL) functionalized TEM grid, using active deposition (by ultracentrifugation) and retention (by PLL interactions with NM surface) of NMs on the substrate, enabling fully quantitative analysis. Similar analysis with AFM was satisfactory in simple media but the lack of chemical-selectivity of AFM limits its applicability for the detection of NMs in complex environmental samples. The sampling approach was validated using both citrate- and PVP-coated AuNMs in pure water, which demonstrated an even distribution of NM on the TEM

\* Corresponding authors.

E-mail addresses: [jlead@mailbox.sc.edu](mailto:jlead@mailbox.sc.edu) (J.R. Lead), [mbsalou@mailbox.sc.edu](mailto:mbsalou@mailbox.sc.edu) (M. Baalousha).

